Mutational analysis of membrane traffic in *Arabidopsis thaliana*

Kin Cheong Kenneth Au

Linacre College

University of Oxford

A thesis submitted for the degree of

Doctor of Philosophy

Trinity Term 2012

I hereby certify that no part of this thesis has already been accepted, or is concurrently being submitted, for any degree or diploma or certificate or other qualification in this University or elsewhere. This thesis constitutes on my own work, except where otherwise stated.

Kin Cheong Kenneth Au
Linacre College
University of Oxford
10 September 2012

Acknowledgement

First, I have to make it clear that this thesis would not have existed if I had not received the financial support from the Clarendon Fund and Linacre Canadian Alumni Scholarship, and the scientific and emotional support from family, friends and colleagues throughout my degree. I would like to express my sincerest gratitude to my academic father (i.e. my primary supervisor), Dr. Ian Moore, for his patience, guidance and support in the past four years. He has been a father figure both inside and outside the lab. Not only has he taught me the proper and meticulous way of doing science, Ian has also inspired and encouraged me to pursue my passion. I also owe much thanks to my parents for their understanding, unrelenting support and boundless love even though I am not a lovable and filial child that they rightly deserve.

I thank my committee members, Prof. Liam Dolan, Prof. Sarah Gurr, Dr. Lee Sweetlove and Dr. Angela Hay for their helpful comments and suggestions.

I also like to thank my collaborators: Drs. Mark Fricker (my second supervisor), Andreas Meyer and Markus Schwarzlander for their contribution on the *gsh2* project and manuscript, Sarah Rodgers and Barry Martin for their assistance with electron microscopy, Drs. Steve Kelly and Chris Greenman for their expertise on bioinformatics, Dr. Imogen Sparkes for the YFP-RTNLB1 construct, Dr. Lorenzo Frigerio for the DER2-YFP construct and the anti-BiP antibody, and Dr. Jurgen Denecke for the anti-CRT antibody.

Past and present members of the Moore lab (Caroline O'Brien, Camille Foucart, Astrid Woollard, Priya Vijayakumar, Claudia Sas, Matthew Spencer, Michal Hala, Monika Kalde and Niloufer Irani)

and some members of the department (notably Xiaoqi Feng, Yuki Yasamura and Sarena Che Omar) also deserve my gratitude. To me they are not just colleagues who make me feel comfortable at work, but also friends who would go out of their way to lend me a hand.

Special thanks goes to Martin Krehenbrink and Monika Kalde who have painstakingly proofread my entire thesis and provided valuable comments and suggestions. I am also grateful for their friendship, assistance and mentoring over these years.

I also thank the Moorwood family who offered me a sanctuary when I most needed it. Hedley, Gloria and Maria Elisa are more than my landlord, but also friends who encouraged me and firmly believed that I can finish my degree and I am capable of making my dream come true.

There were countless occasions when I thought about packing it in. I thank everyone in Linacre Boat Club for giving me the distraction I need at times and providing me a reason to remain in Oxford, and buddies in Hong Kong and Toronto who cheered me on and stuffed my suitcase with encouragement when I was home. Amongst my dear friends I like to acknowledge Ranke, Wing, Sarah and Josi for being there whenever I need to talk to a close friend, their continual emotional support and their faith in me. Now I can go home and say to them in person rather than over the fibre optic cables, “I did it.”

Mutational analysis of membrane traffic in *Arabidopsis thaliana*

Kin Cheong Kenneth Au
Linacre College
A thesis submitted for the degree of *Doctor of Philosophy*
Trinity Term 2012

Abstract

To identify novel and essential components of the plant membrane trafficking mechanisms, *Arabidopsis* membrane trafficking mutants from fluorescent protein-based forward genetic screens were characterized. First, four novel *glutathione synthase* (*GSH2*) mutant alleles featured swollen endoplasmic reticulum (ER)-derived bodies that accumulated a soluble secretory marker. Consistent with the role of GSH2 in glutathione biosynthesis, the loss-of-function mutant alleles exhibited gamma-glutamylcysteine (γ-EC) hyperaccumulation and glutathione deficiency. The aberrant ER morphology was ascribed to the γ-EC accumulation. Redox-sensitive fluorescent protein revealed that *gsh2* seedlings maintained a reduced cytoplasm at steady state but were more sensitive to oxidative challenge. Second, Mut 21 was a conditional mutant that accumulated a secretory marker in the alkalized apoplast at restrictive temperature (31˚C). The mutant was identified as carrying a mutant allele of *tuftelin-interacting protein 11* (*TFIP11*), which has been implicated in regulating redifferentiation and cell proliferation through a cytokinin signalling pathway. Hence, it was postulated that the changes in response to cytokinin affect auxin-mediated acidification of the apoplast. Third, Mut 43 was a conditional mutant that accumulated a soluble secretory marker in the ER and unidentified punctate structures at restrictive temperature, and exhibited perturbations in ER export of a soluble protein marker. Moreover, the mutant showed severe growth defects and abnormal radial root swelling in the apical elongation zone. A mutation identification method through deep-sequencing of the wild-type siblings in outcrossed heterozygous mutant families was developed and tested in Mut 43. At the time when this thesis was prepared, bioinformatic analysis has assigned Mut 43 to the bottom arm of chromosome two and predicted a 300kb mapping interval based on the observed bias in single nucleotide polymorphism ratios. This work demonstrates the feasibility of using forward genetics to study plant-specific aspects of membrane trafficking mechanisms and incorporates new technology to streamline the process of gene identification.

Table of Contents

List of Figures

List of Tables

Abbreviations

ADP- Adenosine diphosphate
AFLP- Amplified fragment length polymorphism
ALP- Alkaline phosphatase
ARF- ADP Ribosylation Factor
ATP- Adenosine-5'-triphosphate
BFA- Brefeldin A
BiFC- Bimolecular fluorescence complementation
BiP- Binding immunoglobulin protein
BOR- Boron transporter
BSA- Bulked segregant analysis
BSO- Buthionine sulfoximine
CAPS- Cleaved amplified polymorphic sequence
Cdc42- Cell division control protein 42
CDNB- 1-chloro-2,4-dinitrobenzene
CIM- Callus-inducing medium
CLT- Chloroquine resistance transporter-like transporter
CoG- Conserved oligomeric Golgi complex
Col-0/ Col- *Arabidopsis* Columbia ecotype
COP- Coat protomer complex
CPY- Carboxypeptidase Y
CRT- Calreticulin
DAPI- 4',6-diamidino-2-phenylindole
dCAPS- Derived cleaved amplified polymorphic sequence
DER2- Derlin 2
DNA- Deoxyribonucleic acid
EE- Early endosome
EFP- Enhanced secGFP fluorescence phenotype
EM- Electron microscopy
EMS- Ethylmethanesulfonate
ER- Endoplasmic reticulum
ERES- Endoplasmic reticulum exit site
ERGIC- Endoplasmic reticulum-Golgi intermediate complex
FRET- Fluorescence resonance energy transfer
GAP- GTPase activating protein
GARP- Golgi-associated retrograde protein complex
GDI- GDP dissociation inhibitor
GDP- Guanosine diphosphate
γ-EC- Gamma-glutamylcysteine
GEF- Guanine nucleotide exchange factor

GFP- Green fluorescent protein
GPOX- Glutathione peroxidise
GRASP- Golgi reassembly stacking protein
GSH/ GSSG- glutathione (reduced/ oxidized form)
GSH1- Gamma-glutamylcysteine ligase
GSH2- Glutathione synthase
GTP- Guanosine-5'-triphosphate
HEPES- 4-(2-hydroxyethyl)-1-piperazineethanesulfonic acid
HMM- Hidden Markov Model
LB- Luria Bertani
LE- Late endosome
L*er*-0/ L*er* - *Arabidopsis* Landsberg *erecta* ecotype
LV- Lytic vacuole
MAGIC- The Multiparent Advanced Generation Inter-Cross
MBB- Monobromobimane
MCB- Monochlorobimane
mRNA- Messenger RNA
MVB- Multivesicular bodies
MS- Murashige & Skoog
NADPH- Nicotinamide adenine dinucleotide phosphate (reduced form)
NEM- N-ethylmaleimide
NIP- Nodulin 26-like intrinsic protein
NPSN- Novel plant SNARE
NSF- N-ethylmaleimide-sensitive factor
OPT- Oligopeptide transporter
PAC- Precursor-accumulating vesicle
PAR- Partition-defective protein
PCR- Polymerase chain reaction
PDI- Protein disulfide isomerise
PID- PINOID
PIN- PIN-FORMED
PIP- Plasma membrane intrinsic protein
PM- Plasma membrane
PP2A- Protein phosphatase 2A
PSV- Protein storage vacuole
PVC- Pre-vacuolar compartment
PVDF- Polyvinylidene fluoride
Rab - Ras-related protein in brain
RAPD- Random amplified polymorphic DNA
RE- Recycling endosome
ROI- Region of interest

RFLP- Restriction fragment length polymorphisms
RFP- Red fluorescent protein
RIM- Root-inducing medium
RNA- Ribonucleic acid
roGFP- Redox-sensitive green fluorescent protein
ROS- Reactive oxygen species
RT-PCR- Reverse transcription polymerase chain reaction
RTNLB- Reticulon-like protein subfamily B
secGFP- Secreted green fluorescent protein
SNAP- Soluble N-ethylmaleimide-sensitive factor attachment protein
SNARE- Soluble N-ethylmaleimide-sensitive factor attachment protein receptor
SNARF- Seminaphtharhodafluor
SNP- Single nucleotide polymorphism
SOC- Super optimal broth with catabolic repression
SSLP- Simple sequence length polymorphisms
STIP1- Septin and tuftelin-interacting protein 1
TFIP11- Tuftelin-interacting protein 11
TGN- Trans-Golgi network
TILLING- Targeted induced local lesions in genomes
TIP- Tonoplast intrinsic protein
TRAPP- Transport protein particle
UPR- Unfolded protein response
VSD- Vacuolar sorting determinant
VSR- Vacuolar sorting receptor
WT- Wild-type
YFP- Yellow fluorescent protein

Chapter 1 General Introduction

1.1 Membrane Trafficking

Eukaryotic and some prokaryotic cells comprise intracellular compartments that are enclosed by one or more lipid bilayer membranes. Each type of compartment, known as an organelle, is functionally distinct from the other and contains its own set of proteins and other macromolecules. Organelles need to interact with each other, the surrounding cytoplasm and also with the cell surface to transmit signals and exchange materials to perform cellular functions. While small molecules, such as ions, monosaccharides and small peptides, can travel across a membrane by passive diffusion or through receptors and transporters on the membrane, macromolecules, such as polysaccharides, lipids and proteins, are ferried between the plasma membrane (PM) and endomembrane organelles through membrane-derived vesicles. This vesicular transport mechanism requires vesicles to bud off from the donor membrane and to fuse to the acceptor membrane. Since not only the cargo molecules, but also membrane materials are trafficked from one compartment to another, this mechanism is also known as membrane trafficking.

Membrane trafficking is fundamental for the survival of a eukaryote as it is implicated in a variety of biological functions and processes. At a subcellular level, it is responsible for the biogenesis and maintenance of the cell wall, PM, vacuoles and other organelles in the endomembrane system. Different components of the membrane trafficking machinery work together to ensure that cargoes are delivered to the right place for organelles to perform their specialized functions; retrograde mechanisms are built in to retrieve escaped components from downstream organelles and to replenish membranes to maintain the function, morphology and identity of organelles (Battey et al., 1999; Sanderfoot and Raikhel, 1999). On a broader scale, membrane trafficking is

implicated in a variety of cellular functions and processes like cell growth. To achieve polarized growth as seen in plants, it is critical for the membrane trafficking mechanism to transport the raw materials and machineries to maintain the polarity and sustain growth, as exemplified by the growth of pollen tubes (Zhang et al., 2010).

Membrane trafficking is also important for responding to biotic and abiotic factors. The former incorporates the interactions with beneficial microorganisms (Mai et al., 2006; Blanco et al., 2009; Ivanov et al., 2012) as well as pathogens (reviewed in Robatzek, 2007). While endocytosis plays a role in pathogen perception (Robatzek et al., 2006), the alteration of secretion is speculated to help divert the cell's resources to withstand attacks (Collins et al., 2003; Assaad et al., 2004; Bhat et al., 2005). Abiotic factor responses include phototropism and gravitropism. Upon perception, the distribution of auxin transporters is changed to alter the flow of auxin, which would in turn trigger changes in plant growth (reviewed in Wiśniewska et al., 2006; Grebe, 2011; Rakusova et al., 2011). Due to its tremendous physiological importance, membrane trafficking processes are temporally and spatially tightly regulated.

1.1.1 Mechanism of vesicular transport

The membrane trafficking mechanism involves macromolecules packed in a membrane-enclosed vesicle that detaches from the donor membrane and fuses to the target membrane. The whole process of transport via vesicles can be divided into three key steps: budding, docking and fusion (Figure 1.1). Each step is highly regulated to provide the specificity necessary to ensure that cargoes are packaged into the right vesicles and are sent to the right compartment at the right time. First, vesicle budding involves the recruitment of coat protein subunits to start forming a protein coat complex. Some coat protein subunits are involved in concentrating selected cargoes

at the site of vesicle formation (Malkus et al., 2002). There are three types of coat proteins: COPI (Orci et al., 1986; Serafini et al., 1991), COPII (Barlowe et al., 1994) and clathrin (Pearse, 1976), which function in distinct parts of the membrane trafficking pathway. COPI is involved in intra-Golgi and Golgi-to-ER retrograde transport; COPII in the ER-to-Golgi pathway; and clathrin in endocytosis, TGN/ PM to endosomes and vacuole/lysosome (reviewed in Bonifacino and Glick, 2004). Each coat protein complex comprises a unique set of subunits, but all operate by a similar mechanism. Recruitment begins with the activation of a specific ARF/SAR1-GTPase in the cytosol and its association with a membrane through a transmembrane guanine nucleotide exchange factor (GEF) protein. The activated GTPase then recruits further coat protein subunits from the cytosol to the vesicle budding site. Cargo selection, packaging and polymerization of the protein coat are mediated by the coat subunits in the case of COPI and COPII mechanisms, and by heterotetrameric adaptor protein complexes in the clathrin-mediated mechanism (Keen et al., 1979). Accessory proteins, such as AP180 and epsin, induce membrane curvature and promote clathrin coat assembly (Ahle and Ungewickell, 1986; Ford et al., 2002). The activity of a GTPase-activating protein (GAP) is stimulated by coatomer-induced membrane curvature and stimulates the GTP hydrolysys activity of the specific GTP-binding protein ARF/SAR1-GTPase (reviewed in Barlowe, 2002). In the COPI and COPII pathways, the coated vesicles then bud off and coat disassembly proceeds due to intrinsic instability while the vesicle is traveling through cytoplasm. In clathrin-mediated pathways, vesicle budding is mediated by the GTPase dynamin which mediates constriction of the vesicle neck (Hinshaw and Schmid, 1995; Takei et al., 1995). The disassembly of the coat is mediated by an uncoating ATPase which requires energy from ATP hydrolysis to strip off the clathrin coat (Braell et al., 1984).

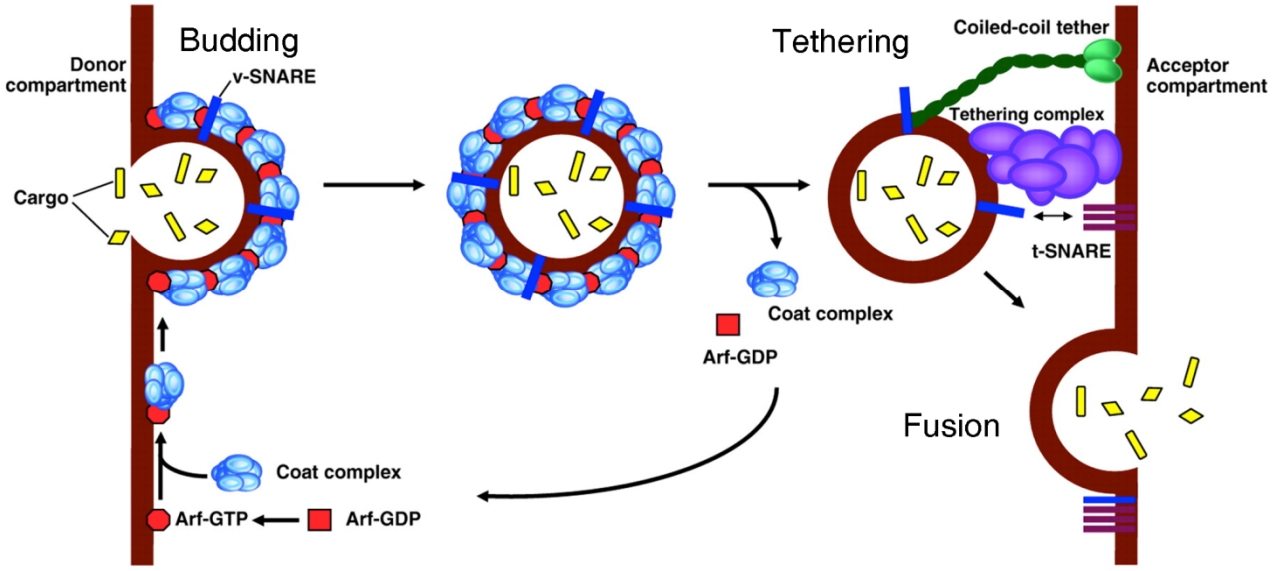

Figure 1.1. Mechanism of vesicular transport.

A vesicle buds from the donor compartment (budding). While it is en-route to the acceptor compartment, the coat protein complex is dissociated from the vesicle. Components of the coat protein return to the donor membrane to participate in another budding event. SNAREs, Rab-GTPase and tethering factors are now exposed on the surface of vesicle. Rab-GTPase on the vesicle can be activated and regulates its effectors; tethering factors on the vesicle and the target membrane facilitate the tethering/docking process (tethering). After the vesicle is brought to the vicinity of the acceptor membrane, SNARE complex is formed and helps fuse the vesicle with the target membrane (fusion).

Figure is modified from Jackson, 2009

After a vesicle has budded off and the coat has disassembled, the lipid bilayer and its embedded membrane proteins are exposed on the vesicle surface. This allows the recruitment of other proteins. While the vesicle is traversing the cytoplasm, tethering factors on the target membrane interact with certain components on the vesicle and guide the vesicle to its destination. There are two general types of tethering factors- the coiled-coil proteins (e.g. GM130, p115, giantin, golgins and GRASP) and multisubunit complexes (e.g. COG, exocyst, GARP and TRAPP) (reviewed in Whyte and Munro, 2002; Sztul and Lupashin, 2006; Yu and Hughson, 2010). Tethering factors can capture vesicles as far as 300nm away from the target membrane and bring them to close proximity for fusion to take place (Sztul and Lupashin, 2006).

Following vesicle tethering and docking, vesicle fusion is mediated by cognate soluble N-ethylmaleimide-sensitive factor attachment protein receptors (SNARE). SNARE motifs are divided into four groups- Qa-, Qb-, Qc- and R-SNARE (reviewed in Hong, 2005). A functional complex must contain one of each motif. The four α-helical motifs interact with each other to form a highly conserved intertwined bundles that facilitate fusion between the vesicle and the target membrane by displacing water molecules between membranes and changing the lipid structure (reviewed in Duman and Forte, 2003). After fusion of the two membranes, N-ethylmaleimide-sensitive factor (NSF) and soluble NSF attachment protein (α-SNAP) bind to the SNARE complex (Sollner et al., 1993). α-SNAP stimulates ATP hydrolysis activity of NSF, thus providing energy for dismantling the SNARE complex (Morgan et al., 1994). Individual SNARE proteins are then recycled for the next fusion event.

Since different SNAREs are located on different organelle membranes and have specific partners for complex formation, they were once thought to be sufficient for defining a vesicle's specificity to the target membrane. However, recent findings suggest otherwise as some SNARE proteins can participate in multiple fusion steps by forming different cognate SNARE complex *in vivo* (Sacher et al., 1997; Xu et al., 2002; Kweon et al., 2003). Moreover, it has been shown both *in vivo* and *in vitro* that vesicles remain tethered to the target membrane in the absence of SNARE-mediated fusion (Broadie et al., 1995; Cao et al., 1998). Hence, it appears that vesicle-targeting specificity is not solely conferred by SNAREs, by also by other factors such as tethering factors and Rab-GTPases.

An introduction to vesicular transport mechanism is not complete without a description of Rab-GTPase, which are molecular switches that oversee the entire process. When it is in its inactive GDP-bound form, a Rab-GTPase is cytosolic and binds to a GDP dissociation inhibitor (GDI). Once the GDP is replaced by GTP by a guanine nucleotide exchange factor (GEF), the active Rab-GTPase is anchored to a specific membrane and recruits various effectors to regulate vesicle budding, to interact with tethering factors and possibly SNAREs for docking and fusion, and to regulate motility of organelles and vesicles by interacting with cytoskeleton elements (reviewed in Segev, 2001; Zerial and McBride, 2001; Nielsen et al., 2008). Effectors of Rab-GTPases include phosphatidylinositol kinases (Camacho et al., 2009), which modify lipids on the membrane to establish membrane identity together with Rab-GTPase itself. Once its job is complete, Rab-GTPase would be inactivated as a GTPase activating protein (GAP) stimulates its GTP hydrolysis activity, it is then detached from the membrane.

1.1.2 Overview of membrane trafficking pathways

Vesicles generated from an organelle cannot be directly targeted to every other organelle in the endomembrane system. Instead, membrane trafficking is a highly regulated and specific process in which cargoes are transported along defined routes. The overall framework of the membrane trafficking is conserved among eukaryotes. There are three main routes: the secretory pathway, the endocytic pathway and the vacuolar/lysosomal pathway. The first station of the secretory pathway is the ER, where proteins that are targeted to endomembrane organelles or the cell exterior enter the pathway from the cytosol. It is where nascent proteins are folded and glycosylated, and lipid is synthesized. The second stop is the Golgi which consists of *cis*, medial and *trans* cisternae. Each cisternum houses a unique set of enzymes and is the site for further N-linked and O-linked glycosylation (reviewed in Kornfeld and Kornfeld, 1985; Schacter and Brockhausen, 1992). From here, cargoes are transported to the trans-Golgi network (TGN), beyond which they are transported either to the plasma membrane (PM) in the case of the secretory pathway or to the endosomes en-route to the vacuole/lysosomes. Vacuole/lysosome-targeted cargoes first arrive at the early endosomes after the TGN, then late endosomes/prevacuolar compartment (PVC)/multivesicular bodies (MVB), and eventually the vacuole/lysosome.

On the other hand, the endocytic pathway begins with extracellular cargoes being internalized by invagination of the PM. Cargoes first arrive at the early endosomes (EE), which are then transported either to the recycling endosomes (RE), where they are recycled back to the PM, or to the late endosomes (LE), from where they are destined to the lysosome/vacuole for degradation.

1.1.3 History of membrane trafficking research

Membrane trafficking research began with the discovery of organelles. The vacuole was visualized by van Leeuwenhoek with a light microscope in the 1600s, followed by the discovery of the Golgi apparatus in 1898 (Golgi, 1898). Then the introduction of electron microscopy in the 1950s allowed researchers to overcome the resolution limit of light microscopy and visualize the fine structures of organelles (Porter et al., 1945; Palade, 1952; Dalton and Felix, 1954; Bainton, 1981) and image vesicle formation (Roth and Porter, 1964).

Palade and Jamieson (1967a, b) developed electron microscopy radioautography to follow the path of secretory proteins. In their pulse-chase method, cells were labelled with a radioactively labelled precursor (pulse) followed by a nonlabelled form (chase). Since only labelled proteins can be detected, the movements of secretory proteins synthesized during the pulse step can be observed. These experiments led to the understanding of the connection between organelles in the secretory pathway and the idea of vesicular transport.

While Palade and his colleagues were plotting the route map of the secretory pathway, the properties of biological membranes were also under investigation. When placed in an aqueous environment, phospholipids spontaneously form a lipid bilayer with the polar head groups facing outward and the hydrophobic tails facing inward. Based on observations with electron microscopy, it was first proposed that a biological membrane comprises three layers, with a lipid bilayer packed between two protein monolayers. However, this trilaminar model was rejected as being thermodynamically unstable and was soon replaced by the fluid mosaic model, which depicts the membrane as a lipid bilayer with proteins embedded within. It classifies membrane proteins as either integral membrane proteins that are embedded within the membrane, or

peripheral membrane proteins that are attached to the surface of the lipid bilayer or to the exposed regions of integral membrane proteins. Since the fluid mosaic model suggests that proteins can diffuse laterally in the bilayer, it initially raised questions on the regulation of membrane identity and vesicle targeting. These concerns were eventually addressed with the proposition of lipid rafts, which establish local membrane domains with cholesterol and sphingolipids (reviewed in Lingwood and Simons, 2010), and the molecular details of organelles that establish membrane identity and vesicle-targeting specificity.

In the 1980s, the work of Rothman and Schekman marked the beginning of the molecular age in membrane trafficking. Rothman reconstituted fusion events of the Golgi apparatus *in vitro* (Fries and Rothman, 1981; Balch et al., 1984). Together with cell-fractionation techniques, the system allowed his group to purify components of vesicular transport, notably NSF, SNAP and eventually SNAREs (Block et al., 1988; Clary et al., 1990; Sollner et al., 1993). Around the same time, Schekman's group took a genetic approach in yeast. By screening for mutants that accumulate secretory organelles, conditional secretory mutants were identified and were categorized into 23 complementation groups or three phenotypic classes based on membrane accumulation (Novick et al., 1980). The *sec* mutants from this screen were identified to be defective in genes involved in various stages of the membrane trafficking process, such as vesicle coat formation (Kaiser and Schekman, 1990; Hicke et al., 1992; Hosobuchi et al., 1992; Oka and Nakano, 1994), regulation with GTP-binding proteins (Salminen and Novick, 1987) and vesicle docking (Novick and Schekman, 1979; Kaiser and Schekman, 1990). The work of Rothman and Schekman has provided the molecular basis of membrane trafficking today. It also paved the way for other researchers to adopt similar approaches to identify further molecular components of the pathway and to

provide explanations for the specificities, the maintenance and maturation of organelles as well as the routing of the trafficking network.

1.1.4 Unique features of membrane trafficking in plants

A general overview of the organization of the endomembrane system in eukaryotic cells has been described in Section 1.1.2. However, it is important to note the clear distinctions in organization between a plant cell and a mammalian cell (Figure 1.2). First, cargoes from the ER are directly transported to the Golgi in plant cells, whereas the vesicles from the ER first arrive at an ER-Golgi intermediate compartment (ERGIC) in mammalian cells. Second, it is not clear if all secretory cargoes in a plant cell are secreted to the PM from the TGN. It has been shown that vesicles that fuse to the plasma membrane can originate directly from the Golgi (Haigler and Brown, 1986) or the TGN (Toyooka et al., 2009) in plants, while cargoes in mammalian cells are generally understood to be exported from the TGN. Third, vesicles that bud off from the PM fuse and release cargoes at the early endosome (EE). While this compartment appears to be distinct from the TGN in mammalian cells, the plant's EE appears to be part of the TGN (Dettmer et al., 2006; Otegui and Spitzer, 2008; Robinson et al., 2008). Fourth, instead of hydrolytic lysosomes, a plant cell has vacuoles that are physically separated into lytic and protein storage vacuoles. Hence, multiple vacuolar sorting pathways have evolved in plants, as explained in Section 1.1.4.5.

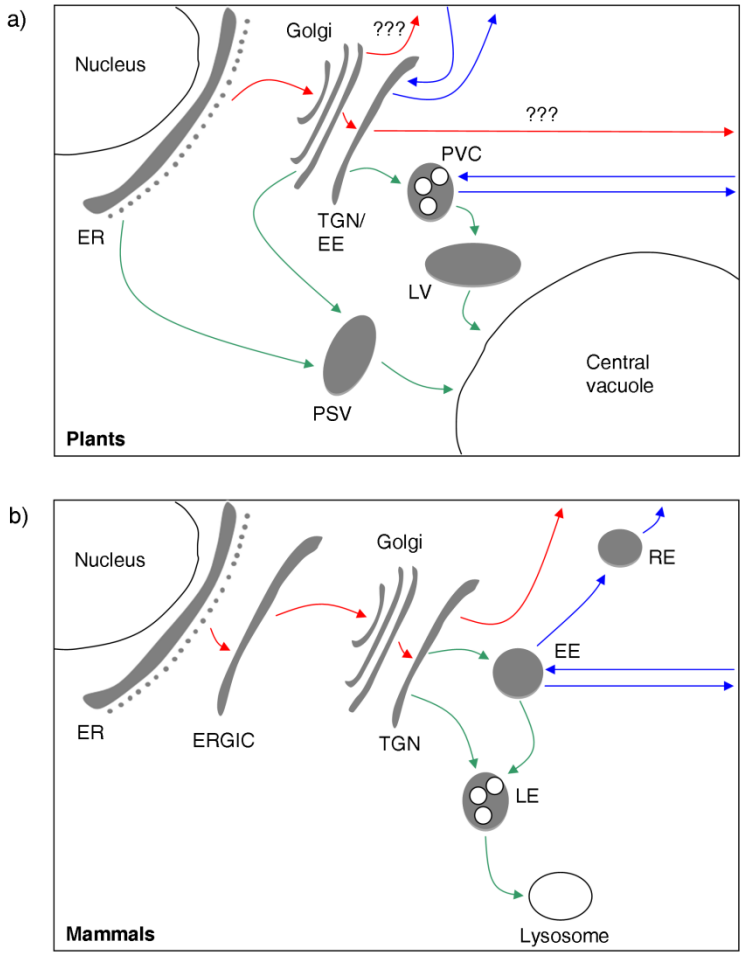

Figure 1.2. Simplified diagrams of the membrane trafficking pathways in plant and mammalian cells.

The secretory (red arrows), endocytic and recycling pathway (blue) and vacuolar/lysosomal sorting pathways (green) in a plant cell (a) and a generic mammalian cell (b) are illustrated.

a) Plant cells- Secretory cargoes are transported from the endoplasmic reticulum (ER) to Golgi, and may or may not pass through the trans-Golgi network (TGN) before they are secreted out of the cell. The endocytic pathway transports extracellular cargoes back to the TGN/early endosomes (EE) or the prevacuolar compartments (PVC), which are multivesicular bodies (MVB). Cargoes then either enter the recycling pathway to return to the plasma membrane (PM) or are directed to vacuolar sorting pathway for degradation. Three vacuolar sorting pathways are characterized. Two are targeted to the protein storage vacuole (PSV) and one to the lytic vacuole (LV). When a cell matures, these vacuoles may fuse into a central vacuole.

b) Mammalian cells in general- Secretory cargoes leave the ER for the ER-Golgi intermediate compartment (ERGIC) before reaching Golgi and TGN. Cargoes are either secreted out of the cell or transported via the late endosome (LE) to the lysosome. Extracellular cargoes are transported to EE via the endocytic pathway, which are either recycled back to the plasma membrane via recycling endosomes (RE) or directed into the lysosomal sorting pathway through late endosome (LE) for degradation.

Note that the retrieval pathways are not shown.

1.1.4.1 ER to Golgi transport

Secretory vesicles depart from the ER at ER exit sites (ERES). In animal cells, ERES are concentrated in the region of the ER that faces the Golgi (Palade, 1975; Hammond and Glick, 2000; Stephens et al., 2000). They are relatively immobile and remain at approximately the same position for several minutes (Stephens, 2003). Vesicles leave the ER for the ERGIC, which is formed as a result of homotypic fusion of COPII vesicles from the ER. Here, protein sorting takes place and cargoes are either ferried to cis-Golgi via long-range transport mediated by microtubule and dynein motors, or recycled back to the ER (reviewed in Appenzeller-Herzog and Hauri, 2006). In plant cells, rather than being confined in a discrete area in the ER, the ERES are widely dispersed in the ER (Boevink et al., 1998). They are stationary for only a short time (half-life of less than 10s in tobacco BY-2 cells) (Yang et al., 2005) and are able to move along with the associated Golgi body as a "secretory unit" (DaSilva et al., 2004). It is clear that ERES in plant cells are more mobile and have an intimate relationship with Golgi stacks, so that ER-derived vesicles travel a much shorter distance to reach their target compared to animal cells.

1.1.4.2 Golgi organization

Differences in organization and functional characteristics of Golgi in animal and plant cells reflect some of the distinct features of membrane trafficking in each lineage. During interphase, a plant cell has a higher number of Golgi stacks than an animal cell (Griffing, 1991). Individual Golgi stacks are dispersed throughout the cytoplasm in plant cells and travel along the underlying actin cytoskeleton (Boevink et al., 1998), whereas the stacks are interconnected and perinuclear in animal cells under the influence of microtubules (Cole et al., 1996). Hence, the traveling distance of Golgi-derived vesicles in plant cells is generally shorter than their animal counterpart.

Furthermore, plant Golgi stacks are much more motile, moving at 3-4μm/s (Boevink et al., 1998; Nebenfuhr et al., 1999) compared to 0.6μm/s for their mammalian counterpart (Sciaky et al., 1997), and their movement appears to be interdependent on ER as the movements of the two organelles are closely associated (Sparkes et al., 2009). Differences are also apparent in mitosis. Animal Golgi undergoes reversible disassembly in early mitosis (Burke et al., 1982) that is mediated by the phosphorylation of GRASP55 and GRASP65 (Xiang and Wang, 2010). Golgi stacks in plant cells, however, do not disintegrate and the secretory pathway is intact throughout mitosis (Faso et al., 2009). This difference is also reflected by the absence of the Golgi reassembly stacking proteins (GRASPs) in plants (Faso et al., 2009).

1.1.4.3 Cell Polarity

Circumstantial evidence suggests that cell polarity arose independently in plants and animals (reviewed in Dettmer and Friml, 2011). Unlike animal cells, many polarized plant cells do not use physical diffusion barriers to segregate proteins to defined domains. Studies on PM proteins (PINs, BOR1 and NIP5;1) revealed that proteins can be targeted to at least three distinct domains (apical, lateral and basal) in root tip epidermal cells (Benková et al., 2003; Wiśniewska et al., 2006; Takano et al., 2010).

Mammalian and yeast cells establish and maintain cell polarity apparently by several mechanisms: 1) active sorting at the TGN and the recycling endosomes, 2) fusion specificities provided by cognate SNAREs in different PM domains, 3) specific domains established by the exocyst complexes and protein complexes on PM such as partitioning defective (PAR), Crumbs and Scribble, and 4) interactions between exocyst complexes and the actin cytoskeleton mediated by a Rho-GTPase Cdc42 (reviewed in Mellman and Nelson, 2008; Orlando and Guo,

2009). Meanwhile, plants do not have any homologues of the mammalian protein complexes that provide landmarks for cell polarity (Dhonukshe, 2009), or Cdc42 (Fu and Yang, 2001), so the third and the fourth mechanisms are not available for plants. The absence of the components used by mammalian and yeast cells suggests that plant cells have to use different strategies for establishing cell polarity.

However, little is known about the exact mechanism by which polarity is established and maintained in the plant cell. Much of the work has focused on the localization of PIN-FORMED (PIN) proteins the auxin transporters. The polarization of PIN1 is established by non-polar secretion followed by GNOM ARF-GEF-mediated polar recycling (Geldner et al., 2003). GNOM is also essential for the redistribution of PIN3 in gravitropic responses (Kleine-Vehn et al., 2010; Rakusova et al., 2011). Similarly, a study on the polar localization of BOR1 on the lateral domain of PM also suggests a postendocytic recycling mechanism for establishing polarity (Takano et al., 2010). Another mechanism regulates PIN localization through phosphorylation. The apical and basal localization of PINs depend on a fine balance between the phosphorylation and dephosphorylation of PINs that are regulated by the protein serine/theonine kinase PINOID (PID) and protein phosphatase 2A (PP2A), respectively. The alteration of relative activities in gain-of-function or loss-of-function mutants results in changes in the polarization of PIN proteins (Michniewicz et al., 2007).

1.1.4.4 Cytokinesis

Cytokinesis is the final step in cell division that separates the daughter cells. An animal cell forms an actomyosin contractile ring at the division plane. As the ring constricts, the cleavage furrow develops and a midbody is formed. The cell is then cleaved into two halves (Zeitlin and Sullivan,

2001). Instead of constriction, a plant cell undergoes cytokinesis by forming a phragmoplast, which is a cytoskeleton-based structure at the midplane, allowing the cell plate to expand centrifugally along the division plane and eventually fuse with the PM (reviewed in Bednarek and Falbel, 2002). The different strategies of cytokinesis have profound implication on the routing of membrane trafficking pathway to ensure components are delivered to the right place. While in animal cells it is important to supply membrane lipids and other molecules to the PM and midbody (Albertson et al., 2005), secretory cargoes are needed at the cell plate rather than at the PM in plant cells (Jürgens, 2004). To deal with this unique cell division strategy, components have evolved that direct vesicles to the cell plate. Most notably, a plant-specific syntaxin KNOLLE interacts with KEULE and SNAP33 to mediate vesicle fusion events at the cell plate (Waizenegger et al., 2000; Assaad et al., 2001; Heese et al., 2001). There is also a report that KNOLLE interacts with another plant-specific SNARE NPSN11 (Zheng et al., 2002). It is unclear whether NPSN11 and SNAP33 form the same SNARE complex with KNOLLE.

1.1.4.5 Vacuolar sorting

In addition to the acidic lytic vacuoles (LV) that resemble LVs in yeast and lysosomes in animal cells, plant cells also possess protein storage vacuoles (PSV) that have a higher pH and different composition. These PSVs are notably present in seeds, root tips and cotyledons. As cells mature, the distinct vacuoles can eventually fuse into a large central vacuole. To ensure delivery of cargoes to the appropriate vacuoles, plant cells have more elaborate vacuolar sorting pathways compared to other eukaryotic cells. Plants have, for example, a larger collection of vacuolar sorting receptors (VSR) than their functional equivalents in other eukaryotes (Shimada et al., 2003). There are three general types vacuolar sorting determinants that are known to be recognized by the vacuolar sorting machineries in plants: 1) sequence-specific N-terminal

propeptides (ssVSD), 2) C-terminal propeptides without clear consensus sequence (ctVSD) and 3) structure-based determinants (psVSD) (Neuhaus and Rogers, 1998). There are also at least three distinct pathways to different vacuoles: 1) a clathrin-coated vesicle-mediated pathway that transports cargoes to the LV (Kirsch et al., 1994; Sanderfoot et al., 1998), 2) a dense vesicle transport pathway to the PSV (Hohl et al., 1996), and 3) an ER-derived precursor-accumulating vesicle (PAC) pathway that bypasses the Golgi to efficiently deliver large amount of storage proteins to the PSV (Hara-Nishimura et al., 1998) (Figure 1.3).

Similar to plants, yeast (*Saccharomyces cerevisiae*) has multiple vacuolar pathways. One is the carboxypeptidase Y (CPY) clathrin-coated vesicle-mediated pathway that transports cargoes from the Golgi to the vacuole via the PVC, and the other is the alkaline phosphatase (ALP) pathway that does not require clathrin and does not pass through the PVC (reviewed in Conibear and Stevens, 1998). Examination of the proteins involved in the yeast and plant clathrin-coated vesicle-mediated pathway reveals that many proteins are homologous, but interestingly some of the functional homologs (e.g. AtVAM3/Vam3p) are localized in different compartments in their respective species (Wada et al., 1997; Sanderfoot et al., 1999). This again validates the notion that knowledge of proteins, even those with conserved functions, cannot simply be transferred from one organism to another.

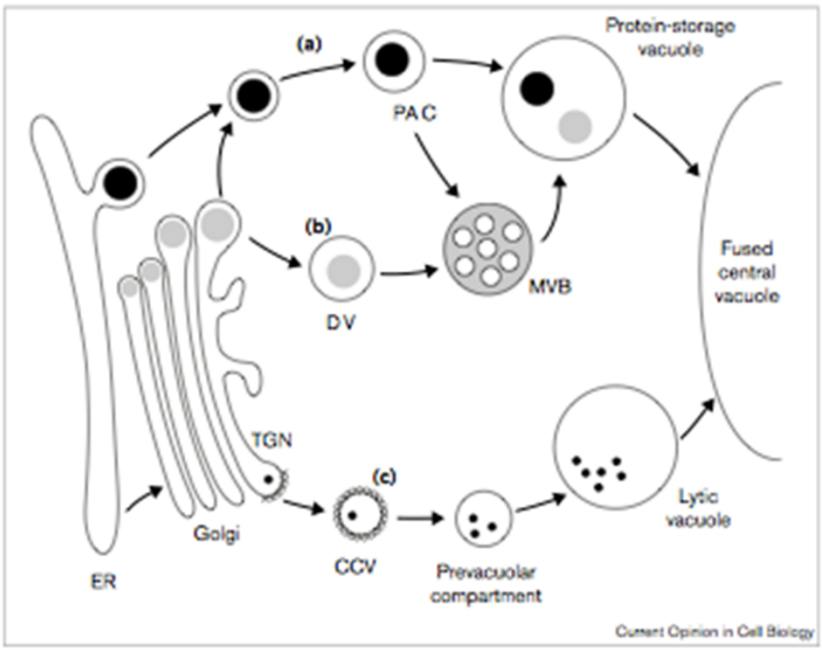

Figure 1.3. Vacuolar sorting pathway in plants.

a) ER-derived precusor-accumulating vesicle (PAC) pathway to the protein storage vacuole (PSV)

b) Dense vesicles (DV) pathway to the PSV

c) Clathrin-coated vesicles (CCV) pathway to the lytic vacuole (LV)

Figure from Bassham and Raikhel, 2000.

1.1.4.6 Genetic composition

It has been hypothesized that the differences in genetic composition reflect the development of unique features in membrane trafficking in each lineage. Numerous gene families essential for membrane trafficking can be found in all eukaryotes, but comparative phylogenetic studies have suggested that several important gene families have undergone independent diversification events in plant and animal lineages (Vernoud et al., 2003; Mouratou et al., 2005). For example, only eight out of 41 mammalian Rab-GTPase subclasses can be found in *Arabidopsis* (Rutherford and Moore, 2002). And these eight subclasses have undergone a plant-specific radiation so that plants have similar number of Rab-GTPases as mammals. Similarly, only two out of the eight ARF-GEF subclasses (ie BIG/SEC7 and GBF/GEA) are found in *Arabidopsis* (Cox et al., 2004). While some members have maintained their ancestral functions (Richter et al., 2007; Teh and Moore, 2007), others have acquired novel plant-specific functions (Geldner et al., 2003). Molecular and cytological studies have suggested that since the time when plants diverged from their shared ancestor with other eukaryotes, plant cells have acquired unique features in various aspects of membrane trafficking (Dacks and Field, 2007). For these reasons, knowledge on membrane trafficking mechanisms in plants cannot be directly inferred from other eukaryotic systems.

1.2 Application of fluorescent proteins and fluorescence microscopy

Fluorescent protein technology provides a non-invasive method for visualizing cellular events *in vivo* and in real-time. Today it is widely used to track the distribution and motility of a protein of interest, to assess gene expression and protein interaction, and in biological screens. Its contribution to membrane trafficking research is also enormous and therefore warrants a section

of its own. In this section, the history of fluorescent protein development is described, followed by its use in membrane trafficking.

1.2.1 History of fluorescent proteins

Green fluorescent protein (GFP) was isolated from jellyfish (*Aequorea victoria*) for the first time in the early 1960s (Shimomura et al., 1962), but it was not until the 1990s that fluorescent proteins were established as a research tool. After GFP was cloned and heterologous expression was established in the 1990s (Prasher et al., 1992; Chalfie et al., 1994; Inouye and Tsuji, 1994), scientists were able to express GFP in model organisms. Based on the understanding of the structures of wild-type GFP and its S65T mutant variant (Heim et al., 1995; Ormö et al., 1996; Yang et al., 1996), variants of GFP with different spectroscopic properties were developed.

Other than the GFP from *Aequorea*, a proportion of fluorescent protein variants that are widely used today stem from a red fluorescent protein (RFP) found in the coral *Discosoma* (Matz et al., 1999). The original tetrameric red fluorescent protein, DsRed, has been engineered extensively to derive a family of stable monomeric proteins whose emission wavelengths range from yellow to red (Campbell et al., 2002; Shaner et al., 2004). These variants complement the collection of GFP and its variants whose emission wavelengths range from blue to yellow. Today, a wide diversity of GFP and RFP variants has been created encompassing different spectroscopic properties, photostabilities, sensitivities to temperature, ionic environment and pH, as reviewed by Shaner et al (2005).

Despite the success in expressing fluorescent recombinant proteins in *E. coli* and *C. elegans* (Chalfie et al., 1994; Inouye and Tsuji, 1994), the application of fluorescent proteins in plant

biology did not have a smooth start. Although a high level of fluorescence was observed in tobacco when GFP was introduced via potato virus X and tobacco mosaic virus (Baulcombe et al., 1995; Heinlein et al., 1995), very little fluorescence was seen in GFP-expressing *Arabidopsis*. To circumvent this, Haseloff et al. (1997) modified the wild-type cDNA GFP for expression in *Arabidopsis* by improving codon usage, removing a cryptic intron and modifying the codons to improve thermotolerance and introduce a dual excitation peak.

1.2.2 The use of fluorescent proteins in membrane trafficking research

Fluorescence microscopy has been an attractive tool for membrane trafficking research because the traffic of macromolecules in the pathway can be visualized in real-time. Even before the era of fluorescent protein technology, fluorescent dyes had already been used to label specific macromolecules or compartments (e.g. DAPI and MBB) (Porter and Feig, 1980; Fahey et al., 1981). The endocytic pathway has also been studied based on the internalization of fluorescent dyes (e.g. FM4-64) (Vida and Emr, 1995). The development of fluorescent proteins has enhanced and popularized the use of fluorescence microscopy in the field.

The most common application of fluorescent proteins in the study of membrane trafficking is protein tagging. By fusing a fluorescent protein with a protein that resides in a specific organelle or an organelle-targeting signal peptide, fusion proteins can be used as organelle markers to examine the morphology and the dynamics of a particular organelle. It is also possible to fuse a fluorescent protein to any proteins of interest to study its trafficking and localization pattern. Having a variety of fluorescent proteins with different spectral properties means that different fluorescently tagged proteins that are coexpressed in the same cell can be imaged simultaneously to examine the relative distribution of the tagged proteins.

The interactions between membrane trafficking regulators can be studied with bimolecular fluorescence complementation (BiFC) or fluorescence resonance energy transfer (FRET) techniques. Both techniques generate fluorescent signals when the candidate proteins are in close proximity. They have been used to identify interactions between SNAREs (Fujikawa and Kato, 2007; Ebine et al., 2008; Grefen et al., 2010; Kwaaitaal et al., 2010), and between Rab proteins and tethering factors in Golgi (Osterrieder et al., 2009).

Another application of fluorescent proteins is their use as markers in genetic screens. After plants with stable expression of a fluorescent protein marker are mutagenized, the resulting mutants can then be identified by visual inspection and confirmed with fluorescence microscopy. A number of research groups have applied this approach to study the genetic basis for membrane trafficking mechanisms, as described in Section 1.3.1.

1.3 Advantages and disadvantages of forward and reverse genetic approach

Forward and reverse genetics are two fundamentally different approaches to elucidate gene functions. While the former starts with a phenotype of interest and works towards pinpointing the gene that is accounting for the phenotype, the latter targets a particular gene and looks for any changes in the phenotype. Reverse genetics has gained popularity in the past decade due to the availability of complete genome sequences and advances in transcriptome analysis. Many resources and techniques, such as site-directed mutagenesis and RNAi silencing, are available for targeting a specific gene in *Arabidopsis*. However, there are two main caveats in the reverse genetic approach. First, some prior knowledge of the function of the candidate gene is required for the experiment; otherwise it would not be possible to determine a suitable gene for study.

But in the *Arabidopsis* genome, 31% of the total predicted gene loci cannot be assigned to any functional groups based on experimental characterization or sequence comparison with other organisms (The Arabidopsis Genome Initiative, 2000). Thus, a large number of genes cannot be easily studied using reverse genetics. Second, in the case of functional redundancy, the true effect of a mutated gene is masked by other genes that can complement it. Studies have shown that significant functional redundancy exists in many gene families associated with membrane trafficking, hampering reverse genetic analysis (Sanderfoot, 2007; Pinheiro et al., 2009; Ebine et al., 2011).

On the other hand, classical forward genetics offers an unbiased approach to identify genes that are attributed to a phenotype of interest. Since no knowledge of gene is required for the mutant screen design, it can potentially identify novel genes that are involved in the process of interest. This approach also avoids the complications associated with functional redundancy as it only identifies mutants with a clear phenotype of interest.

Despite the advantages that forward genetics offer, the major downside is that it has traditionally been a laborious and time-consuming process. Ethylmethanesulfonate (EMS) mutagenesis in *Arabidopsis*, for example, requires a population of at least 125 000 M1 lines to achieve saturation mutagenesis (Haughn and Somerville, 1987; Jander et al., 2003). Once a mutant has been isolated, identification of the gene locus by map-based cloning can be yet another difficult and long process. But recently, the combination of the availability of the reference *Arabidopsis* genome and next-generation sequencing technologies have drastically reduced the time and workload required to identify causative point mutations (Schneeberger et al., 2009; Austin et al.,

2011; Lindner et al., 2012), thus improving the efficiency of high-throughput forward genetic screens.

1.3.1 History of forward genetic screens in membrane trafficking

Forward genetics screens have a long and successful track record in the study of membrane trafficking mechanisms. As described in Section 1.1.3, the yeast *sec* mutants from Novick's conditional mutant screen had a profound impact on establishing the molecular basis of membrane trafficking (Novick et al., 1980). The utility of forward genetic screens of EMS-induced mutants plants was realized when Jurgens et al. (1991) conducted a pioneering forward genetic screen in *Arabidopsis* to study pattern formation in embryos. EMS was chosen as the mutagen as it creates random point mutations across the genome. Its ethyl group specifically reacts with guanine to form O^6-ethylguanine that is paired with thymine by DNA repair mechanisms, resulting in G/C to A/T substitutions most of the time (Greene et al., 2003). Point mutations are desirable as they can create a variety of mutations in a gene ranging from loss-of-function to gain-of-function phenotypes. By isolating mutants with atypical body organization at the seedling stage, nine genes that were important in embryogenesis were discovered (Mayer et al., 1991). Some of these genes, namely *KNOLLE*, *KEULE* and *GNOM*, were later found to be important in the membrane trafficking process throughout a plant's life cycle in addition to embryogenesis. KNOLLE is a plant-specific syntaxin that targets to the cell plate, regulates vesicle fusion to the cell plate and is essential for cytokinesis in plants (Lukowitz et al., 1996; Völker et al., 2001). KEULE is a homologue of Sec1 that regulates vesicle tethering and fusion with the target organelle membrane. It interacts with KNOLLE to mediate vesicle fusion in cytokinesis (Assaad et al., 2001). GNOM is a GTP/GDP exchanger factor for ARF-GTPases proteins. In plants, it plays a

key role in endosomal recycling to establish a polarized localization of PIN1 on the PM (Geldner et al., 2003).

In recent years, forward genetic screens employing fluorescence imaging were used to identify components of the membrane trafficking mechanisms. Plants that stably express a fluorescent protein marker that is known to target a specific compartment through a well-defined membrane trafficking pathway were mutagenized and subsequently screened by fluorescence imaging. The underlying premise of these screens is that any mutations that affect the trafficking of the marker or the morphology of its target organelle would result in aberrant distribution of the fluorescent marker which can be visualized with fluorescence microscopy. This approach has been exploited to study biogenesis of endomembrane organelles and plant-specific regulators in various pathways (Table 1.1). For example, Brandizzi's group has conducted a screen using a Golgi membrane marker (ST-GFP) to study the maintenance of Golgi morphology and to elucidate the intimate relationship between the ER and Golgi in terms of organelle organization (Boulaflous et al., 2008; Faso et al., 2009; Marti et al., 2010a). The mutations that have been characterized so far encompass components that are responsible for ER and Golgi structural maintenance (Faso et al., 2009; Marti et al., 2010b), Golgi motility (Stefano et al., 2012) and ER-to-Golgi transport (Faso et al., 2009; Marti et al., 2010). Similarly, Hara-Nishimura's mutant screen with an ER lumen marker (GFP-HDEL) has led to the identification of components for ER-to-Golgi transport (Nakano et al., 2009) and ER body formation (Matsushima et al., 2003b; Yamada et al., 2008).

Several vacuolar markers have been used in genetic screens that focus on endomembrane organization (GFP-2SC in Tamura et al., 2005), vacuolar sorting (GFP-CT24 in Fuji et al., 2007), and endomembrane protein trafficking and vacuole biogenesis (GFP:δ-TIP) (Cutler et al., 2000; Avila

et al., 2003; Chary et al., 2008; Agee et al., 2010). GFP-2SC is fluorescent in the endomembrane system but not the vacuole (Tamura et al., 2003), making it an ideal endomembrane marker. Indeed, a GFP-2SC-based screen has led to the identification of a Golgi protein (MUR3) that interacts with actin to organize the endomembranes (Tamura et al., 2005). On the other hand, GFP-CT24 is normally only visible in the PSV in seeds. Mutants with vacuolar sorting defects can be identified as the fluorescent protein is secreted to the extracellular matrix, resulting in fluorescent seeds (Fuji et al., 2007). Unlike the other two vacuolar markers, GFP:δ-TIP is targeted to the tonoplast and is therefore insensitive of the light-dependent proteolysis in the vacuolar lumen (Tamura et al., 2003), making it a suitable marker for vacuole biogenesis and the biosynthetic pathway (Chary et al., 2008; Agee et al., 2010).

Furthermore, Friml's group demonstrated the versatility of a polarized PM protein (PIN1-GFP) as a membrane trafficking marker. Following a non-polar secretion, PIN1-GFP is constitutively internalized and recycled to its polar domain on the PM (Geldner et al., 2003). PIN1-GFP was used to screen for two general types of membrane trafficking mutants: endocytic trafficking mutants that exhibited reduced internalization of PIN1-GFP from the PM (Paciorek et al., 2005; Tanaka et al., 2009), and subcellular trafficking mutants that exhibited intracellular accumulation of PIN1-GFP (Feraru et al., 2010; Zwiewka et al., 2011). Interestingly, instead of discovering mutants that are associated with the secretory pathway or the recycling pathway that PIN1 undergoes, the two mutants that have been characterized are both related to vacuolar functions (Feraru et al., 2010; Zwiewka et al., 2011).

Table 1.1. Examples of EMS-induced membrane trafficking mutant alleles identified in fluorescence imaging-based forward genetic screens

Mutant	Gene Product (AGI code)	Screening marker	Phenotype seen with the screening marker	References
nai1	NAI1 (At2g22770)	ER lumen (GFP-HDEL)	Absence of ER bodies	(Matsushima et al., 2003a)
nai2	NAI2 (At3g15950)	ER lumen (GFP-HDEL)	Elongation and reduction of ER bodies	(Yamada et al., 2008)
ermo1	GNL1 (At5g39500)	ER lumen (GFP-HDEL)	Dispersed spherical ER bodies	(Nakano et al., 2009)
gnl1-2, gnl1-3	GNL1 (At5g39500)	Secretory (secGFP)	Accumulation of secGFP in spheroid bodies	(Teh and Moore, 2007)
ermo2/ sec24a	SEC24a (At3g07100)	Golgi membrane (ST-GFP) and ER lumen (GFP-HDEL)	Large aggregates of spherical ER bodies	(Faso et al., 2009; Nakano et al., 2009)
gold36^{P80L}	GOLD36/ MVP1 (At1g54030)	Golgi membrane (ST-GFP)	Retention of Golgi marker in ER	(Marti et al., 2010b)
gom8	RHD3 (At3g13870)	Golgi membrane (ST-GFP)	Reduced Golgi motility and atypical Golgi aggregates	(Stefano et al., 2012)
kam1-1	MUR3 (At2g20370)	Endomembrane and vacuole (GFP-2SC)	Aggregates of endomembranes	(Tamura et al., 2005)
kam2-1	RME8 (At2g26890)	Endomembrane and vacuole (GFP-2SC)	Aggregates of endomembranes	(Tamura et al., 2007)
mvp1-1	GOLD36/ MVP1 (At1g54030)	Tonoplast (GFP:δ-TIP)	Perinuclear aggregates containing GFP:δ-TIP	(Agee et al., 2010)
csp-1	TPS6 (At1g68020)	Tonoplast (GFP:δ-TIP)	Absence of pavement cell lobes	(Chary et al., 2008)
gfs1	VSR1 (At3g52850)	Vacuole (GFP-CT24)	GFP-CT24 was secreted	(Fuji et al., 2007)
gfs2	RME8 (At2g26890)	Vacuole (GFP-CT24)	GFP-CT24 was secreted	(Fuji et al., 2007)
gfs10	(At4g35870)	Vacuole (GFP-CT24)	GFP-CT24 was secreted	(Fuji et al., 2007)
ben1-1	BEN1/ MIN7 (At3g43300)	Polarized PM (PIN1-GFP)	Reduced internalization and agglomeration of PIN1-GFP	(Tanaka et al., 2009)
doc1	BIG (At3g02260)	Polarized PM (PIN1-GFP)	Reduced auxin-mediated inhibition of PIN1-GFP internalization	(Paciorek et al., 2005)
pat2-1	AP3 β Adaptin (At3g55480)	Polarized PM (PIN1-GFP)	Intracellular ectopic accumulation of PIN1-GFP	(Feraru et al., 2010)
pat4-1	AP3 δ Adaptin (At1g48760)	Polarized PM (PIN1-GFP)	Intracellular ectopic accumulation of PIN1-GFP	(Zwiewka et al., 2011)

1.3.2 The principle of using of secretory fluorescent proteins as markers in genetic screens

Instead of using a fluorescent protein marker that targets to a specific organelle, a secreted GFP (secGFP) has been used by our group to assess traffic in the secretory pathway. Essentially, secGFP is made by fusing a sporamin signal peptide for ER translocation on the N-terminus of GFP (Boevink et al., 1999). After secGFP is translocated to the ER, it is transported to the apoplast via the default secretory pathway for soluble cargoes. Once secGFP has reached the apoplast, its fluorescence diminishes due to poor accumulation. Hence, fluorescence is low in wild-type seedlings expressing secGFP under normal growth condition (Zheng et al., 2004). Moreover, the secGFP found in the apoplast is in a truncated form (Zheng et al., 2004).

Based on the premise that the intracellular accumulation secGFP should result in increased fluorescence intensity, a genetic assay using secGFP to identify secretory mutants was developed (Zheng et al., 2004; Teh and Moore, 2007). After EMS mutagenesis, putative mutants with defects in secretion should accumulate secGFP intracellularly in fluorescent form, thus producing an enhanced fluorescence phenotype that can be easily identified using fluorescence imaging (Boevink et al., 1999; Batoko et al., 2000; Zheng et al., 2004). Putative mutants are confirmed by verifying the intracellular secGFP accumulation by confocal fluorescence microscopy. However, a problem with using secGFP as a marker is that its variable expression can interfere the outcome of the analysis, as the enhanced fluorescence phenotype may be due to strong secGFP expression in the mutant line (a false positive), a disruption in secretion (a true positive), or both. To normalize for the variable expression, transgenic plants expressing a self-cleaving marker construct that express a secreted marker and an intracellular reference marker in a fixed stoichiometric ratio (Samalova et al., 2006), were included in subsequent mutant screens. In this

case, the intracellular markers, which is localized in the nucleus (for nlsRFP-2A-secGFP) or the Golgi (for ST-RFP-2A-secGFP), provide a baseline for the expression of the secGFP, thus allowing the application of ratiometric imaging technique to correct for variability in marker expression (Samalova et al., 2006).

1.3.3 secGFP-based forward genetic screens for temperature-sensitive and seedling-lethal secretory mutants

The secretory mutant screen conducted by H Zheng was the first that utilized secGFP as a marker in our group (Zheng, 2001). Zheng was aiming to identify viable mutants that accumulate sufficient intracellular secGFP to exhibit an enhanced fluorescence phenotype. On the putative mutants that he has isolated, Zheng showed that the viable mutants had weak and inconsistent phenotypes, while those that had high level of intracellular secGFP were lethal and therefore could not be propagated to the next generation (Zheng, 2001). It is reasoned that membrane trafficking is an essential cellular process and that any significant perturbations in secretion would jeopardize the viability of the organism. To increase the recovery rate of mutants that exhibit notable membrane trafficking defects, subsequent screens were refined to identify temperature-sensitive and seedling-lethal mutants. Mutants were selected at the seedling stage because it has been speculated that mutations that result in seedling-lethality are less likely to be associated with general defects in development and highly conserved functions compared to embryo- or gametophyte-lethal mutants, as discussed previously (Jürgens et al., 1991; Berná et al., 1999).

The two temperature-sensitive mutants to be described in this thesis, Mut 21 and 43, were isolated from the temperature-sensitive mutant screen by OK Teh (Figure 1.4a). Similar to

Zheng's screen, the seeds from M1 plants were harvested in batches of 120 M1 plants (Teh, 2007). To reduce the number of false positives, the putative mutants were subjected to a second round of heat treatment after recovery. The mutants did not exhibit an enhanced fluorescence phenotype (EFP) until after 24-72h after heat-treatment at 31°C. In total, only two *bona fide* temperature-sensitive mutants were identified from this screen.

The seedling-lethal mutants that are being studied here, G4, N37, S6 and S10, are from the seedling-lethal by H Neto and J Perez-Gomez (Figure 1.4b). Mutants were screened from mutagenized plants expressing secGFP, a ratiometric secGFP construct with a nuclear reference marker (nlsRFP-2A-secGFP) or a Golgi reference marker (ST-RFP-2A-secGFP). Since it was designed to screen for homozygous lethal mutants, the seeds from each M1 plant were harvested individually so that the resulting M2 family can be traced back to allow propagation of the mutation through the heterozygous siblings once a lethal mutant is identified. Eventually, 64 seedling-lethal mutants were identified from the screen (H Neto, J Perez-Gomez and I Moore, unpublished data). The putative mutants are grouped according to the site of secGFP localization as listed on Table 1.2.

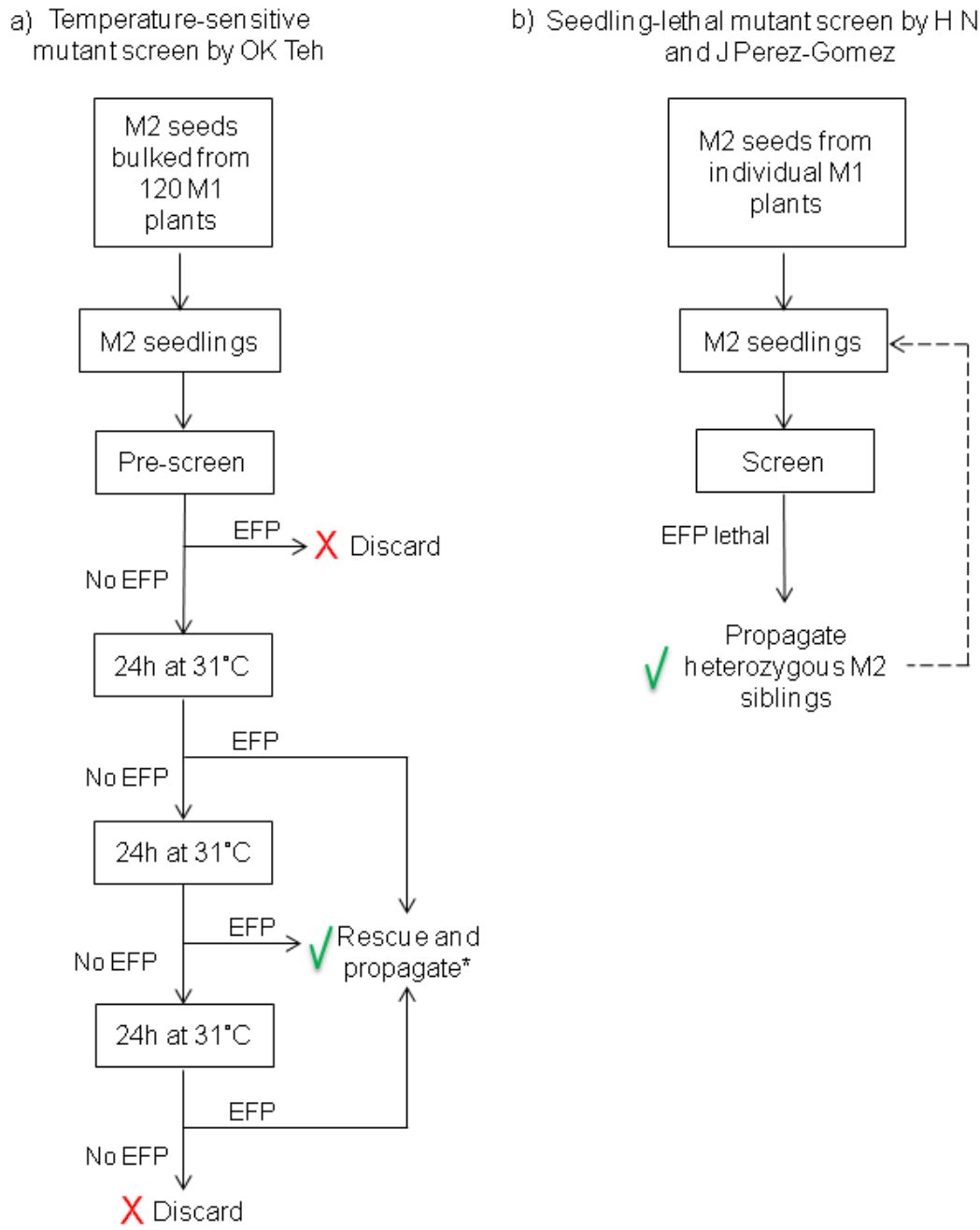

Figure 1.4. Flow-chart of OK Teh's temperature-sensitive mutant screen and H Neto and J Perez-seedling-lethal mutant screen.

* Mutants that weren't rescued were propagated. Repeated heat treatment was conducted on rescued mutants and only those with repeated EFP were propagated.

EFP- Enhanced secGFP fluoresence phenotype

Figure reconstructed from Teh, 2007.

Table 1.2. Putative seedling-lethal mutants grouped according to the site of secGFP localization

Site of secGFP localization	Number of mutants
Tubular fusiform bodies (ER)	34
Tubular fusiform bodies (ER) and vesicles	1
Tubular fusiform bodies (ER) and cytoplasm	1
Plasma membrane/ cell wall / cell surface	8
Vesicles	4
Aggregated bodies	6
Vacuole	2
Unclear	8
Total	**64**

1.4 Thesis objective and overview

Since the ER is the first organelle in the secretory pathway, a block in secretion at this point would compromise all transport of cargoes to downstream endomembrane organelles. Moreover, as described previously, the ER and Golgi in plants are different from their counterparts in other eukaryotic systems in many aspects, such as their morphology, structure, dynamics and motility, which give rise to differences in the early secretory pathway (reviewed in Hanton and Brandizzi, 2006). With the aim of increasing the understanding of the regulation and organization of the early secretory pathway in plants, I have selected mutants that appeared to accumulate secGFP in the tubular fusiform ER bodies in the initial screen for my study of membrane trafficking. Specifically, my study focuses on four seedling-lethal mutants, G4, N37, S6 and S10, and two temperature-sensitive mutants, Mut 21 and Mut 43.

In Chapter 3, the findings on G4, N37, S6 and S10 are presented. These mutants were isolated by H Neto and J Perez-Gomez, who have also shown that secGFP colocalizes with an ER lumen marker in spherical bodies and mapped the mutation to a gene that relates to the glutathione

biosynthetic pathway. Using the mutants as a tool, the link between glutathione synthesis and membrane trafficking is extensively explored. In this work, the mutants are characterized extensively to explore the relationship between ER morphology maintenance and glutathione biosynthesis.

In Chapter 4, the work on characterization and mapping of Mut 21 are presented. Mut 21 is a temperature-sensitive mutant that exhibits an enhanced fluorescence phenotype in the cotyledons 18h after incubation at 31°C. It was first isolated as a mutant that accumulates secGFP in the ER, but more detailed investigation revealed that secGFP actually accumulates in the apoplast. Mapping data identified Mut 21 as a mutant allele of At1g17070, which encodes for tuftelin-interacting protein 11 (TFIP11). As discussed further in this chapter, the study of Mut 21 may provide insight into the behaviour of GFP in the apoplast.

In Chapter 5, the characterization data of Mut 43 is presented. Similar to Mut 21, Mut 43 is a temperature-sensitive mutant that was previously shown to accumulate secGFP in the ER. In addition to the enhanced fluorescence phenotype, Mut 43 also exhibits growth defects and radial root swelling at restrictive temperature. A new mapping and mutation identification method using the next-generation sequencing technology was developed for Mut 43. The preliminary mapping data is described.

Chapter 2 Materials and Methods

2.1 Materials

2.1.1 Plant materials and growth condition

Mutated plants were all in *Arabidopsis thaliana* Columbia ecotype (Col-0). Mapping cross families were generated either by pollinating wild-type Landsberg *erecta* (L*er*-0) stigma with pollens from heterozygous mutant plants, or vice versa (see Section 2.2.5 for details on artificial pollination).

To sterilize seeds to grow in axenic culture, seeds were washed with 70% ethanol for 5 min, stratified at 4°C for two days on Murashige & Skoog (MS) agar plate, which contains 0.44% w/v Murashige & Skoog (MS) basal salt (Sigma Aldrich, United Kingdom), 2.6mM MES, 1% w/v sucrose, pH 5.7 with KOH and 0.7% agar, and cultivated at 20°C with a 16h-photoperiod. Two- to three-week-old seedlings were transplanted to soil. Normally, plants were grown at 20°C with a 16h-photoperiod after transplanting, but homozygous Mut 43 and plants that were used for artificial pollination were grown at 18°C with a 16h-photoperiod.

For temperature-sensitive mutants, heat treatment involved transferring MS agar plates containing seedlings to 31°C with a 24h-photoperiod for 24-48h.

2.1.2 Bacteria and growth condition

Escherichia coli strain DH5α (Hanahan, 1983) was used for recombinant DNA work. Binary vectors other than those derived from pGREEN (Hellens et al., 2000) were transformed into *Agrobacterium tumefaciens* strain GV3101::pMP90 (Koncz and Schell, 1986), which was then used for *Arabidopsis* transformation. pGREEN-based vectors (e.g. pNIGEL in waveline series) were

transformed into *Agrobacterium tumefaciens* strain GV3101::pMP90 containing pSOUP (Hellens et al., 2000).

Bacteria were propagated in Luria Bertani (LB) growth media (1% w/v tryptone, 0.5% w/v yeast extract, 1% NaCl, pH 5.7) with appropriate antibiotics. LB agar selection plates were prepared similarly with the addition of 0.7% agar. Super optimal broth with catabolite repression (SOC) media (2% w/v bacto tryptone, 0.5% bacto yeast extract, 10mM NaCl, 2.5mM KCl, 10mM $MgCl_2$, 10mM $MgSO_4$ and 20mM glucose) were added to the bacteria during the recovery period after a heat shock treatment in transformation.

All media were autoclaved for 20min at 121°C before use.

2.1.3 Chemicals

All chemicals were supplied by Sigma-Aldrich (Dorset, UK), VWR International (Poole, UK), Fisher Scientific (Loughborough, UK), BD (Franklin Lakes, USA) or Melford (Suffolk, UK) unless otherwise stated.

2.1.4 Enzymes

Restriction endonucleases were supplied by New England Biolabs (Hitchin, UK) or Fermentas (part of Thermo Fisher Scientific, Loughborough, UK). DNA polymerases were supplied by Thermo Fisher Scientific (Loughborough, UK), Invitrogen Ltd (Paisley, UK) and New England Biolabs (Hitchin, UK).

2.1.5 Antibiotics

Hygromycin was available as a stock solution from Calbiochem (part of Merck Chemicals, Darmstadt, Germany). Other antibiotics were prepared by dissolving in water or ethanol (for tetracycline) and were filter-sterilized with a 0.22μm syringe filter (Millipore, Cork, Ireland) before use. The antibodies that were used in this study and their stock and final concentrations are listed in Table 2.1.

Table 2.1. Stock and final concentrations of antibiotics used in selection of bacteria and plants

Antibiotics	Stock Concentrations	Final Concentrations	
		Bacteria	Plants
Ampicillin	100mg/mL	100μg/mL	--
Carbenicillin	100mg/mL	200μg/mL	--
Gentamycin	100mg/mL	10μg/mL	--
Hygromycin	417μg/mL	--	15μg/mL
Kanamycin	100mg/mL	50μg/mL	25-30μg/mL
Phosphinothricin	100mg/mL	--	10μg/mL
Tetracycline	50mg/mL	50μg/mL	--
Timentin	2mg/mL	2μg/mL	--

2.1.6 Antibodies

Antibodies containing 27% glycerol were stored at -20°C. The antibodies used and the dilution factors for each antibody were listed in Table 2.2.

Table 2.2. Antibodies used in this work

Name	Host	Source	Dilution Factor
Anti-BiP	Rabbit	Gift from L. Frigerio	1:5000
Anti-CRT	Rabbit	Gift from J. Denecke	1:10000
Anti-GFP	Rabbit	Abcam (ab290)	1:1000
Anti-GFP	Rabbit	Invitrogen Molecular Probe (A6455)	1:1000

2.1.7 Oligonucleotides

PCR oligonucleotide primers were obtained from Bioneer (Daejeon, South Korea) or Sigma Aldrich (Dorset, UK). Sequences are listed in Appendix A.

2.2 Methods

2.2.1 Confocal Laser Scanning Microscopy

2.2.1.1 Zeiss LSM 510 META microscope configuration

Whole seedlings (5-7 days old) were mounted on glass slides with water. Fluorescence was examined with a Plan-Neofluar 25x/0.8NA variable immersion lens or an Apochromat 40x/1.2NA water-immersion lens on Zeiss LSM 510 META laser scanning microscope (Carl Zeiss Ltd., Welwyn Garden City, UK).

Except for simultaneous imaging of GFP and YFP, samples were examined using Zeiss LSM 510 META laser scanning microscope. The settings for imaging GFP, RFP, YFP and simultaneous imaging of GFP and RFP were described previously (Zheng et al., 2004; Samalova et al., 2006; Teh and Moore, 2007). mCHERRY was excited with a 543nm helium-neon laser line and a HFT 458/543 primary dichroic mirror, and was detected with a 565-615nm band pass filter. Bimane was excited with a 405nm blue diode laser and a HFT 458/543 primary dichroic mirror, and was detected with a 475-525nm band pass filter. For simultaneous imaging of mCHERRY and bimane, multi-track line-sequential imaging mode with the configuration mentioned above was used. SNARF was excited with a 543nm helium-neon laser and a HFT458/543 primary dichoric mirror, and was detected with the META detector at 572-604nm and 625-647nm. Images were processed using Zeiss LSM Image Browser (Carl Zeiss Ltd., Welwyn Garden City, UK).

2.2.1.2 roGFP imaging and analysis

roGFP was excited with a 405nm blue diode laser and 488nm argon laser line in multi-track mode and a HFT 405/488/543 primary dichroic mirror. Fluorescence was collected with a 500-530nm band pass filter. Ratiometric analysis was performed using a custom MatLab (MathWorks, Cambridge, UK) software as described previously (Schwarzlander et al., 2008). In the time course experiment with c-roGFP1, the perfusion chamber, which was described previously (Schwarzlander et al., 2008), was connected to a Gilson Minipuls 2 peristaltic pump (Gilson Inc, Middleton, USA) with HPLC-tubing and was mounted on the confocal microscope.

2.2.1.3 Ratiometric construct imaging and analysis

Images were analyzed on Zeiss LSM Image Browser (Carl Zeiss Ltd., Welwyn Garden City, Herts, UK). For quantitative analysis of nlsRFP-2A-secGFP and nlsRFP-2A-GFP-HDEL, RFP intensities were measured by drawing regions of interest (ROI) within a nucleus, while GFP intensities were measured by drawing ROIs around a given cell. Background signals were measured on the vacuole. The data were analyzed on Microsoft Excel. After the GFP and RFP values were subtracted by the background and divided by the laser power, the corrected values were used to generate the GFP/RFP ratio, which represents the fluorescence intensity of GFP that is corrected for protein expression levels.

For secN-RFP-2A-GFP-HDEL, both RFP and GFP were measured on the nuclear envelope. Background signals were measured at the regions outside the sample in each image. The data were subsequently analyzed on Microsoft Excel. After the GFP and RFP values were subtracted by the background and divided by the laser power, the corrected values were used to generate RFP/GFP ratios.

2.2.1.4 Leica TCS SP5 II microscope configuration

Samples coexpressing GFP and YFP were examined using Leica TCS SP5 II with a HC Plan-Apochromat 25x/0.7NA water-immersion lens. Sequential scanning mode was used. GFP was first excited with the 458nm argon laser line and was detected with a PMT channel set to collect signal between 475 and 510nm. YFP was subsequently excited with the 514nm argon laser line and was detected with a second PMT channel set to collect signal between 572 and 613nm. Images were processed using LAS AF (Leica Microsystem (UK) Ltd., Milton Keynes, UK).

2.2.2 Fluorescent dye treatment

Seedlings were immersed in 5μM FM4-64 (Invitrogen Ltd, Paisley, UK; from 5mM stock in water) aqueous solution for 10min to label the plasma membrane and some endosomes, or 60min to label the tonoplast. For bimane labeling, seedlings were immersed in 100μM monochlorobimane (MCB) or monobromobimane (MBB) (Invitrogen Ltd, Paisley, UK; from 100mM stock in ethanol) aqueous solution. For apoplastic pH measurement using SNARF1-Dextran (Invitrogen Ltd, Paisley, UK; from 33mg/mL stock in water), seedlings were immersed in 500μg/mL and the dye was loaded into the cotyledons by vacuum infiltration.

2.2.3 Transmission Electron Microscopy

The sample preparation process was performed with the assistance of S. Rodgers (University of Oxford). 10-day-old seedlings were fixed in 2% (w/v) paraformaldehyde and 1% glutaraldehyde in 20mM K_2HPO_4 buffer (pH 7.0) for 3-5h at room temperature. Samples were washed with 50mM K_2HPO_4 solution before transferring to 2% (w/v) osmium tetroxide for 2h at room temperature. After washing with distilled water, the samples were dehydrated in an ethanol series and

embedded in Spurr's resin. The samples were sectioned with microtome and examined with a Hitachi H7650 transmission electron microscope (Hitachi High-Technologies Europe GmbH, Maidenhead, UK).

2.2.4 Transformation of plant

Arabidopsis Col-0 was transformed by the floral dipping method with *Agrobacterium tumefaciens* (Clough and Bent, 1998). An overnight culture (~50mL for 4-6 plants) of Agrobacteria containing the desired constructs was pelleted by centrifugation at 4500rpm for 10min at room temperature. The pellets were resuspended with 5% sucrose and 0.05% Silwet L-77 (Crompton Europe Ltd., Geneva, Switzerland) in a volume equal to that of the overnight culture. Floral tissues of 4 to 5-week-old *Arabidopsis* were dipped in the mixture for 15-20 seconds. The plants were then laid horizontally in tray on top of wet tissues and covered with cling film for 24h before they were returned to the growth cabinet. The plants were grown until senescence and were allowed to dry before seeds were harvested. The seeds were plated on MS growth medium with the antibiotics for respective constructs, as listed in Table 2.3, for selection.

2.2.5 Artificial pollination

The female flower buds from ~4-week-old *Arabidopsis* plants were prepared by removing their sepals, petals and stamens from unopened flower buds. Pollen grains were obtained by taking stamens of opened flowers and were brushed against the stigma of the female flower buds. Pollinated flowers were covered with cling film for two days. Seeds were harvested after the silique had been desiccated.

2.2.6 Transformation of bacteria

Competent *Escherichia coli* cells for transformation were prepared as described previously (Sambrook and Russell, 2001). *Escherichia coli* were transformed using the heat shock method (Bergmans et al., 1981), in which the cells were incubated with the plasmids at 0°C followed by heat shock at 42°C for 1min. After incubating in ice for 2min, SOC medium was added to the cells. After incubating at 37°C for 45min, the cells were plated on a LB agar plate with antibiotics for selection.

Agrobacterium tumafaciens was transformed by electroporation (Shen and Forde, 1989). 20μL of Agrobacteria cells and 1μL of plasmids were combined in an electroporation cuvette. Electroporation was done with a BioRad Gene Pulser (Hemel Hempstead, UK) connected to a 200Ω resistor. The voltage and capacitance were set to 2.5kV and 25μF, respectively. After the electroporation, LB was added to the cells immediately followed by 2h of incubation at 28°C. The cells were then plated on a LB agar plate with the antibiotics for the respective constructs (Table 2.3) for selection.

Table 2.3. Selection antibiotics for constructs used in this study

Construct	Selection Antibiotics in Bacteria	Selection Antibiotics in Plants	References
pVKH-P35S-secGFP	Kanamycin	Hygromycin	(Batoko et al., 2000)
pVKH-P35S-GFP-HDEL	Kanamycin	Hygromycin	(Batoko et al., 2000)
pVKH-P35S-secN-RFP_m-2A-GFP-HDEL	Kanamycin	Hygromycin	(Samalova et al., 2006)
pVKH-P35S-nlsRFP$_m$-2A-secGFP$_f$	Kanamycin	Hygromycin	(Samalova et al., 2006)
pVKH-P35S-nlsRFP$_m$-2A-GFP-HDEL	Kanamycin	Hygromycin	(Samalova et al., 2006)
pH2GW7-P35S-roGFP1	Spectinomycin	Hygromycin	(Schwarzlander et al., 2008)
pH2GW7-P35S-roGFP2	Spectinomycin	Hygromycin	(Schwarzlander et al., 2008)
pWEN22-P35S-roGFP2iLH148S-HDEL	Spectinomycin	Hygromycin	(A Meyer, personal communication)
P35S-RTNLB1-eYFP-Nos::pCAMBIA 1300	Kanamycin	Hygromycin	(Sparkes et al., 2010)
pGREEN0029-P35S-DER2-YFP	Kanamycin	Kanamycin	(L Frigerio, personal communication)
pNIGEL07-PUBQ10-YFP-VAMP711	Kanamycin and Ampicillin	Phosphinothricin (BASTA)	(Geldner et al., 2009)
pBIN20-P35S-mCHERRY-HDEL (ER-rk)	Kanamycin	Kanamycin	(Nelson et al., 2007)
pBIN20-P35S-ST-mCHERRY (G-rk)	Kanamycin	Kanamycin	(Nelson et al., 2007)
pBIN20-P35S-γTIP-mCHERRY (Vac-rk)	Kanamycin	Kanamycin	(Nelson et al., 2007)

2.2.7 DNA extraction from plants

Genomic DNA for routine PCR was isolated from 6 to 8-day-old *Arabidopsis* tissues according to Edwards et al. (1991) or the sucrose prep method (Berendzen et al., 2005). After DNA precipitation, DNA was resuspended in 20μL water. 1-2μL of DNA prepared from these two methods was used for PCR reaction.

For whole-genome sequencing, genomic DNA was extracted from the rosette leaves of 4-week-old plants with Qiagen DNeasy Plant Kit (West Sussex, UK) or Promega Wizard® Genomic DNA Purification Kit (Southampton, UK) according to manufacturers' instructions, followed by phenol-chloroform extraction (see Section 2.2.9.1).

2.2.8 Plasmid DNA extraction from bacteria

Plasmids were extracted from bacteria using an alkaline lysis miniprep protocol modified from Birnboin and Doly (1979). 1.5mL overnight culture was pelleted and washed with Solution I (50mM glucose, 25mM Tris and 10mM EDTA adjusted to pH 8 with hydrochloric acid). The pellet was resuspended in 200μL Solution I and 10μL of 10mg/mL lysozyme. After incubating on ice for 10min, 400μL Solution II (0.2M NaOH and 1% SDS) was added and incubated on ice for 10min or until clear. Next, 300μL of Solution III (3M KCH_3COO solution with pH adjusted to pH 4.8 with acetic acid) was added and incubated on ice for 5min. After centrifuging at 13 000rpm for 20min at 4°C, the DNA was precipitated from the supernatant with 0.7 volume of isopropanol (propan-2-ol). After centrifuging at 13 000rpm for 30min at 4°C, the pellet was washed with 70% ethanol and subsequently resuspended in 20-30μL water.

2.2.9 DNA Purification

2.2.9.1 Phenol-chloroform extraction

After DNA extraction, DNA was purified using phenol-chloroform extraction if high-quality DNA was desired. One volume of saturated phenol (pH 8) was added, vortexed and centrifuged at maximum speed for 1min. Then one volume of chloroform was added and centrifuged. The upper aqueous phase was transferred to another tube, combined with one volume of chloroform, mixed and centrifuged. Once again, the upper phase was removed to another tube after centrifugation. 0.1-0.3M NaCl and three volumes of ice-cold 100% ethanol were then added to precipitate the DNA. After leaving on ice for two to three hours, precipitated DNA was sedimented by centrifuging at maximum speed for 10min. The pellet was then washed with 70% ethanol, dried and resuspended in TE buffer (10mM Tris-HCl at pH 7.6 and 0.1mM EDTA).

2.2.9.2 Sodium acetate precipitation

DNA was precipitated by adding 1/10 of 3M sodium acetate solution (pH 5.2) and 2.5 volume of cold 100% ethanol. After incubating at room temperature for 15min, the sample was centrifuged at 13 000rpm for 20min at 16°C. The DNA pellet was then washed with 70% ethanol, dried, and resuspended in water or TE buffer (10mM Tris-HCl at pH 7.6 and 0.1mM EDTA).

2.2.10 Polymerase Chain Reaction

For routine polymerase chain reaction (PCR) reaction, 20-50μL reaction mixtures were set up according to manufacturers' instructions for DreamTaq DNA Polymerase (Fermentas, part of Thermo Fisher Scientific, Loughborough, UK) or Invitrogen Taq Polymerase (Invitrogen Ltd., Paisley, UK). For high fidelity PCR, Phusion High-Fidelity DNA Polymerase (New England Biolab,

Hitchin, UK) was used and the reaction mixture was set up according to manufacturer's instructions.

PCR took place in a Biometra T1 Thermocycler or T-Gradient thermocycler (Biometra GmbH, Goettingen, Germany). PCR programme included an initial heating step at ~95°C, then 28-35 cycles of denaturation, annealing and extension, followed by a final extension step at ~72°C. The annealing temperature and extension time were adjusted for the reaction.

If the PCR products were used for reactions downstream (e.g. sequencing or restriction digestion), the products were purified using QIAquick PCR Purification Kit (Qiagen, West Sussex, UK) according to manufacturer's instruction and the purified DNA was resuspended in water.

2.2.11 Restriction digest

Restriction digests were set up according to instructions from New England Biolabs or Fermentas. Typically, 10μL of PCR products or 2-5μL of miniprep plasmid were added to the 20μL mixture. The mixture was incubated at appropriate incubation temperature (usually 37°C or 60°C) for one hour followed by 20min of inactivation at 80°C on a thermal cycler.

2.2.12 Agarose gel electrophoresis

0.5x TBE was used as running buffer and for dissolving agarose. It was prepared by diluting 5x stock solution (55g Tris, 27.5g orthoboric acid and 3.72g EDTA in 1L H_2O at pH 8.0). 0.8-3.0% agarose gel was made by dissolving molecular grade agarose (Bioline, London, UK) or MetaPhor Agarose (Cambrex, Rockland, USA) in 0.5x TBE. After the agarose was dissolved by heating and cooled to ~50°C, 0.5μg/mL of ethidium bromide was added to the solution from a stock of 10g/L,

and poured into a gel tray. The gel was cooled and then mounted onto the gel electrophoresis unit with 0.5x TBE as running buffer.

To load DNA sample onto the gel, each sample was diluted to at least 10μL with water and mixed with 6x loading dye (0.25% w/v bromophenol blue and 30% v/v glycerol in water). 3-6μL of 1kB or 100bp DNA ladders (Fermentas) were loaded as markers. The gel was run at 360-480V/m on Horizon 11.14 Gel Electrophoresis Equipment (Life Technologies, Paisley, UK) and was visualized with a UV trans-illuminator.

2.2.13 Sanger sequencing reaction

Sanger sequencing was done using Applied Biosystem 3730xl DNA Analyzer (part of Life Technologies, Paisley, UK) in Department of Zoology, University of Oxford. The 10μL reaction mixture consisted of 5x Big Dye sequencing buffer (Applied Biosystem, part of Life Technologies Corp, Carlsbad, USA), 2.5x ready reaction mix, 3.2pmol of primer and 5-20ng of purified PCR product (500-1000bp). The sequencing PCR programme started with heating the mixture at 96°C for 2min, then 25 cycles of 96°C for 30s, 50°C for 15s and 60°C for 4min. Following the PCR, samples were precipitated by sodium acetate precipitation (Section 2.2.9.2) and submitted to the sequencing facility in dried form. The sequence output file was viewed and analyzed using MacVector 11.1.2 (MacVector Inc, Cambridge, UK).

2.2.14 Protein extraction from plants

Proteins of 7 to 10-day-old whole seedlings were extracted by homogenization in two volumes of extraction buffer: 4% SDS (w/v), 100mM Tris-HCl (pH 6.8), 400μg/mL bromophenol blue, 200mM DTT, 20% glycerol, 0.2% β-mercaptoethanol and 1μL of plant protease inhibitor cocktail solution

(Sigma-Aldrich, Poole, UK). Samples were then boiled for 10min followed by centrifugation at 10 000*g* for 5min. The supernatant containing the extracted proteins was then transferred to a new tube.

2.2.15 Immunoblot analysis

Proteins were separated by SDS-PAGE (4% stacking gel and 14% separating gel) and were blotted onto a polyvinylidene fluoride (PVDF) membrane as described previously (Batoko *et al.*, 2000). Before incubating with primary antibody, the blot was stained with Ponceau S solution: 0.5% Ponceau S and 1% acetic acid for 5min and subsequently washed with 1% acetic acid. An image of the blot was taken with a Nikon D700 camera (Nikon UK Ltd, Kingston upon Thames, UK) before being completely destained with 1% acetic acid. The blot was incubated with primary antibodies at appropriate concentration (Table 2.2), followed by incubation with alkaline phosphatase-conjugated secondary antibodies (anti-rabbit IgG) (Sigma-Aldrich, Poole, UK), which was used at 1:10 000 dilution. The alkaline phosphatase was then developed by adding Western Blue® Stabilized Substrate for Alkaline Phosphatase (Promega, Madison, USA). Once the bands were observed, the blot was washed with water and with 20mM EDTA solution (pH 8) to stop the reaction.

Chapter 3 Characterization of novel *GSH2* mutant alleles

3.1 Chapter Summary

G4, N37, S6 and S10 were identified as putative seedling-lethal secretory mutants. Despite the differences in their developmental phenotypes, they all accumulated secGFP in large spherical bodies, and for this reason they were studied collectively. Indeed, all of the mutations were mapped to the *GSH2* locus and therefore were renamed *gsh2-3* to *gsh2-6*. *GSH2* encodes GSH synthase, which synthesizes a ubiquitous tripeptide- glutathione. Previous studies have shown that the ER-derived spherical bodies accumulated membrane proteins targeted to the PM and the tonoplast. Here, the spherical bodies were further characterized by confocal fluorescence imaging of several ER-localized fluorescent protein markers and electron microscopy. Since glutathione is important in cellular redox reactions, some redox-related processes that utilize glutathione were also assessed in the mutants.

3.2 Introduction

3.2.1 Physiological significance of glutathione

Glutathione (GSH) is a tripeptide composed of glutamate, cysteine and glycine and is the most abundant small thiol molecule in a cell with cytosolic concentration of 2-3mM in plant cells (Meyer et al., 2001). Glutathione serves a diverse range of cellular functions and processes including cell division (Vernoux et al., 2000), heavy metal detoxification (Cobbett et al., 1998) and environmental stress responses (Foyer and Noctor, 2011). Most importantly, glutathione plays a major role in redox reactions and has been associated with redox state maintenance, oxidative stress signaling and disulfide bond regulation in the ER (Noctor et al., 2000; Chakravarthi et al., 2006; Meyer, 2008). It can exist either in reduced (GSH) or oxidized form (GSSG) (Banhegyi et al., 2007; Meyer, 2008). The thiol group in cysteine allows glutathione to form a disulfide bond with

either another glutathione molecule or proteins containing accessible thiols. GSSG can be reduced to GSH by GSH reductase that transfers electrons from NADPH to glutathione. Different compartments of a eukaryotic cell may have different GSSG:GSH ratios. For instance, the GSSG:GSH ratios in the *Arabidopsis* ER lumen and cytosol are ~1:3 and ~1:100, respectively (Cairns et al., 2006). A glutathione molecule oscillates between the reduced and the oxidized form to resist any changes in cellular oxidation state. When reactive oxygen species (ROS) such as hydrogen peroxide (H_2O_2) and lipid peroxide are present, glutathione peroxidase (GPOX) transfers electrons from GSH to the peroxides, thereby relieving oxidative stress (Dixon et al., 1998). Glutathione can also couple with ascorbate to establish the glutathione-ascorbate cycle, which is important in cellular ROS detoxification and redox signal transmission (Meyer, 2008). Furthermore, glutathione is capable of reducing proteins directly so that proteins like oxidoreductases are maintained in the reduced state (Jessop and Bulleid, 2004). Hence, glutathione is involved in many cellular pathways and is indispensable for cellular redox homeostasis and signalling.

3.2.2 Glutathione biosynthesis pathway

Glutathione biosynthesis is a two-step process that first combines glutamate and cysteine to form gamma-glutamylcysteine (γ-EC), followed by the addition of glycine to γ-EC to form glutathione (GSH). These two steps require ATP hydrolysis and are catalyzed by γ-EC ligase (GSH1) and GSH synthase (GSH2), respectively (Figure 3.1).

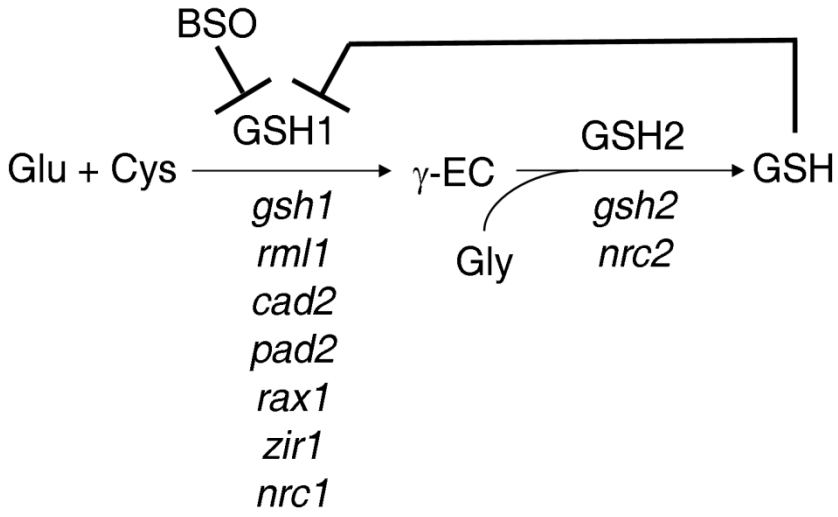

Figure 3.1. Schematic diagram of the glutathione biosynthesis pathway

γ-EC ligase (GSH1) converts glutamate and cystein into γ-EC, then GSH synthase (GSH2) converts γ-EC to GSH, which can in turn feed back on GSH1. BSO is a reversible inhibitor of GSH1. *gsh1, rml1, cad2, pad2, rax1, zir1* and *nrc1* are mutant alleles of *GSH1*, *gsh2* and *nrc2* are mutant alleles of *GSH2*.

In *Arabidopsis*, GSH1 is localized exclusively in the plastids and GSH2 in both the plastids and the cytosol (Wachter et al., 2005). Given that glutathione feeds back on GSH1 to inhibit glutathione biosynthesis (Hell and Bergmann, 1990) and cytosolic GSH2 is sufficient for normal plant development (Pasternak et al., 2008), it is likely that transport mechanisms exist that permit movement of γ-EC from the plastids to cytosol and GSH from cytosol to plastids. Genetic analysis suggests that in *Arabidopsis* γ-EC and glutathione are transported from plastids to the cytosol by chloroquine resistance transporter-like transporters (CLT1-3) (Maughan et al., 2010).

3.2.3 Mutants that affect the glutathione biosynthesis pathway

Several mutants of *GSH1* and *GSH2* in *Arabidopsis* have been characterized previously. Work on various mutants of GSH1 has revealed the role of glutathione in heavy metal tolerance (Cobbett et al., 1998; Jobe et al., 2012; Shanmugam et al., 2012), photo-oxidative stress response (Ball et al., 2004), disease resistance (Parisy et al., 2006) and postembryonic root growth (Vernoux et al.,

2000). A *gsh1* null mutant was described and shown to exhibit an embryo-lethal phenotype (Cairns et al., 2006). In all *GSH1* mutants, the level of γ-EC and GSH were reduced, but the level of cysteine was higher than in the WT (Cobbett et al., 1998; Vernoux et al., 2000; Cairns et al., 2006; Parisy et al., 2007; Jobe et al., 2012; Shanmugam et al., 2012). The presence of GSH in homozygous *gsh1* mutant embryos that lack *GSH1* expression suggests that maternal tissues supply the embryo with a low level of GSH that is however insufficient for normal growth (Cairns et al., 2006). In contrast, *gsh2* insertion mutants exhibited a seedling-lethal rather than embryo-lethal phenotype in *Arabidopsis* (Pasternak et al., 2008). Hyperaccumulation of γ-EC was observed in loss-of-function *GSH2* mutant alleles (Pasternak et al., 2008; Jobe et al., 2012).

3.2.4 Knowledge of G4, N37, S6 and S10 prior to this study (Work from H Neto and J Perez-Gomez)

G4, N37, S6 and S10 were isolated as seedling-lethal biosynthetic membrane trafficking mutants by H. Neto and J. Perez-Gomez in the Moore laboratory. G4 was isolated from a line expressing ST-RFP-2A-secGFP, N37 from a line expressing nlsRFP-2A-secGFP, and S6 and S10 from the original secGFP line (Zheng et al., 2004; Samalova et al., 2006). These four mutants showed different degrees of developmental impairment after seven days of growth (Figure 3.2a). G4 and S10 terminated growth soon after germination; N37 had severely reduced root growth and died within three weeks; S6 was similar to the WT in morphology but was always smaller in size. It was later revealed that homozygous S6 was viable but produced many fewer seeds than the WT (data not shown). Despite such variation in developmental phenotypes, analysis with confocal fluorescence microscopy revealed that all four mutants accumulated secGFP in characteristic swollen bodies that were 5-10μm in diameter (Figure 3.2b).

To investigate the localization of secGFP and the trafficking pattern of different organelle markers, H Neto and J Perez-Gomez expressed various fluorescent protein-tagged markers of the endomembrane system in N37. An ER lumen marker (GFP-HDEL) (Boevink et al., 1998; Crofts et al., 1999), which localized to the lumen of tubular fusiform bodies and ER network in the WT, was observed exclusively in the swollen bodies of N37 (Figure 3.3a and b). Tonoplast (BobTIP-GFP) (Reisen et al., 2003) and plasma membrane marker proteins (PIP-GFP) (Cutler et al., 2000) were trapped on the membrane of swollen bodies in N37 (Figure 3.3c to f). FM4-64, a lipophilic styryl dye (Ueda et al., 2001; Bolte et al., 2004; Dettmer et al., 2006), was endocytosed into the tonoplast of WT and N37, and did not completely colocalize with BobTIP-GFP (Figure 3.7a). Hence, it appears that the endocytic pathway was unperturbed in the mutant and the swollen bodies were distinct from the vacuole. Furthermore, the trafficking of Golgi (ST-RFP) (Batoko et al., 2000) and TGN markers (VHA-a1:GFP) (Dettmer et al., 2006) and the morphology of these compartments observed under confocal fluorescence microscopy appeared unaffected in the mutants (Figure 3.3g to j), suggesting that the secretory pathway was not completely disrupted.

Genetic complementation and subsequent sequencing showed that all mutations resided in the *GSH2* locus (At5g27380) which encodes GSH2 (Figure 3.4a). Each mutant carries a single base-pair substitution that results in either a non-sense mutation W130Stop in S10 (*gsh2-3*), or a missense mutation G434E in G4 (*gsh2-4*), P364S in N37 (*gsh2-5*) and G94E in S6 (*gsh2-6*) (Figure 3.4a). Sequence alignment of the *Arabidopsis* GSH2 sequence with that of human and yeast (*Saccharomyces cerevisiae*) revealed that *gsh2-4*, *gsh2-5* and *gsh2-6* result in changes in conserved amino acid residues (Figure 3.4b). With S10 and G4 considered as the stronger, and N37 and S6 as the weaker mutant alleles, the mutants were renamed *gsh2-3* to *gsh2-6* in decreasing order of severity of the developmental phenotype (Figure 3.2a).

The work presented in this chapter aims to investigate how a loss-of-function mutation in a glutathione biosynthetic enzyme affects ER morphology and the secretory pathway in a cell. First, the intracellular secGFP accumulation was validated by western blot analysis. Then the ER morphology was analyzed extensively with light microscopy and electron microscopy. Next, the effects of varying level of glutathione and its precursor, γ-EC, on ER morphology, growth and cellular redox state were explored.

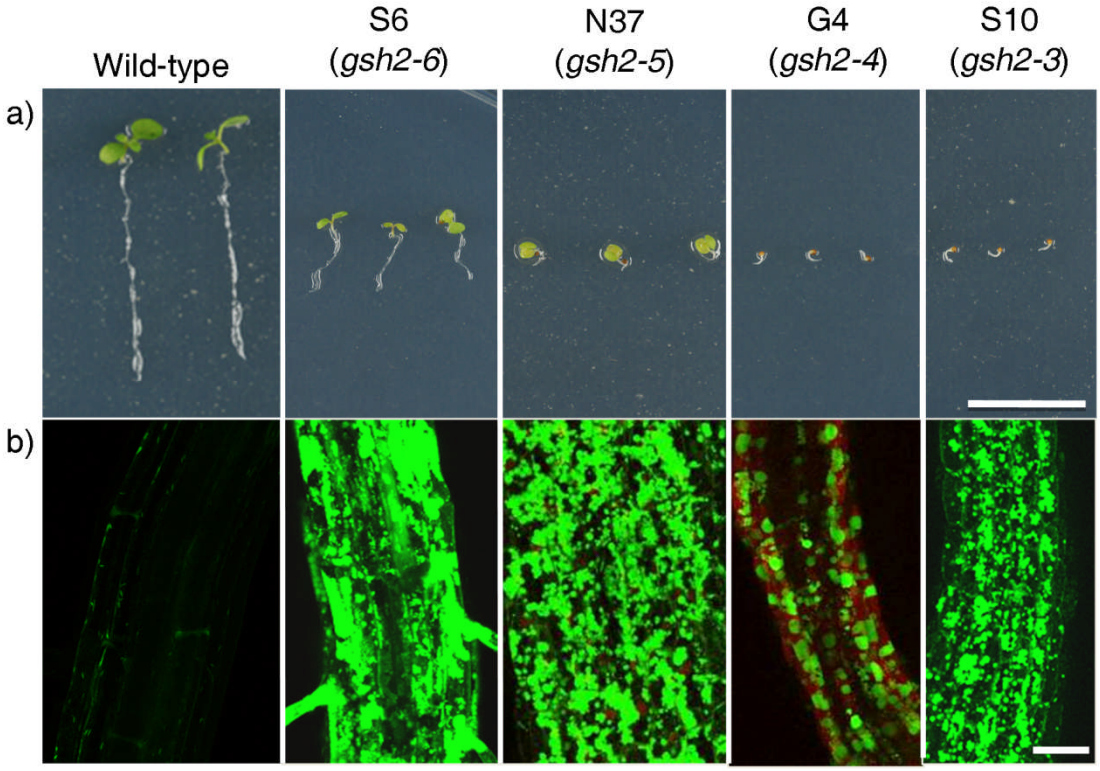

Figure 3.2. Four putative membrane trafficking mutants with similar phenotype were identified in the secGFP seedling-lethal mutant screen

a) Bright-field images of 7-day old wild type secGFP line (S76), S6, N37, G4 and S10 whole seedlings.

b) Confocal images of wild type (S76), S6, N37, G4 and S10 epidermal root cells. Green colour represents secGFP; red colour in G4 represents Golgi marker (ST-RFP).

Bar=1cm in (a) and 50μm in (b).

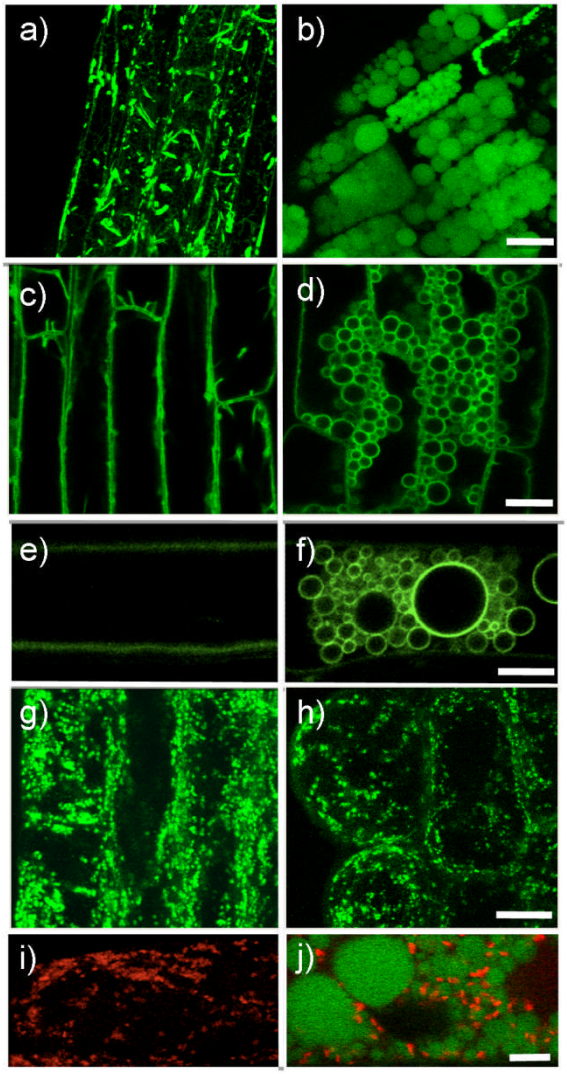

Figure 3.3. ER, tonoplast, PM markers were accumulated in swollen bodies in *gsh2*

a) to h) Epidermal root cells of six-day-old WT (a, c, e and g) and N37 (*gsh2-5)* (b, d, f, and h) seedlings expressing ER marker (GFP-HDEL) (a and b), tonoplast marker (BobTIP-GFP) (c and d), PM marker (PIP-GFP) (e and f) and TGN marker (VHA-a1:GFP) (g and h).

i) and j) Six-day-old WT (i) and G4 (*gsh2-4)* (j) seedlings expressing ST-RFP-2A-secGFP. ST-RFP and secGFP were represented in red and green, respectively.

Images from H Neto and J Perez-Gomez

Bar=20μm in (b), (d) and (h); 10μm in (f) and 5μm in (j).

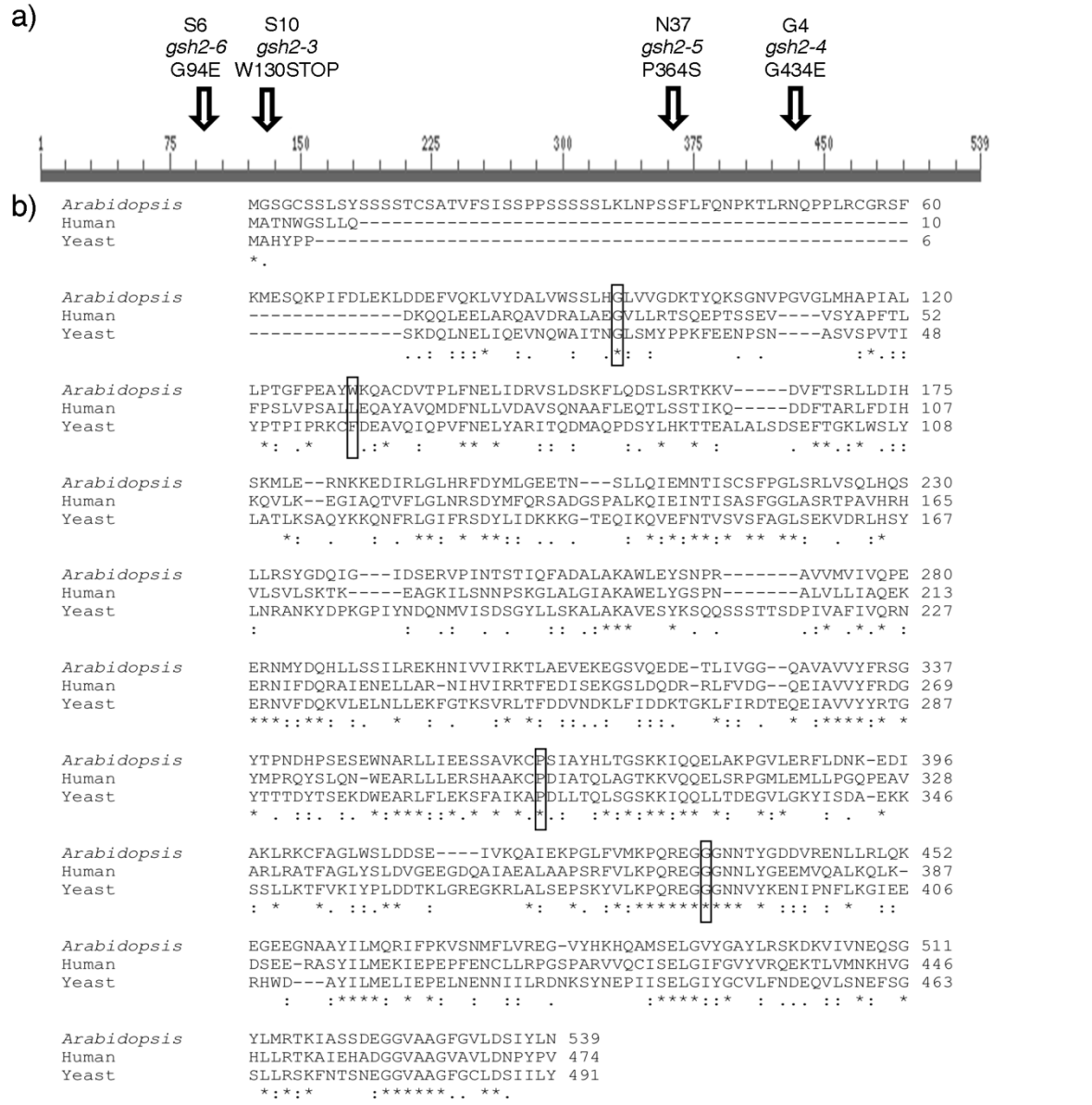

Figure 3.4. S10, G4, N37 and S6 were all mapped to the *GSH2* locus (At5g27380)

a) Location in the *GSH2* locus of the mutation in each allele (numbering refers to codons). S10, G4, N37 and S6 were renamed to *gsh2-3*, *gsh2-4*, *gsh2-5* and *gsh2-6*, respectively.

b) Alignment of GSH synthase protein sequence of *Arabidopsis*, human (*Homo sapiens*) and yeast (*Saccharomyces cerevisia*e) using ClustalW. Mutations of G4, N37, S6 and S10 were boxed. Symbols below the sequences denote the degree of conservation. Asterisks (*) indicate identical residues; semi-colon (:) and period (.) indicate conserved and semi-conserved substitutions, respectively.

3.3 Results

3.3.1 Genotyping markers for the novel *GSH2* mutant alleles

PCR markers were designed to distinguish each mutant allele to facilitate the genotyping process (Table 3.1). These genotyping markers were especially useful in distinguishing between heterozygous and WT plants, and confirming genotypes. Since the point mutation in *gsh2-5* created an *XhoI* restriction site, a cleaved amplified polymorphism sequence (CAPS) was created by designing a pair of primers to amplify the mutation by PCR. Following an *XhoI* restriction digest, the *gsh2-5* allele exhibited a unique band pattern (Table 3.1). For *gsh2-3, gsh2-4* and *gsh2-6*, because their point mutations did not generate any polymorphic restriction sites, mismatches were introduced in the PCR primers to form an artificial *XmnI* restriction site for each point mutation. Following an *XmnI* restriction digest, the PCR products that correspond to the mutant alleles were digested to generate a unique band pattern (Table 3.1).

Table 3.1. Genotyping markers for novel *GSH2* mutant alleles

Mutant	Forward Primer	Reverse Primer*	Restriction Enzyme	WT Fragments (bp)**	Mutant Fragments (bp)**
G4 (*gsh2-4*)	GCTTACCATTTAA CTGGCTCCA	GATATTGGGGGACTCA ATTGGGTGAAAAC	*XmnI*	314	28, 286
N37 (*gsh2-5*)	TGTACGATCAAC ATTTGCTGAG	GCCTGCTTGACAATTT CTGAG	*XhoI*	177, 584	67, 177, 517
S6 (*gsh2-6*)	GTGGCTGCTCTT CTCTCTCTTACTC	CTGATTTCTGATAACTT TTGTCACCAAGAACGA G	*XmnI*	309	32, 277
S10 (*gsh2-3*)	CTTGCCCACCACT AAAGTTCC	CATTGAAAAGAGGAG TAACATTACAAGAATG CTT	*XmnI*	330	31, 299

* Red letters represent mismatches between the primer and the template to create a restriction site on the mutant allele

** Expected fragment sizes after restriction digestion of PCR products

3.3.2 secGFP immunoblot analysis

Since secGFP is found in a truncated form in the apoplast or in the lytic vacuole (Tamura et al., 2003; Zheng et al., 2004), secGFP that localizes intracellularly along the secretory pathway is expected to be in the full-length form. To assess the intracellular accumulation of secGFP, whole seedling protein extracts from the WT and the mutants were analyzed on an immunoblot with anti-GFP antibodies. The secGFP protein was present in both full-length and truncated form in the WT, with the latter form being slightly more abundant (Figure 3.5). In contrast, the full-length secGFP was predominant in both *gsh2-5* and *gsh2-6*, consistent with the intracellular localization of secGFP previously observed by confocal microscopy. secGFP secretion appeared to be less inhibited in *gsh2-6* than in *gsh2-5* as more of the truncated form was present in *gsh2-6*.

3.3.3 Identity of swollen bodies in *gsh2*

Since tonoplast and PM markers were localized in the bodies with the ER lumen marker GFP-HDEL, these bodies were hypothesized to be ER-derived structures. To confirm that these structures were indeed ER-derived, an ER membrane marker, DER2-YFP (L Frigerio, unpublished data), was coexpressed with GFP-HDEL. In the WT, the ER network was labelled by both DER2-YFP and GFP-HDEL (Figure 3.6a and b). In *gsh2-5*, both markers labelled the swollen bodies with GFP-HDEL in the lumen and DER2-YFP in the perimeter (Figure 3.6c and d). In addition, DER2-YFP was seen to occasionally label the ER network (Figure 3.6d), thereby proving the presence of a residual ER network in *gsh2-5*.

Previous experiments with FM4-64 have shown that the endocytic pathway was unperturbed in *gsh2-5* and that the tonoplast was distinct from the swollen bodies that were labelled by BobTIP-GFP (Figure 3.7a) (H Neto, J Perez-Gomez, I Moore, unpublished data). To test this further, the

vacuolar lumen was labelled using monochlorobimane (MCB), which becomes fluorescent and membrane-impermeant only after it conjugates to reduced glutathione in the cytosol. The conjugated product, glutathione-S-bimane (GSB), is then actively transported to the vacuole (Fricker et al., 2000). In *gsh2-5*, GSB accumulated in the vacuole but did not colocalize with an ER lumen marker (mCHERRY-HDEL) (Nelson et al., 2007) in swollen bodies (Figure 3.7b and c). Hence, I concluded that the swollen bodies were distinct from the vacuoles.

Transmission electron microscopy revealed that swollen bodies in the epidermal cells at the root tips of *gsh2*-3 and *gsh2-6* were surrounded by electron-dense structures that resembled ribosomes (Figure 3.8). The ER tubules were dilated in younger cells of *gsh2-6* compared to the WT (Figure 3.8g). Similar structures were also observed with confocal microscopy (Figure 3.8h to j). These findings suggest that ER morphology is perturbed in *gsh2* mutants and the swollen bodies are indeed derived from the ER.

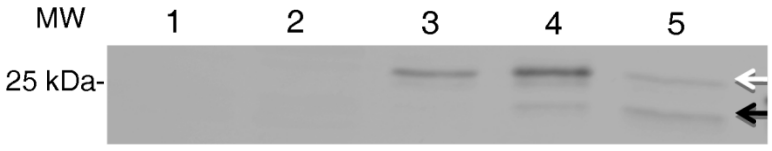

Lane 1. Col-0
2. *gsh2-5* (N37) WT segregant
3. *gsh2-5* (N37) mutant segregant
4. *gsh2-6* (S6) mutant segregant
5. secGFP (S76)

Figure 3.5. *gsh2* accumulated the truncated form of secGFP

Anti-GFP immunoblot analysis of proteins extracted from seven-day-old seedlings. *gsh2-5* (N37; lane 3) and *gsh2-6* (S6*;* lane 4) had substantially higher proportion of full-length secGFP than in the WT (lane 5). Molecular weight marker is indicated on the left. White arrow- full-length secGFP; black arrow- truncated secGFP.

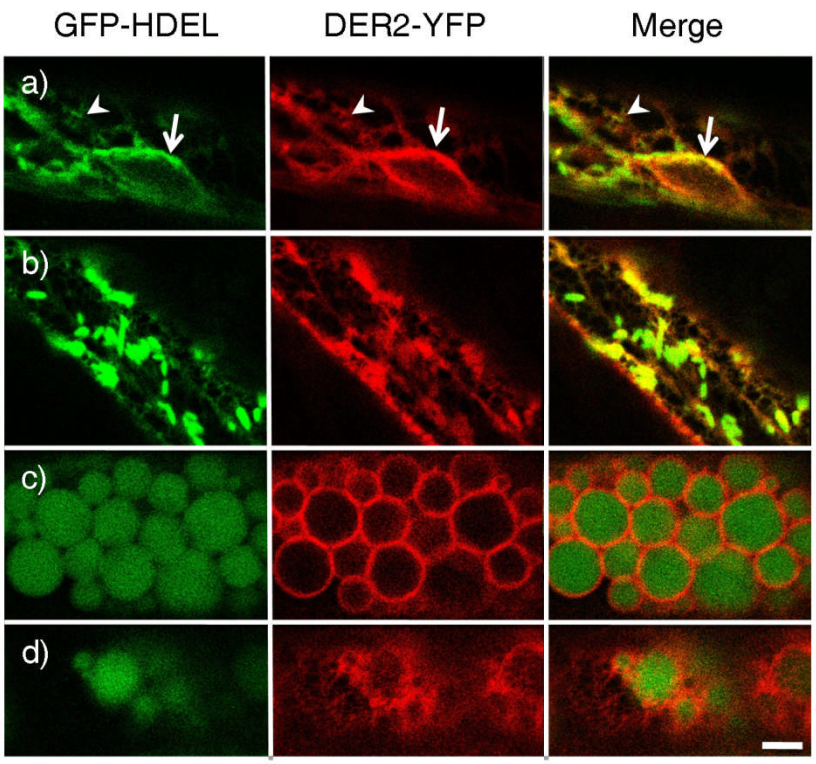

Figure 3.6. GFP-HDEL and DER2-YFP labelled the same compartments in WT and *gsh2-5*

a) and b) Epidermal root cells of WT. GFP-HDEL and DER2-YFP colocalized at nuclear envelope (arrow) and mesh-like ER network (arrowhead) (a). In addition. GFP-HDEL labeled tubular fusiform bodies (b).

c) and d) Epidermal root cells of *gsh2-5*. Both GFP-HDEL and DER2-YFP localized in the lumen and membrane of swollen bodies, respectively (c). DER2-YFP also labeled the residual ER network (d).

Bar=5μm.

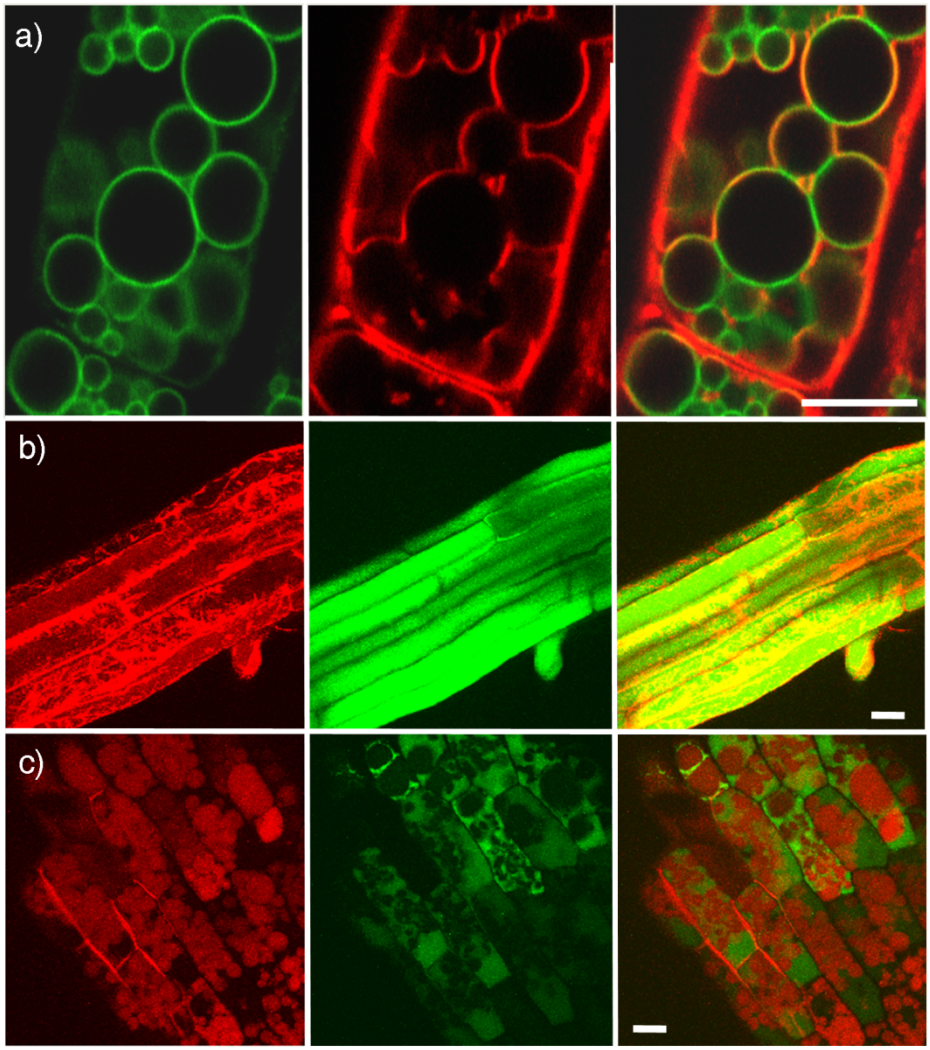

Figure 3.7. Swollen bodies are distinct from vacuoles

a) Epidermal root cell of a *gsh2-5* seedling expressing BobTIP-GFP (green) was stained with FM4-64 (red) for 60min.

b) and c) WT (b) and *gsh2-5* (c) expressing mCHERRY-HDEL (red) were incubated in 100μM MCB for 15min. Bimane became fluorescent after it was conjugated to thiols (green).

Bar=5μm (a) and 20μm in (b) and (c).

Image (a) from H Neto and J Perez-Gomez.

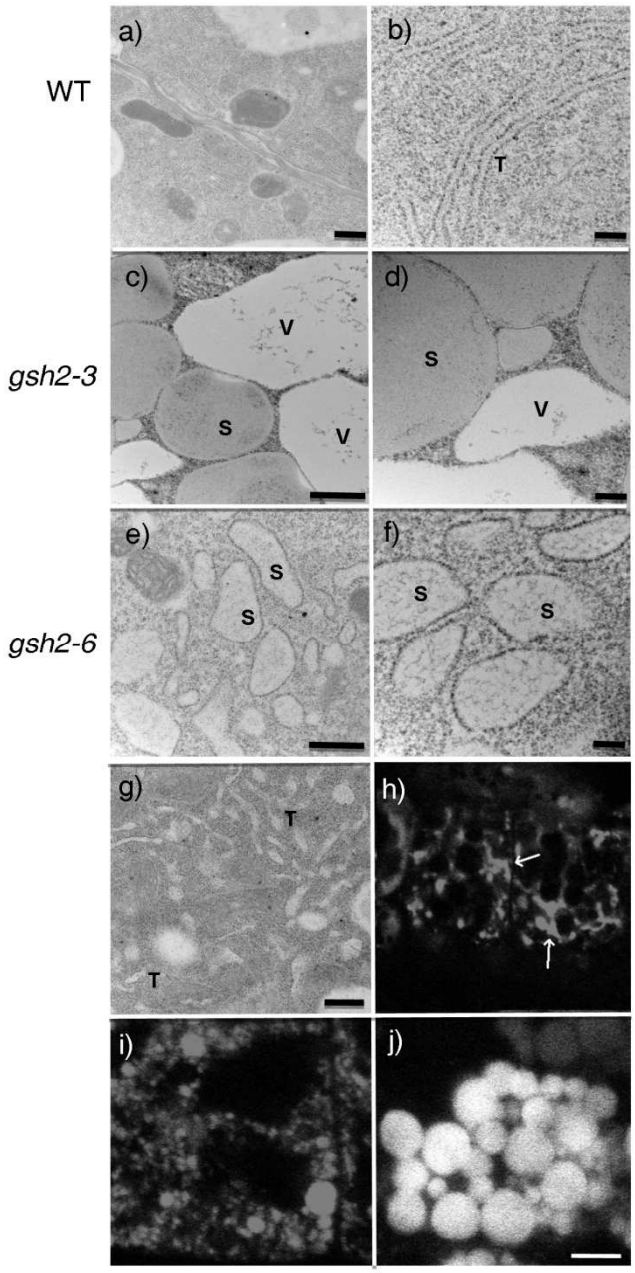

Figure 3.8. Electron microscopy (EM) revealed that *gsh2* swollen bodies are surrounded by ribosomes.

Images of epidermal root cells of 7-day-old seedlings

a) and b) EM images of WT cells showing tubular ER and absence of swollen bodies.

c) to f) Swollen bodies are present in *gsh2-3* (c and d) and *gsh2-6* (e and f). The swollen bodies are surrounded by ribosomes as indicated by the black dots around the swollen bodies. g) Some younger cells of *gsh2-6* had dilated ER tubules.

h) to j) Confocal images of epidermal cells in the root tip region of *gsh2-6* (h and i) and *gsh2-3* (j) expressing secGFP. The apparently dilated tubules are indicated by arrows in (h)

T=tubular ER, S=swollen bodies, V=vacuole. Bar=500nm in (a), (c), (e) and (g); 100nm in (b), (d) and (f); 5μm in (j)

3.3.4 Effect of *GSH2* mutations on cytosolic γ-EC and GSH level

To examine whether glutathione biosynthesis was affected by the *GSH2* mutations, the content of cytosolic γ-EC and GSH in 10-day-old seedlings of *gsh2* alleles was measured by C Müller and A Meyer (University of Heidelberg). *gsh2-1* and *rml1* were also included in this analysis, which are a null T-DNA insertion allele of *GSH2* (Pasternak et al., 2008) and a hypomorphic *GSH1* allele (Vernoux et al., 2000), respectively. While the level of GSH was much higher than that of γ-EC in the WT, γ-EC was the predominant low-molecular thiol molecule in all *gsh2* mutants (Figure 3.9a). Among the *gsh2* mutants, *gsh2-3*, *gsh2-4* and the null T-DNA insertion allele showed the greatest degree of γ-EC hyperaccumulation and GSH deficiency. The γ-EC content in these mutants was about 400-fold greater than in WT and GSH was undetectable, suggesting that there is little or no GSH2 activity. γ-EC hyperaccumulation was also observed in *gsh2-5* and *gsh2-6*, though to a less extent (170-fold greater than in the WT), and GSH content was 26% and 33% of WT level, respectively. These results confirmed that all the new *gsh2* alleles caused a reduction in GSH2 activity, thereby increasing the content of its substrate γ-EC and decreasing the content of its product GSH.

To visualize the low-molecular weight thiol molecules in swollen bodies, roots were stained with monobromobimane (MBB) and monochlorobimane (MCB). Unlike MCB which preferentially labels reduced glutathione through an enzymatic reaction (Meyer et al., 2001), MBB labels small thiols non-specifically (Fahey et al., 1981). As the analysis of low-molecular weight thiols of *gsh2* had revealed that γ-EC replaced GSH as the most abundant small thiol molecule, MBB was expected to mostly label γ-EC. As bimane becomes fluorescent and membrane-impermeant after it is conjugated to a thiol molecule, the γ-EC-bimane adduct should be trapped in the membrane-

bound swollen bodies. Indeed, higher bimane fluorescence was detected in swollen bodies of *gsh2-5* root cells after MBB labeling compared to MCB labeling (Figure 3.9b and c), suggesting that swollen bodies contained particularly high quantities of γ-EC.

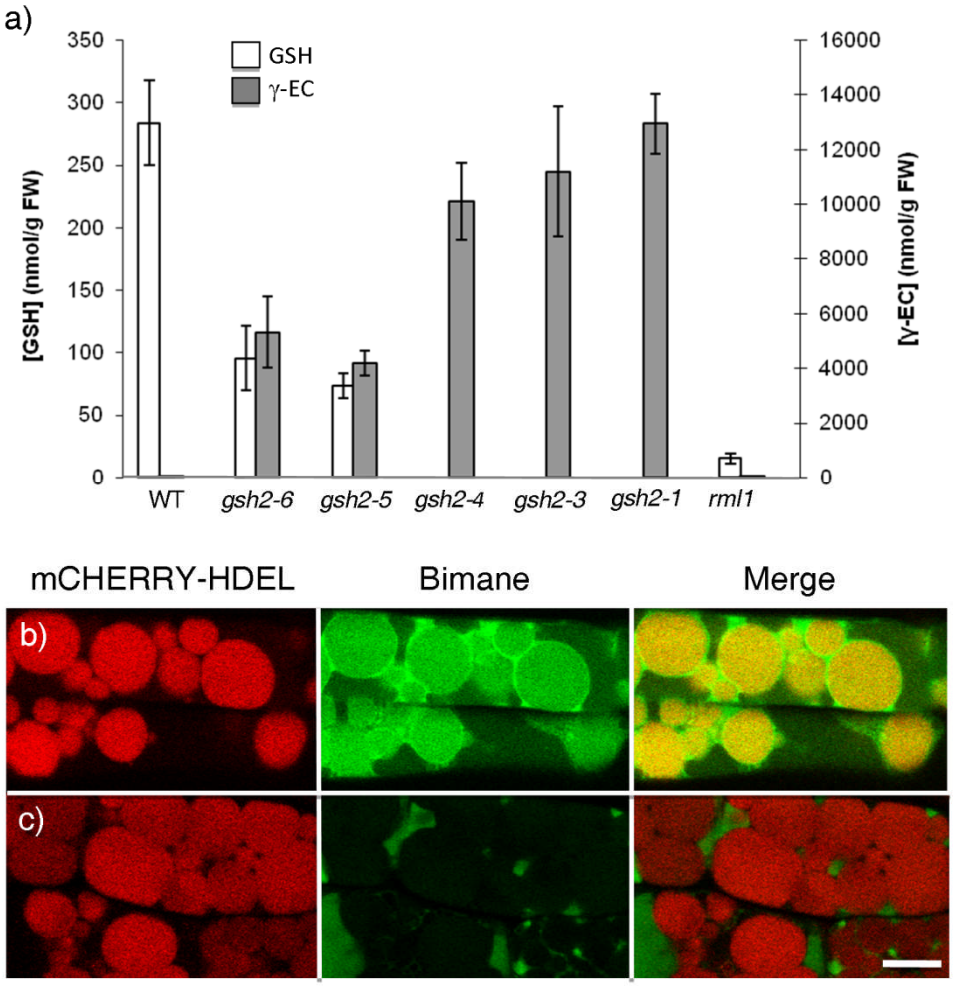

Figure 3.9. Low-molecular thiol profile of *GSH2* mutant alleles

a) Low-molecular weight thiol analysis of WT, *gsh2* and *rml1*. GSH and γ-EC are represented by white and grey bars, respectively. Data from C Müller and A Meyer.

b and c) MBB and MCB labelling of low-molecular weight thiols suggested that γ-EC are in the swollen bodies in epidermal root cells. Six-day old *gsh2-5* seedlings expressing mCHERRY-HDEL were incubated with 100μM MBB (b) or 100μM MCB (c) for 1h. Bimane signal is present in swollen bodies with MBB labelling but not with MCB labelling.

Bar=10μm.

3.3.5 Effect of *GSH2* mutations cellular redox state

Although glutathione is associated with a variety of cellular functions, it is primarily known for its role in redox homeostasis by reversible formation of disulfide bridges (Jessop and Bulleid, 2004; Meyer, 2008). To assess the cellular redox state, a GFP-derived ratiometric redox-sensitive transgenic construct, roGFP, was used to measure the gluathione redox potential of cotyledon epidermis cells *in vivo* by confocal fluorescence imaging (Schwarzlander et al., 2008; Marty et al., 2009). The redox sensitivity of the probe is based on the formation or disruption of the disulfide bridge linking its engineered cysteine residues, which in turn changes the fluorophore's conformation and ultimately the spectroscopic properties. First, cytosolic roGFP1 (c-roGFP1) was expressed in *rml1*, *gsh2-5* and WT. The probe was fully reduced in both the WT and *gsh2-5*, but significantly more oxidized in *rml1* ($P<0.01$) (Figure 3.10a) at steady state. To evaluate the redox buffer capacity, *gsh2-5* and WT seedlings were perfused in half-strength MS medium in a time-course experiment. Compared to the WT, the glutathione redox potential of *gsh2-5* was highly variable under steady state conditions. Upon challenge with 10mM H_2O_2, both the WT and mutant showed full oxidation of roGFP. Washout of H_2O_2 resulted in full recovery of the highly reducing redox potential in the WT after 15-20min, while the mutant remained significantly more oxidized ($P<0.01$). It thus appeared that *gsh2-5* had a weaker redox buffer capacity than WT (Figure 3.10b and c).

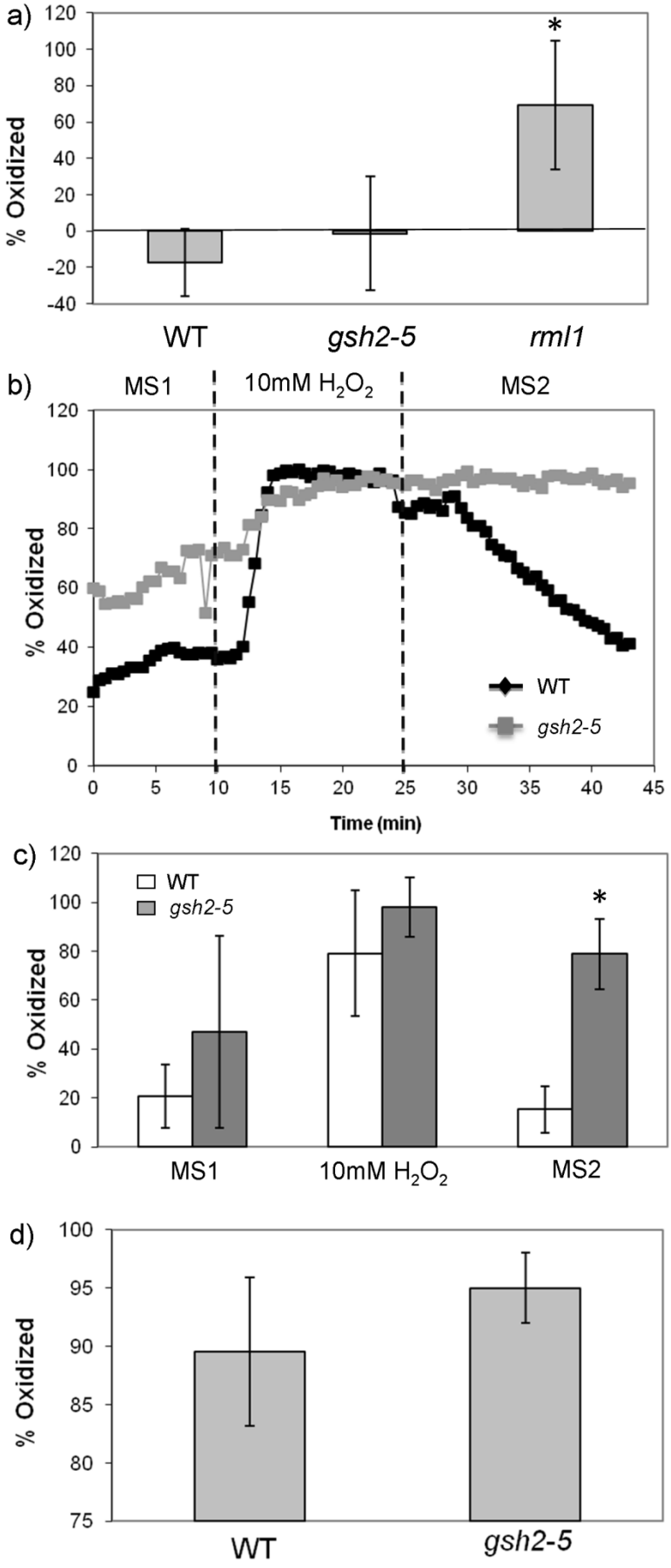
a)
% Oxidized
120
100
80
60
40
20
0
-20
-40
*
WT
gsh2-5
rml1
b)
MS1
10mM H_2O_2
MS2
% Oxidized
120
100
80
60
40
20
0
0
5
10
15
20
25
30
35
40
45
Time (min)
WT
gsh2-5
c)
% Oxidized
120
100
80
60
40
20
0
WT
gsh2-5
*
MS1
10mM H_2O_2
MS2
d)
% Oxidized
100
95
90
85
80
75
WT
gsh2-5

Since I hypothesized that changes in glutathione level may affect the redox state in the ER as well as in the cytosol, I attempted to measure the glutathione redox potential in the ER. Because the ER is notorious for its oxidizing environment, an ER-localized modified roGFP with a relatively oxidized midpoint potential (ER-roGFP2iL) (Lohman and Remington, 2008; I Aller, A Meyer, unpublished data) was expressed in *gsh2-5* and WT plants. Although ER-roGFP2iL was slightly more oxidized in *gsh2-5*, the difference between the two genotypes was not statistically significant (Figure 3.10d). Since the probe was almost fully oxidized in both genotypes, the measurement may not truly reflect the redox state in the ER. A probe with an even more oxidized midpoint potential is likely to provide a more accurate measurement.

Figure 3.10. *gsh2* redox state in the ER and cytosol

a) *rml1* has a more oxidized cytosol than WT and *gsh2-5*. Cytosolic glutathione redox potential was measured in WT, *gsh2-5* and *rml1* by expressing cytosolic roGFP (c-roGFP1). c-roGFP1 were fully reduced in both WT and *gsh2-5*; *rml1* cytosol is significantly more oxidized than WT (Asterisk, $P<0.01$). Each bar represents data from 10 seedlings.

b) Representative time-course traces showing the dynamic response of glutathione redox potential in WT (black) and *gsh2-5* (grey) seedlings to transient oxidation. Samples were first perfused in half-strength MS (MS1) for 10min, then in medium containing 10mM H_2O_2 (10mM H_2O_2) for 15min, followed by half-strength MS (MS2) for 20min.

c) Based on the time-course in (b), average glutathione redox potential in WT (white) and *gsh2-5* (grey) was measured after each perfusion step as shown in (b). Asterisks indicate the value that is significantly different from WT under the same treatment ($P<0.01$).

d) ER glutathione redox potential in six-day-old WT and *gsh2-5* seedlings as measured by ER-localized roGFP (ER-roGFP2iL). Each bar represents data from 10 seedlings.

All error bars represent SD

3.3.6 The contribution of glutathione to the *gsh2* phenotypes

Since *gsh2* mutants had low concentrations of glutathione, *gsh2-5* was grown in medium supplemented with glutathione to determine whether any phenotypes of *gsh2* can be rescued by exogenous glutathione. I first attempted to restore normal ER morphology by adding exogenous GSH to *gsh2* mutants after germination in normal growth media, but the no substantial change in ER morphology was observed (data not shown). Next, I germinated *gsh2* in the presence of exogenous GSH. Strikingly, normal root growth was recovered in all tested alleles (Figure 3.11a). With 1mM GSH, the primary root length of the WT was reduced by 35% and was comparable to those of *gsh2* under the same treatment. It appeared that exogenous GSH could rescue root growth of seedlings that were deficient of GSH, but somewhat inhibited the growth of seedlings with normal GSH level. To explore the effect of exogenous GSH further, WT and *gsh2-5* plants were grown in media supplemented with a series of concentrations of GSH. As the concentration of GSH was serially diluted from 0.33mM to 0.012mM, root growth was also reduced in a dose-dependent manner (Figure 3.11b). Interestingly, both WT and *gsh2-5* plants had longer roots at 0.33mM GSH than at 1mM GSH, implying excess glutathione was inhibitory to root growth. At 1mM GSH, the ER phenotype of *gsh2-5* was completely rescued as no trace of swollen bodies was found in root epidermal cells and normal ER morphology was observed as examined by confocal microscopy of the ER lumen marker GFP-HDEL (Figure 3.11d). At 0.33mM GSH, the recovery appeared patchy such that normal ER was found in some areas (Figure 3.11e), while small circular bodies labelled by GFP-HDEL were found elsewhere in the same seedling (Figure 3.11f and g). At concentration below 0.33mM, the effect of glutathione on ER morphology was not apparent (Figure 3.11h to j).

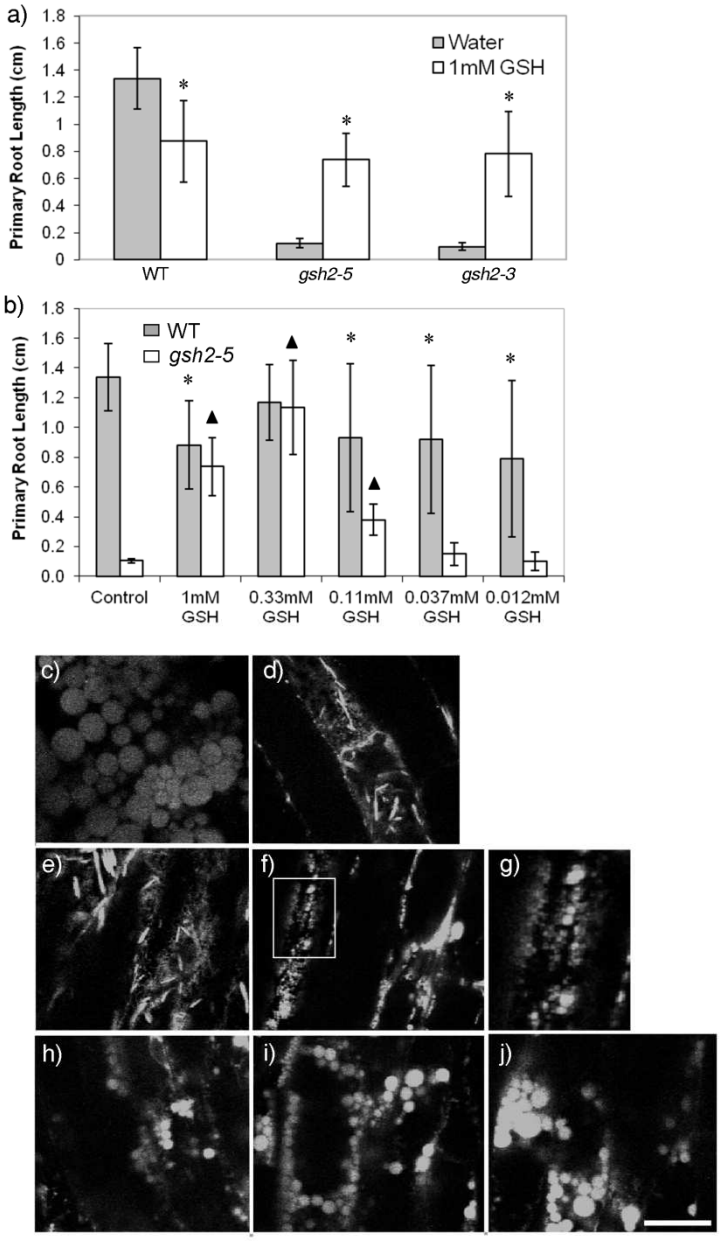

Figure 3.11. *gsh2* mutant phenotypes were rescued by exogenous GSH

a) Primary root lengths of WT, *gsh2-3* and *gsh2-5* after seedlings were grown in media with or without 1mM GSH for six days. Asterisks indicate values that are significantly different from those of the same genotype in water control (P<0.01).

b) WT and *gsh2-5* seedlings expressing an ER marker (GFP-HDEL) were germinated and grown in medium supplemented with a series of gluathione concentration. b) Primary root lengths of six-day-old WT and *gsh2-5* seedlings grown in media supplemented with water (control) or the listed concentration of glutathione. Asterisks and triangles indicate values that are statistically significantly different from those of WT and mutant in control, respectively (P<0.01). Error bars represent SD.

c) to j) Confocal fluorescence images of seedlings grown with no exogenous GSH (c), 1mM GSH (d), 0.33mM GSH (e to g), 0.11mM GSH (h), 0.037mM GSH (i) or 0.012mM GSH (j). (g) is a zoomed image of the boxed area in (f). Root epidermal cells are shown.

Bar=20μm

3.3.7 Effect of γ-EC hyperaccumulation on ER morphology

Since γ-EC synthesis can be inhibited by GSH through feedback inhibition on GSH1 (Figure 3.1) (Hell and Bergmann, 1990), exogenous GSH can abolish γ-EC hyperaccumulation as well as GSH deficiency in *gsh2*. Hence, the fact that exogenous glutathione can restore normal ER in *gsh2* could not discriminate whether γ-EC hyperaccumulation or GSH deficiency alone could trigger the phenotype. I attempted to resolve the two phenomena by examining the phenotypes of *rml1* plants and inhibiting γ-EC production in *gsh2* plants. Although *rml1* was also deficient in GSH and had a similar growth reduction as *gsh2-5* in seedling stage (Figure 3.12a), its ER morphology appeared similar to the WT (Figure 3.12b). It therefore seems that depletion of GSH alone was insufficient to induce the swollen ER phenotype. To test if the swollen phenotype could be attributed to γ-EC hyperaccumulation, I inhibited γ-EC and GSH production in *gsh2-5* by using buthionine sulfoximine (BSO), which is a reversible inhibitor of GSH1 (Figure 3.1) (Griffith, 1982). Seven days after germination and growth in media containing 1mM BSO, root growth was significantly reduced in WT but no developmental change was observed in *gsh2-5* (Figure 3.12c to f). Strikingly, ER morphology was unaffected in WT and normal ER was completely restored in cotyledons and hypocotyls of *gsh2-5* (Figure 3.12g to j). The recovery in the root was partial as ER network was observed but tubular fusiform bodies were absent in many cells. Because this was similar to what was observed in WT plants treated with 10mM H_2O_2 (Figure 3.13), I suspect the root of *gsh2-5* was suffering oxidative stress in the presence of BSO. Since the swollen ER phenotype was never observed without γ-EC accumulation, the evidence here suggests that the swollen ER phenotype ascribes to γ-EC hyperaccumulation rather than GSH depletion.

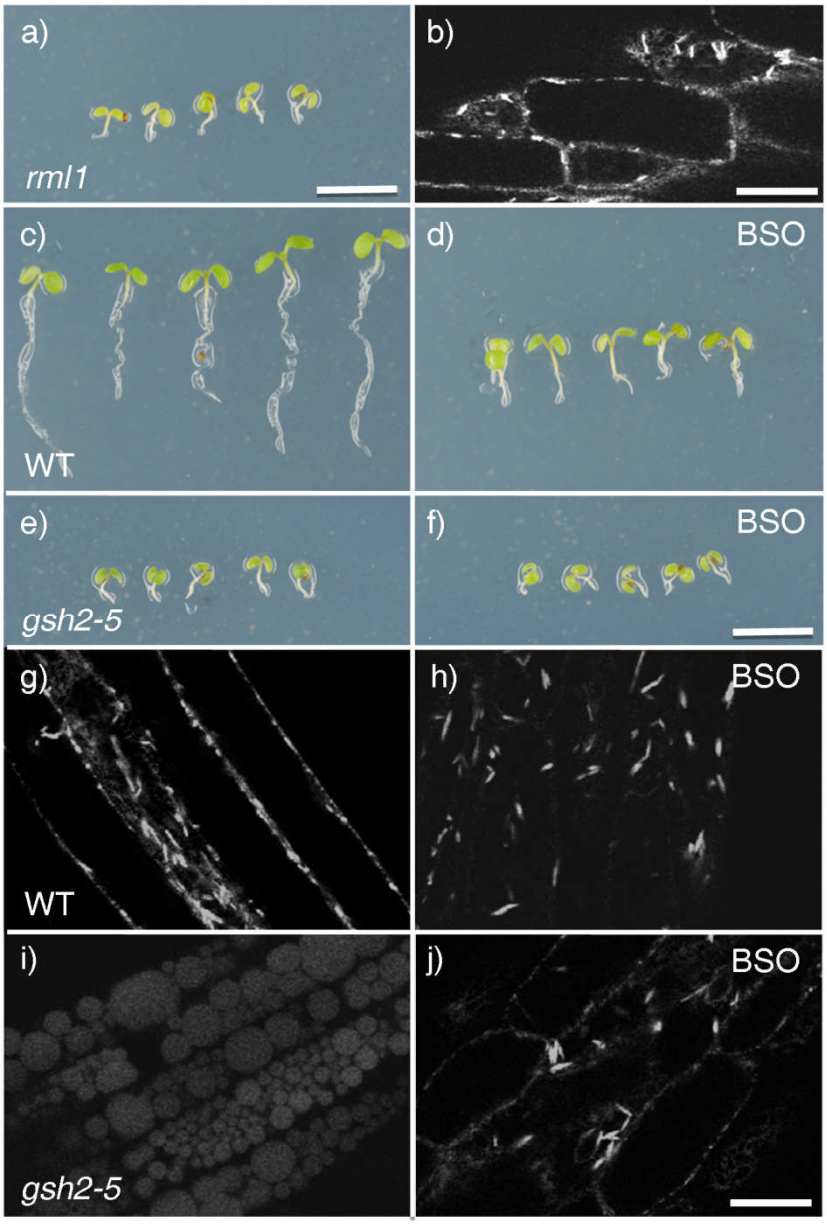

Figure 3.12. *gsh2* swollen body phenotype was attributed to γ-EC hyperaccumulation rather than GSH deficiency

a) and b) Bright-field (a) and confocal images of hypocotyl (b) of seven-day-old *rml1* seedlings expressing an ER lumen marker (N-YFP-HDEL).

c) to f) Bright-field images of seven-day-old WT (c and d) and *gsh2-5* (e and f) seedlings grown in media without (c and e) and with 1mM BSO (d and f).

g) to j) Confocal images of hypocotyl of seven-day-old WT (g and h) and *gsh2-5* (i and j) seedlings expressing an ER lumen marker (GFP-HDEL). Seedlings were grown in normal growth media (g and i) or growth media supplemented with 1mM BSO (h and j).

Bar=5mm in (a) and (f), 20μm in (b) and (j).

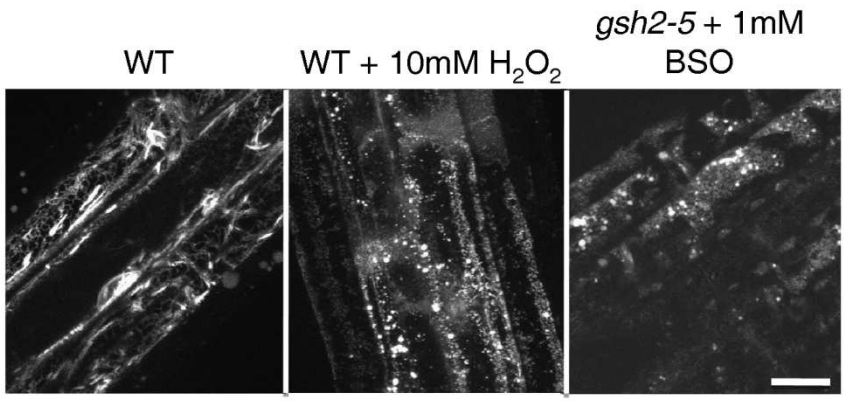

Figure 3.13. BSO-treated *gsh2-5* root cells show similar pattern as wild type (WT) root cells that are under oxidative stress

Confocal images epidermal root cells of six-day-old WT and *gsh2-5* seedlings expressing an ER lumen marker (GFP-HDEL). Seedlings were grown in medium supplemented with water or 10mM H_2O_2 for WT, or 1mM BSO for *gsh2-5*.

Bar=20μm.

3.3.8 Gluathione depletion did not affect secGFP secretion

To test whether the secretory pathway is sensitive to GSH level, GSH was depleted in WT seedlings with a GSH1 inhibitor BSO and a GSH-conjugating compound 1-chloro-2, 4-dinitrobenzene (CDNB) (Coleman et al., 1997). Seedlings were incubated in liquid medium with 1mM BSO and 1mM CDNB for six hours to deplete all the glutathione in the seedlings. To quantify biosynthetic traffic, the treated seedlings were expressing a ratiometric marker nlsRFP-2A-secGFP or nlsRFP-2A-GFP-HDEL, which provide stoichiometric expressions of a nuclear-targeted mRFP1 and a secreted GFP (for secGFP) or an ER-localized GFP (GFP-HDEL) (Samalova et al., 2006). Here, a series of confocal fluorescence images of an epidermal root cell was taken along the z-axis. The absolute mean fluorescence intensity of RFP in the nucleus, which represents the baseline for transgene expression in that cell, was measured at the plane with the highest mean RFP intensity. Similarly, the absolute mean intensity of GFP in the cytoplasm was measured at the plane with the highest mean GFP intensity. The resultant GFP/RFP ratios plotted

in Figure 3.14 represent the level of GFP in the cytoplasm after correcting for variability in transgene expression and background fluorescence. The GFP/RFP ratios for nlsRFP-2A-secGFP reflect the quantity of the secreted marker accumulating in the cytoplasm due to perturbation in secretory traffic. Seedlings expressing another ratiometric marker nlsRFP-2A-GFP-HDEL, was included in the analysis as a control. Theoretically, the GFP/RFP ratio observed in this marker is the expected value when secGFP is completely trapped in the cytoplasm (Zheng et al., 2005; Samalova et al., 2006). The analysis showed that the glutathione depletion treatment did not affect the ratios of either marker (Figure 3.14), suggesting that biosynthetic traffic is not affected by decreased level of GSH.

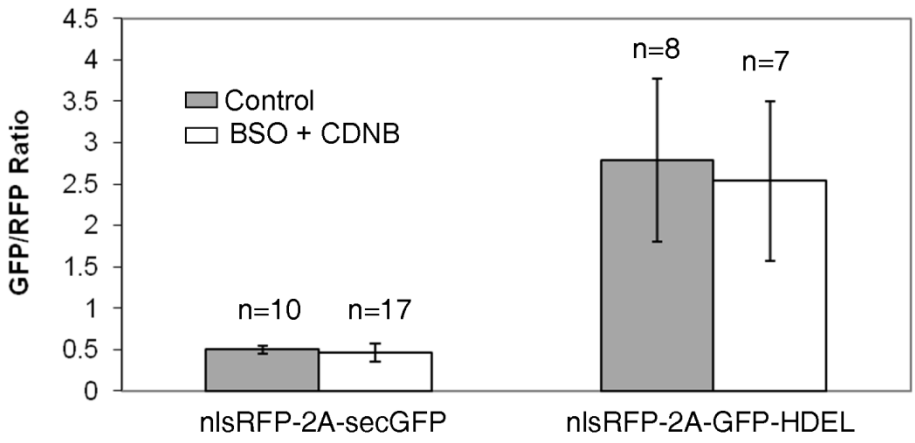

Figure 3.14. secGFP secretion is not affected by GSH depletion

1mM BSO and CDNB were added to six-day-old WT seedlings expressing nlsRFP-2A-secGFP or nlsRFP-2A-GFP-HDEL to deplete the endogenous glutathione pool. Ratios of GFP and RFP intensities are shown.

3.3.9 Comparison of unfolded protein response between WT and *gsh2*

Correct disulfide bridge formation is crucial for proteins to attain their native conformation. A collection of oxidoreductases and protein disulfide isomerases (PDI) work with chaperones in the ER to assist correct protein folding by promoting disulfide bond formation (Onda et al., 2009; Liu and Howell, 2010). It has been shown in mammalian cells that oxidoreductases in the ER are

reduced by GSH (Jessop and Bulleid, 2004), thus GSH plays a key role in the electron transfer process that is required for disulfide bond formation. To investigate the possibility that reduced GSH content of *gsh2* may compromise protein folding and therefore lead to accumulation of secreted proteins in the ER and constitutive ER stress, I analyzed the accumulation of the ER resident chaperones Binding Protein (BiP) and calreticulin (CRT), whose expression is upregulated as part of the unfolded protein response (UPR) (Koizumi et al., 2001; Christensen et al., 2008; Costa et al., 2008). As shown in Figure 3.15, the expression of BiP and CRT in *gsh2-5* did not appear to differ from that of the WT, implying that the mutant was not under constitutive ER stress. Next, to examine whether *gsh2* was sensitive to an accumulation of unfolded proteins in the ER, the UPR between the WT and *gsh2-5* was compared by treating the seedlings with the ER stress-inducing drug tunicamycin (Bertolotti et al., 2000; Iwata and Koizumi, 2005). After a seven-hour treatment, the abundance of BiP and CRT was increased in both WT and *gsh2-5* with no apparent difference between the genotypes. Not only did the constitutive isoforms of BiP and CRT increase in abundance, but the inducible isoforms were also evident. Hence, the ability to respond to UPR did not appear to be compromised in *gsh2-5*.

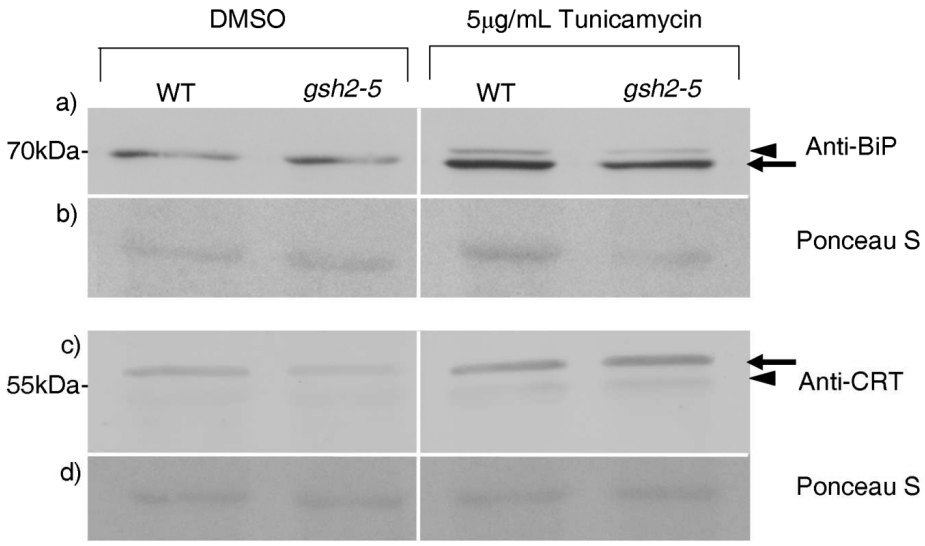

Figure 3.15. *gsh2* does not have constitutive unfolded protein response (UPR) and responds to chemically induced UPR in similar manner as WT

Eight-day old WT and *gsh2-5* seedlings were incubated in liquid MS medium with DMSO (control) or 5μg/mL tunicamycin for 7h before whole-seedling proteins were extracted.

a)and c) Immunoblot analysis of BiP (a) and CRT (c) expression using anti-BiP and anti-CRT antibodies. Arrows indicate bands that correspond to constitutive BiP and CRT. Arrowheads indicate bands that appear in UPR.

b) and d) Ponceau S stain of the same blot to demonstrate equal loading.

Molecular weight markers are indicated on the left.

3.3.10 Overexpression of ER-shaping reticulon in *gsh2*

Reticulons localize in the membrane of the tubular ER and are responsible for maintaining ER morphology by inducing membrane curvature (Voeltz et al., 2006; Tolley et al., 2008; Sparkes et al., 2010; West et al., 2011). In *Arabidopsis*, there are 21 genes encoding reticulon-like proteins, namely AtRTNLB1-21 (Oertle et al., 2003; Nziengui et al., 2007). It has been shown that AtRTNLB1-4 and 13 can remodel the ER lumen without affecting secretory transport (Tolley et al., 2008; Sparkes et al., 2010). It has also been shown *in vitro* that a mammalian reticulon, RTN4a, can be inhibited by thiol-modifying reagents, resulting in a perturbation of ER tubule morphology

(Voeltz et al., 2006). For these reasons, I hypothesized that γ-EC affected ER morphology through reticulons.

To test whether normal ER morphology can be restored in *gsh2* by overexpression of reticulons, YFP-tagged *Arabidopsis* reticulon (RTNLB1-YFP) (Sparkes et al., 2010) and ER lumen marker (mCHERRY-HDEL) (Nelson et al., 2007) were coexpressed in the WT and *gsh2-5*. While RTNLB1-YFP clearly labelled the ER network in both WT and *gsh2-5*, mCHERRY-HDEL labelled the tubular fusiform bodies in WT and the swollen bodies in *gsh2-5* (Figure 3.16a to d). There was little colocalization between RTNLB1-YFP and mCHERRY-HDEL. Although DER2-YFP and RTNLB1-YFP are both ER membrane markers, the localization patterns of RTNLB1-YFP and DER2-YFP were noticeably different such that the former localized in tubular ER network and the latter localized in the membrane of swollen bodies (compare Figure 3.6c and d with 3.16b and d).

Next, to find out whether the ER-shaping function of plant reticulons, like their mammalian counterparts, can be inhibited by thiol-modifying reagents and result in swollen body formation, WT seedlings were grown with N-ethyl-maleimide (NEM), which can react with the free thiol group on a cysteine residue (Riordan and Vallee, 1972) and can therefore inactivate a protein if its thiol groups are required for function. Although NEM reduced root growth substantially (Figure 3.16 e and f), it did not appear to affect ER morphology (Figure 3.16g and h). Therefore, it appeared that plant reticulons are insensitive to thiol-modifying reagents.

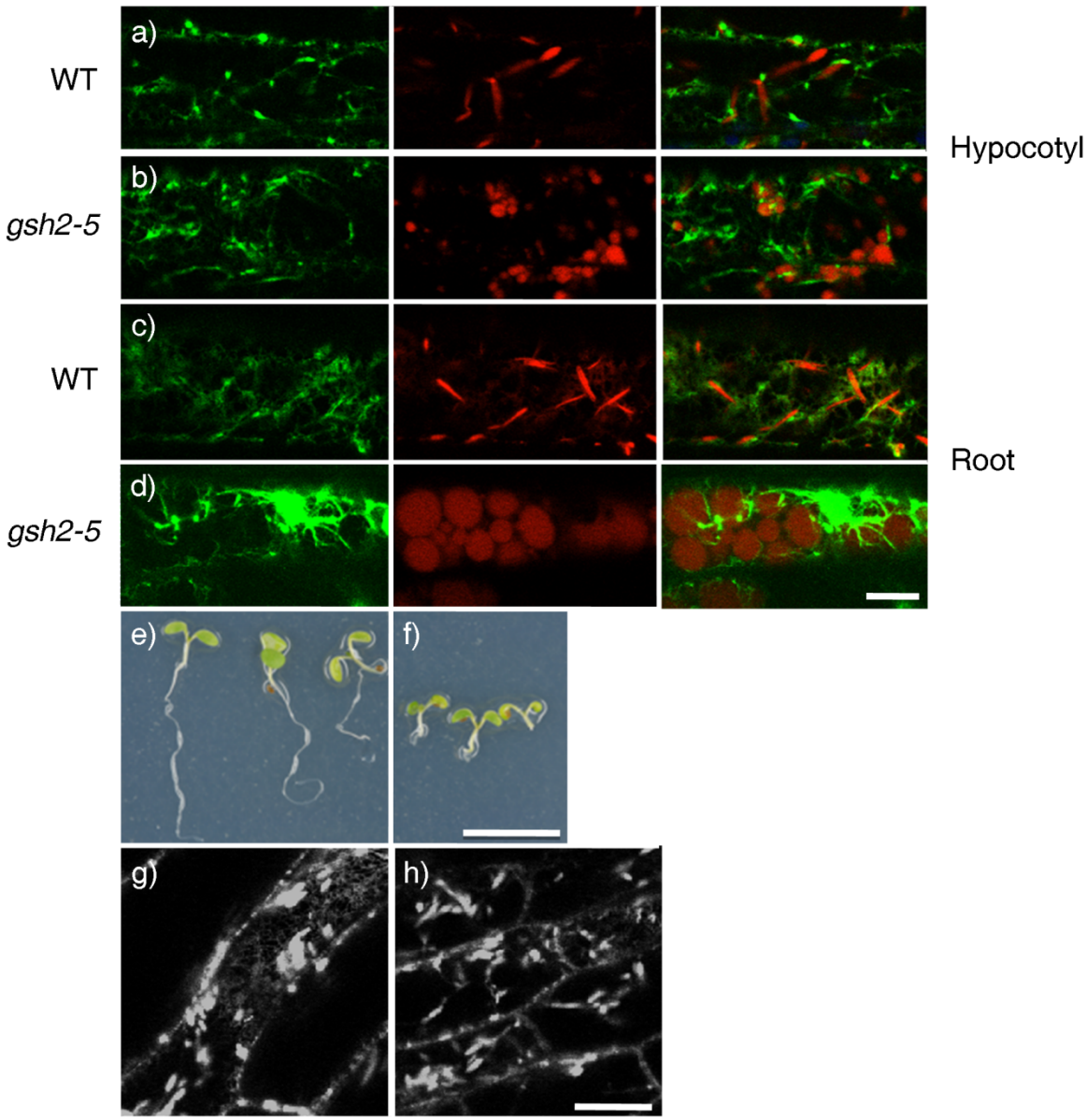

Figure 3.16. ER network is labelled by RTNLB1-YFP in *gsh2-5*; NEM does not affect reticulon function in root

a) to d) Six-day-old WT (a and c) and *gsh2-5* (b and d) seedlings expressing RTNLB1-YFP (green) and mCHERRY-HDEL (red). Hypocotyl (a and b) and root (c and d) epidermal cells are shown.

e) and f) Bright-field images of six-day-old WT seedlings growing in MS medium supplemented with DMSO (e) and 50μM NEM (f).

g) and h) Confocal images of WT seedlings expressing N-YFP-HDEL in MS medium supplemented with DMSO (g) and 50μM NEM (h).

Bar=10μm in (d), 5mm in (f) and 20μm in (f).

3.4 Discussion

3.4.1 Membrane trafficking in *gsh2*

The four novel mutant alleles of *GSH2* described in this chapter all accumulated secGFP in characteristic ER-derived swollen bodies. Since Golgi (ST-RFP) and TGN (VHA-a1:GFP) markers are able to reach their target compartments in *gsh2* but secGFP, PM (PIP-GFP) and tonoplast (BobTIP-GFP) markers are not, ER export appears to be partially blocked in *gsh2*. Even in the WT, PIP-GFP and BobTIP-GFP can be observed not only on the membrane of their targeted compartment but occasionally also in the ER, suggesting that they are not efficiently transported and therefore more sensitive to perturbations in secretory traffic.

I have attempted to disrupt the secretory pathway by depleting cytosolic glutathione and inhibiting glutathione synthesis in the WT, but secGFP secretion was unaffected by the treatment. The evidence available so far suggests that glutathione depletion is not sufficient to block the secretory pathway, so γ-EC accumulation alone may be sufficient to partially block secretion in addition to changing the ER morphology.

3.4.2 ER morphology in *gsh2*

The ER is a morphologically dynamic structure that changes frequently during development (Ridge et al., 1999). In many *Brassicaceae* plants including *Arabidopsis*, parts of the ER also exists as spindle-shaped structures known as ER bodies (Iversen, 1970; Behnke and Eschlbeck, 1978; Matsushima et al., 2003b). These structures accumulate fluorescent proteins that carry an ER signal peptide and a C-terminal H/KDEL retrieval motif (Toyooka et al., 2000; Hawes et al., 2001; Yamada et al., 2008). Indeed, such markers predominantly label ER bodies in the WT, and swollen

ER in *gsh2*. Similar to the tubular ER bodies (Hawes et al., 2001), the swollen bodies in *gsh2* were also surrounded by ribosomes. Because tubular ER bodies have never been observed in *gsh2* under normal growth condition, I suspect that the swollen bodies in *gsh2* may be derived from the tubular bodies. To investigate the relationship between the tubular fusiform bodies and the swollen bodies, one could perhaps compare the composition of the two compartments. Previous studies have shown that the β-glucosidase PYK10 is abundant in tubular ER bodies and is implicated in defence against herbivore or fungal attacks (Matsushima et al., 2002; Yamada et al., 2011). Meanwhile, a comprehensive analysis of the composition of swollen bodies is yet to be conducted, but this study has shown that γ-EC is present in the swollen bodies of *gsh2-5* in significant quantity. It is possible that large swollen bodies arise as a consequence of excessive accumulation of γ-EC. Since *gsh2* mutants do not exhibit a constitutive UPR, we can assume that the proteins that occupy the ER have attained their native conformation and are functional.

The ER also forms an elaborate membrane network throughout the cytoplasm (reviewed in Sparkes et al., 2009). Different ER markers expressed in *gsh2* provide different perspective of the ER morphology in the mutant. In this study, the ER was labelled with soluble fluorescent proteins with the HDEL retention motif (e.g. GFP-HDEL and mCHERRY-HDEL), and with DER2-YFP and RTNLB1-YFP. The HDEL markers exclusively labelled the swollen bodies in *gsh2* and did not show any signs of an ER network. DER2-YFP was also mostly on the membrane of swollen bodies, but was occasionally observed on the tubular network. Since there was no evidence that DER2-YFP affects the shape of ER network (L Frigerio, personal communication), I conclude that a residual ER network does exist in *gsh2* mutants. The reason that the network is not visibly labelled by the HDEL markers is likely because the soluble markers can concentrate in voluminous compartments

like the swollen bodies and therefore label those compartments much more intensely compared to the narrow tubules where less proteins can occupy.

In contrast to the HDEL markers and DER2-YFP, reticulon (RTNLB1-YFP) is the only marker that exclusively labels the ER network in *gsh2-5*. This may be attributed to the fact that reticulons preferentially localize in membrane of high curvature like the tubular ER network, and are excluded from less curved surfaces like the spherical swollen bodies (Tolley et al., 2008; Sparkes et al., 2010). Given that the reticulons preferentially reside in the tubular ER and affect ER morphology in mammals and plants (Voeltz et al., 2006; Shibata et al., 2008; Tolley et al., 2008; Sparkes et al., 2010), I hypothesized that γ-EC may affect ER morphology by interacting with one or more of the 21 plant reticulons in *Arabidopsis* (Oertle et al., 2003; Nziengui et al., 2007). However, swollen bodies were still present in *gsh2* despite overexpression of reticulons, therefore the formation of swollen bodies does not appear to be a consequence of perturbing reticulon function. To find out if there are any cysteine residues in reticulons with which thiol molecules can interact to disrupt the ER-shaping function, I attempted to inactivate the free thiol groups with NEM. Although NEM has significantly reduced seedling growth, ER morphology was not affected as seen from confocal fluorescence microscopy. Therefore, unlike their mammalian counterparts, plant reticulons do not appear to be sensitive to thiol-reacting reagents.

3.4.3 γ-EC hyperaccumulation and GSH deficiency contribute to the *gsh2* phenotype independently

Genetic and pharmacological perturbation of GSH1 activity shows that the atypical ER morphology in *gsh2* plants is attributed to γ-EC accumulation rather than GSH deficiency. It has been shown here and previously that *gsh2* null mutants can be rescued by exogenous GSH

(Pasternak et al., 2008). Though normal ER morphology in *gsh2* can be restored by exogenous GSH (Figure 3.11), the effect of GSH on ER morphology is indirect by alleviating γ-EC accumulation through feedback inhibition of GSH1 activity (Hell and Bergmann, 1990). This is consistent with 1) the observation that exogenous GSH failed to rescue the swollen ER phenotype in *gsh2* if it was applied after germination as γ-EC may have already hyperaccumulated to a significant level (data not shown); 2) the observation that *rml1* does not exhibit a swollen ER phenotype despite low cytosolic GSH content; and 3) the restoration of normal ER morphology in *gsh2-5* in the presence of the GSH1 inhibitor BSO.

It has been reported previously that the complete absence of GSH in *gsh1* null mutants confers embryo-lethality (Cairns et al., 2006), whereas *gsh2* null mutants are seedling-lethal (Pasternak et al., 2008). Here the role of GSH in development is again demonstrated, as the developmental phenotype of *gsh2* seedlings correlates with their cytosolic GSH level, and as the root growth of *gsh2-5* responds to exogenous GSH in a dose-dependent manner.

3.4.4 ER transport of γ-EC and GSH

The data in this work suggests that γ-EC is present in the swollen bodies of *gsh2* in significant quantity (Figure 3.9), so how does excess γ-EC end up in the ER? The transport of γ-EC and glutathione across the ER membrane is poorly understood. Although some members of the oligopeptide transporter (OPT) family in *Arabidopsis* can transport glutathione and its derivatives (Cagnac et al., 2004), it is not known whether any of these transporters reside on the ER membrane. Evidence from mammalian skeletal muscle cells suggests a correlation between ryanodine receptor channel activity and glutathione influx into the sarcoplasmic reticulum (Csala et al., 2003), but *in vitro* experiments showed that reduced glutathione (GSH) could diffuse into

the ER (Bánhegyi et al., 1999; Le Gall et al., 2004). Although glutathione is known to reside in the ER (Zechmann et al., 2008), it is not so clear for γ-EC. Given that γ-EC primarily acts as a substrate for GSH2 in plastids and the cytosol, I hypothesize that no exclusive mechanism is present for transporting γ-EC into the ER, and so γ-EC and glutathione may share the same transport mechanism across the ER membrane. To test this idea, we would first need to identify all the transporters on the ER membrane that can potentially transport γ-EC and/or GSH, and the specificity of each transporter may be characterized *in vitro* to find out whether there are any transporters that interact with γ-EC but not GSH.

3.4.5 Redox state in ER and cytosol

The redox state in the ER and the cytosol of *gsh2-5* was measured using roGFP. The data indicates no significant difference in the ER redox state between the WT and *gsh2-5*. As the ER is known to be a highly oxidized environment (Hwang et al., 1992; Meyer et al., 2007), a probe with a highly oxidized midpoint potential (roGFP2iL) was used to measure the redox state in this compartment, but the probe was almost fully oxidized. Thus the probe may not accurately determine the true redox state of the ER as the compartment's redox potential may fall outside the probe's sensitive range. The probe roGFP2iL currently has the most oxidized midpoint potential in the roGFP family (Lohman and Remington, 2008), but unfortunately it is still not ideal for measurement in the ER. When a probe capable of measuring even more oxidized redox potential becomes available, the measurement should be repeated with the new probe.

In contrast, measurements made with roGFP1 show that the cytosol is highly reduced in both the WT and *gsh2-5* at steady state. And since the *rml1* cytosol is more oxidized than *gsh2-5*, it suggests that γ-EC can at least partially substitute GSH as redox buffer. But at the same time,

gsh2-5 has decreased redox buffer capacity and increased sensitivity to oxidative stress. One possible explanation is that GSH participates in enzymatic reactions to maintain the redox state, whereas γ-EC is recognized by very few enzymes and with much lower affinity, so it can restore the redox state mainly through non-enzymatic reaction.

3.4.6 Future Direction

In this chapter, four *gsh2* mutants were presented as membrane trafficking mutants with abnormal ER morphology. Prior to this study, the role of γ-EC in *Arabidopsis* has been largely ignored as it is assumed to be a short-lived intermediate in the glutathione biosynthesis pathway that has no biological function in *Arabidopsis*. This view is challenged in this study as the evidence suggests that excess γ-EC can perturb ER morphology and that γ-EC can partially substitute the function of glutathione. It would be interesting to identify the interactors of γ-EC and therefore the mechanism that leads to the changes in ER morphology and to the potential perturbation of the secretory pathway. A good starting point would be to analyze the composition of the swollen ER bodies in *gsh2*. Another important point raised in this study is the affinity of γ-EC to glutathione-specific enzymes. Under normal conditions, when glutathione is the predominant low-molecular weight thiol molecule, many enzymes show high specificity to glutathione. Do these enzymes have the capacity to use γ-EC when glutathione is depleted? The answer to this question has a notable impact on the capability of γ-EC as a substitute for glutathione. The different γ-EC and GSH profiles in the new *GSH2* mutant alleles can be used to study this question *in vivo*.

Chapter 4 Characterization of Mut 21

4.1 Chapter Summary

Mut 21 was isolated from OK Teh's temperature-sensitive screen (Teh, 2007). The enhanced secGFP phenotype is observed in cotyledons as early as 18h after incubation at restrictive temperature. Here, the enhanced fluorescence phenotype was extensively characterized. The mutation was assigned to the first half of chromosome one in the previous study (Teh, 2007), and was further mapped and identified as a non-sense mutation on the gene locus At1g17070. The steps that have been taken to identify and confirm the mutation are presented in this chapter, followed by discussion on the relationship between the previously known function of TFIP11 and Mut 21's phenotypes.

4.2 Introduction

4.2.1 Temperature-sensitive mutants

A temperature sensitive mutant has a reversible phenotype that is triggered upon restrictive temperature and would revert to WT phenotype in permissive temperature. However, complete reversibility is rarely the case and the time it takes to trigger and reverse the mutant phenotype can vary. Temperature-sensitive mutants arise either because they are involved in a temperature-dependent biological process, or because the mutations affect the gene product in a way that results in structural changes and therefore gain or loss of activities at restrictive temperature. Mutants in the latter category are particularly useful for studying essential gene functions that would result in lethality upon inactivation, such as membrane trafficking. Temperature-sensitive mutants provide temporal control for the induction of a phenotype so that the function of the mutated gene product and the development of phenotypes can be

observed at different stages of a biological process. In addition, conditional mutants allow lethal mutations to be propagated and the separation of accumulated effects due to loss of viability.

The values of temperature-sensitive mutants in membrane trafficking research have been demonstrated through Novick and Schekman's yeast *sec* (secretory) mutants, which accumulate invertase and acid phosphatase at restrictive temperature (Novick et al., 1980). The mutants were invaluable in understanding the mechanism of vesicular transport as well as establishing the molecular basis and epistatic relationships between the regulators of secretory pathway in eukaryotes.

Despite their potential in studying essential processes, a major problem with temperature-sensitive mutants is the rare occurrence of conditional mutants in *Arabidopsis*. It is expected that only 1-2% of all EMS-induced mutations result in temperature-sensitive mutations (Rennell et al., 1991; Suckow et al., 1996; Shiraishi et al., 2004), in contrast to 5% and 65% that result in nonsense and missense mutations, respectively (McCallum et al., 2000). Despite the low frequency, a few temperature-sensitive mutants in *Arabidopsis* have been isolated from EMS mutagenesis screen (Yasutani et al., 1994; Meisel et al., 1996; Whittington et al., 2001; Long et al., 2002; Sugiyama, 2003). Amongst these are the temperature-sensitive membrane trafficking mutants *hit1-1* and *hit1-2* which helped to establish a connection between the membrane trafficking process and the maintenance of plasma membrane integrity at high temperature; and *scd1-1* which displays cytokinesis defects in guard cells and pavement cells (Falbel et al., 2003), 2003).

4.2.2 Mut 21 as a putative temperature-sensitive membrane trafficking mutant

Mut 21 was first isolated as a monogenic recessive conditional mutant that exhibits enhanced secGFP fluorescence 18h after growing at 31°C (Teh, 2007). Even at permissive temperature, the vegetative development of Mut 21 is delayed (Figure 4.1a and b). The rosette leaves of Mut 21 are slightly smaller with a flatter shape (Figure 4.1c), while the size of the siliques between Mut 21 and WT are similar (Figure 4.1d). The enhanced fluorescence phenotype occurs exclusively in the cotyledons (Figure 4.1f to m). Although the secGFP transcript is slightly more abundant in Mut 21 than in WT (Figure 4.1e), the difference is not sufficient to account for the marked increase in fluorescence.

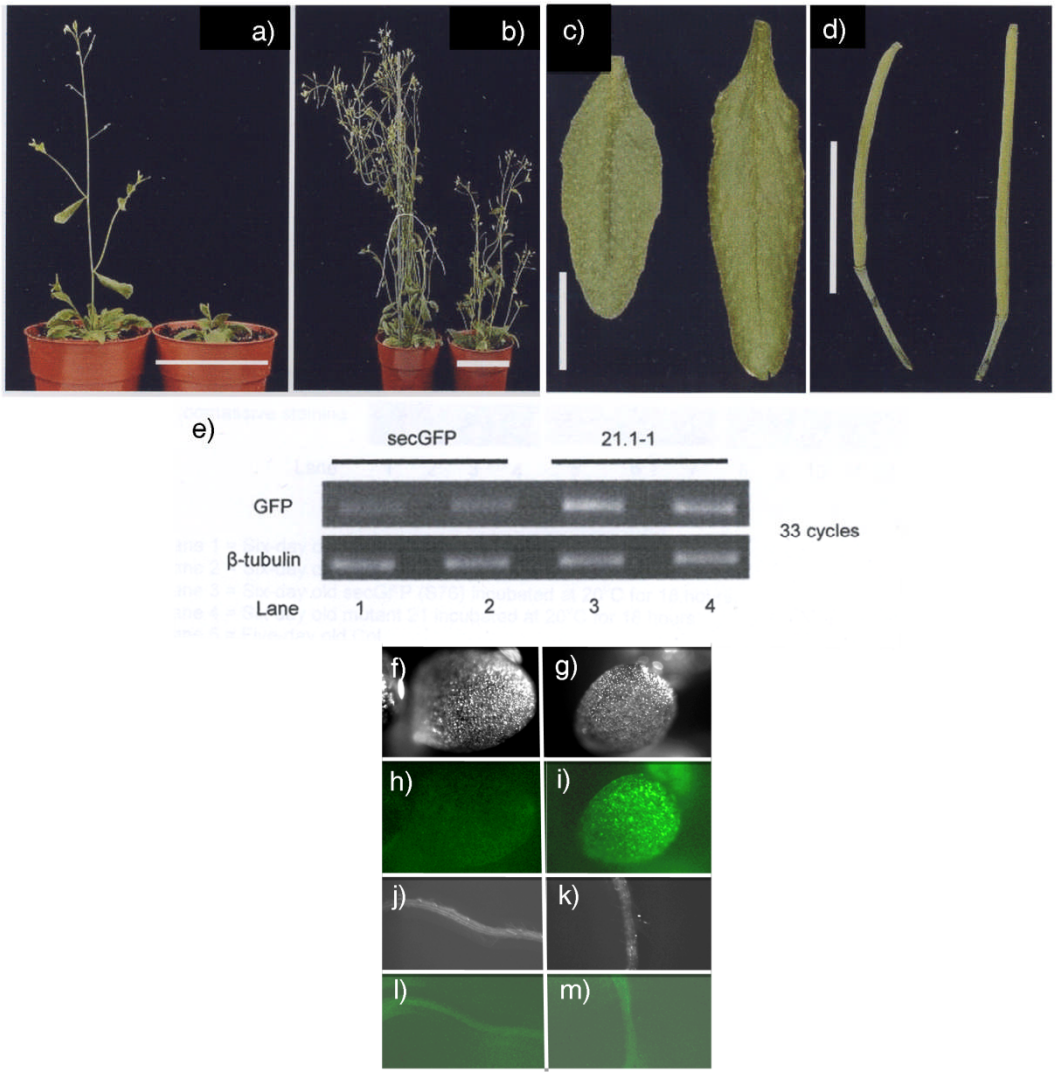

Figure 4.1. Growth of Mut 21 is slightly delayed under permissive temperature

a) and b) 28-day-old (a) and 42-day-old (b) WT (left) and Mut 21 (right) plants.

c) Rosette leaves of Mut 21 (left) and WT (right) plants.

d) Siliques of Mut 21 (left) and WT (right) plants.

e) Expression profile of secGFP and β-tubulin transcripts of WT expressing secGFP (Lane 1 and 2) and Mut 21 (Lane 3 and 4) at restrictive temperature. RNA was extracted from whole-seedlings and analyzed by RT-PCR. Number of PCR cycles is shown on the left.

f) and g) Bright-field images of WT (f) and Mut 21 (g) cotyledons.

h) and i) Fluorescence images of WT (h) and Mut 21 (i) cotyledons expressing secGFP.

j) and k) Bright field images of WT (j) and Mut 21 (k) roots.

l) and m) Fluorescence image of WT (l) and Mut 21 (m) roots expressing secGFP.

Bars=5cm in (a) and (b), 1cm in (c) and (d).

Images from Teh, 2007.

4.2.3 Map-based Cloning

4.2.3.1 The principle of map-based cloning

Map-based cloning (also known as positional cloning) is an invaluable technique to complement a forward genetic screen. It is applied to identify the gene that causes the mutant phenotype by looking for linkages between genetic markers and the mutated gene (Jander et al., 2002). The technique depends on the recombination events that occur during prophase I of meiosis. Fragments of DNA are swapped between homologous chromosomes in a process known as chromosomal crossover, and so each chromosome has a new combination of alleles (hence the term recombination). For gene loci that are sufficiently far apart on the same chromosome or on different chromosomes, there is a 50-50 chance for them to be arranged on the same chromosome, hence the recombination frequency is 50%. In this case, alleles in one locus segregate independently of the alleles in the other locus. But when two gene loci are physically close together, the probability of recombination events occurring between them decreases, so their alleles tend to stay in the same chromosome. This is known as genetic linkage, in which the recombination frequency is less than 50% and the alleles on the two gene loci do not segregate independently. Using this principle, the genetic distance can be determined between two loci on a chromosome. Map-based cloning is about building a genetic map of the position of the causative mutation to a phenotype of interest relative to genetic markers whose positions on the chromosome are known.

The concept of constructing a genetic map was developed by Thomas Morgan and his pupil Alfred Sturtevant. Based on the inheritance of the sex-linked eye colour trait in *Drosophila*, Morgan established the principle of genetic linkage (Morgan, 1910). Sturtevant demonstrated

that the relative position of three of more loci on a chromosome can be determined by the recombination frequencies between them. He subsequently generated the first genetic map in *Drosophila* (Sturtevant, 1913). Morgan and Sturtevant defined the genetic distance in terms of map unit, which equals to recombination frequency of 1%. A map unit is also equivalent to a hundredth of a Morgan, or one centiMorgan (cM).

4.2.3.2 Strategy for map-based cloning

The availability of high-quality DNA genome and polymorphism data make *Arabidopsis* an ideal model plant species for genetic study. Following the Columbia ecotype (Col-0) genome in 2000 (The Arabidopsis Genome Initiative, 2000), sequence data of other ecotypes have also become widely available (Gan et al., 2011). The DNA differences among ecotypes are used to construct genetic markers, which are to be used to establish recombination frequencies for positional cloning. In this study, the polymorphisms between Col-0 and Landsberg *erecta* (L*er*) are exploited to identify the mutation of Mut 21.

A flow-chart that outlines the steps in map-based cloning is shown in Figure 4.2a. In this study, double-backcrossed Mut 21 plants in Col-0 background were outcrossed to L*er*-0 to generate heterozygous F1 progenies, which were then self-fertilized to generate segregating mapping families. The mutant segregants in these F2 families were selected and classified as the mapping population.

Since the mutated locus originates from the Col background, markers that are linked to the mutated locus are expected to show bias to the Col-specific alleles, which can be visualized as the increased intensity of the Col band on an agarose gel following electrophoresis. Alternatively, if

no bias in the Col allele is observed, it is concluded that a recombination event has taken place between the marker and the mutated locus.

As one can imagine, an enormous number of PCR reactions must be performed to analyze the genetic markers in all five chromosomes of *Arabidopsis* for every individual in the mapping population. Instead, DNA of about 100 mutants can be pooled and analyzed with a set of genetic markers that are evenly dispersed over the entire genome in Bulk Segregant Analysis (BSA) (Michelmore et al., 1991; Lukowitz et al., 2000). The purpose of BSA is to roughly locate regions of chromosome where linkage is present, as defined by over-representation of the Col alleles on three consecutive genetic markers on the same arm of a chromosome. Once a particular region of chromosome is identified, the mutation can be fine-mapped by analyzing individuals in the mapping population with markers that are spaced closer together on the chromosome.

Fine-mapping first requires the establishment of two markers that flank the mutation through three-point mapping. Starting from the flanking markers on both sides of the mutation, genetic markers positioned within the flanking markers are analyzed for recombination events. The idea is to find the recombinants that are in close proximity of the mutation. As the markers are closer to the mutation, the recombination frequencies decrease and so fewer recombinants can be found. The probability of finding recombinants at a given distance of DNA correlates with the size of the mapping population (Figure 4.2b). The last markers in which recombinants are found on either side of the mutation define the final mapping interval.

Following fine-mapping, mutations in the gene loci within the mapping interval were identified in this work by whole-genome sequencing and comparing the sequencing data with the reference

genome. Candidate genes were then determined and confirmed with complementation experiments.

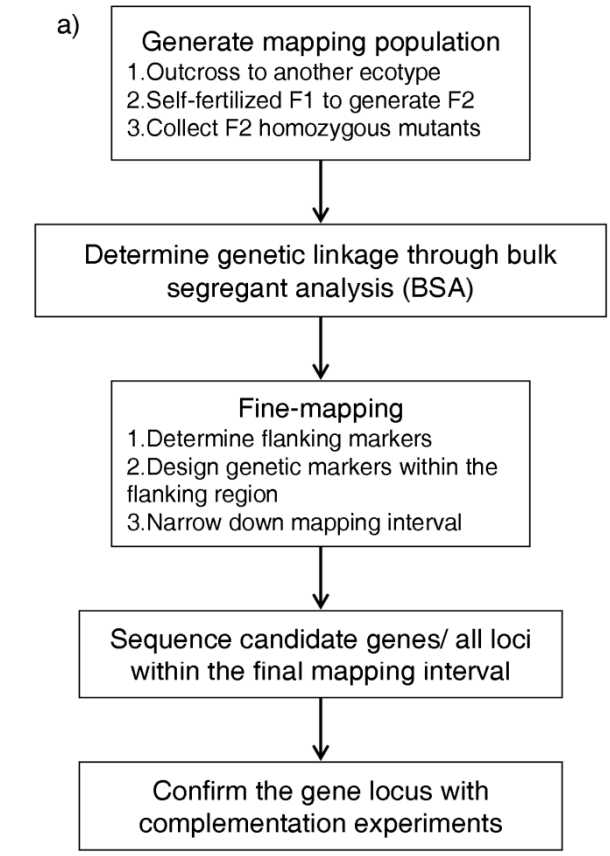

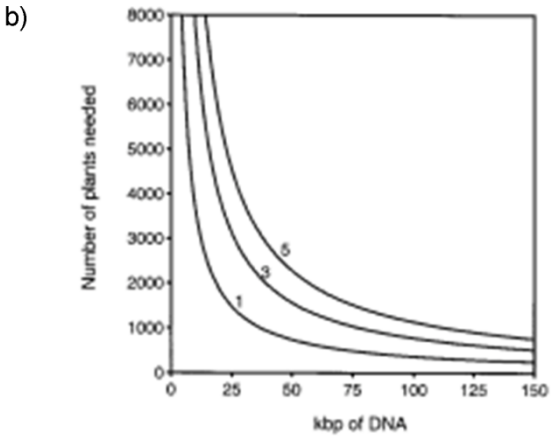

Figure 4.2. Strategy for map-based cloning

a) Flow-chart outlining the steps in map-based cloning

b) The probability of having recombination events within a given physical interval of DNA increases with population size. Number of plants required to find at least one (1), three (2) or five (3) recombinants at a given physical interval of DNA.

Figure (b) from Jander et al., 2002.

4.2.3.3 Genetic markers

In the past, one had to perform the laborious and technically challenging process of chromosome walking to identify the mutated gene locus without actually knowing the genome sequence. The molecular markers that were used at the time to develop a genetic map were restriction fragment length polymorphisms (RFLPs), amplified fragment length polymorphisms (AFLPs) and random amplified polymorphic DNAs (RAPDs). RFLPs involve digesting the DNA sample with restriction enzymes followed by comparing fragment lengths on a Southern blot to determine genetic linkage groups (Tanksley et al., 1989). AFLPs are very similar to RFLPs but instead of analyzing the DNA fragments on a Southern blot, the fragments are amplified in a PCR and are then visualized on an agarose gel (Vos et al., 1995). On the other hand, RAPDs utilize multiple and arbitrary primers for a PCR and separate the PCR products on an agarose gel. Polymorphisms can be identified by the different band patterns on the gel (Williams et al., 1993).

Modern markers are all PCR-based markers. The most commonly used markers are derived from simple tandem repeats, insertions/ deletions or single nucleotide polymorphisms (SNP) in the genome (Lukowitz et al., 2000; Hou et al., 2010). Simple sequence length polymorphisms (SSLP) are based on the different length of a short repetitive element between two ecotypes. Insertion/deletion (Indel) markers are derived from a region containing an insertion or deletion sequence. Cleaved amplified polymorphic sequence (CAPS) markers are based on SNP that results in a restriction site sequence in one allele. Following a PCR, the products are digested by restriction enzymes before being analyzed on a gel. In most cases, SNPs do not form any polymorphic restriction sites. A mismatch is then introduced in the primer to create an artificial restriction site with one of the polymorphisms. This is known as derived CAPS (dCAPS) and can be designed from many SNPs.

4.2.4 Objective

In this chapter, the localization pattern of secGFP was examined by coexpressing secGFP with organelle markers. It was revealed that secGFP actually accumulated in the apoplast. Since the application of secGFP as a secretory marker was based on the assumption that its fluorescence is quenched at the apoplast, Mut 21 was an interesting mutant for identifying factors that affect the behaviour of secGFP. It was found that Mut 21 had an alkaline apoplast in the cotyledons, which may relate to the fluorescence phenotype. Furthermore, the mutation of Mut 21 was identified with map-based cloning and confirmed by complementation experiments.

4.3 Results

4.3.1 Temperature sensitivity of Mut 21

The phenotypes of Mut 21 of seven-day-old seedlings are very similar to WT at permissive temperature (20°C) (Figure 4.3a and b). However, after 24h of growth at restrictive temperature of 31°C, changes in hypocotyl and root growth were observed (Figure 4.3c and d). To follow up on this observation, hypocotyl and root length were compared between six-day-old seedlings of WT and Mut 21. Though the lengths of hypocotyl in WT and mutant seedlings were similar at permissive temperature, the hypocotyls of Mut 21 seedlings elongated an order of magnitude less than those of WT after 24h of growth at restrictive temperature (Figure 4.3e). Similarly, root growth was similar in WT and Mut 21 at permissive temperature, but was significantly reduced at restrictive temperature ($P<0.01$) (Figure 4.3f). Mut 21's root growth was more affected than WT. While WT's root growth was reduced by 33% at restrictive temperature, Mut 21's growth was reduced by 80%.

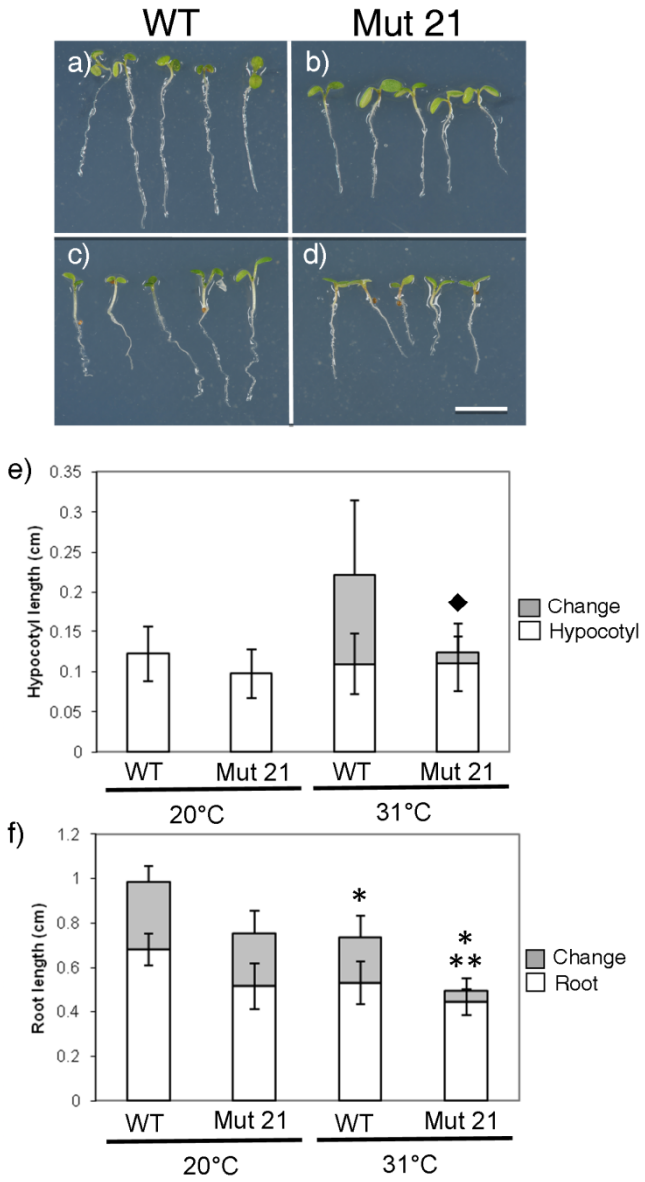

Figure 4.3. Mut 21 exhibits enhanced secGFP fluorescence and elongates less than WT at restrictive temperature

a) to d) Bright-field images of seven-day-old WT (a and c) and Mut 21 (b and d) seedlings growing at 20°C (a and b) and 31°C (c and d) in the last 24h.

e) and f) Hypocotyl (e) and root (f) growth upon heat treatment. Hypocotyl and root length before the heat treatment are represented by white bars. Seedlings were then grown in 20°C or 31°C for 24h. Changes in hypocotyl and root length in the 24h treatment period are represented by grey bars. Diamond indicates changes in hypocotyl length that are significantly different from WT under the same treatment ($P<0.01$). Single asterisks indicate changes in root length that are significantly different from the same genotype grown at 20°C ($P<0.01$). Double asterisks indicate changes in root length that are significantly different from WT under the same treatment ($P<0.01$).

Error bars represent SD

Bar=50mm in (d)

4.3.2 secGFP localized in apoplastic space in cotyledons

The distribution of secGFP was characterized with confocal fluorescence microscopy. In the cotyledons, secGFP weakly labelled the tubular fusiform bodies in WT (Figure 4.4a and c), while in the mutant it could be observed intracellularly, noticeably in the ER, and in the apoplastic space (Figure 4.4b and d). Hence, it appeared that secGFP was also secreted out of the cell in Mut 21, but unlike WT the fluorescent proteins remained fluorescent in the apoplast. In roots, however, secGFP was weakly fluorescent in both genotypes. The signals on the root images (Figure 4.4e and f) were mostly identified to be autofluorescence on the cell wall. Hence, consistent with previous observations (Teh, 2007), the enhanced secGFP fluorescence phenotype was exclusive to the cotyledons in seedlings.

The C-terminal region of secGFP undergoes proteolysis shortly before or after reaching the apoplast, thus secGFP is present in the apoplast as truncated form (Zheng et al., 2004). To confirm the apoplastic localization of secGFP in Mut 21, whole seedling protein extracts from WT and Mut 21 at different growth condition were analyzed on an immunoblot with anti-GFP antibodies. Consistent with previous findings (Zheng et al., 2004), the intracellular GFP-HDEL marker was largely present in its full-length form (Lane 7, Figure 4.5), while the secGFP in WT and Mut 21 exists in both the full-length and truncated form (Lane 2 to 6, Figure 4.5). Growth at restrictive temperature did not change the relative abundance of the form of secGFP in WT (Lane 2 and 3, Figure 4.5), but it significantly increased the proportion of the truncated form in Mut 21 (Lane 4 and 5, Figure 4.5). These results show that GFP cleavage was not disrupted in Mut 21, and verified the apoplastic localization of secGFP in Mut 21 at restrictive temperature as observed under confocal fluorescence microscopy.

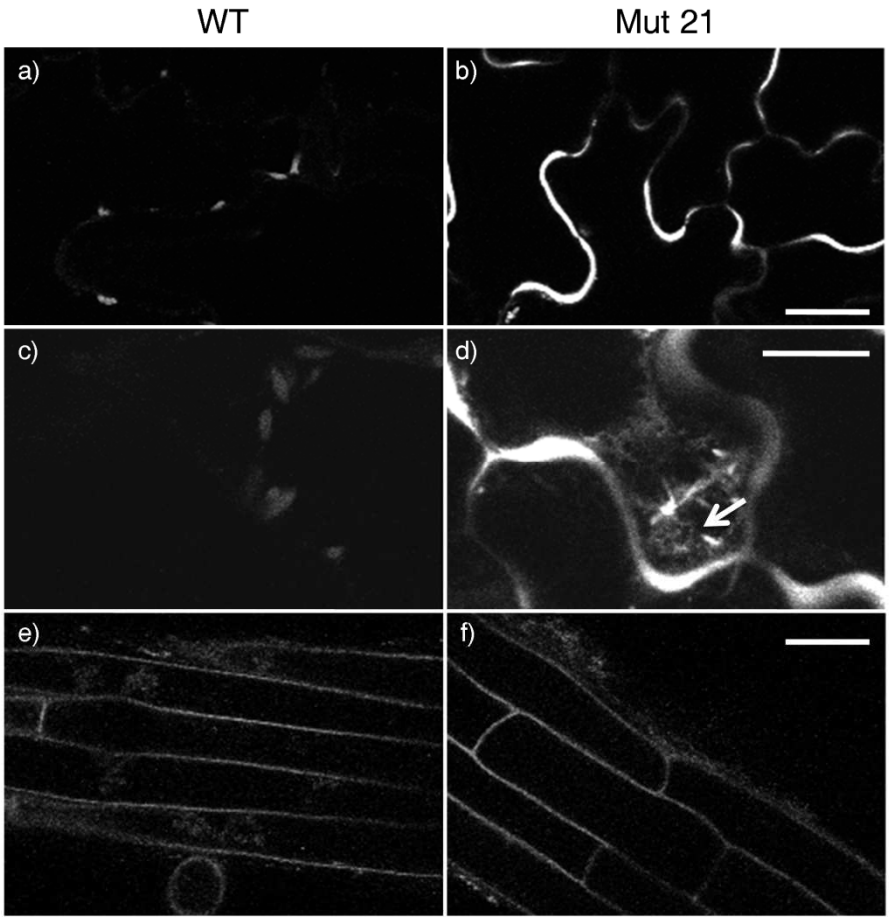

Figure 4.4. Mut 21 shows enhanced secGFP fluorescence in the cotyledons at restrictive temperature

Six-day-old WT (a, c and e) and Mut 21 (b, d and f) seedlings expressing secGFP after growing at 31°C for 24h. Epidermal cells in the cotyledons (a to d) and roots (e and f) are shown. The arrow in (d) indicates ER network.

Bars=20μm in (b) and (f), 10μm (d).

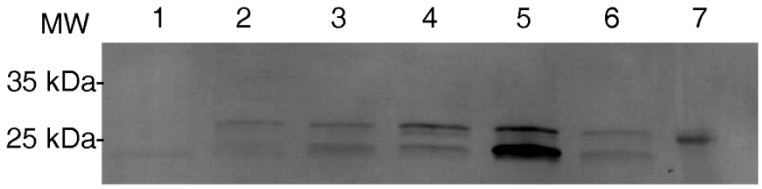

Lane 1. Col-0
2. Mut 21 WT segregant at 20°C
3. Mut 21 WT segregant at 31°C
4. Mut 21 mutant segregant at 20°C
5. Mut 21 mutant segregant at 31°C
6. secGFP WT
7. ER lumen marker (GFP-HDEL)

Figure 4.5. Anti-GFP immunoblot analysis of whole-seedling protein extracts from seven-day-old seedlings

Molecular weight markers are indicated on the left.

4.3.3 Localization pattern of ER, Golgi and tonoplast marker in Mut 21

ER (mCHERRY-HDEL), Golgi (ST-mCHERRY) and tonoplast marker (γTIP-mCHERRY) (Nelson et al., 2007) were coexpressed with secGFP in WT and Mut 21 to further characterize the distribution pattern of secGFP. The ER and Golgi markers revealed that there was no perturbation in ER or Golgi morphology observed under confocal fluorescence microscopy (Figure 4.6a and b). Other than localizing in their target organelles, mCHERRY-HDEL and ST-mCHERRY were often seen to colocalize with secGFP in the apoplast in Mut 21 similar to WT cells that strongly expressed the markers. Furthermore, γTIP-mCHERRY was localized on the tonoplast and did not colocalize with secGFP in Mut 21 (Figure 4.6c). This confirmed that secGFP did not accumulate in the ER, Golgi or the vacuole, but in the apoplastic space in cotyledons.

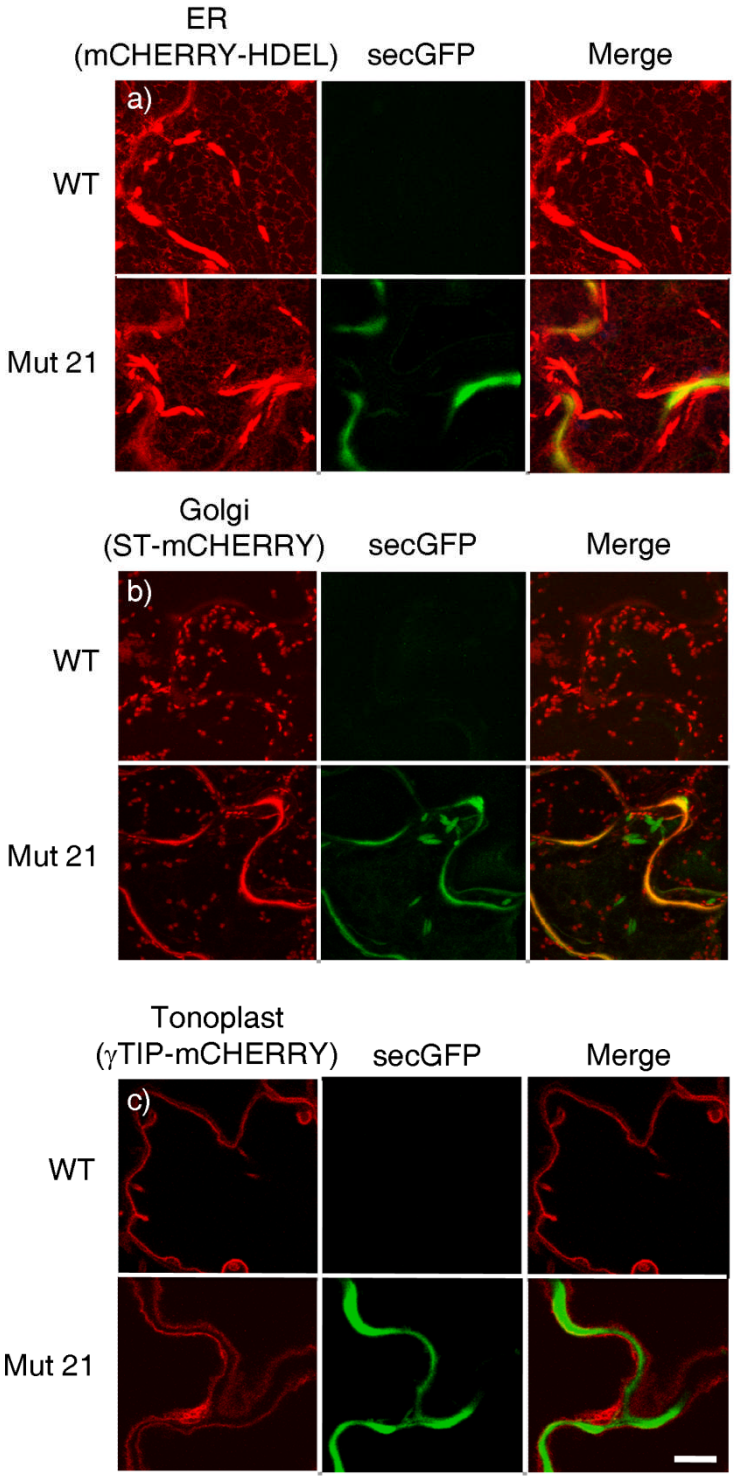

Figure 4.6. secGFPs are localized in Mut 21 cotyledon apoplast

Images of cotyledons of six-day-old seedlings after 24h of heat treatment at 31°C. secGFP is coexpressed with mCHERRY-HDEL (a), ST-mCHERRY (b) and γTIP-mCHERRY (c). While mCHERRY-HDEL and ST-mCHERRY are localized in ER and Golgi, respectively, and in the apoplast where both markers colocalized with secGFP. γTIP-mCHERRY do not colocalize with secGFP.

Bar=10μm

4.3.4 Measurement of the apoplastic pH

Given that secGFP is not fluorescent in the acidic apoplast (Zheng et al., 2004), it is possible that Mut 21's apoplast was alkalized upon heat treatment. To test this, the pH of Mut 21 apoplast in cotyledons was measured using SNARF1 that is conjugated to dextran (SNARF1-Dextran). SNARF1 has a pH-sensitive emission spectrum that comprises two peaks, which can be used to determine pH through ratiometric fluorescence imaging (Albrechtova et al., 2003; Jia and Davies, 2007; Li et al., 2008). SNARF1-Dextran remained in the apoplast of cotyledons after it was loaded by vacuum infiltration (Figure 4.7a to d). Apoplastic pH in WT and Mut 21 was determined by measuring the ratio between the fluorescent intensities of the "acidic peak" (572-604nm) and of the "basic peak" (625-647nm). As shown in Figure 4.7e, Mut 21 at restrictive temperature had a significantly lower ratio than Mut 21 at permissive temperature and WT in either condition ($P<0.01$). To determine the apoplastic pH, SNARF1-Dextran was calibrated *in vivo* by infiltrating WT cotyledons in a series of pH buffered solutions (100mM acetate at pH 5.5; 100mM HEPES at pH 6.0, 6.5, 7.0 and 7.5; 100mM Tris-HCl at pH 8.5). The ratios of SNARF1-Dextran were found to be linearly dependent on pH in the range of 6 to 8 (Figure 4.7f). The pH of WT and Mut 21 was determined by interpolating the pH value that corresponds to each ratio on the calibration curve (Figure 4.7f). With the exception of Mut 21 at restrictive temperature that had a pH of 7.2, all other samples had pH between 6.6 and 6.8. Hence, Mut 21's apoplast in cotyledons became more alkaline upon growth at restrictive temperature.

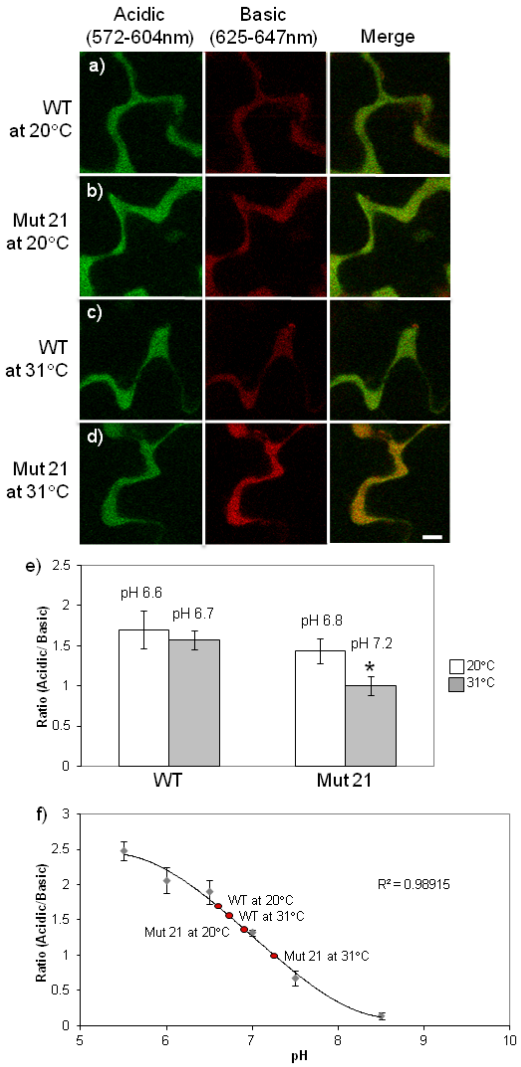

Figure 4.7. The apoplast of Mut 21 cotyledons was alkalized after heat treatment

After five days of growth at 20°C, WT and Mut 21 seedlings were either transferred to 31°C or remained in 20°C for 24h. SNARF1-Dextran was then infiltrated into cotyledons and apoplastic pH was determined by ratiometric fluorescence imaging.

a) to d) SNARF1-Dextran labeled the apoplast of cotyledons. Images of apoplasts in WT (a) and Mut 21 (b) at 20°C, and in WT (c) and Mut 21 (d) at 31°C were shown. Emissions of SNARF1-Dextran were collected at 572-604nm (the acidic channel, green) and at 625-647nm (the basic channel, red).

e) Average ratio of emission intensity of SNARF1-Dextran in WT and Mut 21 in 20°C (white) and 31°C (grey). pH values on top of each bar were determined by interpolating the *in vivo* calibration curve in (f). The ratio in Mut 21 at 31°C (asterisk) was statistically significantly different from all other values ($P<0.01$). n=10 for WT and 9 for Mut 21. Error bars represent SE of means.

f) *In vivo* calibration for SNARF1-Dextran. WT cotyledons were infiltrated with SNARF1-Dextran in pH buffered solutions (pH 5.5, 6.0, 6.5, 7.0, 7.5 and 8.5; n=5) and were subsequently imaged. The regression coefficient (r-squared) value of the calibration curve are shown. The emission ratio in (e) are plotted onto the curve to interpolate the corresponding pH values. Error bars represent SD.

Bar=10μm in (d)

4.3.5 Mapping and Identification of Mut 21

After characterizing the phenotypes of Mut 21, the following sections relate to the identification of Mut 21. The first step was to assign the mutation to one of the five chromosomes in *Arabidopsis* using BSA. Then the mapping interval was narrowed down with the process of fine-mapping. Once an interval was established based on a number of mapping cross population, mutations within the region were identified by genome sequencing, followed by confirming the mutation that is causative to the phenotype of interest.

4.3.5.1 Verification of Bulk Segregant Analysis

Previous BSA data indicated that the gene locus of Mut 21 is on the top arm of *Arabidopsis* chromosome one (Teh, 2007). Another independent BSA was performed with a different set of markers to validate the genetic linkages in Mut 21 (Table 4.1; Figure 4.8). Similar to previous findings, linkages were observed on the top arm of chromosome one and the bottom arm of chromosome five. Specifically, over-representation of the Col alleles was observed in markers F21M12, F20D23 and ciw12 on chromosome one; ciw9, MPL12 and K9P8 on chromosome five (Figure 4.8). Since it has been reported that the linkage on chromosome five was associated to the secGFP transgene in the secGFP (S76) line (Teh, 2007), the location of Mut 21 gene locus on chromosome one has been confirmed by two independent BSA.

Table 4.1. Comparison of BSA markers used in Teh, 2007 and in this study

Chromosome	Marker used in Teh, 2007	Marker used in this study
I	F21M12	F21M12
	ciw12	F20D23
	ciw1	ciw12
	nga280	NF514a
	ATPASE	
II	ciw2	F18P14
	PLS2	nga1126
	nga1126	nga168
	nga168	
III	nga162	nga172
	ciw11	N7N14
	ciw4	T6H20
	nga6	K27K19
IV	ciw5	ciw5
	nga1111	F14G16
	ciw7	F6E21
	nga1107	
V	CTR1	nga151a
	ciw8	PHYC
	PHYC	ciw9
	ciw9	K9P8
	ciw10	MNC17

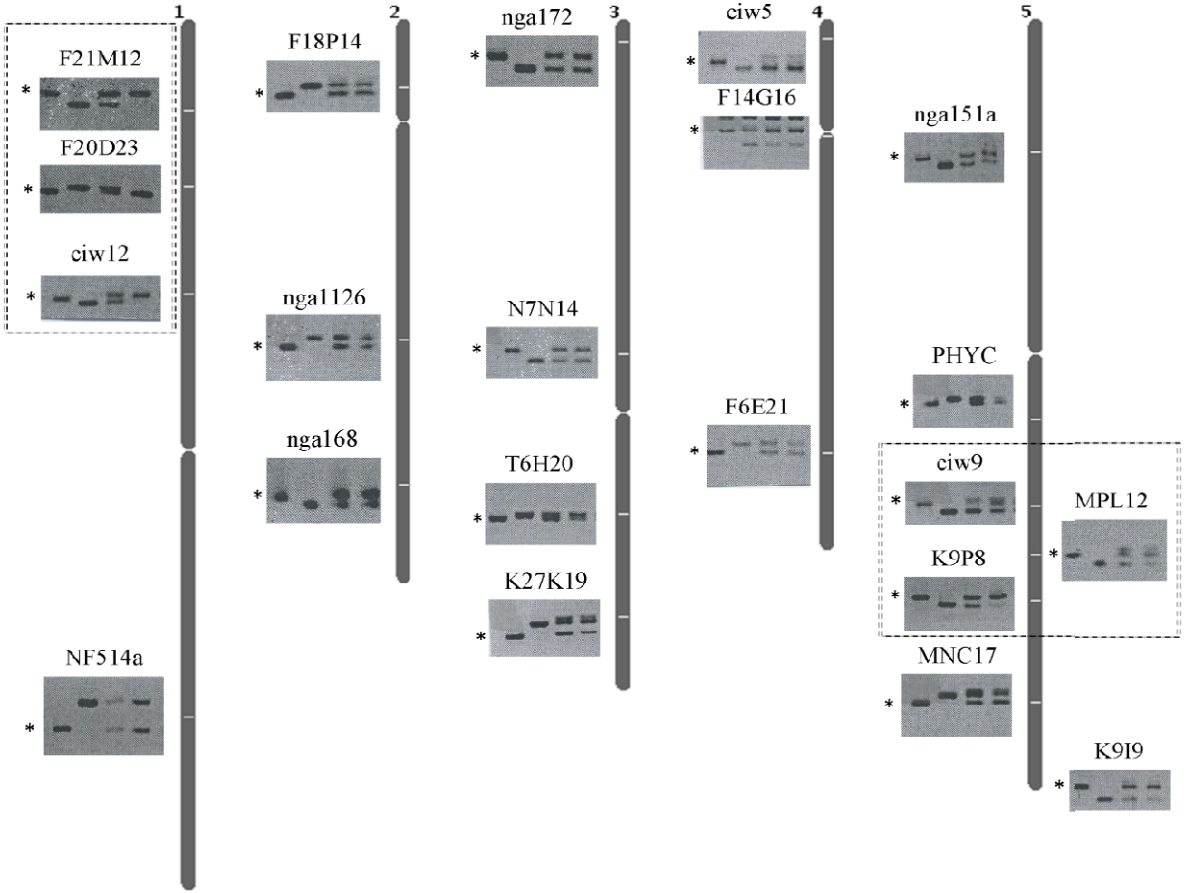

Figure 4.8. Verification of bulk segregant analysis

A set of 21 genetic markers were used to verify previous BSA results. In each gel image, the first two lanes from the left re present wild type Col and L*er*, respectively. The third lane represents the mapping cross F1 population which is heterozygous. The fourth lane represents the mapping cross F2 homozygous Mut 21 population. Consistent with previous findings, Mut 21 shows linkage to the Col-specific alleles on chromosome one and five (boxed area). Asterisks indicate PCR fragments corresponding to the Col-specific allele of each marker.

4.3.5.2 Fine-mapping

The next step was to identify a starting point for fine-mapping. Based on the BSA data (Figure 4.8), I hypothesized that the mutation was between F21M12 and F7P12 which is located between F20D23 and ciw12 on chromosome one. Flanking markers of Mut 21 were determined based on the recombination frequencies between Mut 21 and the two putative flanking markers. As shown in Table 4.2, the recombination frequency between F21M12 and Mut 21 was four-fold less than that between F7P12 and Mut 21, so the mutation was closer to F21M12 in terms of genetic distance and it could be on either side of F21M12 (Figure 4.9). Since the sum of the recombination frequencies between F12M12 and Mut 21 (5.71cM) and between Mut 21 and F7P12 (20.4cM) was almost equal to the recombination frequency between F21M12 and F7P12 (23.7cM), it was more plausible that Mut 21 was between the two markers similar to Figure 4.9b. Hence, it was concluded that F21M12 and F7P12 were indeed the flanking markers of Mut 21.

Table 4.2. Determination of flanking markers for fine-mapping

	Number of recombinants	Total number of chromosomes	Recombination frequency (%)	Genetic distance (cM)
Mut 21 and F21M12	25	438	5.71	5.71
Mut 21 and F7P12	87	426	20.4	20.4
F21M12 and F7P12	100	422	23.7	23.7

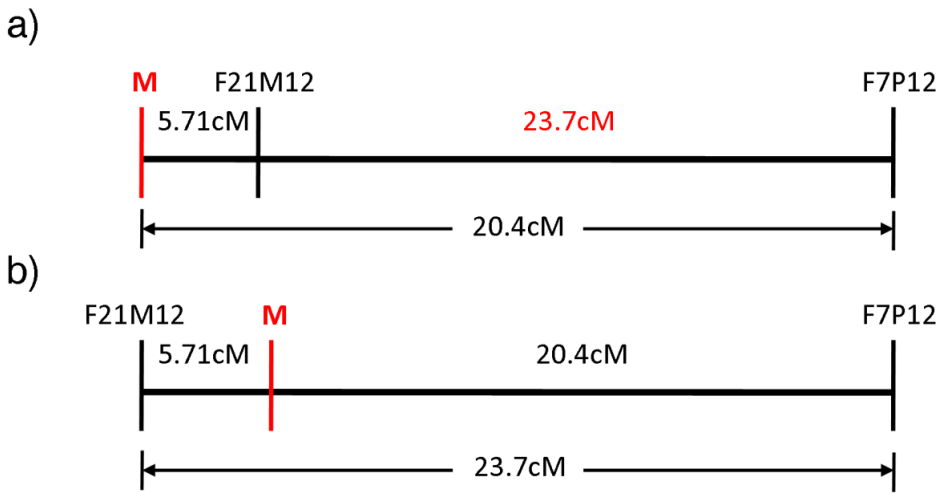

Figure 4.9. F21M12 and F7P12 are the flanking markers of Mut 21 that mark the starting points for fine-mapping

Mut 21 gene locus (M) is 5.71cM and 20.4cM from F21M12 and F7P12, respectively. Since Mut 21 gene locus is closer to F21M12, Mut 21 gene locus can be on either side of F21M12 (a or b). The scenario in (a) suggests that the genetic distance between F21M12 and F7P12 is ~14.69cM, which is inconsistent with experimental value of 23.7cM. Meanwhile, the scenario in (b) is more consistent to the experimental value as the calculated genetic distance between the two markers is ~26.11cM. Hence, it is concluded that F21M12 and F7P12 are the flanking markers of Mut 21.

All 499 individuals in the mapping population were analyzed for recombination using genetic markers between F21M12 and F7P12 (Table 4.3). As the markers were positioned closer to the mutation, fewer recombinants were found (Figure 4.10; Table 4.3 and 4.4). Eventually, only one recombinant was found on F17F16 (above the mutation) and F20D23 (below the mutation). The physical distance between F17F16 and F20D23 was about 170kB with 74 predicted gene loci in the region.

Table 4.3. Genetic markers for fine-mapping Mut 21

Marker	Type	Start position	Number of recombinant chromatids	Total number of chromatids
F21M12	SSLP	3212189	25	448
F3F19	SSLP	4507836	14	448
T24D18	SSLP	5487434	2	998
F19K19	SSLP	5722172	1	998
F17F16	CAPS	5721172	1	998
PERL42164	dCAPS	5803149	0	998
PERL42230	dCAPS	5215283	0	998
F20D23	SSLP	5889509	1	998
F11A6	CAPS	6090186	1	998
F15H18	SSLP	6327111	3	998
F6A14	CAPS	6510519	4	998
T26F17	SSLP	7729031	50	998
T17H3	SSLP	9559718	25	448
F7P12	SSLP	12535670	87	448

Table 4.4. Fine-mapping results of Mut 21

Marker	F21M12	T24D18	F19K19	F17F16	PERL42164	PERL42230	F20D23	F11A6	F15H18	F6A14	T26F17	T17H3
Plant ID												
3	C						C				C	
4	C						C					
7	C						C					
8	C						C					
9	C											
10	C						C					
13	C						C					
14	C						C					
23	H						C			C	H	H
24	H	C					C					
31	C						C			C	H	H
39	H	H	H	H	C	C	C	C			C	
43	C						C			C	H	H
54	C						C	C	H	H	H	H
64	C						C			C	H	
66	C						C			C	H	C
71	C						C			C	H	C
73	C						C			C	H	C
75	H	H	C	C			C				C	C
78	C						C				C	H
85	C						C			C	H	
96	C						C			C	H	H
97	C						C					
98	C						C			C	H	
99	C						C					
107			C	C	C	C	H	H	H		H	
108			C						C		H	
111			C						C		H	

117			C						C		H	
118			C						C		H	
121			C						C		H	
123			C						C		H	
126			C						C		H	
130			C						C		H	
133			C						C		H	
150			C						C		H	
168			C						C		H	
173			C						C		H	
185			C						C		H	
223	C						C			C	H	H
224	C						C				C	C
233	C						C			C	H	H
251	C						C	C	C	H	H	H
252	C						C	C	H	H	H	H
331		C							C		H	
332		H	C								C	

A subset of recombinants in the total mapping population was shown, including the only recombinants for F17F16 and F20D23. C represents Columbia non-recombinants; H represents heterozygous recombinants. Grey area represents genotype not determined; yellow area represents the mapping interval.

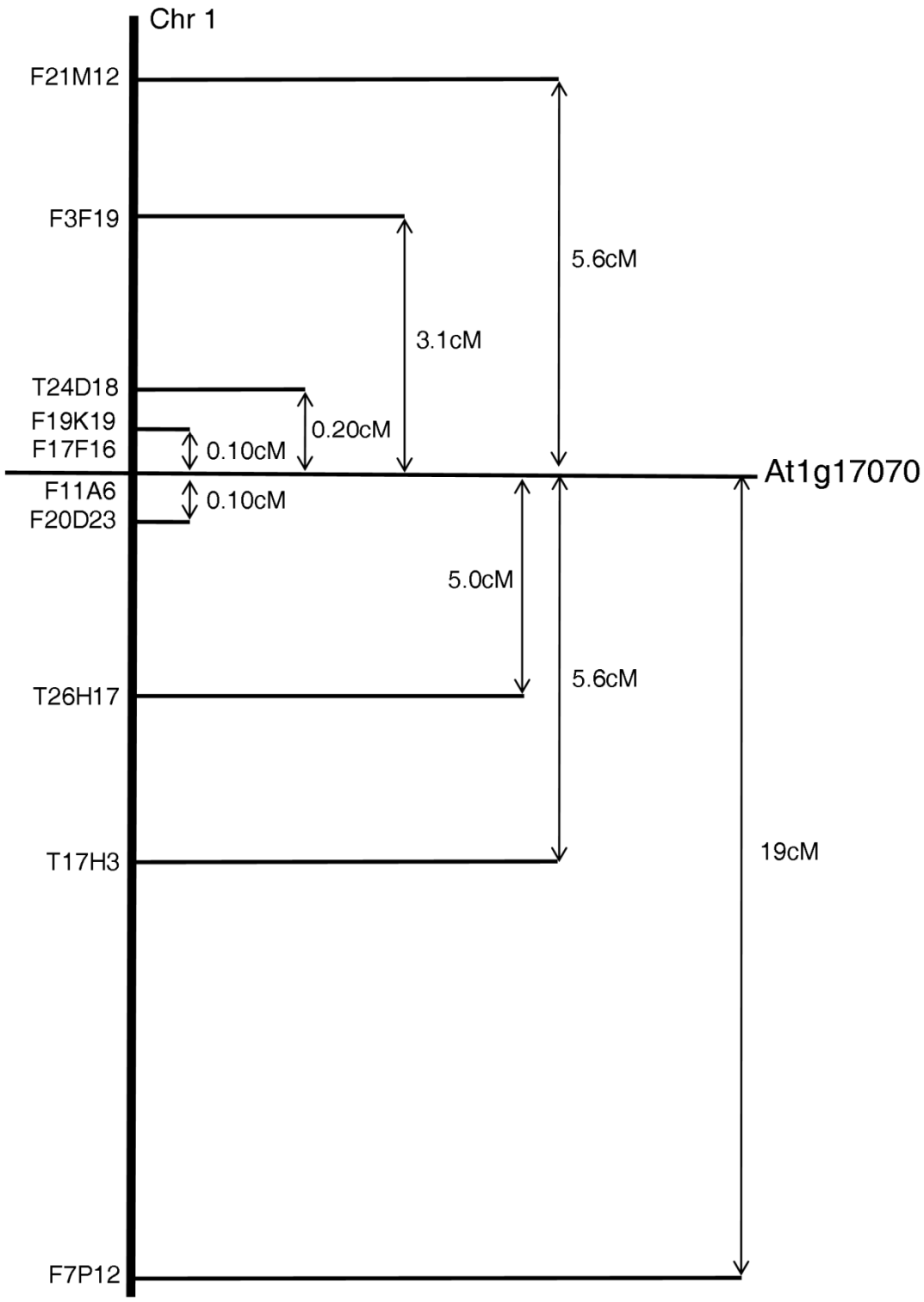

Figure 4.10. Fine-mapping results of Mut 21

Genetic distance of each genetic marker (in cM) was calculated based on the percentages of recombinants chromatids in a mapping population of 224 plants (for F12M12, F3F19, T17H3 and F7P12) or 499 plants (for T24D18, F19K19, F17F16, F20D23, F11A6, F15H18, F6A14 and T26H17).

4.3.5.3 Identifying mutation within the mapping interval through whole genome sequencing

The gene locus of Mut 21 was determined by whole-genome resequencing to identify polymorphisms in the mapping region. DNA samples from 24 homozygous mutants from a backcross family were pooled and sequenced using Illumina sequencing-by-synthesis technology. After low-quality reads have been filtered out, 118 million reads provided ~60x coverage of the *Arabidopsis* genome and were aligned to the reference Col-0 genome (available on TAIR). One insertion and three single nucleotide polymorphisms (SNPs) were identified within the mapping region in Mut 21 genome (Figure 4.11; Table 4.5). The gene locus At1g17000 had a silent G to A mutation on the first exon (Figure 4.11a); At1g17060 had an insertion on the fourth intron (Figure 4.11b); At1g17070 had a nonsense G to A mutation that changed a codon for tryptophan to a stop signal (Figure 4.11c); At1g17110 had a missense C to T mutation that changed a proline to a leucine (Figure 4.11d). Since mutations on the last two loci resulted in a change in amino acid or a truncated protein, they were selected as the candidate genes.

At1g17070 encodes for tuftelin-interacting protein 11 (TFIP11), which is predicted to have three domains according to the Pfam database (http://pfam.sanger.ac.uk/). The point mutation in Mut 21 is located in the GC-rich DNA-binding factor-like protein domain (Figure 4.12a), thus resulting in truncation of this domain. Meanwhile, At1g17110 encodes for ubiquitin-specific protease 15 (UBP15), which consists of a zinc finger at the N-terminal region in addition to the main ubiquitin hydrolase domain (Liu et al., 2008). The point mutation is situated between the two domains (Figure 4.12b).

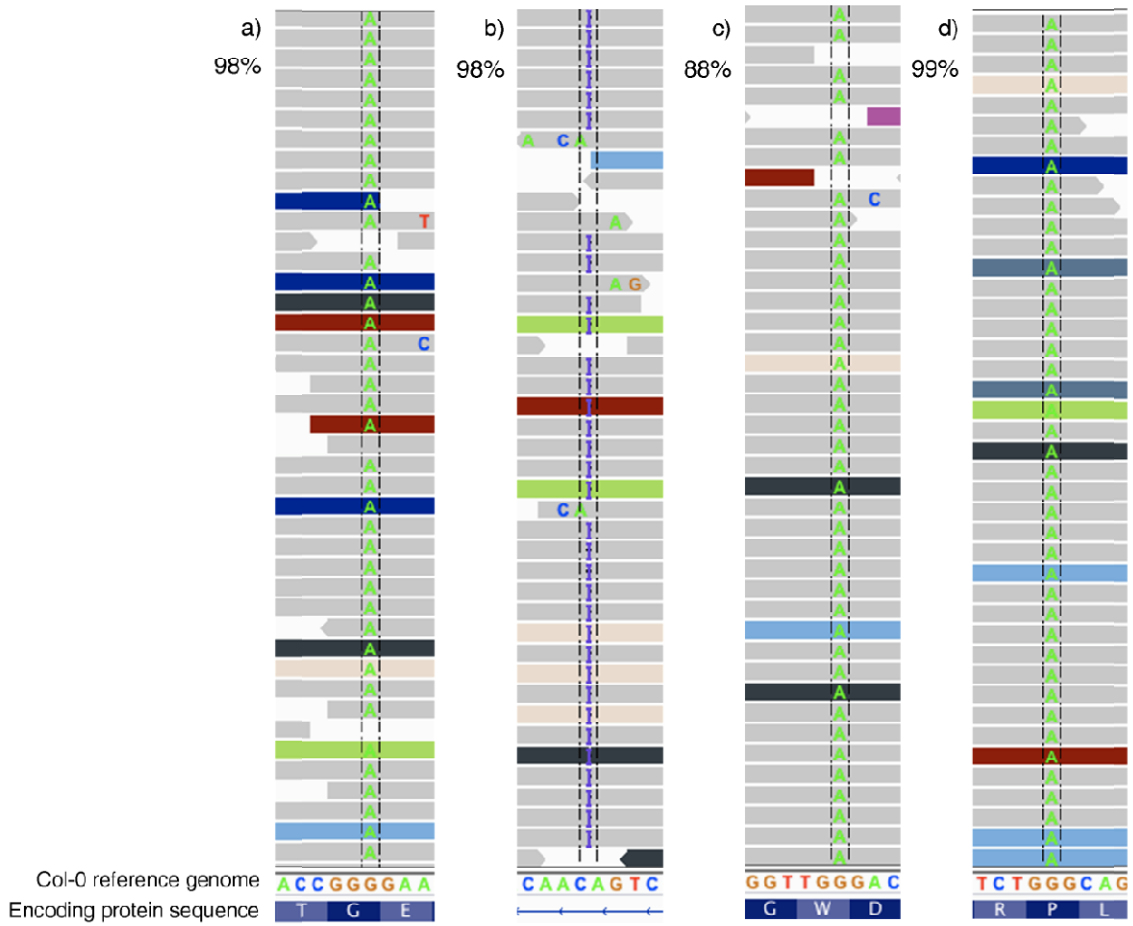

Figure 4.11. Four polymorphisms are found on gene loci within the final mapping interval

Screenshots of a subset of sequence reads that show the polymorphisms on At1g17000 (a), At1g17060 (b), At1g17070 (c) and At1g 17110 (d). The Col-0 reference genome is shown at the bottom along with the corresponding coded amino acid residues except for (b) where a nucleotide is inserted in an intron. The percentage values represent the percentages of aligned reads that show the indicated polymorphism.

Table 4.5. Polymorphisms in the mapping region

Gene name	Position on chromosome one	Part of gene	Mutation	Change in amino acid residue
At1g17000	5812811	1st exon	G → A	None
At1g17060	5833053/4	4th intron	T insertion	None
At1g17070	5839038	1st exon	G → A	W → Stop
At1g17110	5848490	4th exon	C → T	P → L

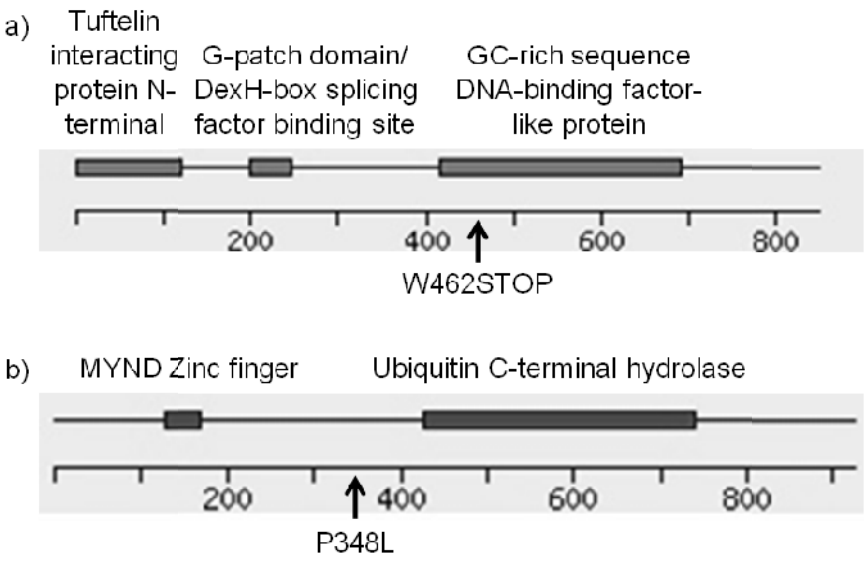

Figure 4.12. Domains of proteins encoded by At1g17070 (TFIP11) and At1g17110 (UBP15)

Schematic diagrams of TFIP11 (a) and UBP15 (b). The mutated amino acid residues in Mut 21 are shown.

4.3.5.4 Complementation experiments

The genetic cause to the phenotypes in a monogenic recessive mutant like Mut 21 can be identified by complementation experiments, in which genetic materials are introduced into the mutant to see whether the WT phenotype can be restored. Molecular complementation involves cloning the WT allele on the candidate gene locus and transforming to the mutant. If the mutant is complemented by the transgene, the tested locus is causative to the mutant phenotype. Meanwhile, genetic complementation exchanges genetic materials through cross-fertilization. In plants, recessive mutant alleles of the candidate gene locus are cross-pollinated to the mutant. If there is no complementation in the F1 progeny, then it can be said that both mutants belong to the same complementation group and they are likely to be allelic.

To identify the causative mutation, I made use of the independent alleles at the two candidate loci. *rrd4* is the only point mutation allele of At1g17070 that has been characterized (Sugiyama, 2003). Interestingly, it is a temperature-sensitive mutant that also experiences growth retardation at restrictive temperature and was characterized as a root and hypocotyl redifferentiation mutant (Sugiyama, 2003). The missense mutation of *rrd4* is located one nucleotide upstream of Mut 21, resulting in identical tryptophan to stop codon mutation in the coding sequence (M Sugiyama, personal communication). For At1g17110, two T-DNA knockout mutant alleles have been described. Both mutant alleles, *ubp15-1* and *ubp15-2*, had flat rosettes, narrow and serrated leaves (Liu et al., 2008).

To test for complementation of the secGFP accumulation phenotype of Mut 21, homozygous plants were used to pollinate emasculated *rrd4*, *ubp15-1* and *ubp15-2*. The F1 progenies were grown for seven days and were observed after a further 24h at restrictive temperature (Figure

4.13). The number of F1 individuals from each cross with enhanced fluorescence was summarized in Table 4.6. All 60 *ubp15* Mut 21 seedlings had similar growth as secGFP-expressing WT (Figure 4.13a, d and e), and did not exhibit the enhanced fluorescence phenotype (Figure 4.13i and j). Hence, Mut 21 was genetically complemented by *ubp15*. In contrast, all seven Mut 21 *rrd4* seedlings showed a similar degree of growth reduction as homozygous Mut 21 mutants (Figure 4.13b and c). Also, enhanced fluorescence phenotype was observed in the F1 plants, with secGFP labelling the apoplast in the cotyledons similar to Mut 21 (Figure 4.13g and h).

PCR genotyping markers were used to confirm that the crosses were successful and the observed F1 plants had the expected alleles (Table 4.7). The *rrd4* marker was a dCAPS marker whose artificial *ApaI* restriction site is disrupted by the point mutation in *rrd4* (M Sugiyama, personal communication). Meanwhile, the Mut 21 marker was a CAPS marker in which one of the two *AvaII* restriction sites was disrupted by the Mut 21 point mutation. As expected, both mutant alleles were present in all seven F1 progenies of the *rrd4* x Mut 21 cross (Figure 4.14). Hence, *rrd4* failed to complement Mut 21 and its mutation in the At1g17070 gene locus was causative to the phenotypes observed in Mut 21.

Molecular complementation experiments were initiated using a 5.2kb fragment of WT DNA from the At1g17070 locus. This fragment encompasses the 5’ untranslated region, the coding region and the 3’ untranslated region of At1g17070 and was cloned to the binary vector pBIN+. But due to time-constraints, the molecular complementation experiment of Mut 21 was incomplete.

Table 4.6. Genetic complementation results

Associated locus	Cross (female ♀ x male ♂)	Number of seeds examined	Seedlings with enhanced fluorescence
At1g17070	*rrd4* x Mut 21	7	7
At1g17110	*ubp15-1* x Mut 21	34	0
	ubp15-2 x Mut 21	26	0

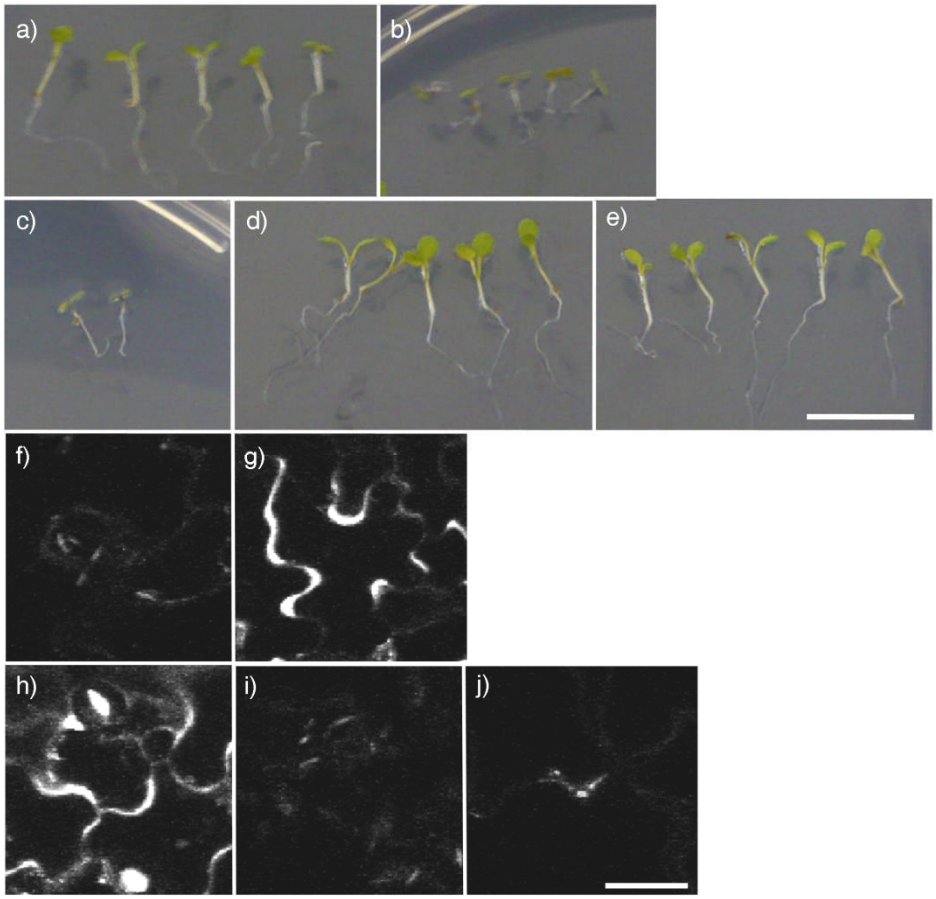

Figure 4.13. Genetic complementation of Mut 21

Bright-field images of whole seedlings (a to e) and confocal images of cotyledons (f to j) of WT seedlings expressing secGFP (a and f), Mut 21 (b and g), Mut 21 *rrd4* (c and h), Mut 21 *ubp15-1* (d and i) and Mut 21 *ubp15-2* (e and j). All seedlings were treated at 31˚C for 24h before imaging.

Bar= 1cm in (d) and 20µm in (j)

Table 4.7. Genotyping markers for At1g17070 mutant alleles

	Forward Primer	Reverse Primer*	Restriction Enzyme	WT Bands (bp)**	Mutant Bands (bp)**
rrd4	CGCTGGACTCACTTGC TATTCG	CACTGCATCACTAA GAGGGGCC	*ApaI*	18, 134	152
Mut 21	AGGAAGAGAAACAAA AAAGACAC	TTGGCTATAAGGCG TTGAGA	*AvaII*	102, 111, 122	122, 213

* Red letters represent mismatches between the primer and the template to create a restriction site on the WT allele

** Expected fragment sizes after restriction digestion of PCR products

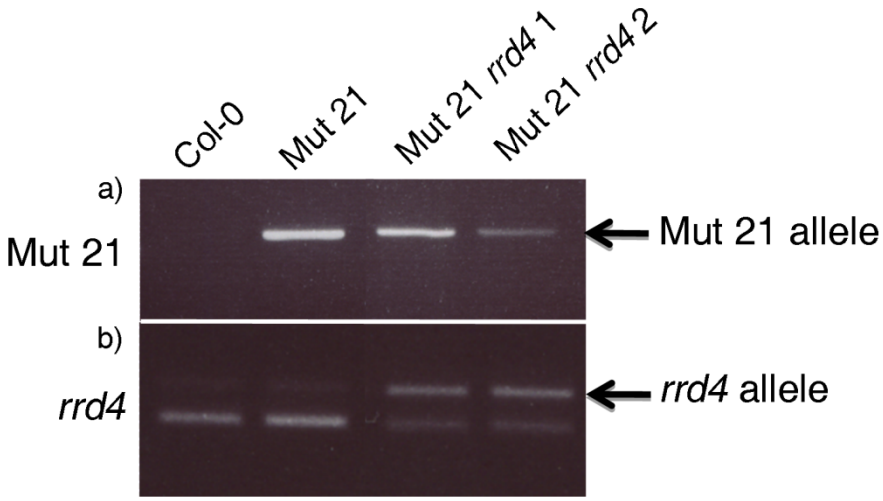

Figure 4.14. PCR genotyping of Mut 21 *rrd4*

Col-0, Mut 21 and the two F1 seedlings generated from the *rrd4* x Mut 21 cross were genotyped using PCR genotyping markers for the Mut 21 allele (a) and the *rrd4* allele (b). Bands that correspond to the mutant alleles are indicated by arrows.

4.3.5.5 Domain analysis of TFIP11

TFIP11 has a paralogue in *Arabidopsis* that is encoded by the gene locus At2g42330. Alignment of the two protein sequences revealed high degree of similarity between the two proteins (Figure 4.15), strongly suggesting an occurrence of a gene duplication event. The *Arabidopsis* TFIP11 protein sequence was also aligned with some common homologs in human (TFIP11), mouse (TFIP11) and *C. elegans* (STIP1) with the Cobalt constraint-based multiple protein alignment tool (http://www.ncbi.nlm.nih.gov/tools/cobalt/) (Figure 4.16a). Although the G-patch domain may not appear to be more conserved than the intergenic region at first glance, the key features of the domain are the six highly conserved glycine residues and the signature motif that contains five of the conserved glycine- hhxxxGaxxGxGhGxxxxG (h is hydrophobic residues (ILVM), a is aromatic residues (FYW) and x is any residues) (Aravind and Koonin, 1999). These elements are all present in *Arabidopsis* TFIP11. Furthermore, alignment of the GC-rich sequence DNA-binding factor-like domain of *Arabidopsis* TFIP11 with the domain's consensus sequence from other species reveals high degree of similarity between the two (Figure 4.16b). The mutated tryptophan in Mut 21 is a highly conserved residue in the GC-rich DNA-binding factor-like domain.

```
At1g17070       MDEYQDMERFSMDNDYEGGRWEGDEFVYQKRKEKRKQTKNDATYGIFAESDSDSDDSGGG 60
At2g42330       M--------------------GDEG----KKEKRRQTKEDAVYGFVFESDSNSDDSGG- 34
                *                     ***     :****:***:**.**:. ****:******

At1g17070       GSRRKRRKDRDSGRKADLTKPVNFVSTGTVMPNQEIDKDSREHNDEKDRDKIEDNDMIDE 120
At2g42330       -SRRKKRRK---------TKPVKFSSAGNI---DQVLKQNRGNC------KIDEND---- 71
                 ****:*:.         ****:* *:*.:   ::: *:.* :       **::**

At1g17070       DVEVRGGLGIGSSGLGLGFNANGFDDEDNLLPGALGKKIADRAKMRGKAKVEKRGQEGGG 180
At2g42330       -------------------------DTILPIALGKKIADKAHVR-------------- 90
                                         *.:** ********:*::*

At1g17070       AKGGKKNTLGSDIGQFEKSTKGIGMKLLEKMGYKGGGLGKNQQGIVAPIEAQLRPKNMGM 240
At2g42330       EKNNKKEN-------FEKFSGGIGMKLLEKMGYKGRGLGKNQQGIVAPIEVQLRPKNMGM 143
                 *..**:.       *** : ************** **************.*********

At1g17070       GYNDFKEAK---LPDLKKVEEKK-IIGVSVSENEQSHGDRGGKNLWKKKKVRKAVYVTAE 296
At2g42330       GYNDFKEKNAPLFPCLNKVEEKKKSVVVTVSEN---HGD-GRRDLWKKKNVRKEVYITAE 199
                ******* :   :* *:******  : *:****   *** * ::*****:*** **:***

At1g17070       ELLEKKQEAGFGGGQTIIDMRGPQVRVVTNLENLDAEEKAKEADVPMPELQHNLRLIVDL 356
At2g42330       EFLGKKQEEGFGCDQLIIDKRGPQDRVVNSLRNLYAEEKATDANVQQPELQHNLRFIVKS 259
                *:* **** *** .* *** **** ***..*.** *****.:*:*  ********:**.

At1g17070       VEHEIQKIDRDLRNERESALSLQQEKEMLINEEEKQKRHLENMEYIADEISRIELENTSG 416
At2g42330       LEHGILKTDKDLRNEKGLALSLQQEKEKFKMGVKKQKTLFDNLGYVAEEIDRIEVEIASG 319
                :** * * *:*****:  ******** :    :***  ::*: *:*:**.***:* :**

At1g17070       NLTLDSLAIRFEDLQTSYPDDYKLCSLSTIACSLALPLFIRMFQGWDPLSDAVHGLKAIS 476
At2g42330       NLTLDSLANRFKDLRSSYPDDYKCCNLSCIASSLALPLFIRMFQGWDPLSDAEHGIEAIS 379
                ******** **:**::******* *.** **.****************** **::***

At1g17070       SWRKLLEVEEDHNIWVVSTPYSQLVSEVVLPAVRIAGINTWEPRDPEPMLRFLETWETLL 536
At2g42330       SWKMLLEVEDNQSI---STPYSQLVSEVILPAVRVSGINTWEPRDPEPMLRLLETWEKML 436
                **: *****:::.*   ***********:*****::***************:*****.:*

At1g17070       PSSVLQTILDTVVLPKLSTAVEYWDPRRELVAIHVWVHPWLPILGQKLEFLYQIIQMKLS 596
At2g42330       PSLIFETILTTVVLPKLSIAIESWEPRLETVPIHFWVHPWLPVLGQKLESAYQIIRMKFG 496
                ** :::*** ******** *:* *:** * *.**.*******:******  ****:**:.

At1g17070       NVLDAWHPSDSSAYTILSPWKTVFDTTSWEQLMRRYIVPKLQLALQEFQVNPANQNLERF 656
At2g42330       NLLDAWHPSDVSVHTILSPWKTVFDAASWEQLMRRYIVPKLQVALQEFQINPADQNLDEF 556
                *:******** *.:**********::***************:******:***:***:.*

At1g17070       DWVMKWASAVPIHLMADMMERFFFPKWLDVLYHWLRAKPRFEEIQGWYYGWKELFPQELT 716
At2g42330       NLVMGWVSSVPIHLMTDLMERFFFPKWLDVLYHWLCSEPKFDEIMKWFLGWKGTFPQELS 616
                : ** *.*:******:*:***************** ::*:*:**  *: ***  *****:

At1g17070       ANERIRIQLKRGLDMLMEAVEGVEVSQPRA-------KANERTQSVPAQAQAQAKAQMDS 769
At2g42330       ANRRIEIQFKRGLDMAREAVERMEMSQPGARENISYHKAQEQRQS---EGRAKVQAQVDD 673
                **.**.**:******  **** :*:*** *       **:*: **   :.:*:.:**:*.

At1g17070       TEVLSLKEVLEVFAQEQELLFKPKPNRMHNGLQIYGFGNVSVIIDSVNQKLLAQKDGGWF 829
At2g42330       PEELSFKEAVELFAQEKELLLKPKPHRMHNGLQIYRFGNVSVLLDSANSKLLAQEEGRWF 733
                .* **:**.:*:****:***:****:********* ******::**.*.*****::* **

At1g17070       LVTPDDLLRMHNNTTVSAKR 849
At2g42330       PVDLDSLLKMH-YSAVTGKQ 752
                 *  *.**:**  ::*:.*:
```

Figure 4.15. Alignment of *Arabidopsis* TFIP11 (At1g17070) and its paralogue At2g42330

Asterisks (*) indicate identical residues; semi-colon (:) and period (.) indicate conserved and semi-conserved substitutions, respectively. The mutated amino acid residue of Mut 21 is highlighted in yellow.

a)

```
Human          MSLSHLYRDGEGRIDDDDD-ER----ENFEITDWDLQNEF--NPNRQRHWQTKEEATYGV 53
Mouse          MSLSHLYRDGEGHLDDDDDDER----ENFEITDWDLQNEF--NPNRQRHWQTKEEATYGV 54
A.thaliana     ------------MDEYQDMERFSMDNDYEGGRWE-GDEFVYQKRKEKRKQTKNDATYGI 46
C.elegans      M--------------EDDDGR----ESFEINDMDL--EYAMNPGGRRRFQNKDQATYGV 39
                                :*  *    :.:*    :   *:  :   .:: *.*::****:

Human          WAERDSDDERPSFGGKRAR-----------DYSAPVNFISAG-------LKKGAAEEAEL 95
Mouse          WAERDSDEERPSFGGKRAR-----------DYSAPVNFISAG-------LKKGAAEEADS 96
A.thaliana     FAESDSDSDDSGGGGSRRKRRKDRDSGRKADLTKPVNFVSTGTVMPNQEIDKDSREHNDE 106
C.elegans      FAP-DSDDDDDEQGTSRGPYKK------RSKISAPMSFVSGG-IQQGNKIDKDDPASLNL 91
               :*  ***.:    * .*             . : *:.*:* *       :.*.     :

Human          EDSDD-EEKPVKQDD----------------------------FPKDFGPR---KLKTG 122
Mouse          EDSDA-EEKPVKQED----------------------------FPKDLGPK---KLKTG 123
A.thaliana     KDRDKIEDNDMIDEDVEVRGGLGIGSSGLGLGFNANGFDDEDNLLPGALGKKIADRAKMR 166
C.elegans      NLGGE--KKPKEDDE----GSIQID------------FDKRTKKAPKQNGAQVFAGMRSS 133
               :  .   .:   :::                              *   * :    :

Human          GNFKPSQKG-----FAGGTKSFM--DFGSWERH--TKGIGQKLLQKMGYVPGRGLGKNAQ 173
Mouse          GNFKPSQKG-----FSGGTKSFM--DFGSWERH--TKGIGQKLLQKMGYVPGRGLGKNAQ 174
A.thaliana     GKAKVEKRGQEGGGAKGGKKNTLGSDIGQFEKS--TKGIGMKLLEKMGYK-GGGLGKNQQ 223
C.elegans      ANHGAADINQ---------------FGSWMRGDGNSNKIMKMMQAMGYKPGEGLGAQGQ 177
               .:    . .                :*.: :   ...   *::: ***  * *** : *

Human          GIINPIEAKQRKGKGAVGAYGSERT--------T---------QSMQDFPVVDSEEEAEE 216
Mouse          GIINPIEAKQRKGKGAVGAYGSERT--------T---------QSLQDFPVADSEEEAEE 217
A.thaliana     GIVAPIEAQLRPKNMGMGYNDFKEA--------KLPDLKKVEEKKIIGVSVSENEQSHGD 275
C.elegans      GIVEPVQAQLRKGRGAVGAYGKESTATGPKFGESAADAQK--RMAQEGTSSRPTNDDQEK 235
               **: *::*: *  . .:*  . : :         .             . .   .::.  .

Human          EFQKELSQWRKDPSGSKKKPKYSYKTVEELKAKGRISKKLTAPQK--ELSQVKVIDMTGR 274
Mouse          EFQKELSQWRKDPSGSKKKPKYSYKTVEELKAKGRVSKKLTAPQK--ELSQVKVIDMTGR 275
A.thaliana     RGGKNL--WKK-----KKVRKAVYVTAEEL-----LEKKQEAGFG----GGQTIIDMRGP 319
C.elegans      SGLKIKGSWKK-----SQTVKTKYRTIEDVMEEGMSASRPASHQQSQQYSNIKVIDMTGK 290
                  *    *:*     .:  *  * * *::       .:  :       .  .:*** *

Human          EQKVYYSYSQISHKHNVPDDGLPLQSQQLPQSGKEAKAPGFALPELEHNLQLLIDLTEQE 334
Mouse          EQKVYYSYSQISHKHSVPDEGVPLLAQLPPTAGKEARMPGFALPELEHNLQLLIERTEQE 335
A.thaliana     QVRVVTNLENLDAEEKA---------------KEADVP---MPELQHNLRLIVDLVEHE 360
C.elegans      QQKIYSGYDSFSMKTRSEYDTVD----------DEERTVFDVPELIHNLNLLVDLTEEG 339
               : ::  . ..:. :                   :   .   :*** ***.*::: .*.

Human          IIQNDRQLQYERDMVVNLFHELEKMTEVLDHEERVISNLSKVLEMVEECERRMQPDCSNP 394
Mouse          IIQSDRQLQYERDMVVSLSHELEKTAEVLAHEERVISNLSKVLALVEECERRMQPHGADP 395
A.thaliana     IQKIDRDLRNERESALSLQQEKEMLINEEEKQKRHLENMEYI---ADEISRIELENTSGN 417
C.elegans      IRRSNQQLISLKDQTTALEYDLQQVQKSLGTEEQEAQHIKDVYELIDGFS------SNRS 393
               * : :::*   :: .  *  : :   :    :::  .::. :    :  .

Human          LTLDECARIFETLQDKYYEEYRMSDRVDLAVAIVYPLMKEYFKEWDPLKDCTYGTEIISK 454
Mouse          LTLDECARIFETLQDKYYEEYRLADRADLAVAIVYPLVKDYFKDWHPLEDGSYGTQIISK 455
A.thaliana     LTLDSLAIRFEDLQTSYPDDYKLCSLSTIACSLALPLFIRMFQGWDPLSDAVHGLKAISS 477
C.elegans      PSMEECQELFRRLRSEFPHEYELYSLETVAIPTVLPLIQKYFVAWKPLEDKNYGCELIST 453
                :::.    *. *: .: .:*.: .   :* . . **.   *  *.**.*  :* : **.

Human          WKSLLENDQLLSHGGQD------LSADAFHRLIWEVWMPFVR-NIVTQWQPR-NCDPMVD 506
Mouse          WKSLLENDQLLSHSSQD------LSSDAFHRLMWEVWMPFVR-NVVAQWQPR-NCEPMVD 507
A.thaliana     WRKLLEVEEDHNIW---------VVSTPYSQLVSEVVLPAVRIAGINTWEPR-DPEPMLR 527
C.elegans      WRDILDDSKNGRKMTFGHNKTKGDEIRAYDRIIWEGILPSIR-RACLQWDPSTQMHEMIE 512
               *:.:*: .:                .: ::: *  :* :*      *:*  : . *:

Human          FLDSWVHIIPVWILDNILDQLIFPKLQKEVENWNPLTDTVPIHSWIHPWLPLMQARLEPL 566
Mouse          FLDSWAHIIPVWILDNILDQLIFPKLQKEVDNWNPLTDTVPIHSWIHPWLPLMQARLEPL 567
A.thaliana     FLETWETLLPSSVLQTILDTVVLPKLSTAVEYWDPRRELVAIHVWVHPWLPILGQKLEFL 587
C.elegans      LVEQWIPLLSAWITENILEQLVVPKIAERVNQWDPMTDEIPIHEWLVPWLVLLGDRIQTV 572
               ::: *  ::.  : :.**: ::.**:   *: *:*  : :.** *: *** ::  ::: :
```

```
Human          YSPIRSKLSSALQKWHPSDSSAKLILQPWKDVFTPGSWEAFMVKNIVPKLGMCLGELVIN 626
Mouse          YSPVRSKLSSALQKWHPSDASAKLILQPWKEVLTPGSWEAFMLRNIVPKLGMCLGELVIN 627
A.thaliana     YQIIQMKLSNVLDAWHPSDSSAYTILSPWKTVFDTTSWEQLMRRYIVPKLQLALQEFQVN 647
C.elegans      MPPIRQKLSKALKLWDPMDRSALETLRPWQNVWSAATFSAFIAQNIVPKLGVALDTMELN 632
                  :: ***..*. *.* * **   * **: *  . ::. :: : ***** :.*  : :*

Human          PHQQHMDAFYWV--IDWEGMISVSSLVGLLEKHFFPKWLQVLCSWL-SNSPNYEEITKWY 683
Mouse          PHQQHMDAFYWV--MDWEGMISVSSLVGLLEKHFFPKWLQVLCSWL-SNSPNYEEITKWY 684
A.thaliana     PANQNLERFDWV--MKWASAVPIHLMADMMERFFFPKWLDVLYHWL-RAKPRFEEIQGWY 704
C.elegans      P-TMNPEYPEWTACMEWLEFTHPDAIANIVTKYFFPRFYNCLCLWLDSPGVDYNEVKRWY 691
               *   : :   *.  :.*        :.:: :.***:: : *  **      ::*:  **

Human          LGWKSMFSDQVLAHPSVKDKFNEALDIMNRAVSSNVGAYMQPGARENIAYLTHTERRKDF 743
Mouse          LGWKSMFSDQVLAHPSVKDKFNEALDIMNRAVSSNVGAYMQPGARENIAYLTHTERRKDF 744
A.thaliana     YGWKELFPQELTANERIRIQLKRGLDMLMEAVEGV--EVSQPRAKAN-------ERTQSV 755
C.elegans      GSWKARIPQVLVNYPTVNENLRRSMIAIGRSLQG-------------------EKVGGL 731
                .**  :.: :     :. ::...:  : .::..                    *:  ..

Human          QYEAMQERREAENMAQRGIGVAASSVPMNFKDLIETKAEEHNIVFMPVIGKRHEGKQLYT 803
Mouse          QYEAMQERREAENMAQRGIGVAASSVPMNFKDLIETKAEEHNIVFMPVIGKRHEGKQLYT 804
A.thaliana     PAQA-----QAQAKAQMD-----STEVLSLKEVLEVFAQEQELLFKPKPNRMHNGLQIYG 805
C.elegans      QATPIAPMAPPPPMAPHFTQ-AAPVQKLSLKEIIEYTAGKNGFTYHPQKDRYKDGRQVFW 790
                  .      .   *        .   :.:*:::*  * :: : : *  .: ::* *::

Human          FGRIVIYID--RGVVFVQGEKTWVPTSLQSLIDMAK-------- 837
Mouse          FGRIVIYID--RGVVFVQGEKTWVPTSLQSLIDMAK-------- 838
A.thaliana     FGNVSVIIDSVNQKLLAQKDGGWFLVTPDDLLRMHNNTTVSAKR 849
C.elegans      FGALSIYLDSEMVYVMDPIEFVWRPSGLNELIQMAQG----AQG 830
               ** : : :*     ::   :  *     :.*: * :
```

b)

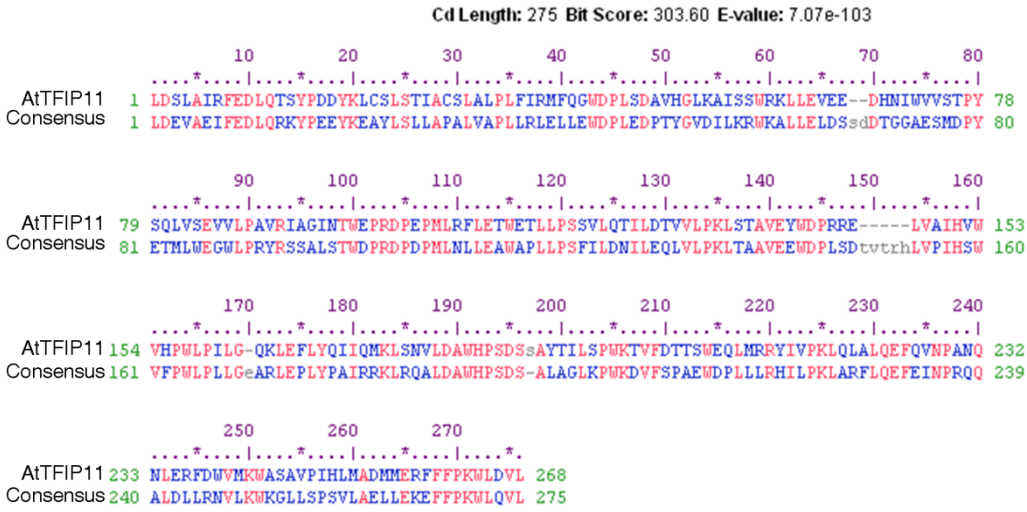

Figure 4.16. Comparison of Arabidopsis *TFIP11* protein sequence with other species

a) Alignment of *Arabidopsis* TFIP11 protein sequence with *Caenorhabditis elegans* STIP1 (NCBI: NP_496226), human (*Homo sapiens*) (NCBI: NP_036275) and mouse (*Mus musculus*) TFIP11 (NCBI: NP_061253). The tuftelin-interacting domain, G-patch domain and GC-rich sequence DNA-binding factor-like domain on the *Arabidopsis* TFIP11 are highlighted in green, cyan and purple, respectively. The signature G-patch motif is boxed in black; the last highly conserved glycine outside the signature motif is boxed in red. The mutated amino acid residue of Mut 21 is highlighted in yellow. Symbols below the sequences denote the degree of conservation. Asterisks (*) indicate identical residues; semi-colon (:) and period (.) indicate conserved and semi-conserved substitutions, respectively.

b) Alignment of the GC-rich sequence DNA-binding factor-like domain of *Arabidopsis* TFIP11 with the consensus sequence (Pfam_07842) (Marchler-Bauer et al., 2011). Identical residues are represented in red letters.

4.4 Discussion

4.4.1 Mut 21 is a temperature-sensitive, but not a membrane trafficking mutant

As described previously (Teh, 2007) and in this study, Mut 21 is a temperature-sensitive mutant that closely resembles WT under permissive temperature. After 24h of growth at 31°C, however, Mut 21 exhibits both developmental and enhanced secGFP fluorescence phenotypes. Despite the dramatic heat-induced changes, Mut 21 is able to fully recover after it is returned to permissive temperature.

Although Mut 21 exhibits an enhanced secGFP fluorescence phenotype, it does not appear that Mut 21 is a secretory mutant because secGFP accumulates in the apoplast. The apoplastic accumulation of secGFP is supported by the anti-GFP immunoblot as the presence of cleaved secGFP increased substantially in Mut 21 after the heat treatment. secGFP is proteolyzed shortly before or after being secreted out of the cell or delivered to the lytic vacuole (Tamura et al., 2003; Zheng et al., 2004). Given that no secGFP is observed in the vacuole, it is concluded that the truncated secGFP is located in the apoplast.

4.4.2 Apoplastic localization pattern of secGFP

GFP fluorescence is often quenched in acidic environments such as the lytic vacuole and the apoplast (Di Sansebastiano et al., 1998; Batoko et al., 2000; Tamura et al., 2003; Zheng et al., 2004; Pinheiro et al., 2009). The apoplastic pH of plant aerial organs is generally described to be between pH 5 and 6.5 (Grignon and Sentenac, 1991; Pitann et al., 2009). This study has established that the apoplastic pH of WT *Arabidopsis* cotyledons is around pH 6.6-6.8, which is slightly higher than the consensus value. Given that GFP is reported to be stable between pH 5.5 and 12 *in vitro* (Ward, 1981), it is surprising to see that GFP fluorescence is attenuated at such pH

range. One possible explanation is that the stability of GFP is compromised by proteolytic events, as it has been shown previously that light-dependent proteinases in lytic vacuole render GFP unstable (Tamura et al., 2003).

The fact that fluorescent secGFP accumulates in the apoplast prompted me to hypothesize an alkaline apoplast in Mut 21. Indeed, I established that upon heat treatment, Mut 21's apoplastic pH is 0.5 unit higher than WT. Thus the presence of fluorescent GFP in the apoplast is correlated with the increase in apoplastic pH.

The enhanced secGFP fluorescence was only observed in the cotyledons, but not in other regions of the seedling. This is either because the mutation specifically affects the cotyledons, or because the pH in other regions of the seedling is more strongly influenced by environmental factors such as the growth medium. While knowledge about the mutated gene locus and its function may provide evidence for the former scenario, it has been shown that apoplastic pH in the root is sensitive to the pH of growth medium (Gao et al., 2004; Zheng et al., 2004). Since our growth medium is buffered at pH 5.7, there is a possibility that the change in apoplastic pH in the root is neutralized by the buffer capacity of the growth medium. Also, secGFP can diffuse away from the root. For these reasons, no enhanced fluorescence is observed in the root of Mut 21 seedlings upon heat treatment.

4.4.3 pH and hypocotyl elongation

A notable developmental phenotype of Mut 21 is the inhibition of hypocotyl elongation in response to heat. Heat-induced hypocotyl elongation is mediated by auxin (Gray et al., 1998). The acid growth theory proposes that auxin promotes cell elongation by regulating the activity of

the H^+-ATPases on the plasma membrane. The decrease in pH further promotes bond cleavage and realignment of cell wall polymers (Rayle and Cleland, 1970; Hager et al., 1971). Indeed, Staal et al., (2011) have established a relationship between the growth rate and the change in surface pH in the *Arabidopsis* root. Since acidification of the apoplast is essential for cell elongation, the drastic inhibition of hypocotyl in Mut 21 may be related to the apoplastic alkalinization that is induced by the mutation. In the future, it may be worthwhile to study whether Mut 21 mutation has any direct effects on the apoplastic pH and cell elongation.

4.4.4 Implication of Mut 21 on using secGFP as a reporter of membrane trafficking event

The primary goal of our forward genetic screens was to identify mutants that exhibit defects in the secretory pathway. The screen is based on the assumption that secGFP fluorescence is quenched in the acidic apoplast. Mut 21 provides an example of a mutant that shows an enhanced fluorescence phenotype in extracellular matrix. Moreover, with respect to our membrane trafficking mutant screen, Mut 21 can be used as a tool to understand more about the processing and behaviour of GFP so that we may improve the use of fluorescent proteins in the future.

Despite the knowledge that was gained from Mut 21, the mutant selection process must be improved to identify true positive membrane trafficking mutants for characterization in the future. The intracellular accumulation of secGFP must be established meticulously using confocal microscopy and anti-GFP immunoblot. In the case of Mut 21, though secGFP is observed in the tubular fusiform bodies of ER, the fluorescent marker is actually en route to the apoplast where it accumulates. Following examination with confocal microscopy, processing and turnover of secGFP should be analyzed with anti-GFP immunoblot. Putative secretory mutants should have

increased ratio of full-length GFP band (upper band) to cleaved GFP band (lower band) (Zheng et al., 2004). If the lower band is dominant, it is likely that secGFP secretion is not blocked, or secGFP is redirected to the lytic vacuole (Tamura et al., 2003; Zheng et al., 2004). If vacuolar localization of a secretion marker is suspected, one can validate the finding by comparing the marker's fluorescence intensities in the vacuole between WT and mutant in the dark, where the observation is not influenced by the different levels of light-dependent protease activities (Tamura et al., 2003). One must be cautious about selecting a putative mutant with no vacuolar localization pattern of secGFP and with a major proportion of secGFP in the truncated form.

It is also advisable to compare the abundance of secGFP transcripts between WT and mutants with RT-PCR, as high expression of secGFP may lead to enhanced fluorescence. It has been established previously that GFP expression in Mut 21 was increased upon heat treatment, but the increase appeared insufficient to account for the observed enhanced fluorescence phenotype (Teh, 2007). secGFP expression analysis is not essential for mutants expressing ratiometric trafficking markers since the expression and intracellular accumulation of secGFP can be quantified by determining the ratio between GFP and another fluorescent protein that is targeted to a specific organelle (Samalova et al., 2006).

4.4.5 Structure and subcellular localization of tuftelin-interacting proteins

At1g17070 encodes for TFIP11, which consists of three domains- the tuftelin-interacting domain, G-patch domain and GC-rich DNA-binding factor-like protein (Figure 4.12a). The G-patch domain is found in proteins with RNA-processing activities (Silverman et al., 2004), and also in proteins that interact with tuftelin or septin in animals in yeast two-hybrid screens (Shih et al., 2002; Wen et al., 2005). While tuftelin is an acidic glycoprotein in the extracellular matrix of enamel that

contributes to enamel mineralization in mammalian teeth (Deutsch et al., 1997), septin is a GTPase that is required for cytokinesis in animals, yeast, fungi and insects (reviewed in Longtine et al., 1996). Tuftelin and septin do not appear to be related as there is no functional connection or sequence similarity between the two proteins. In humans, TFIP11 is expressed not only in the teeth but also in a number of tissues (Mao et al., 2001). It interacts with components that are involved in pre-mRNA splicing (Tannukit et al., 2008; Wen et al., 2008). In *Caenorhabditis elegans*, septin and tuftelin interacting protein 1 (STIP1), is essential for embryogenesis and development (Ji et al., 2007).

Subcellular localization of TFIP homologs in human, mice and *C. elegans* has been investigated. The human and *C. elegans* homologs were both localized in the nucleus (Beausoleil et al., 2004; Ji et al., 2007). This finding was consistent with the idea that the protein is involved in RNA-splicing through the G-patch domain.

4.4.6 Tuftelin-interacting protein in *Arabidopsis*

4.4.6.1 TFIP11 expression in endosperm

Protein sequence alignment shows a high degree of similarity between TFIP11 and At2g42330. However, little is known about TFIP11 and its paralogue that is encoded by At2g42330 in *Arabidopsis*. Gene expression data on different tissue types (https://www.genevestigator.com/) reveals that At2g42330 and *TFIP11* have different gene expression patterns. The former has low to medium expression in endosperm, seed coats and influorescence, and remarkably high expression in sperm cells (Figure 4.17); *TFIP11* has low to medium expression in all parts of seedlings and the highest level of expression in chalazal endosperm of seeds (seven-fold higher than most other tissues) (Figure 4.18). An endosperm inside a seed is a source of nutrients for the

embryo, containing carbohydrates, minerals, fatty acids, amino acids and growth factors. In particular, cytokinin is a growth factor that is found in endosperm in higher plants (Lenton and Appleford, 1987; Lorenzi et al., 1988; Martin et al., 1989; Kobayashi et al., 1995; Banowetz et al., 1999). In *Arabidopsis*, endosperm first develops into a multinucleate syncytium, followed by cellularization events that form the micropylar, central and chalazal domains (Brown et al., 1999). Chalazal endosperm is distinct from the other two domains such that the chalazal cyst remains syncytial even after the micropylar and the central domains have cellularized (Mansfield and Briarty, 1990; Brown et al., 1999). Minerals are stored in the elaborated vacuole and ER in the chalazal domain and are translocated to the embryo at specific development stages (Otegui et al., 2002). So far, no abnormalities have been observed with embryo development of Mut 21, but it may simply be because the mutant embryo and endosperm have always been developed at permissive temperature.

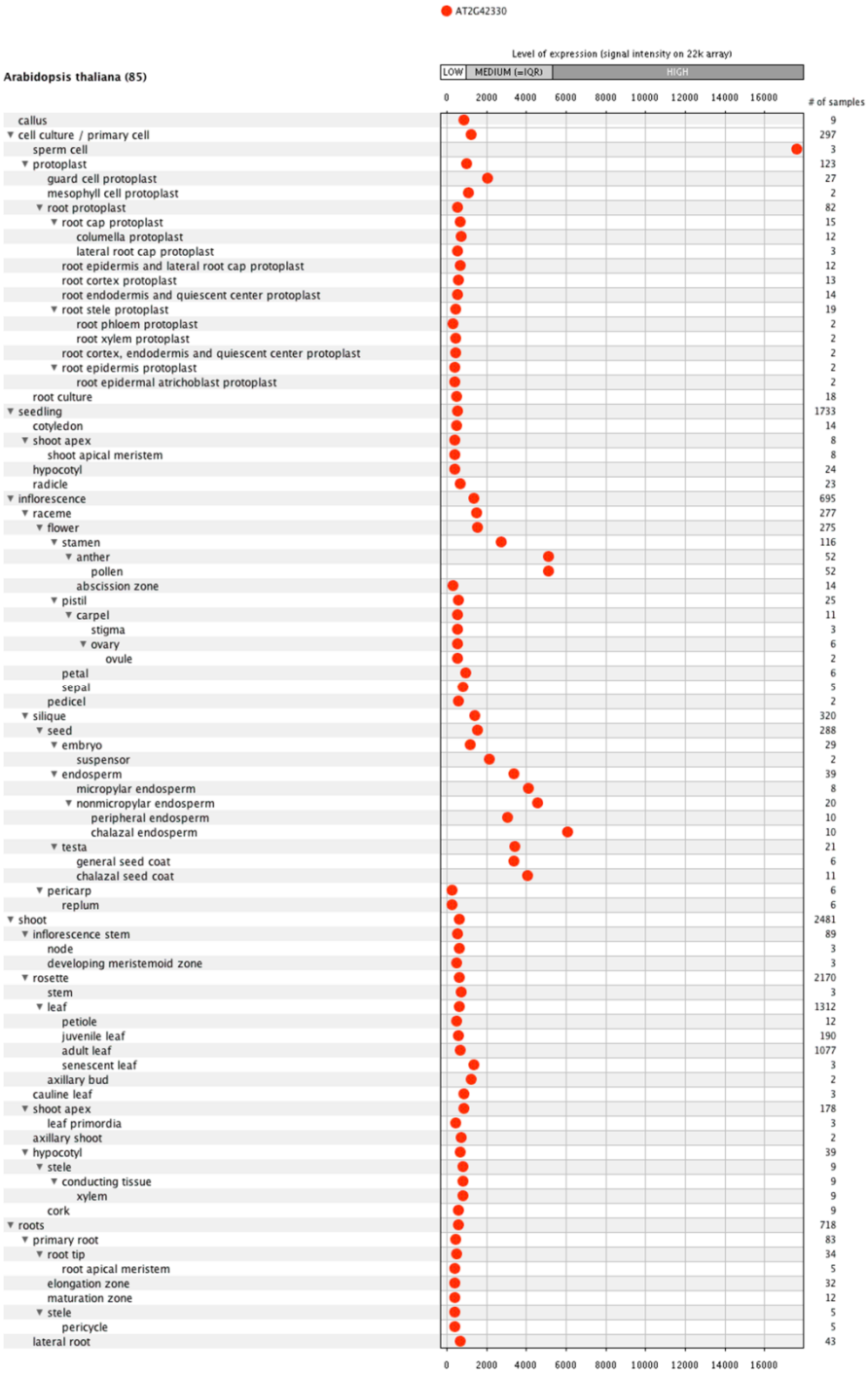

Figure 4.17. Expression pattern of *Arabidopsis* At2g42330 in various tissues

Level of expression is based on signal intensity on 22k arrays and is displayed in linear scale.

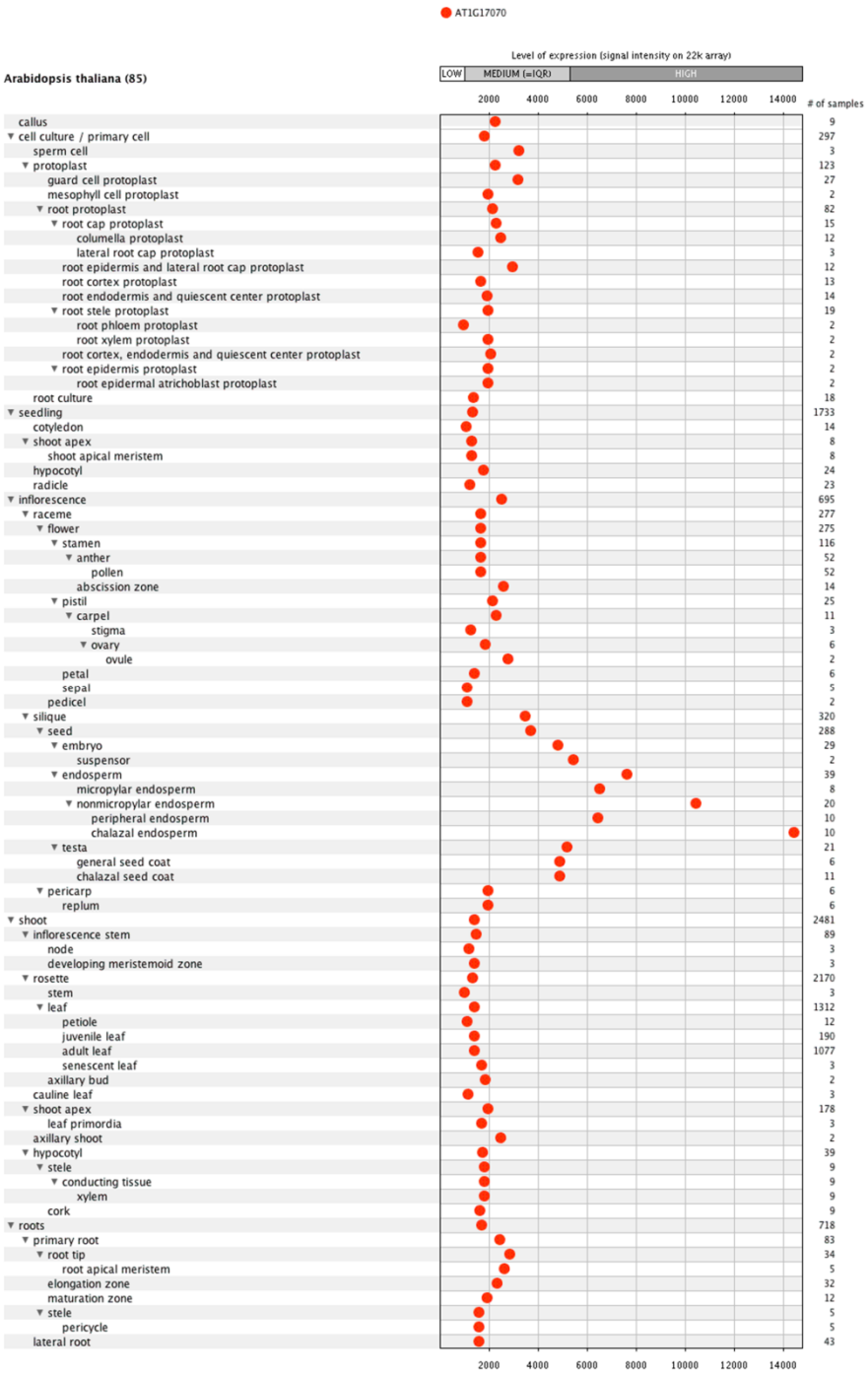

Figure 4.18. Expression pattern of *Arabidopsis* TFIP11 in various tissues

Level of expression is based on signal intensity on 22k arrays and is displayed in linear scale.

4.4.6.2 TFIP11 expression at non-permissive temperature

To investigate whether the WT *TFIP11* expression is heat-sensitive, the array data from different heat stress and heat shock experiments was also compiled and analyzed. As shown in Figure 4.19, various heat treatments do not seem to markedly affect transcript abundance. Hence, it does not appear that expression of *TFIP11* is correlated to temperature.

Based on the current findings, two possible explanations regarding to the temperature sensitivity of Mut 21 can be inferred. First, TFIP11 activity is required at both permissive and restrictive temperature, but the mutation only perturbs its activity at restrictive temperature. This is seen in proteins with an amino acid substitution that destablizes their native conformation only at restrictive temperature (e.g. Hawkes et al., 1984; Hecht et al., 1984; Gordon and King, 1994), but is uncommon for mutations that result in truncated proteins like Mut 21 and therefore I conclude it is not the most plausible explanation for Mut 21's temperature sensitive phenotypes. The second explanation is that TFIP11 is not essential at permissive temperature but is necessary at restrictive temperature. This implies that TFIP11 participates in a pathway that is intrinsically sensitive to temperature (e.g. Thomas et al., 1993). Consistent with this explanation, Mut 21 has exhibited defects in heat-induced hypocotyl elongation. Other temperature-sensitive phenotypes in Mut 21 may be attributed to the fact that there are redundant pathways functioning at permissive temperature to compensate for the loss of TFIP11 function, but not at restrictive temperature. For this reason, though TFIP11's expression is not temperature-dependent, the mutant phenotypes are only apparent at restrictive temperature when the redundant pathways have been inhibited.

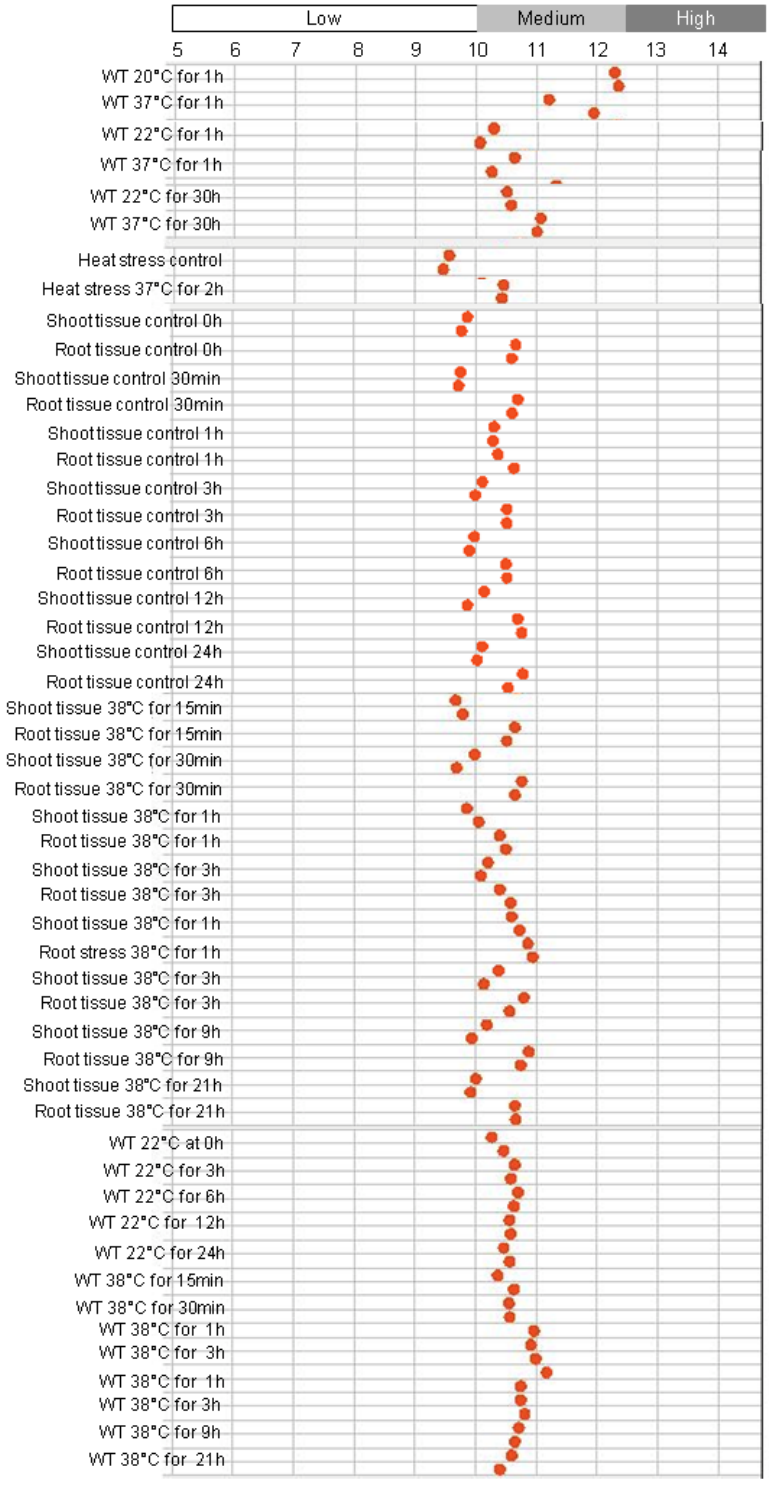

Figure 4.19. Heat treatment array data for *TFIP11* mRNA transcripts

Different heat experiments involving WT plants are shown. Temperature and duration of the heat treatment are displayed in some of the names. Level of expression is based on signal intensity on 22k arrays and is displayed in logarithmic scale.

4.4.6.3 TFIP11 and cell wall synthesis protein

This study shows that a point mutation in TFIP11 is correlated with the alkalization of the apoplast in cotyledons at restrictive temperature, but a causal relationship has yet to be established. A computational prediction procedure that gathers information from several cell wall protein databases has predicted that *Arabidopsis* TFIP11 coexpresses and interacts with a soluble cell wall synthesis-related protein, beta-galactosidase 17 (BGAL17) and is involved in the secretory pathway (Zhou et al., 2010). Since BGAL17 has an ER translocation signal peptide, BGAL17 has been speculated to be transported to the cell wall via the secretory pathway. If the interaction is true, then it may provide an explanation for the alteration of apoplastic pH in Mut 21. But based on what is known, it is difficult to imagine how the two proteins can physically interact. First, there is no evidence that TFIP11 is in the secretory pathway as no signal peptide is identified by the signal peptide prediction program SIG-Pred (Bradford, 2001). Second, as mentioned above, there is strong evidence suggesting that TFIP11 regulates pre-mRNA splicing in the nucleus through its G-patch domain. So unless there is any experimental evidence showing the interaction between TFIP11 and BGAL17, it seems unlikely that the two proteins colocalize, though there is still a possibility that the expression of TFIP11 correlates with BGAL17 and TFIP11 regulates the expression of one or more factors that are essential for BGAL17 activity on the cell wall.

4.4.6.4 Proposed relationship between TFIP11 and phytohormone signalling

A mutant allele of *TFIP11*, *rrd4*, has a nonsense mutation in the same codon as Mut 21, resulting in the same tryptophan to stop codon change in TFIP11. *rrd4* was identified as its hypocotyl explants failed to proliferate in callus-induction media and it showed limited adventitious root growth in root-induction media at restrictive temperature (Sugiyama, 2003). In contrast to this

study, Sugiyama (2003) focused on the redifferentiation phenotypes in hypocotyls and roots. Following the pre-culture of hypocotyl explants at restrictive temperature, *rrd4* failed to redifferentiate into roots (Figure 4.20a and b). Callus formation in both hypocotyl and root explants is also strongly inhibited at restrictive temperature (Figure 4.20c) (Sugiyama, 2003). Furthermore, Sugiyama has found that *rrd4* explant dedifferentiation and seedling growth were more sensitive to the inhibitory effects of the phytohormone cytokinin at restrictive temperature. He therefore proposes a model in which TFIP11 is a positive regulator in a cytokinin pathway (M Sugiyama, personal communication). He reasoned that a cell's resultant response to cytokinin is a balance between the promoting and the inhibitory pathways of cytokinin. Since TFIP11 is hypothesized to promote the positive effects of cytokinin, the loss of TFIP11 activity would lower the cell's sensitivity to the positive pathway and therefore enhance the inhibitory effects. This model coincides with the finding that cytokinin is abundant in endosperm where TFIP11 is also highly expressed, corroborating with the model that TFIP11 is present in cytokinin's site of action to modulate a cell's sensitivity.

While Sugiyama speculates that the role of TFIP11 is on a cytokinin-mediated pathway, the alkaline apoplast phenotype in Mut 21 suggests to me the possibility of an auxin-mediated process. In accordance to the acid growth theory (Rayle and Cleland, 1970; Hager et al., 1971), auxin promotes cell expansion by stimulating the activity of proton pumps on the PM to lower the apoplastic pH and to trigger cell wall loosening (Hager, 2003; Takahashi et al., 2012). Therefore, it is possible that Mut 21 affects the acidification of apoplast through auxin. The two apparently conflicting speculations may be resolved by the fact that cytokinin and auxin often interact to regulate plant growth and development processes, including embryogenesis (Muller and Sheen, 2008), meristerm development (Su et al., 2011), lateral root formation (Casimiro et

al., 2003; De Smet et al., 2006) and vascular differentiation (Aloni et al., 2006). So if TFIP11 does indeed promote cytokinin functions, it is not difficult to envisage that reduction in TFIP11 activity may also affect auxin biosynthesis or response through auxin-cytokinin crosstalk mechanisms.

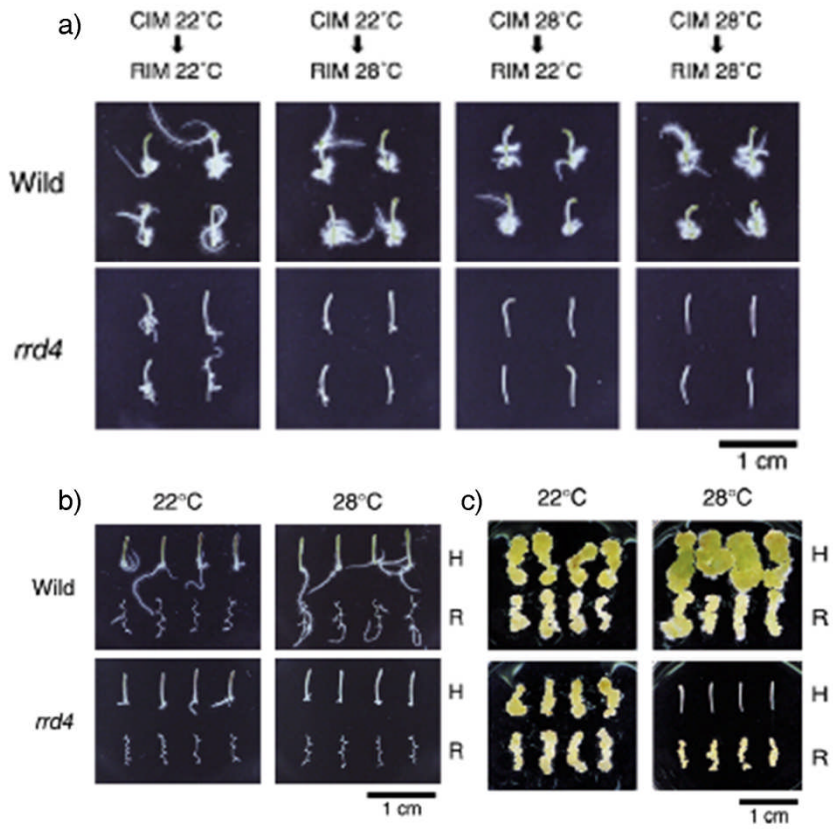

Figure 4.20. *rrd4* displays defects in redifferentiation at restrictive temperature

a) Hypocotyl explants were grown in callus-inducing medium (CIM) at permissive temperature (22°C) for 4d or restrictive temperature (28°C) before transferring to root-inducing medium (RIM) and grown for 8d at permissive or restrictive temperature.

b) Hypocotyl (H) or root explants (R) were cultured in RIM for 12d at permissive temperature (left) and restrictive temperature (right)

c) Hypocotyl (H) or root explants (R) were cultured in CIM for 24d at permissive temperature (left) and restrictive temperature (right)

Figures from Sugiyama, 2003.

4.4.7 Future Directions

To validate the mutant identification results, the WT allele of *TFIP11* should be cloned into homozygous Mut 21 to see whether the mutant phenotypes are suppressed. Though I have started the cloning process, the molecular complementation experiment is yet to be completed. The secGFP localization in *rrd4* should be analyzed to verify that it has the same enhanced secGFP phenotype as Mut 21. The function of TFIP11 in *Arabidopsis* is still elusive at this point. A good starting point in studying this protein in more detail would be to examine the subcellular localization of TFIP11, possibly by tagging it with a fluorescent protein and visualizing it with confocal fluorescence microscopy. Here I have established a correlation between the mutation and the apoplastic pH in cotyledons, but further work is required to possibly infer a causative relationship between the two events. Based on the localization of TFIP11, one can form hypothesis regarding its influence on cotyledon apoplastic pH regulation. Since it is predicted to be in the nucleus, TFIP11 is not likely to play a direct role on apoplastic pH. It may, however, regulate apoplastic pH through one or more proteins. One may be able to gather some leads by identifying genes whose expression is regulated by TFIP11. Mut 21 and *rrd4* are valuable tools for studying the function of TFIP11. However, the activity of the truncated protein at different temperatures is yet to be established. It may be useful to generate knockout mutants or silence the gene by RNA interference to compare the phenotypes and activities with the temperature-sensitive mutants and WT to analyze the relationship between protein activities and phenotypes.

Chapter 5 Characterization of Mut 43

5.1 Chapter Summary

As described in the General Introduction, Mut 43 was selected for this study as it accumulates secGFP in the ER after being incubated at 31°C for 24h (Teh, 2007). This study reveals that secGFP accumulates intracellularly in Mut 43 even at permissive temperature and is further enhanced at restrictive temperature. The localization of the intracellular secGFP was examined using ER, Golgi and tonoplast markers. Apart from the enhanced fluorescence phenotype, Mut 43 also exhibited developmental defects such that it is always smaller and takes longer to develop than in WT. A large proportion of Mut 43 plants lost their viability beyond the seedling stage, posing a challenge for extracting sufficient DNA from each seedling for traditional map-based cloning similar to the problems encountered with studying early-lethal mutants. For this reason, a new mapping method based on next-generation sequencing technology was developed to identify the causative mutations in early-lethal mutants and was tested on Mut 43.

5.2 Introduction

5.2.1 Mut 43 as a putative temperature-sensitive membrane trafficking mutant

Mut 43 is a monogenic recessive secGFP-accumulating mutant that was previously isolated from a temperature-sensitive mutant screen. The enhanced secGFP fluorescence phenotype in Mut 43 was observed in all parts of the seedling after 24h at restrictive temperature (31°C) (Figure 5.1a to h). The secGFP transcript abundance in Mut 43 is slightly higher than in WT (Figure 5.1i), but the increase does not seem to be sufficient to result in the big difference in secGFP fluorescence level. The secGFP phenotype is irreversible after 48h of heat treatment. After incubating at restrictive temperature for 24h or longer, the homozygous mutant loses its viability at the seedling stage and thus cannot be propagated (Teh, 2007). Even when maintained at permissive

temperature, it has been reported that only about 60% of seedlings that have been transplanted to soil can reach maturity (Teh, 2007). It shows conspicuous developmental defects even at permissive temperature (Figure 5.2) (Teh, 2007). The growth stages of Mut 43 are significantly delayed and the mutant seedlings are always smaller than WT (Figure 5.2a and b) (Teh, 2007). Likewise, a mature adult Mut 43 is considerably shorter and smaller compared to WT (Figure 5.2d) and has smaller siliques (Figure 5.2e). Another interesting aspect of Mut 43 is its temperature-sensitive swollen root-tip phenotype. As visualized by light microscopy, the swelling occurred at the most apical portion of the elongation zone in Mut 43 seedlings after a heat treatment.

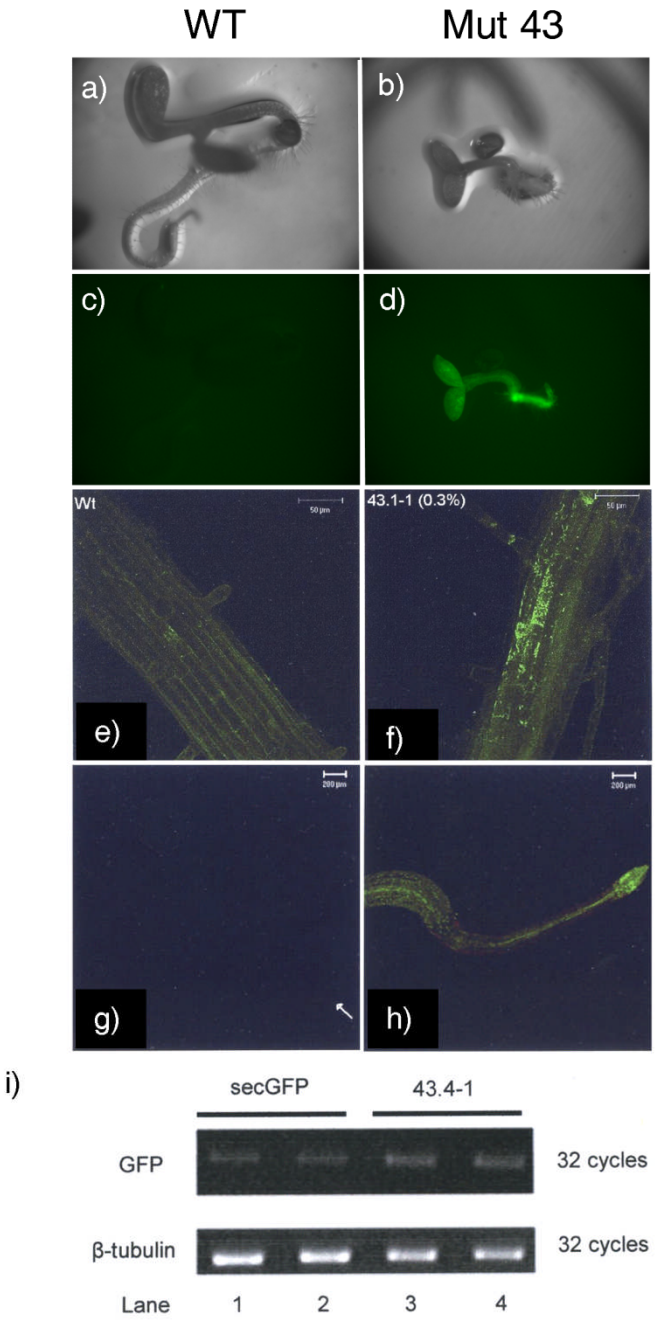

Figure 5.1. Mut 43 exhibits enhanced secGFP fluorescence phenotype at restrictive temperature

a) to d) Bright-field images (a and b) and fluorescence images (c and d) of WT (a and c) and Mut 43 (b and d).

e) to h) Confocal fluorescence images of WT (e and g) and Mut 43 (f and h) expressing secGFP at restrictive temperature (31°C). Mature roots (e and f) and root tips (g and h) of seedlings are shown

i) Expression profile of secGFP and β-tubulin transcripts of WT expressing secGFP (Lane 1 and 2) and Mut 43 (Lane 3 and 4) at restrictive temperature. RNA was extracted from whole seedlings and analyzed by RT-PCR. Number of PCR cycles is indicated on the left.

Figures (e) to (i) were taken from Teh, 2007.

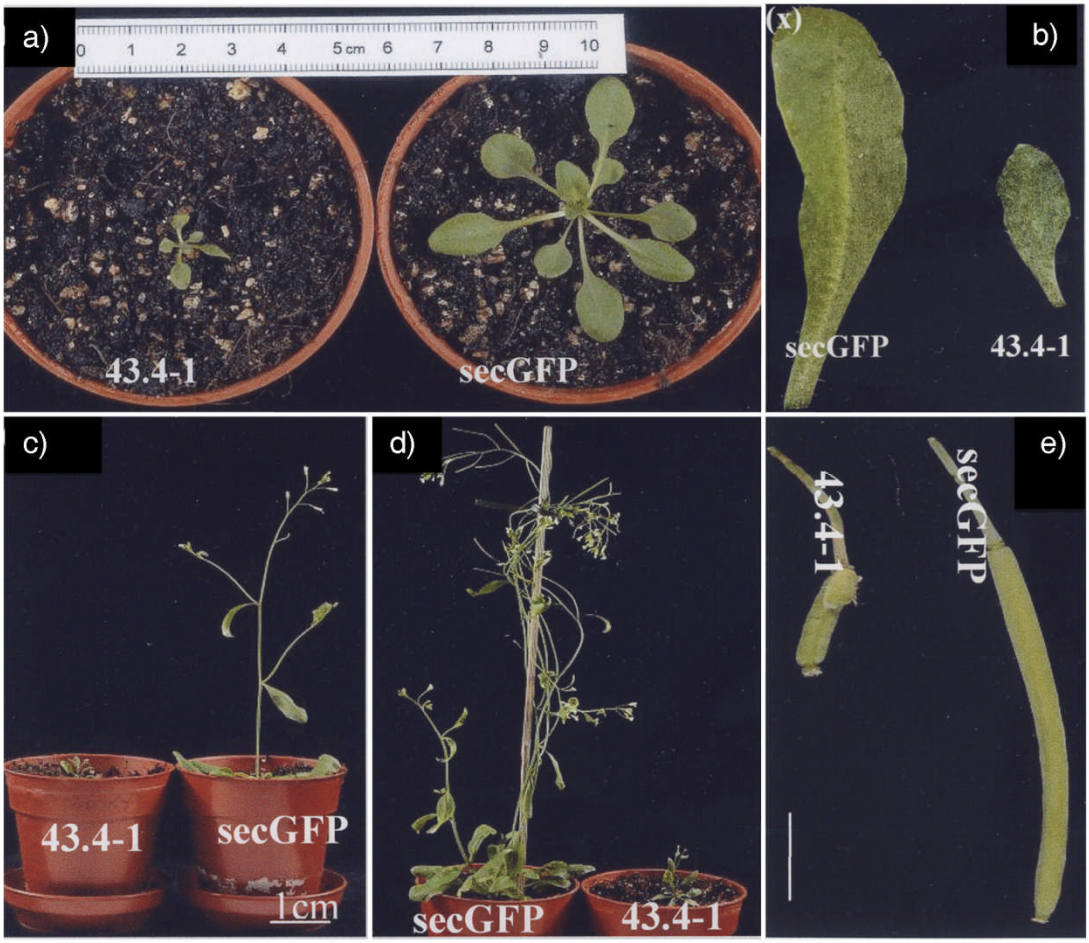

Figure 5.2. Developmental phenotypes of Mut 43

a) 25-day-old rosettes

b) Rosette leaves

c) 30-day-old plants

d) 36-day-old plants

e) Siliques

Bar=1cm in (e)

Figures from Teh, 2007.

5.2.2 Complications with mapping early-lethal mutants using the traditional map-based cloning method

As demonstrated with Mut 21, the mutation underlying a phenotype can be mapped using conventional map-based cloning. Col-0 plants carrying the mutant allele were outcrossed to the L*er*-0 ecotype to generate a mapping cross family. The mutant segregants in the F2 generation of the family were isolated, and their genomic DNA was extracted individually. The recombination events in each individual are then analyzed using genetic markers that are generated based on the polymorphisms between two *Arabidopsis* ecotypes. The approximate position of the mutant gene locus is defined by a set of genetic markers that co-segregate with the mutant allele. Since the probability of finding a recombination event close to the gene of interest increases with the size of the population, genetic resolution can be enhanced by increasing the mapping population. For Mut 21, with about 500 individuals, the mutation was mapped to a region of 170kb on chromosome one.

Although the conventional mapping method is robust for viable mutants with a distinct phenotype, it cannot be easily applied to mutants with low viability like Mut 43 because of the problems in extracting a sufficient quantity of DNA from individuals. A viable alternative is to utilize next-generation sequencing technology to identify the mutation (Hillier et al., 2008; Sarin et al., 2008; Smith et al., 2008; Srivatsan et al., 2008; Blumenstiel et al., 2009; Huang et al., 2009; Schneeberger et al., 2009; Zuryn et al., 2010; Austin et al., 2011). An attractive feature of next-generation sequencing is that it can quantify both rare and common variants in a population. Here, the samples are pooled together, thereby increasing the chance of isolating sufficient quantity of DNA for the sequencing reactions. There are currently a number of next-generation

sequencing methods available (reviewed in Mardis, 2008; Ansorge, 2009), but the common principle is that the pooled DNA is sampled randomly and each nucleotide is read multiple times (hence the term deep-sequencing). As a result, it can be used to identify polymorphisms within a population. By comparing the polymorphisms with the reference genome, one can then map the mutation by identifying areas of genetic linkage and ultimately identify the causal mutation. The feasibility of this approach to identify the causative mutation of a recessive *Arabidopsis* mutant has been demonstrated based on the polymorphisms between the Col-0 and L*er*-0 ecotypes (Schneeberger et al., 2009; Austin et al., 2011).

5.2.3 Objective

In this chapter, the phenotypes of Mut 43 were confirmed and further characterized. Although the mutant exhibits growth defects and enhanced secGFP fluorescence even at permissive temperature, the phenotypes were indeed exacerbated at restrictive temperature. Furthermore, a standard condition for triggering the root-tip swelling phenotype was sought so that the root-tip of Mut 43 could be studied systematically.

I have also attempted to map Mut 43 using next-generation sequencing technology in collaboration with The Genome Analysis Centre (TGAC). Two approaches were attempted to identify the mutation in Mut 43. The first method involves sequencing DNA from pooled mutants in the F2 generation of mapping cross families. Similar to Schneeberger's approach (2009), the mutation can be identified as an EMS-induced SNP near the region of the genome that shows 1:0 ratio of Col:L*er* SNPs. But due to the technical difficulties experienced in isolating sufficient good-quality DNA from mutant seedlings for next-generation sequencing, an alternative mapping strategy needed to be developed based on sequencing the phenotypically WT siblings in the

population. The second method is a newly developed one that sequences the WT siblings of the mapping cross families instead. Since the alleles of gene loci that are linked to a lethal mutation would have a distinct segregation pattern that is not only apparent in the mutant but also in the WT siblings, it is hypothesized that this property can be used to map the mutation. But a major uncertainty with this approach is whether the sequencing technology can produce the depth of sequence coverage required to precisely quantify the polymorphisms in the sample. In the following sections, the preliminary mapping data of Mut 43 are shown and the method is evaluated.

5.3 Results

5.3.1 The enhanced fluorescence phenotype of Mut 43 changes with temperature

The distribution of secGFP was examined by confocal fluorescence microscopy at both permissive and restrictive temperatures (Figure 5.3). When WT seedlings were imaged with the same microscope settings, secGFP was shown to label the tubular fusiform bodies and displayed similar fluorescence level at both temperatures (Figure 5.3a to f), thus implying that temperature alone does not affect secGFP distribution. In contrast, changes in the distribution pattern of secGFP were observed in Mut 43 at different temperatures. At permissive temperature, secGFP was localized in the tubular fusiform bodies and the ER network in all parts of the seedling (Figure 5.3g to i). At restrictive temperature, secGFP was also apparent in the vacuole in addition to the ER (Figure 5.3l) in root epidermal cells. Despite the changes in the root, secGFP in cotyledons and hypocotyls were still observed mostly in the ER. Hence, Mut 43 exhibits an enhanced secGFP fluorescence phenotype even at permissive temperature, but the heat treatment affects the distribution of fluorescent secGFP in root cells.

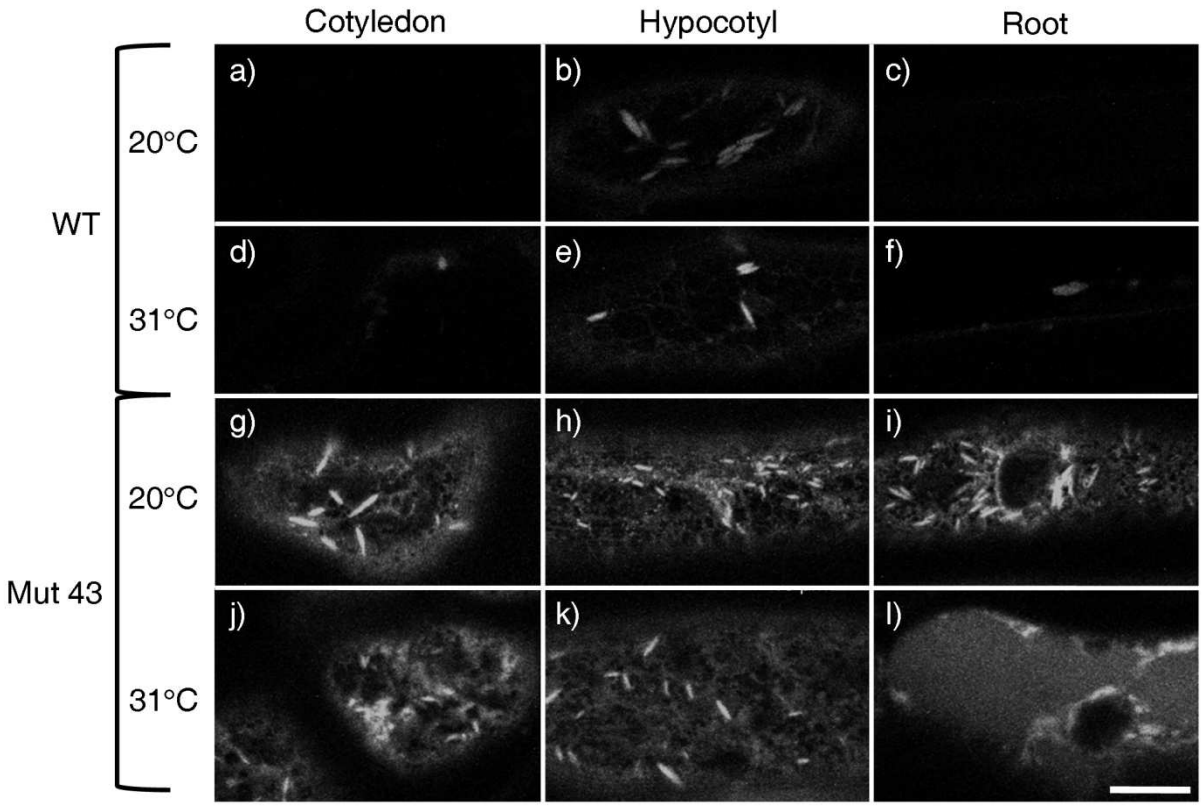

Figure 5.3. Mut 43 secGFP fluorescence is enhanced at restrictive temperature

Six-day-old WT (a to f) and Mut 43 (g to l) seedlings expressing secGFP were grown in 20°C or 31°C for 24h after five days of growth under normal condition. Epidermal cells in cotyledons (a, d, g and j), hypocotyls (b, e, h and k) and mature roots (c, f, i, l) are shown.

Bar=10μm

Though the abundance of the secGFP transcript was assessed previously (Figure 5.1i) (Teh, 2007), the secGFP protein expressions of WT and Mut 43 were never assessed. To analyze the accumulation and processing of secGFP, whole protein extracts of WT and Mut43 seedlings expressing secGFP or an ER lumen marker (GFP-HDEL) were immunoblotted with anti-GFP antibodies (Figure 5.4). The majority of the ER lumenal marker GFP-HDEL was in the full-length form (Lane 7), consistent with its intracellular localization. As described previously, secGFP is present in truncated form in the apoplast and the vacuole (Tamura et al., 2003; Zheng et al., 2004). At permissive temperature, Mut 43 homozygous mutants accumulated more full-length

secGFP than their WT siblings (Lane 2 and 4), reflecting the intracellular accumulation of secGFP in the mutant (Zheng et al., 2004) as seen by confocal fluorescence imaging (Figure 5.3). At restrictive temperature, the truncated secGFP in the WT segregants was slightly more abundant than at permissive temperature (Lane 3). In Mut 43, both the full-length and the truncated forms of secGFP were more abundant at restrictive temperature than at permissive temperature (Lane 5). This suggest a slight increase of secGFP in the secretory pathway at restrictive temperature in both WT and Mut 43; and the increased presence of the truncated secGFP in the mutant reflects the presence of secGFP in the vacuole in the root cells at restrictive temperature.

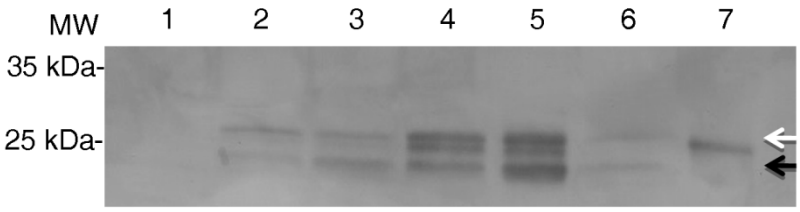

Lane 1. Col-0
2. Mut 43 WT segregant at 20°C
3. Mut 43 WT segregant at 31°C
4. Mut 43 mutant segregant at 20°C
5. Mut 43 mutant segregant at 31°C
6. secGFP
7. ER lumen marker (GFP-HDEL)

Figure 5.4. Mut 43 accumulates more full-length and truncated forms of secGFP than WT

Anti-GFP immunoblot analysis of whole-seedling protein extracts of seven-day old seedlings expressing secGFP or GFP-HDEL. Mut 43 mutant segregants accumulate more full-length secGFP than WT at permissive temperature (20°C) (compare Lane 2 and 4). At restrictive temperature (31°C), both WT and Mut 43 seedlings increased the expression of the truncated secGFP. Particularly in Mut 43, there is also a slight increase in the expression of the full-length secGFP.

5.3.2 Localization pattern of ER, Golgi and tonoplast marker in Mut 43

Since secGFP was apparent in the ER in all parts of Mut 43 seedlings, secGFP localization was characterized further by visualizing secGFP with markers for the ER lumen (mCHERRY-HDEL) and Golgi membrane (ST-mCHERRY) (Nelson et al., 2007) in Mut 43 and WT at restrictive temperature. Figure 5.5 shows that there was a high degree of colocalization between secGFP and mCHERRY-HDEL in Mut 43 seedlings. In addition to labeling the ER, secGFP also appeared in the vacuole of the epidermal root cells of the root (Figure 5.5f), consistent with previous observations (Figure 5.3l). Moreover, secGFP often labelled punctate structures that did not colocalize with mCHERRY-HDEL (arrows in Figure 5.5f), suggesting these punctate structures are not ER.

ST-mCHERRY labelled the ER network in addition to the Golgi bodies in Mut 43 seedlings but not in the WT. In contrast to the ER marker, very little colocalization was observed between secGFP and the Golgi bodies that were labelled by ST-mCHERRY in Mut 43 (Figure 5.6). Confocal fluorescence microscopy did not reveal any changes in Golgi morphology. The Golgi bodies appeared larger than the secGFP-labelled punctate structures (Figure 5.7), which did not colocalize with ST-mCHERRY (Figure 5.7b) or mCHERRY-HDEL, and so are likely to be distinct from the Golgi bodies and the ER.

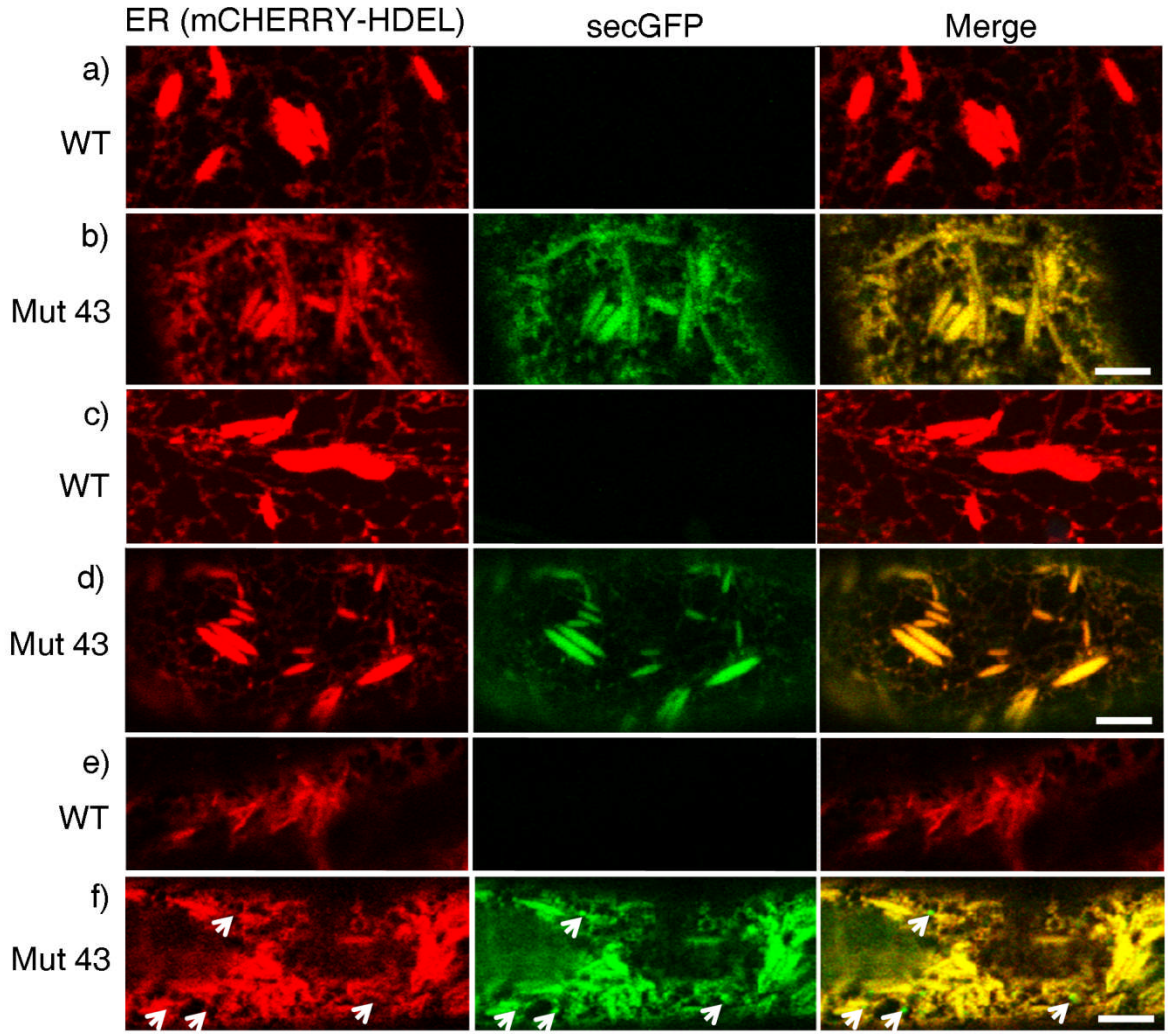

Figure 5.5. secGFPs colocalize with an ER marker in Mut 43

Confocal images of six-day-old WT (a, c and e) and Mut 43 (b, d and f) seedlings coexpressing secGFP and an ER lumen marker (mCHERRY-HDEL) after growth at 31°C for 24h. Images of cotyledons (a and b), hypocotyl (c and d) and root epidermal cells (e and f) are shown. Arrows indicate punctate structures that are labelled by secGFP but not mCHERRY-HDEL (also see Figure 5.7).

Bars=5μm

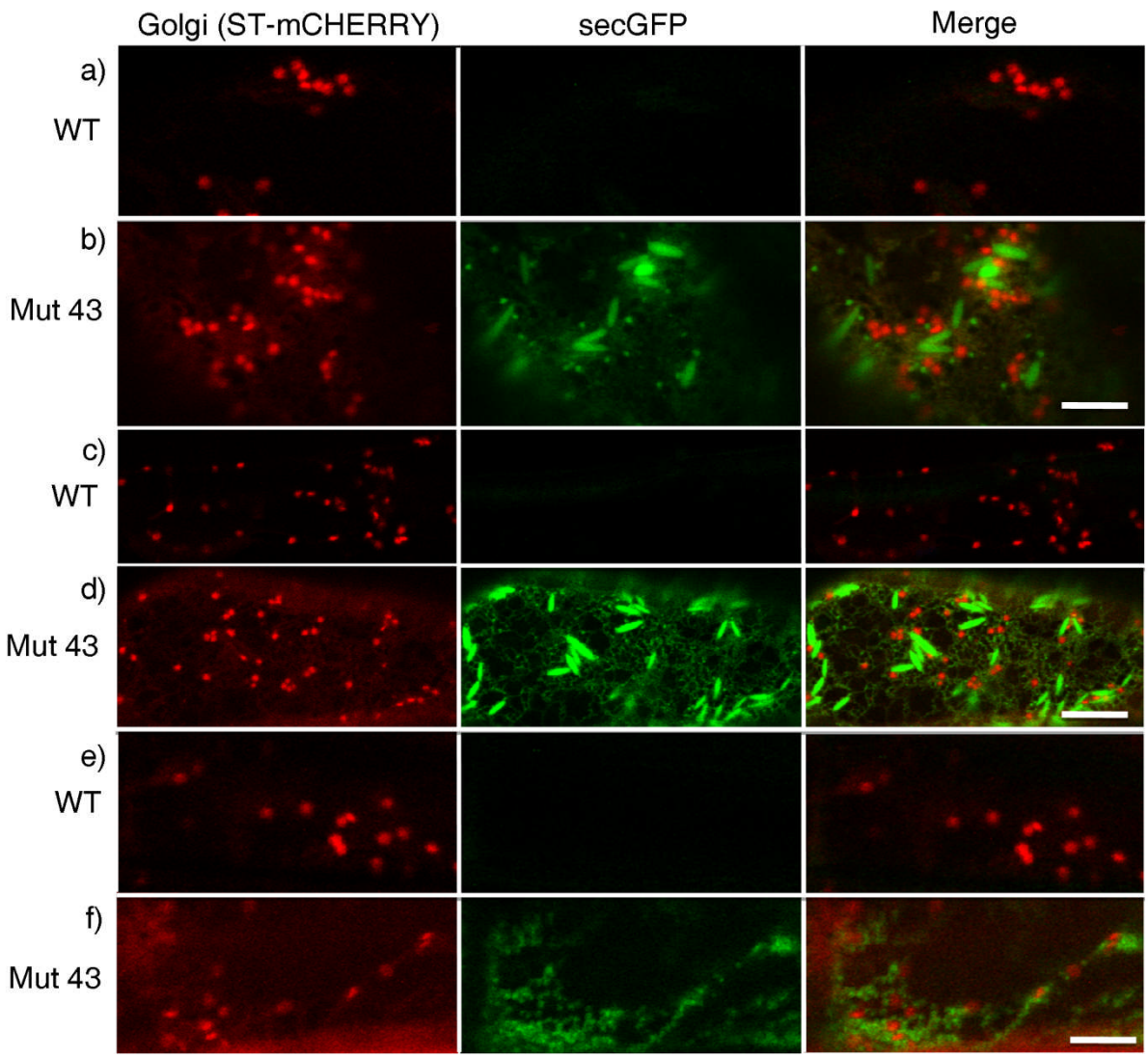

Figure 5.6. secGFP do not colocalize with the mCHERRY-labelled Golgi bodies in Mut 43.

Confocal images of six-day-old WT (a, c and e) and Mut 43 (b, d and f) seedlings coexpressing secGFP and a Golgi marker (ST-mCHERRY) after growth at 31°C for 24h. Images of cotyledons (a and b), hypocotyl (c and d) and root epidermal cells (e and f) are shown.

Bars=5μm

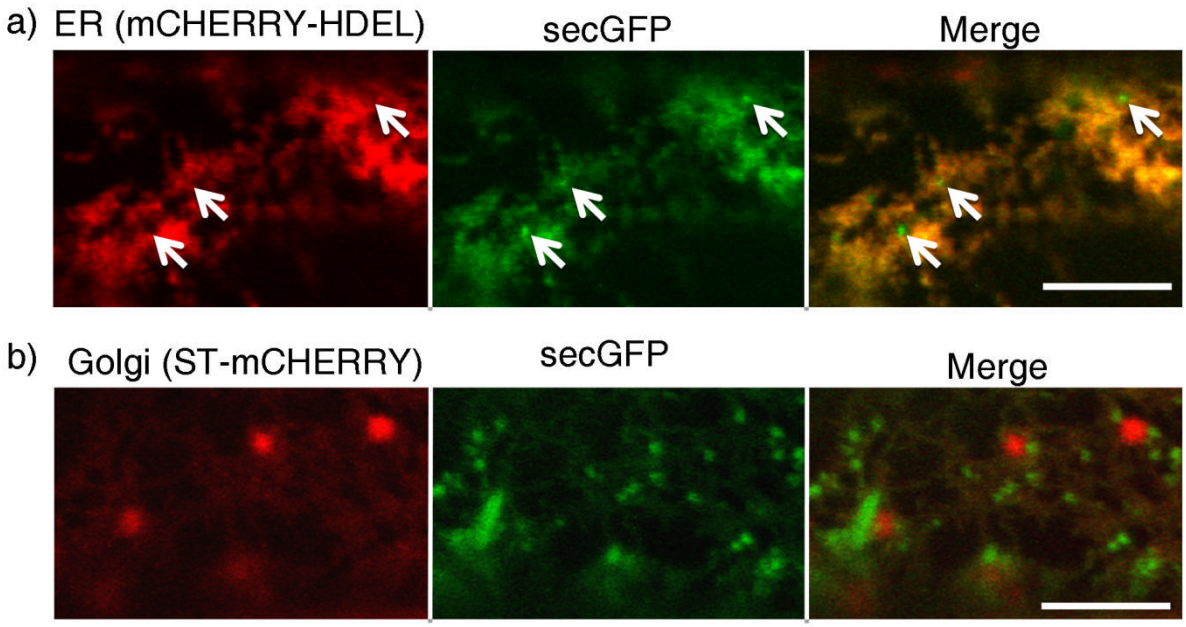

Figure 5.7. secGFP-labelled punctate structures in Mut 43

Hypocotyl cells of six-day-old Mut 43 seedlings coexpressing secGFP and mCHERRY-HDEL (a) or ST-mCHERRY in (b) after growth at 31°C for 24h. Arrows in (a) indicate secGFP-labelled punctate structures that exclude mCHERRY-HDEL.

Bars=5μm

Intriguingly, the fluorescence intensities of the fluorescent protein organelle markers tested were much higher in Mut 43 than in WT, such that the laser power often had to be decreased 4-20-fold in Mut 43, depending on the marker, to visualize a marker in WT and Mut 43 at similar intensities. This led to the speculation that the accumulation of secGFP in the ER of Mut 43 may be a consequence of saturated ER export due to transgene overexpression, rather than a *bona fide* phenotype of Mut 43. To distinguish the two effects, I used a ratiometric fluorescent protein construct secN-RFP-2A-GFP-HDEL, which is stoichiometrically cleaved into a vacuole-targeted protein (secN-RFP-2A) and an ER-localized protein (GFP-HDEL) (Samalova et al., 2006), to assay ER export. Here, the GFP-HDEL provides a reference for transgene expression that can be quantified by measuring the absolute GFP fluorescence intensity in the nuclear envelope. On the other hand, the quantity of secN-RFP-2A in the ER inversely reflects ER export traffic and can be

quantified by measuring the absolute RFP fluorescence intensity in the nuclear envelope. The resultant RFP/GFP ratio then represents the quantity of secN-RFP-2A in the ER after transgene expression has been normalized. For example, if secN-RFP-2A is not exported from the ER, a high RFP/GFP ratio is expected; whereas if the transgene is simply overexpressed, an unaltered RFP/GFP ratio is expected.

The absolute RFP and GFP fluorescence intensities were measured at the nuclear envelope which is connected to the ER and where the intensities of both markers are independent of the size and shape of the ER (Figure 5.8a). A series of confocal fluorescence images of nuclear envelopes were taken along the z-axis; a transect was then drawn across the nuclear envelope to locate the plane with the highest GFP intensity from which the absolute fluorescence intensity values were recorded. As shown in Table 5.1, the absolute GFP intensity in Mut 43 was 5.7- and 4.3-fold greater than in the WT at permissive and restrictive temperature, respectively. This suggests that the mutant has higher transgene expression than the WT under both conditions. However, the increase in transgene expression is not sufficient to account for the increase in RFP intensity of the ER. As shown in Figure 5.8b, the RFP/GFP ratio of Mut 43 increased by 2.7-fold and 4.7-fold compared to the WT at permissive and restrictive temperature, respectively, suggesting increased presence of the export marker relative to the reference in the nuclear envelope. In contrast, although transgene expression also increased two-fold in the WT at restrictive temperature, the overall RFP/GFP ratio did not change significantly, thereby suggesting that the observed increase in RFP intensity in this case is a direct consequence of increased transgene expression. Hence, the higher RFP/GFP ratio in Mut 43 implied that the increased presence of the exported marker in the ER and nuclear envelope was attributable to factors other than differences in the fluorescent protein transgene expression level.

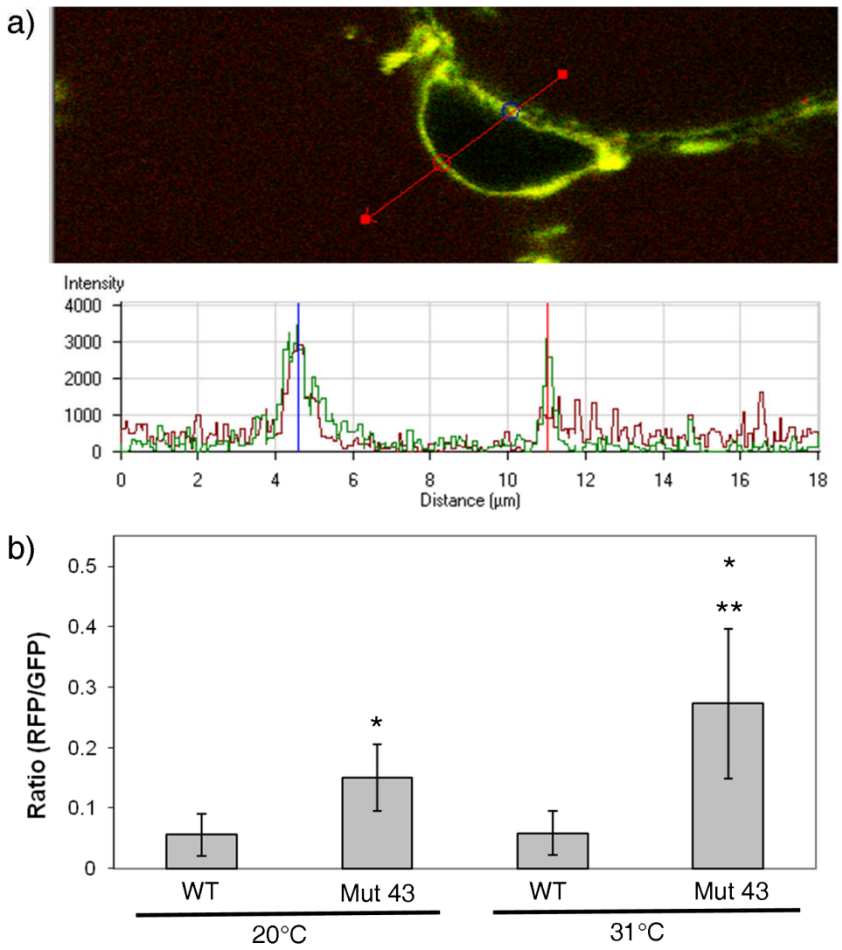

Figure 5.8. Increased presence of secN-RFP-2A in nuclear envelope of Mut 43

Ratios of RFP (secN-RFP-2A) to GFP (GFP-HDEL) were measured from the cotyledon epidermal cells of six-day-old WT and Mut 43 seedlings expressing the ratiometric fluorescent protein construct secN-RFP-2A-GFP-HDEL after 24h growth at 20°C or 31°C.

a) An illustration of quantitative analysis of ER export with secN-RFP-2A-GFP-HDEL.

Top: A confocal image showing a transect drawn across a nuclear envelope. Bottom: Graph representing the GFP (green) and RFP (red) fluorescence intensity profiles along the transect.

The red and blue vertical lines on the graph below highlight the positions of GFP fluorescence intensity peaks along the transect, and correspond to the red and blue circles, respectively, on the image above. The absolute RFP and GFP fluorescence intensities at the position of maximum GFP fluorescence intensity are recorded.

b) Graph showing the RFP/GFP ratios in the WT and Mut 43 seedlings at 20°C and 31°C. Single asterisks (*) represent values that are significantly different from WT under the same condition; double asterisk (**) represents value that is significantly different from the same genotype at permissive temperature ($P<0.01$).

Each bar represents measurements from five seedlings. Error bars represent SD.

Table 5.1. Quantitative measurement of secN-RFP-2A-GFP-HDEL intensities in WT and Mut 43

		RFP Intensity		GFP Intensity	
		Absolute fluorescence (Arbitrary units ± SD)	**Fold increase compared with WT**	**Absolute fluorescence (Arbitrary units ± SD)**	**Fold increase compared with WT**
Permissive Temperature (20°C)	**WT**	7.6 ± 6.4	--	140 ± 62	--
	Mut 43	120 ± 89	16	780 ± 420	5.7
Restrictive Temperature (31°C)	**WT**	15 ± 8.7	--	300 ± 170	--
	Mut 43	340 ± 180	22	1300 ± 460	4.3

To assess the vacuolar traffic in Mut 43, the distribution pattern of a tonoplast marker (YFP-VAMP711) (Geldner et al., 2009) was analyzed. Unfortunately, marker lines coexpressing YFP-VAMP711 and secGFP could not be isolated likely due to silencing of the secGFP transgene, so a colocalization study of secGFP and a vacuolar marker could not be conducted. Looking at the outer surface of epidermal cells, it appeared that YFP-VAMP711 consistently labelled more punctate structures in Mut 43 than in the WT (Figure 5.9a, c, e, g, i and k). Indeed, the number of YFP-YAMP711-labelled punctate structures per unit area of cytoplasm is significantly greater in Mut 43 than in the WT throughout the seedling ($P<0.05$) (Figure 5.9m). However, YFP-VAMP711 still localized on the tonoplast of the central vacuole in both genotypes (Figure 5.9b, d, f, h, j and l), thus suggesting that the tonoplast marker could still reach the vacuole in Mut 43 despite increased labelling of punctate structures that are apparently upstream of the vacuole in the vacuolar sorting pathway.

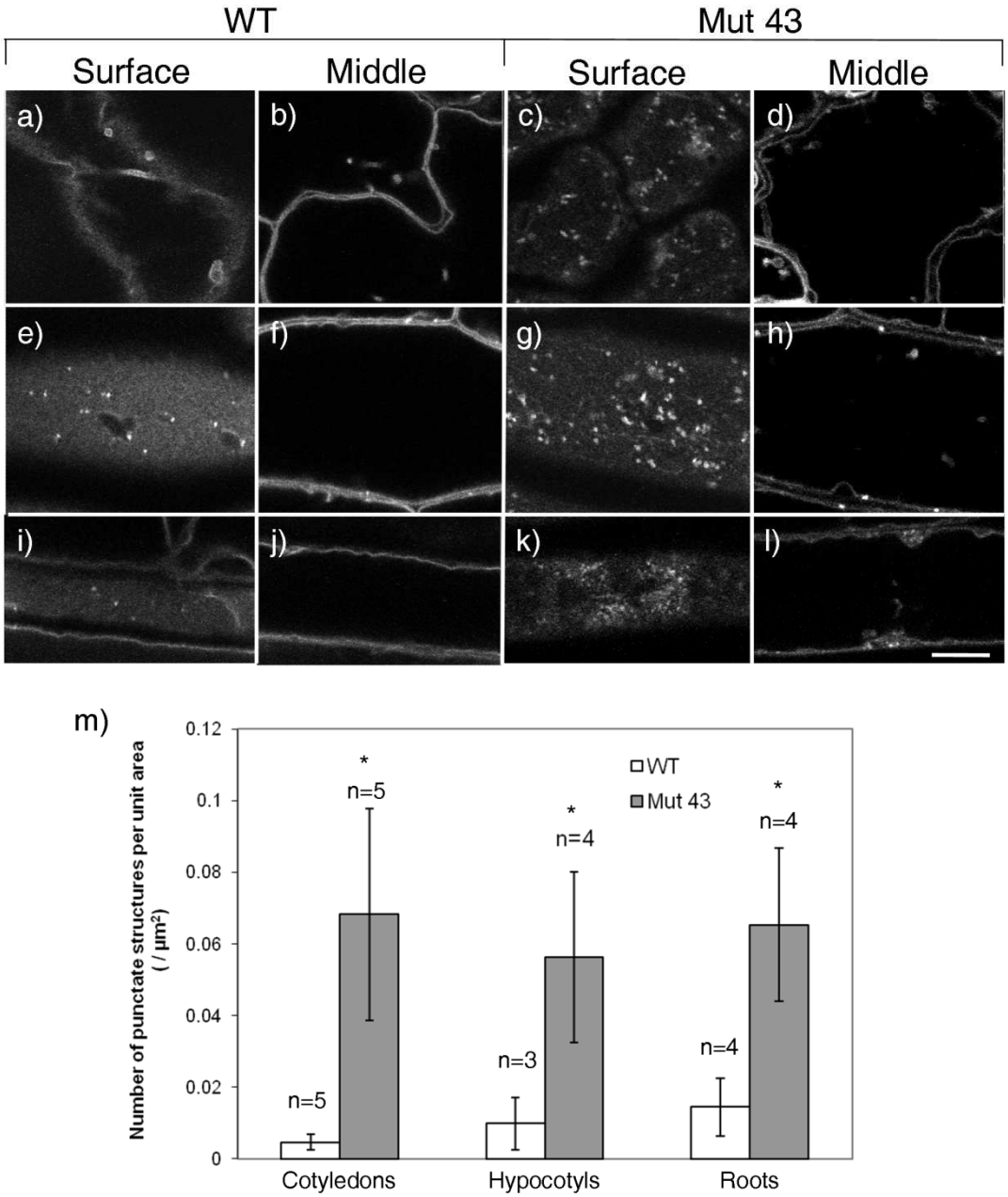

Figure 5.9. Tonoplast marker labelled more punctate structures in Mut 43

Epidermal cells in cotyledons (a to d), hypocotyls (e to h) and roots (i to l) of WT (a, b, e, f, i and j) and Mut 43 (c, d, g, h, k and l) expressing YFP-VAMP711. Images show punctate structures on the cell surface, and tonoplast of central vacuole in the middle plane.

m) Density of punctate structures that are labelled by YFP-VAMP711. Asterisks (*) indicate values that are statistically different from WT ($P<0.05$). n= number of seedlings.

Error bars represent SD.

Bar=10µm

5.3.3 The developmental phenotypes of Mut 43

In the seedling stage, the mutants had smaller cotyledons with colours ranging from dark green to brown. As seen by confocal fluorescence imaging, the epidermal cells in cotyledons were smaller and shaped differently compared to the WT such that that the jigsaw shape of the cells was less apparent in Mut 43 (Figure 5.10). Mut 43 took a much longer time to develop and never reached the same height as the WT. Consistent with previous findings (Teh, 2007), the homozygous mutant plants could only be propagated at permissive temperature, but even in that case were less fertile than the WT. It has been reported that about 64% of the transplanted Mut 43 seedlings could reach maturity (Teh, 2007). Though I have achieved a higher success rate (about 88%), many plants had already lost viability before the transplant stage (3-4 weeks post-germination). Overall, only 20% of the seedlings germinated on growth media agar plates survived at the transplant stage.

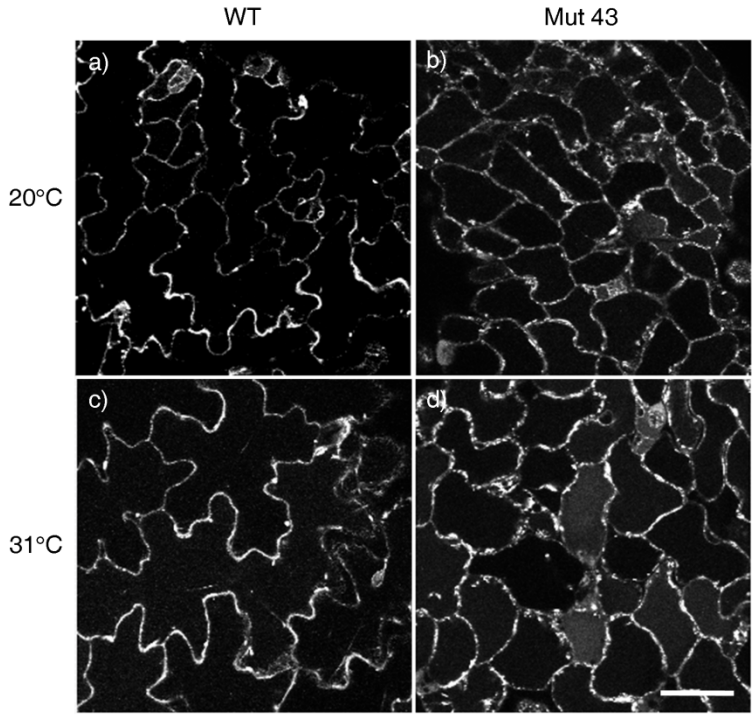

Figure 5.10. The irregular cell shape of epidermal cells in cotyledons of Mut 43

Cotyledon epidermal cells of six-day-old WT (a and c) and Mut 43 (b and d) seedlings expressing mCHERRY-HDEL are shown. Seedlings were incubated at 20°C (a and b) or 31°C (c and d) for 24h.

Bar=50μm

As mentioned previously, Mut 43 exhibits a temperature-dependent radially swollen root-tip phenotype (Teh, 2007). The induction of this phenotype does not coincide with the enhanced secGFP fluorescence phenotype. To find a condition for triggering the radial swelling in Mut 43, seedlings were observed for the swelling phenotype after three different heat treatment regimes: after 24h at 31˚C, 48h at 31˚C followed by 24h at 20˚C, and 48h at 31˚C followed by 48h at 20˚C. While the WT did not show swollen root-tips following any treatment (Figure 5.11a and b), the mutant showed various degrees of swollen root-tip phenotype (Figure 5.11c and d). After 24h at 31˚C, increased secGFP fluorescence was observed with no swollen root-tip. After 48h at 31˚C followed by 24h of recovery time at 20°C, the swelling phenotype was observed. Another 24h later, the root-tips were slightly more swollen with the presence of root hair. Out of the three regimes, It was determined that the best condition for triggering the swollen root-tip phenotype in Mut 43 was 48h of heat treatment at 31°C followed by 48h of recovery time at the permissive temperature of 20°C. It is important to note that even under this condition only about half of the total Mut 43 seedlings examined exhibited the radial swelling phenotype, implying that the trait is not highly penetrant.

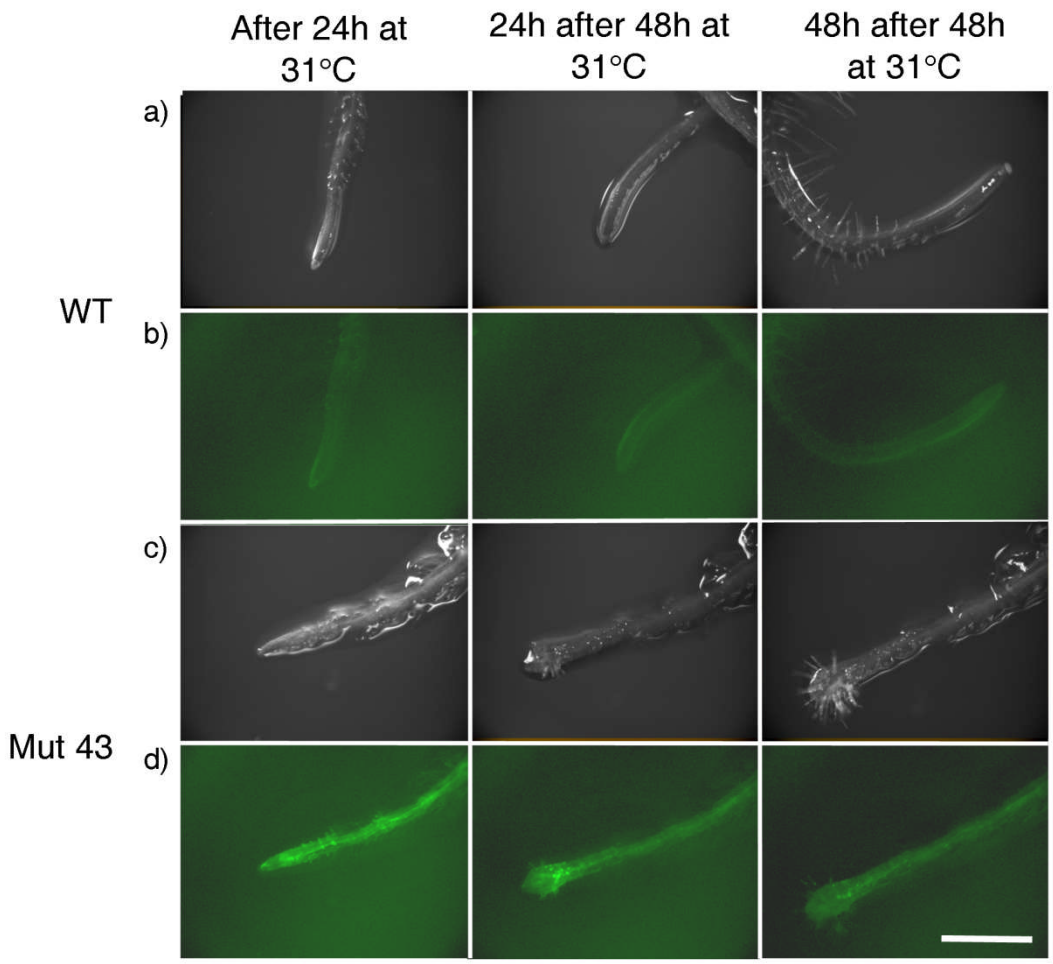

Figure 5.11. The root-swelling phenotype in Mut 43 is more pronounced two days after 48h at restrictive temperature (31°C)

Bright-field (a and c) and fluorescent images (b and d) of WT (a and b) and Mut 43 (c and d) at the indicated time-points.

Bar=1mm

The ER and Golgi morphology in the radial swelling region was examined in seedlings expressing an ER (mCHERRY-HDEL) or Golgi (ST-mCHERRY) marker. Abnormal cells were found in the elongation zone immediately basal to the meristematic cells (Figure 5.12b). As seen in a light microscope, the cells in this region of WT root were rectangular and lined up in an organized array (Figue 5.12a). Each cell appeared tightly packed with its neighbours. In contrast, the cells of Mut 43 appeared in various shapes and sizes (Figure 5.12b). They were generally larger, more

rounded and less tightly packed with larger area of extracellular space found between the neighbouring cells.

While mCHERRY-HDEL labelled the ER network in the WT (Figure 5.12a and c), this marker labelled the ER as well as the vacuole in Mut 43 (Figure 5.12b and d). Interestingly, mCHERRY-HDEL also revealed the pleiomorphic ER morphology of Mut 43 root-tip cells (Figure 5.12e to g). Some cells had more cisternal ER (Figure 5.12e) and some had more tubular ER (Figure 5.12f). In contrast, as revealed by ST-mCHERRY, the morphology of the Golgi was apparently similar between the WT and Mut 43 (Figure 5.12g and h). Other than the Golgi bodies, ST-mCHERRY also localized on the nuclear envelope and the ER membrane in Mut 43.

In summary, Mut 43 accumulates secGFP in ER and punctate structures throughout the seedling. At restrictive temperature, secGFP is also visible in the central vacuole of root cells. Quantitative confocal fluorescence imaging reveals that inhibition of ER export is enhanced at restrictive temperature. Other than its secGFP accumulation phenotype, Mut 43 also exhibits conspicuous developmental phenotypes, such as growth defects, abnormal cell shape and sizes and root swelling. Although it was initially recovered as a temperature-sensitive mutant, it is effectively a seedling-lethal mutant due to its low viability even at permissive temperature.

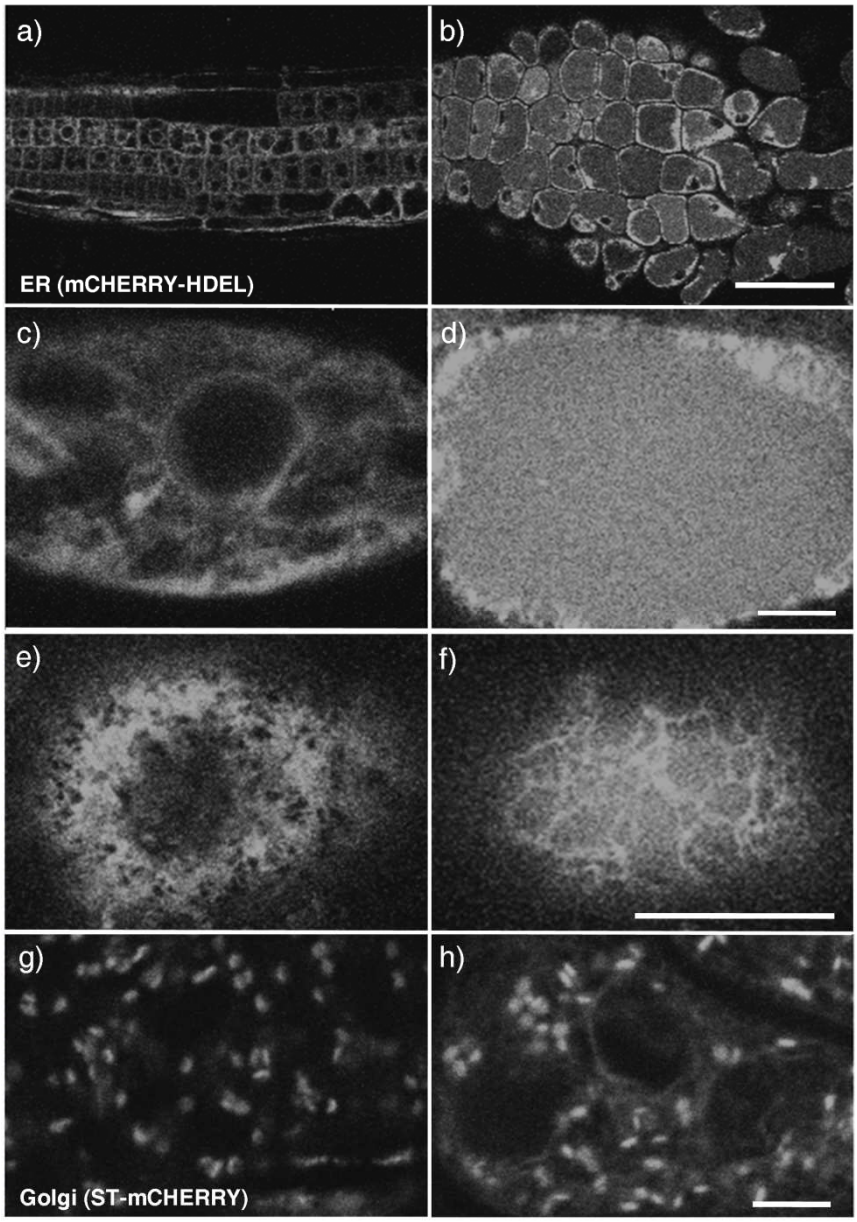

Figure 5.12. Mut 43 radial swelling root tip

Six-day-old WT and Mut 43 seedlings were grown at 31°C for 48h, followed by recovery at 20°C for 48h.

a)and b) Low-zoom images of WT (a) and Mut 43 (b) seedling primary roots expressing mCHERRY-HDEL.

c) and d) High-zoom images of WT (c) and Mut 43 (d) root epidermal cells in the apical elongation zone, showing the localization of mCHERRY-HDEL.

e) to f) Pleiomorphic ER morphology of the swollen cells.

g) and h) Root epidermal cells WT (g) and Mut 43 (h) expressing ST-mCHERRY in the apical elongation zone.

Bars=50μm in (b); 5μm in (d) and (h) and 10μm in (f)

5.3.4 Mapping and identification of Mut 43

5.3.4.1 Generation of mapping cross families

Previous BSA had assigned Mut 43 to the lower half of chromosome two (Teh, 2007). To identify the mutation, a mapping cross family had to be generated by outcrossing the mutant allele to a polymorphic WT. But since homozygous mutants had low viability, the phenotypically WT siblings in a heterozygous mutant family were crossed to L*er*-0 instead. The resulting F1 progenies were genotyped using a PCR-based genetic marker to confirm their Col/L*er* heterozygosity and were selfed to generate the F2 generations. Only the mutant-segregating F2 families were used for mapping. Interestingly, all the mutant-segregating mapping cross families were from crosses with Mut 43 as male and L*er*-0 as female. And out of 65 F1 plants, only 22% were heterozygotes instead of the expected 1:1 ratio between homozygous WT and heterozygous mutant plants. These findings suggest a reduced transmission of the Mut 43 allele through both male and female gametes. However, a more systematic investigation is required to precisely quantify the transmission rate.

5.3.4.2 Preparation of homozygous mutant samples for deep-sequencing

I made two attempts to prepare samples of the mapping cross F2 mutants for deep-sequencing. As mutant seedlings start to lose viability 10 days after germination, I decided to extract DNA from 7-day-old seedlings. At this age, almost all the seedlings are viable and so a large population can be gathered, albeit with low fresh weight for each seedling. After DNA extraction and purification, the amount of DNA was determined by Nanodrop and agarose gel electrophoresis (Table 5.2). Both mapping cross mutant samples yielded at least 1μg of DNA. Ultraviolet light absorption spectra were generated for each sample to assess the purity of the DNA sample (Figure 5.13a and b), and the A260/A280 and A260/A230 ratios were determined to assess the

quality of the samples (Table 5.2). Considering that a pure DNA sample is expected to have an A260/A280 ratio between 1.8 and 2.0 and an A260/A230 ratio between 2.0 and 2.2 (Manchester, 1995), the first sample pool containing 526 homozygous seedlings, mapping cross mutant 1, was slightly sub-optimal. Indeed, DNA libraries for deep-sequencing could not be constructed from this sample. Next, 329 individuals were pooled in the second mapping cross mutant sample-Mapping cross mutant 2 (Table 5.2). Instead of using the Qiagen DNeasy Plant kit, the Promega Wizard® Genomic DNA Purification Kit was used as an attempt to improve quality and yield of DNA. Compared to the previous sample pool, both the quality and the quantity of this pool was better despite a smaller population size (Table 5.2 and Figure 5.13b). Although the sample passed TGAC's initial quality control stage, a problem was once again encountered in the library construction process. Therefore, none of the mapping cross mutant samples prepared could be used for deep-sequencing reactions.

Table 5.2. Mapping cross samples submitted for deep-sequencing

Sample Pool	Number of Individuals	Fresh Weight (mg)	Amount of DNA (ng)	A260/A280	A260/A230
Mapping cross mutant 1	562	360	1000	1.76	1.89
Mapping cross mutant 2	329	182	1800	1.85	2.09
Mapping Cross WT	492	6400	4400	1.86	1.90

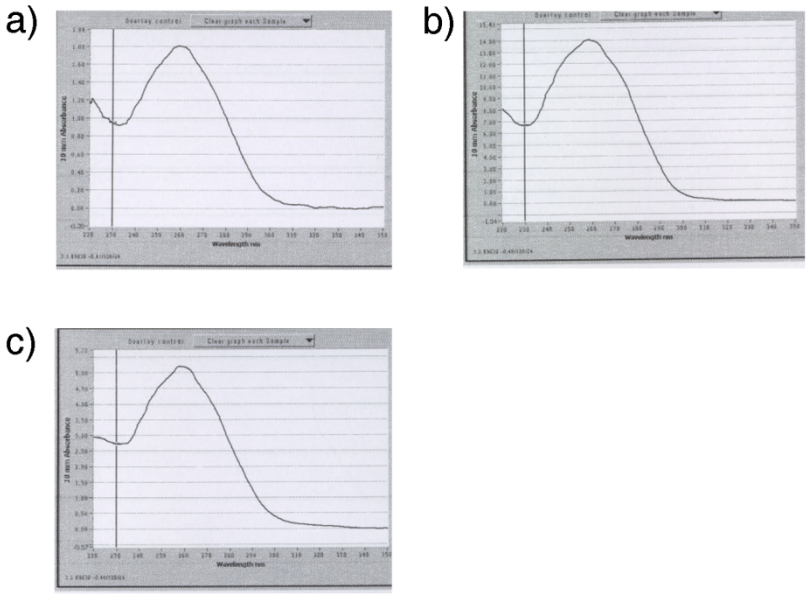

Figure 5.13. Ultraviolet light absorption spectra of the DNA samples submitted for deep-sequencing

a) Mapping cross mutant 1

b) Mapping cross mutant 2

c) Mapping cross WT

5.3.4.3 Mapping Mut 43 through deep-sequencing of WT siblings

Due to time-constraints, I was unable to generate a third pool of mapping cross mutant samples for deep-sequencing. So instead, a collaboration with TGAC was established to explore the feasibility of using the remaining WT siblings in the Mut 43 mapping cross families for mapping and mutation identification. It has been reasoned that the bias against the homozygous mutants would shift the ratio of WT-genome to Mut 43-genome of the mutant locus from 1:1 towards 2:1 (Figure 5.14). The WT-genome and the mutant-genome are distinguished using the polymorphisms between two ecotypes. In our case, since the mutant originates from Col-0 background and is crossed to L*er*-0, the mutant-genome and the WT-genome are represented by the Col-0 and L*er*-0 SNPs, respectively. To find out whether the current deep-sequencing technology has the capacity to generate data with sufficient quality to detect this shift in the SNP ratio and ultimately map Mut 43, WT segregants of the F2 generation of mapping cross families were pooled together. 4.4μg of DNA was extracted from the flower buds of 492 plants (Table 5.2). Despite the sub-optimal A260/A230 ratio (Table 5.2, Figure 5.13c), a DNA library was successfully constructed and the sequencing reaction was performed successfully.

Sequencing reads of 30-40 base pairs from Illumina Genome Analyzer were aligned to the Col-0 reference genome. After the genome was assembled, it was established that the overall sequencing coverage was 40x, which means each nucleotide of the genome was sampled 40 times on average. Since the SNPs between Col and L*er* are 50 times more common than EMS-induced SNPs (1 SNP per kb between Col and L*er* compared to 0.020 SNP per kb in EMS mutagenesis) (Ossowski et al., 2008 and in this study), it was expected that most observed SNPs represent the polymorphisms between the two ecotypes. The concordance of each SNP, which represents the percentage of total reads that supports the SNP, is plotted against the SNP's

position on each chromosome in Figure 5.15 (C Greenman, unpublished data). On chromosome one to four, there was a distinct region with very few reads on each chromosome. These regions are presumably the centromeric regions with highly repetitive sequences that are poorly read and assembled. A Hidden Markov Model (HMM) was used to classify the genome into regions with equal representation of L*er* and Col SNPs and regions that show bias in the SNP ratio. The algorithm was designed to call for the 0.5 state which represents L*er*:Col ratio of 1:1 and the 0.33/0.67 state which represents L*er*:Col ratio of 2:1 (Figure 5.15). No significant bias was observed in chromosome one, three, four and five as the HMM called the 0.5 state throughout each chromosome. However, a strong bias was observed on the bottom arm of chromosome two. Not only did the HMM call the biased state in the entire region, the SNPs also appeared to cluster above the 0.67 line. Hence, it was concluded that genetic linkage was observed on chromosome two. The data are consistent with the previous BSA result (Teh, 2007) that assigned the causative mutation to the bottom arm of chromosome two.

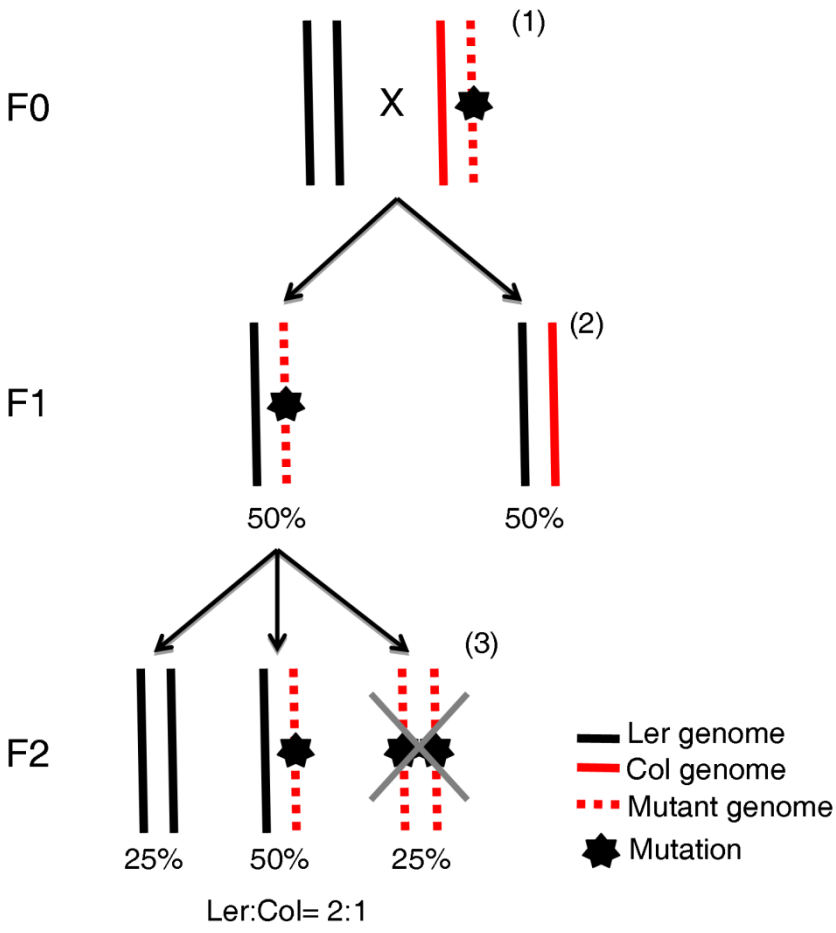

Figure 5.14. Principle of mapping early-lethal mutants through deep-sequencing of wild-type siblings of a mapping cross family

The monogenic recessive early-lethal mutant is propagated in heterozygous form in the Columbia (Col) background before being crossed to Landsberg erecta (L*er*) ecotype to create mapping cross families (1). After crossing to L*er*, 50% of the F1 progeny are heterozygous for the WT L*er* allele and the mutant allele (2). When these plants are selfed, three genotypes are apparent in the F2 progenies- 25% of the F2 are homozygous L*er* WT, 50% are heterozygous for the L*er* WT allele and the mutant allele, and 25% are homozygous mutant (3). Since the homozygous mutants are lethal, they are excluded in this sample. Therefore, for the mutated gene locus and its linked loci, the L*er*:Col ratio is shifted towards 2:1 as there is a selection against homozygous Col alleles on these loci. Conversely, for loci that are unlinked to the mutation, the Col and L*er* alleles are equally represented, hence the L*er*:Col= 1:1.

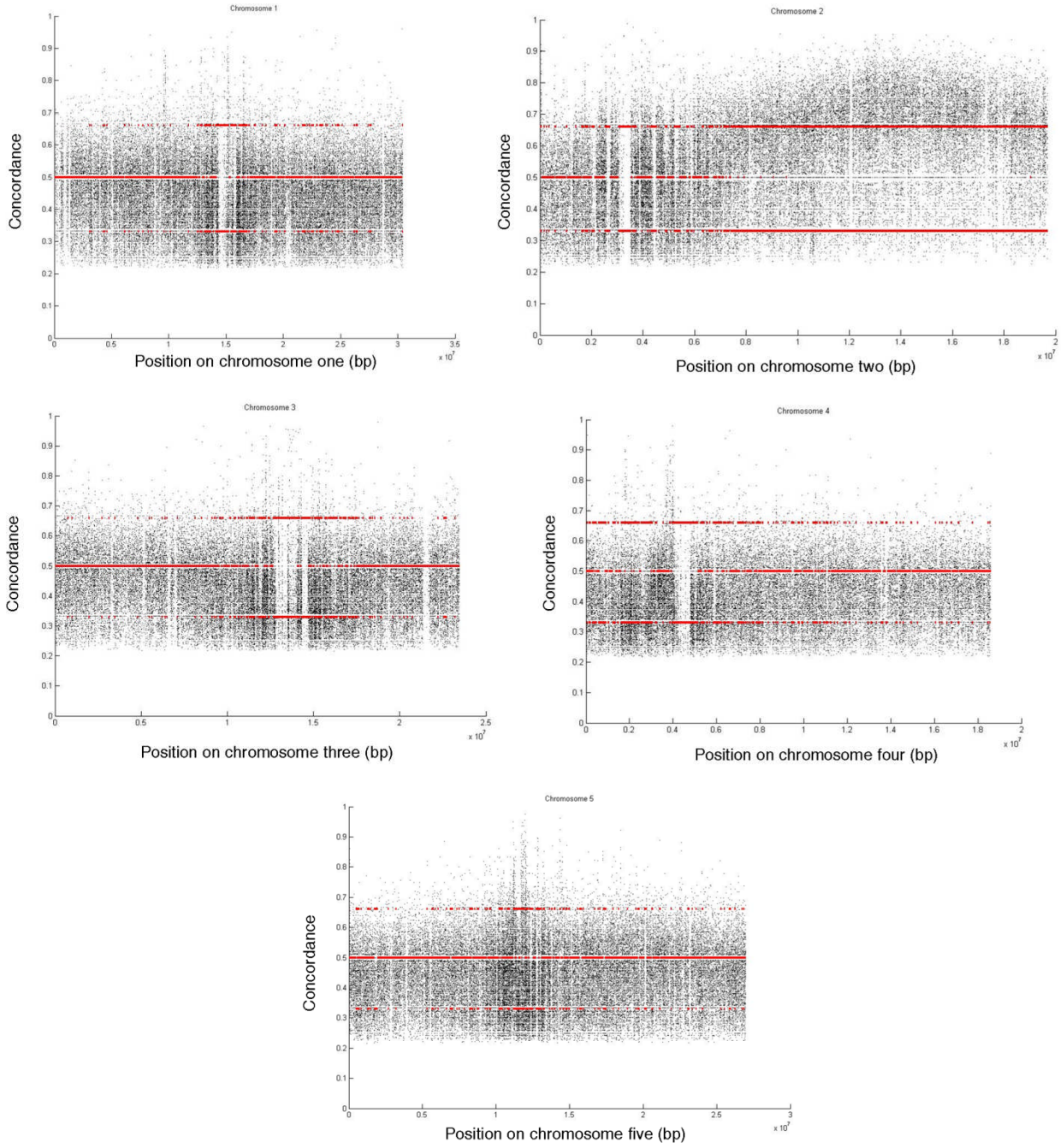

Figure 5.15. SNP data and genotype states called by HMM

Black dots represent individual SNPs along each chromosome. Red lines represent the hidden states called by the Hidden Markov Model (HMM), which calls for either the 0.5 state (1:1 ratio) or the 0.33/0.67 state (2:1 ratio).

Figure from C Greenman (TGAC)

To improve the data quality, another analysis conducted by S Kelly (University of Oxford) only included known SNPs between Col and L*er* (Gan et al., 2011) that were supported by at least 15 reads. The SNPs were collectively evaluated in a series of overlapping windows that group consecutive SNPs within a 30kb interval over a step size of 15kb. The L*er*:Col SNP ratios were calculated in each window and plotted in Figure 5.16 (S Kelly, unpublished data). A notable feature of the plot is that the broad peak on chromosome two has a maximum concordance value of 0.75 instead of the expected 0.67 that corresponds to 2:1 L*er*:Col SNP ratio. A plausible explanation is the bias in transmission of the mutant allele (Section 5.3.4.1). Based on the observed male transmission bias, I determined that the segregation ratio between the WT and the mutant allele is 1.86:1 instead of the theoretical 1:1 ratio (Calculation 5.1). From this ratio, I then determined that the frequency of the WT-allele in the WT segregant population is 0.74, which corroborates to the data in Figure 5.16.

Calculation 5.1. Determination of the segregation ratio and the frequency of the WT allele in a population of WT segregants of heterozygous mutant families

Let A and a be the WT and the mutant allele, respectively. Assuming the male transmission rate of the mutant allele is 0.2, and no bias in female transmission.

			Male	
			0.8	**0.2**
			A	**a**
Female	**0.5**	**A**	0.4 AA	0.1 Aa
	0.5	**a**	0.4 Aa	0.1 aa

Frequencies of each genotype are:
AA= 0.4, Aa= 0.5, aa= 0.1

Frequencies of each allele are:
A= 0.4 + 0.5x0.5= 0.65
a= 0.5x0.5 + 0.1= 0.35
A:a= 0.65:0.35 = 1.86

Hence, the WT to mutant allele segregation ratio is 1.86:1 in contrast to the expected 1:1.

According to the Hardy-Weinberg principle, the frequencies of each genotype in the F2 generation are:
AA= 0.65^2= 0.423
Aa= 2x0.65x0.35= 0.455
aa= 0.35^2= 0.123

Since aa is lethal, only AA and Aa can be found in the mapping population, so the frequencies of each allele are:

A= 0.423 + 0.5x0.455= 0.651
a= 0.5x0.455= 0.228

Therefore, the expected frequency of the WT allele = A/ (A+a)= 0.651/ (0.651 + 0.228)= 0.74.

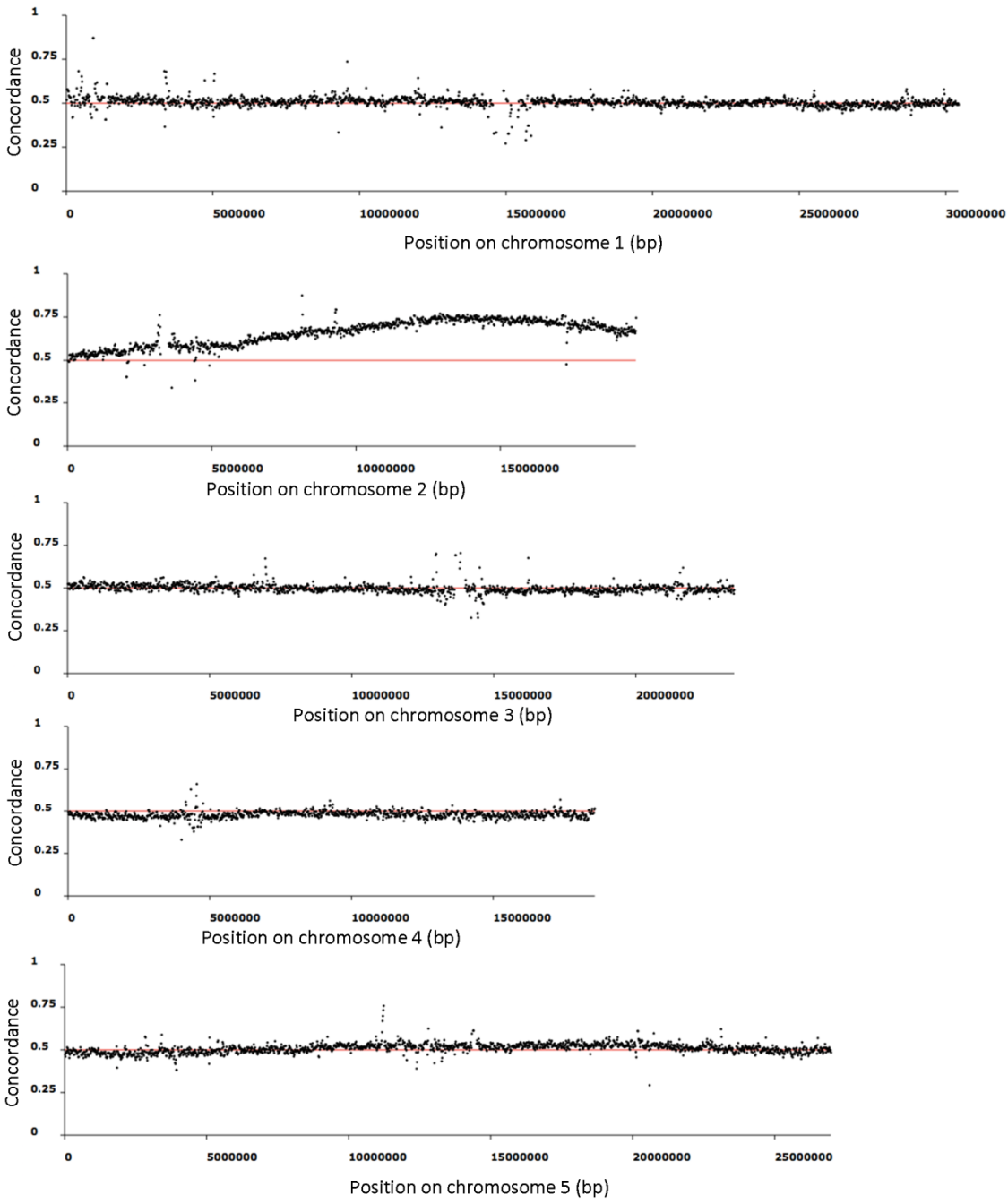

Figure 5.16. Genome-wide SNP frequencies along each chromosome

Only previously confirmed Col/L*er* SNPs with a minimum read depth of 15 bases are included in the analysis. The filtered SNPs were binned at 30kb intervals with a step size of 15kb.

Figure was constructed by S Kelly (unpublished data).

Since the linked region is represented by a broad peak that spans the entire bottom arm of chromosome two, I wondered if this resembles the distribution of SNP ratios as determined from the traditional gel-based method. To answer this, the distributions of SNP ratios over the linked region for *gnl1-2* (Teh, 2007), Mut 21 and Mut 43 were plotted on the same graph (Figure 5.17). *gnl1-2* and Mut 21 were previously identified using the traditional map-based cloning method with a population size of 998 and 1990 chromosomes, respectively (Teh, 2007). As shown in Figure 5.16, *gnl1-2* had a sharp peak, suggesting the increase in genetic resolution with size of the mapping population. Meanwhile, the peaks for Mut 21 and Mut 43 were similarly broad, suggesting similar distribution of recombination frequency. Next, the breadth of each curve was measured by calculating the intervals with less than 5% recombination frequency based on the equation of each curve. The calculated intervals were 2.8Mb, 6.1Mb and 7.9Mb for *gnl1-2*, Mut 21 and Mut 43, respectively. In other words, the the interval of Mut 43 was 21% greater than that of Mut 21 and three-fold greater than that of *gnl1-2*. Given that the population size of Mut 43 is slight smaller than that of Mut 21, I conclude that distribution of recombination frequency observed from deep-sequencing WT segregants of Mut 43 family is similar to what would have been observed using the traditional method with a similar number of homozygous mutant individuals.

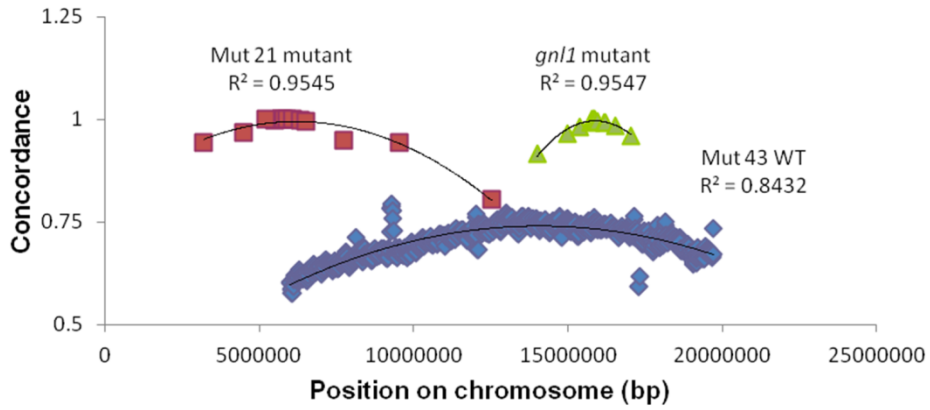

Figure 5.17. Distribution of SNP ratios in *gnl1-2*, Mut 21 and Mut 43

L*er*:Col SNP ratios were determined either by conventional map-based cloning method with homozygous mutant individuals for Mut 21 (red squares) and *gnl1-2* (green triangles), or by deep-sequencing of WT segregants for Mut 43 (blue diamonds). n= number of chromosomes in the mapping population. The regression coefficient (r-squared) values of each curve of best fit are shown.

Comparing Figure 5.15 and 5.16, the SNPs in the latter figure are less stochastic. The strong bias on the bottom arm of chromosome two becomes more apparent. Next, the effects of the binned window size and the read depth filter on the broad peak of chromosome two were evaluated. Three window sizes (30kb, 60kb and 120kb) and three read depth filters (15bp, 30bp and 45bp) were tested. Despite the changing window size, the step size was kept at 15kb to maintain the same number of data points. As shown in Figure 5.18, the data points were less scattered and some outliers were eliminated as the size of sliding window increased. The apex of the curve also became more apparent with increasing window size. On the other hand, increasing the stringency of the read depth filter beyond 15bp did not have any significant improvements on the data quality. In fact, increasing the filter from 30bp to 45bp appeared to have a detrimental effect on the quality as the regression coefficient of the best fit curve has decreased slightly when the read depth filter was increased from 30bp to 45bp. The predicted positions of maximum SNP ratio were determined by calculating the maximum values of each best fit curve. The six plots all point to positions within an 85kb region of chromosome two (Table 5.3).

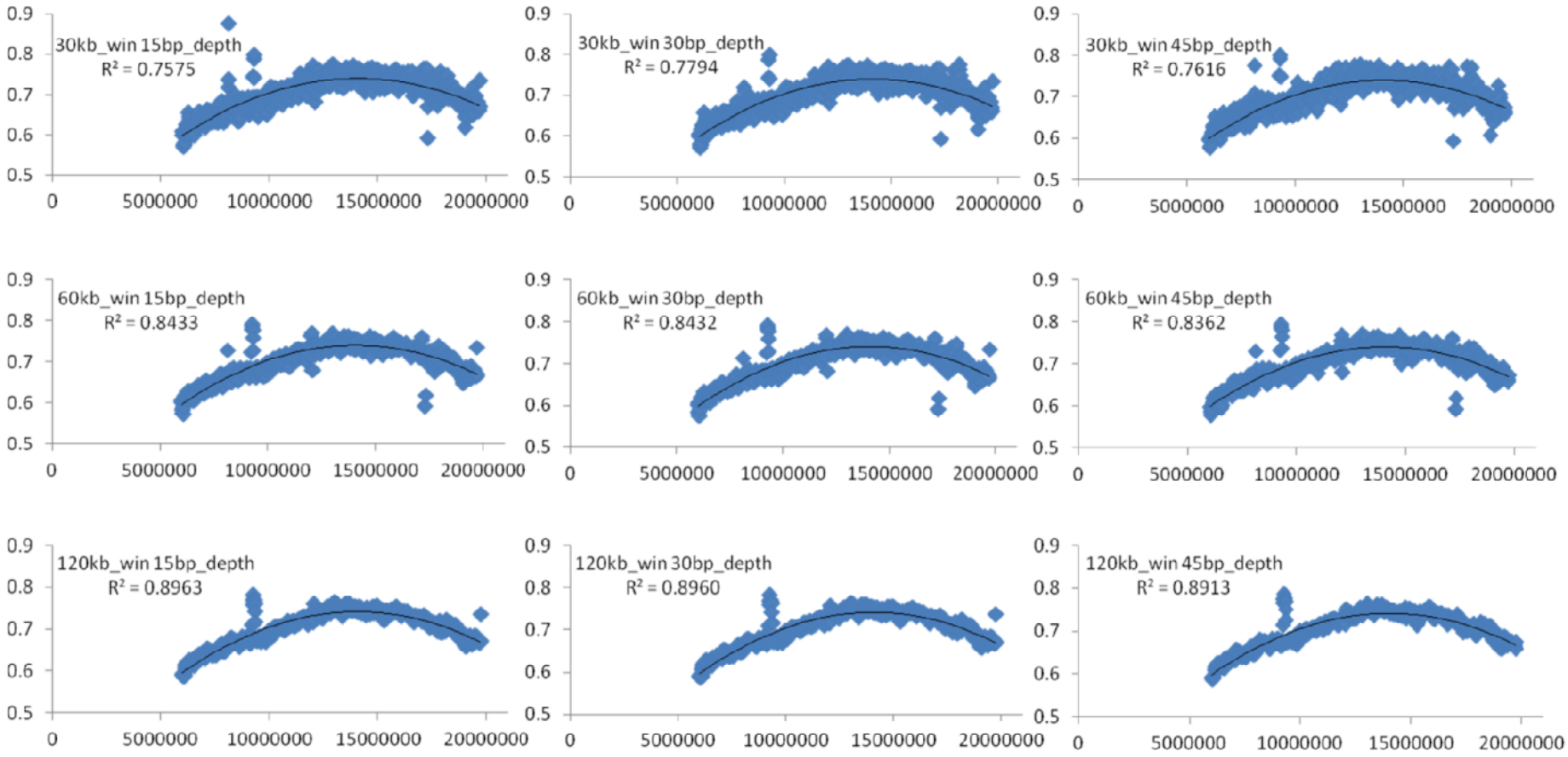

Figure 5.18. The effect of sliding window size and minimum data depth on output

Consecutive SNPs with read-depth (depth) of at least 15bp, 30bp or 45bp were binned in 30kb, 60kb or 120kb windows (win) with a step size of 15kb. The regression coefficient (r-squared) values of each curve of best fit are shown. x-axis represents position on chromosome two; y-axis represents SNP concordance.

Table 5.3. Predicted maximum SNP ratio position in different sliding window size and minimum read-depth filter settings

Sliding Window Size (kb)	Minimum Read-depth (bp)		
	15	30	45
30	14 095 000bp	14 120 000bp	14 093 000bp
60	14 078 000bp	14 082 000bp	14 055 000bp
120	14 072 000bp	14 071 000bp	14 035 000bp

To generate a more reliable prediction of the position of maximum SNP ratio, only regions with high SNP ratios (from 9Mb to the end of chromosome) were included in the plot in Figure 5.19. And to reduce artefacts from low-coverage and high-coverage SNPs, only SNPs that are supported by 30-80 reads were included in this analysis. The resulting plot appeared have fewer outliers than the curves in Figure 5.18. Based on this new plot, a best fit curve was drawn and its maximum value, which represents the maximum SNP ratio, is at position 14 317 000bp on chromosome two (Figure 5.19).

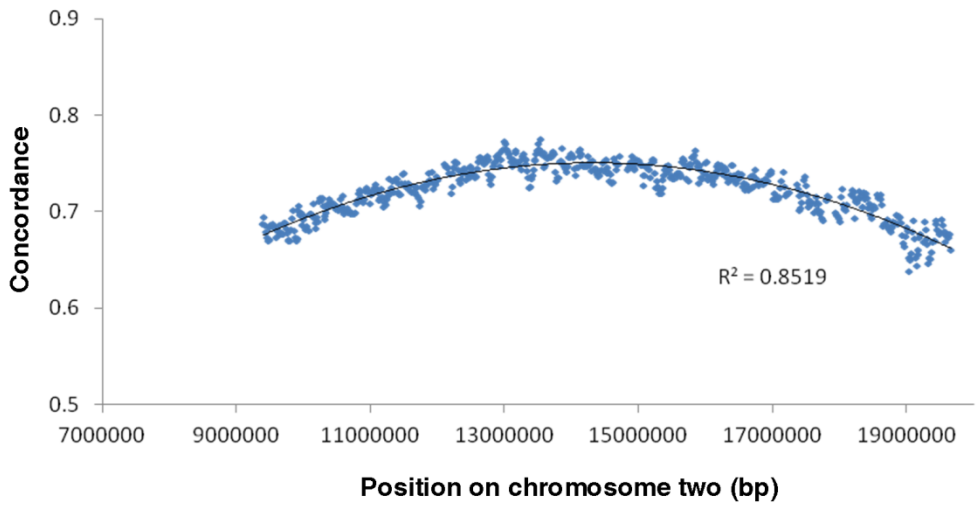

Figure 5.19. Determination of the position of maximum SNP ratio

SNPs with read-depths between 30 and 80bp were binned in 60kb windows with a step size of 15kb. Only SNPs from 9000000bp to the end of chromosome two were analyzed. The regression coefficient (r-squared) values of each curve of best fit are shown. The position where the curve of best fit has the maximum SNP ratio is 14316828bp.

SNPs were ranked according to their distance from the maximum SNP ratio to identify likely candidates of the causative EMS-induced mutation. Since it has been projected that there is a 95% chance of finding a recombinant 75kb away from a given chromosome position with 500 individuals (Figure 4.2b; Jander et al., 2002), SNPs that are positioned within 150kb from the predicted maximum SNP ratio were evaluated. Unlike in the mapping process, known polymorphisms between Col and L*er* were filtered out; and only SNPs that are within a coding sequence and those that show canonical EMS-induced G/C to A/T transition were included. The SNPs were identified by a SNP-calling algorithm written by S Kelly (University of Oxford) and visually on Integrative Genomic Viewer (Robinson et al., 2011). Both approaches identified some SNPs with concordance of over 60%. Since the frequency of the Mut 43 allele is only 25%, the SNPs with high concordance are likely to represent the variants between the reference L*er*-0 sequence and the L*er* used in our lab. Hence, those SNPs were filtered out by only including SNPs with 60% concordance or less. The remaining SNPs were ranked according to their distance from the predicted peak and their chi-square values calculated from an expected value of 0.25 (Table 5.4 and 5.5). A notable observation is that the list does not include any classical membrane trafficking genes and there are not any obvious candidate genes based on the observations on Mut 43.

Table 5.4. Putative EMS-induced SNPs ranked according to chi-square values and distance from the maximum L*er*:Col SNP ratio

Accession	Distance to Peak (bp)	Position on Chromosome (bp)	Reference Base	Mutant Base	Codon change*	Amino Acid Change	Support**	Concordance	Annotation
AT2G34110	85332	14402332	G	A	Intron		5	0.25	Forkhead-associated (FHA) domain-containing protein
AT2G34130	95362	14412362	G	A	GGG to GAG	G to E	3	0.25	CACTA-like transposase family
AT2G33790	21910	14295090	G	A	CTA to TTA	Silent	21	0.35	AGP30 (ARABINOGALACTAN PROTEIN30)
AT2G33790	21906	14295094	G	A	ATC to ATT	Silent	25	0.373134	AGP30 (ARABINOGALACTAN PROTEIN30)
AT2G33980	34973	14351973	G	A	Intron		10	0.166667	AtNUDT22 (Arabidopsis thaliana Nudix hydrolase homolog 22); hydrolase
AT2G33790	21928	14295072	C	T	GCC to ACC	A to T	30	0.491803	AGP30 (ARABINOGALACTAN PROTEIN30)
AT2G33980	34984	14351984	G	A	Intron		9	0.155172	AtNUDT22 (Arabidopsis thaliana Nudix hydrolase homolog 22); hydrolase
AT2G33670	71613	14245387	G	A	AAG to AAA	Silent	8	0.205128	MLO5 (MILDEW RESISTANCE LOCUS O 5); calmodulin binding
AT2G34130	92640	14409640	C	T	AAC to AAT	Silent	4	0.210526	CACTA-like transposase family
AT2G37780	25729	14291271	C	T	AGC to AAC	S to N	25	0.6098	Cysteine/Histidine-rich C1 domain family protein

AT2G34130	92926	14409926	G	A	TGG to TGA	W to Stop	6	0.214286	CACTA-like transposase family
AT2G34040	63680	14380680	C	T	Intron		11	0.314286	Apoptosis inhibitory 5 (API5) family protein
AT2G34110	85357	14402357	C	T	Intron		5	0.333333	Forkhead-associated (FHA) domain-containing protein
AT2G34130	93544	14410544	G	A	GGT to GAT	G to D	10	0.212766	CACTA-like transposase family
AT2G34130	92630	14409630	C	T	CTC to CTT	Silent	4	0.190476	CACTA-like transposase family
AT2G33790	22776	14294224	G	A	Intron		65	0.833333	AGP30 (ARABINOGALACTAN PROTEIN30)
AT2G33720	52217	14264783	G	A	GTG to ATG	V to M	6	0.130435	AP2/B3-like transcriptional factor family protein
AT2G33735	48375	14268625	G	A	Intron		16	0.470588	DNA J-domain heat shock N-terminal domain-containing protein
AT2G34130	93127	14410127	C	T	GCG tp GTG	A to V	2	0.153846	CACTA-like transposase family
AT2G34130	93374	14410374	C	T	GCG to GCT	Silent	2	0.153846	CACTA-like transposase family
AT2G33735	48388	14268612	G	A	Intron		26	0.6341	DNA J-domain heat shock N-terminal domain-containing protein

AT2G34030	58802	14375802	G	A	Intron		23	0.442308	Calcium-binding EF hand family protein
AT2G34040	64459	14381459	G	A	Intron		15	0.357143	Apoptosis inhibitory 5 (API5) family protein
AT2G34130	95347	14412347	G	A	TGT to TAT	C to Y	1	0.125	CACTA-like transposase family
AT2G33670	71620	14245380	G	A	AGA to AAA	R to K	5	0.128205	MLO5 (MILDEW RESISTANCE LOCUS O 5); calmodulin binding
AT2G34040	64210	14381210	C	T	Intron		21	0.411765	Apoptosis inhibitory 5 (API5) family protein
AT2G34040	64437	14381437	G	A	Intron		19	0.38	Apoptosis inhibitory 5 (API5) family protein
AT2G34040	64430	14381430	G	A	Intron		21	0.42	Apoptosis inhibitory 5 (API5) family protein
AT2G34040	64198	14381198	C	T	Intron		23	0.442308	Apoptosis inhibitory 5 (API5) family protein
AT2G34040	64433	14381433	G	A	Intron		21	0.42	Apoptosis inhibitory 5 (API5) family protein
AT2G34040	60909	14377909	C	T	3' UTR		40	0.625	Apoptosis inhibitory 5 (API5) family protein
AT2G34040	62083	14379083	G	A	Intron		33	0.5593	Apoptosis inhibitory 5 (API5) family protein
AT2G34130	92525	14409525	C	T	AAC to AAT	Silent	8	0.4	CACTA-like transposase family

AT2G34040	61870	14378870	C	T	Intron		38	0.791667	Apoptosis inhibitory 5 (API5) family protein
AT2G34100	96354	14413354	C	T	Intron		3	0.12	Unknown protein
AT2G34130	94472	14411472	C	T	TTC to TTT	Silent	3	0.115385	CACTA-like transposase family
AT2G34110	81583	14398583	G	A	Unknown		28	0.54902	Forkhead-associated (FHA) domain-containing protein
AT2G33220	237600	14079400	G	A	Intron		12	0.352941	GRIM-19 protein
AT2G34130	92527	14409527	G	A	AGC to AAC	S to N	9	0.45	CACTA-like transposase family
AT2G34130	93229	14410229	C	T	GCT to GTT	A to V	9	0.140625	CACTA-like transposase family
AT2G33490	130006	14186994	G	A	CCT to CCA	silent	4	0.117647	Hydroxyproline-rich glycoprotein family protein
AT2G33550	105754	14211246	G	A	TCG to TTG	S to L	5	0.119048	Homeodomain-like superfamily protein
AT2G34315	163618	14480618	C	T	AGG to ATG	R to M	10	0.153846	Disease resistance protein-related
AT2G34315	163611	14480611	C	T	CGG to CGA	Silent	9	0.138462	Disease resistance protein-related
AT2G33220	236922	14080078	G	A	3' UTR		30	0.535714	GRIM-19 protein

* 5’ UTR- 5’ Untranslated region; 3’UTR- 3’ Untranslated region

** Number of reads supporting the mutant base

Table 5.5. Scores for each ranked SNPs

Accession	Chi-square	Chi-square rank	Distance Rank	Score (Chi-square Rank x Distance Rank)
AT2G34110	0.000	1	48	48
AT2G34130	0.000	2	78	156
AT2G33790	2.400	39	6	234
AT2G33790	4.063	47	5	235
AT2G33980	1.667	30	12	360
AT2G33790	14.266	57	7	399
AT2G33980	2.086	36	13	468
AT2G33670	0.314	13	43	559
AT2G34130	0.118	8	70	560
AT2G37780	21.229	60	10	600
AT2G34130	0.143	9	71	639
AT2G34040	0.579	22	33	726
AT2G34110	0.417	15	49	735
AT2G34130	0.261	10	75	750
AT2G34130	0.298	12	69	828
AT2G33790	106.167	95	9	855
AT2G33720	2.630	41	22	902
AT2G33735	6.618	52	19	988
AT2G34130	0.481	16	72	1152
AT2G34130	0.481	17	74	1258
AT2G33735	24.197	63	20	1260
AT2G34030	7.692	53	25	1325
AT2G34040	1.929	35	41	1435
AT2G34130	0.500	21	77	1617
AT2G33670	2.314	37	44	1628
AT2G34040	5.338	48	36	1728
AT2G34040	3.380	46	39	1794
AT2G34040	5.780	49	37	1813
AT2G34040	7.692	54	35	1890
AT2G34040	5.780	50	38	1900
AT2G34040	36.000	71	27	1917
AT2G34040	22.578	62	31	1922
AT2G34130	1.800	33	67	2211
AT2G34040	56.333	84	30	2520
AT2G34100	1.690	31	83	2573
AT2G34130	1.885	34	76	2584
AT2G34110	18.240	58	45	2610
AT2G33220	1.441	28	96	2688
AT2G34130	3.200	44	68	2992
AT2G34130	3.063	43	73	3139

AT2G33490	2.382	38	85	3230
AT2G33550	2.881	42	84	3528
AT2G34315	2.404	40	89	3560
AT2G34315	3.235	45	88	3960
AT2G33220	18.286	59	95	5605

5.4 Discussion

5.4.1 Mut 43 as a temperature-sensitive membrane trafficking mutant

Although it was isolated from a temperature-sensitive mutant screen, Mut 43 shows both developmental and enhanced secGFP fluorescence phenotypes even at permissive temperature. However, the phenotypes are enhanced by the heat treatment, with the mutant having a different pattern of secGFP localization and ultimately losing viability upon heat treatment. The secGFP marker is localized in the ER and in small punctate structures. In root epidermal cells, secGFP is observed in the vacuole in addition to the ER after 24h of heat treatment. The vacuolar localization of secGFP is consistent with the increased level of truncated secGFP in Mut 43 after the heat treatment as shown by the immunoblot analysis. It is likely that the majority of the cleaved secGFP represents the population in the vacuole, where GFP-fusion proteins can be efficiently cleaved (Tamura et al., 2003).

It has been proposed that GFP contains a weak vacuolar sorting determinant, so that secGFP would enter the vacuolar pathway upon perturbation of post-Golgi secretory traffic (Zheng et al., 2005). The increased abundance of secGFP in the vacuole at restrictive temperature suggests a change in turnover of secGFP in the vacuole. This may be due to an increase in secGFP expression, a decrease in hydrolytic activities in the vacuole and/or an increase in inhibition of secretion. According to mRNA expression data (Teh, 2007), the slight increase in secGFP transcript level in Mut 43 does not seem to be sufficient to entirely contribute to the observed increase in fluorescence intensity. Another possible explanation for the observed increase in secGFP protein is a change in turnover due to a reduction in hydrolytic enzyme activities in the vacuole. Hydrolase activities are optimal at acidic pH (Boller and Kende, 1979). The pH in the lytic vacuole is regulated by two proton pumps on the tonoplast- V-type H^+ ATPase (V-ATPase) and H^+

pyrophosphatase (V-PPase). It has been shown that mutants that are deficient in V-ATPase have a more alkaline vacuolar pH (Krebs et al., 2010). Hence, a defect in one of the proton pumps may contribute to the secGFP phenotype in Mut 43. If this is the case, then it can explain the vacuolar accumulation of secGFP but does not adequately explain why the vacuolar localization is observed in the root but not in other tissues of Mut 43 seedlings. Therefore, it comes down to the last explanation, which is membrane trafficking defects that perturb the secretion of soluble proteins.

5.4.2 Transgene expression in Mut 43

A surprising observation in Mut 43 is that the fluorescent intensities of organelle markers were often significantly higher than in the WT. These markers were regulated by the 35S promoter from cauliflower mosaic virus (for mCHERRY-HDEL, ST-mCHERRY and ratiometric marker) or the endogenous UBQ10 promoter (for YFP-VAMP711). Both are known for stable expressions ranging from moderate to high level in most cell types (Nelson et al., 2007; Geldner et al., 2009). A ratiometric marker, secN-RFP-2A-GFP-HDEL, was used to examine ER export relative to the transgene expression. Quantitative analysis revealed that the marker had a higher expression in Mut 43 than in the WT at both permissive and restrictive temperatures. After the difference in expression was accounted for, there was still a greater quantity of the ER export marker, secN-RFP-2A, in the nuclear envelope of Mut 43 than in the WT, suggesting that the observed increase in RFP fluorescence intensity in Mut 43 is not solely an effect of higher transgene expression.

5.4.3 The root radial swelling phenotype

Another interesting phenotype of Mut 43 is the radial swelling of the root tip upon extended heat treatment. Based on light microscopy, the epidermal cells in the most apical part of the root

elongation zone are no longer arranged in regular files. Instead, cell shapes and sizes became irregular and cells in the epidermal cell layer appeared larger in general compared to the WT. It is uncertain whether other cell types in the swollen area are also abnormal since they cannot be visualized clearly. Unfortunately, due to time-constraints, the swelling phenotype could not be characterized extensively. The current data could only establish that the radial swelling is caused by the enlarged cells in the epidermal layer. It would be interesting to examine the root cross-section at the swollen region to measure the root diameter, to determine whether there are additional cell layers and to examine more carefully the cell size in each layer.

The root-tip swelling phenotype is not highly penetrant as only 50% of the mutant seedlings exhibit this phenotype. While the intracellular secGFP accumulation phenotype is enhanced after 24h at restrictive temperature, the root-tip swelling phenotype took 48h at restrictive temperature to fully develop. It suggests that the swelling phenotype is a secondary effect of the mutation possibly due to intracellular accumulation of secretory cargoes. A survey of root morphology mutants in *Arabidopsis* reveals that the observed phenotypes in many mutants are generally ascribed to either perturbation in cell wall polysaccharide synthesis or processing (Arioli et al., 1998; Lane et al., 2001; Burn et al., 2002; Roudier et al., 2005; Wang et al., 2006a), or disruption in microtubule organization and/or related elements (Bannigan et al., 2006; Bannigan et al., 2007; Yang et al., 2011). Since membrane trafficking is associated with the delivery of polysaccharides to the cell wall (Wightman and Turner, 2010) and cytoskeleton dynamics (Vale, 2003; Wang et al., 2006b; Zhang et al., 2010), it is speculated that a mutant with secretion defects can also develop atypical root morphology as a consequence.

5.4.4 Mapping Mut 43 through deep-sequencing

Map-based cloning cannot be easily applied to embryo- or seedling-lethal mutants because of the limited amounts of DNA that can be isolated from individuals. I have first attempted to extract DNA from seven-day-old Mut 43 seedlings. Despite two attempts with the pooled mutants from mapping cross families, a sufficient quantity of high-quality DNA required for deep-sequencing could not be obtained. Besides these two attempts, I was also unable to extract DNA from 300 backcrossed homozygous mutant seedlings (data not shown). These experiences reflect the difficulties in conducting genomic studies on early-lethal mutants. To overcome the problems with DNA extraction, I have tested the feasibility of using the WT segregants of the Mut 43 heterozygous mapping cross families for mapping through deep-sequencing. If this is successful, it will immeasurably reduce the time and cost for mapping other seedling-lethal membrane trafficking mutants that have limited prospects of isolating sufficient DNA for traditional map-based cloning.

Next-generation sequencing technologies have been widely used for mapping and identifying the causative point mutation by sequencing homozygous mutant individuals (Sarin et al., 2008; Srivatsan et al., 2008; Blumenstiel et al., 2009; Schneeberger et al., 2009; Austin et al., 2011), but reports on mapping with the WT siblings of a heterozygous family have been limited (Lindner et al., 2012). Though the approach is theoretically sound, in practice it faces the uncertainty of whether the current sequencing technology can generate data of sufficient quality to precisely quantify the polymorphisms within the pooled population. Recently, a method was developed to map a homozygous lethal mutant in *Arabidopsis* by analyzing the segregation ratios of EMS-induced mutations in backcrossed heterozygous mutants (Lindner et al., 2012).

In this work, the Mut 43 locus was mapped using the phenotypically WT individuals in the F2 generation of mapping cross families. The data were refined by excluding EMS-induced SNPs in the mapping process, filtering out low read-depth SNPs that are likely to yield spurious ratios due to small sampling size and evaluating SNPs collectively using a sliding window approach to average out the intrinsic noise. It was found that increasing the minimum read depth filter from 15bp did not result in significant improvements to data quality, and having a stringent filter (45bp in our 40x-coverage data) is in fact detrimental to the data quality likely because it creates a bias towards reads on repetitive and transposable elements that are prone to high-coverage artefacts (Lindner et al., 2012). On the other hand, the size of the sliding window has a noticeable impact on the distribution of the SNP data points. By averaging more consecutive SNPs in a bigger window, the data points become less scattered. We have also attempted averaging individual SNPs so all SNPs are equally weighted, or averaging individual reads so the SNPs are differentially weighted according to their read depths, it was concluded that the two averaging methods did not change the data quality significantly (data not shown). Consistent with previous BSA results (Teh, 2007), a strong bias in the SNP ratio was observed on the bottom arm of chromosome two. After a highly refined SNP ratio plot is generated, the position of Mut 43 is predicted based on the maximum SNP ratio. SNPs that are positioned within 150kb away from the predicted position were examined. Surprisingly, after eliminating all the known SNPs between Col and L*er*, there are still a significant number of non-reference SNPs with concordance above 0.60. The high concordance suggests that it is likely to be polymorphisms in L*er* that are not in the L*er* reference genome either because they are not recorded in the reference genome or they reflect the variation between the reference L*er*-0 and the L*er*-0 in our laboratory. After these SNPs are also removed from the list, it was found that none of the SNPs represent mutations from a gene that is known to relate to membrane trafficking function. This implies that Mut 43 is a mutant allele of

a novel membrane trafficking gene. But before this claim is substantiated, it is imperative to seek other ways to improve the accuracy of the predicted position.

There are other analyses that can be conducted in the dataset to infer the position of the causal mutation. It may be possible to infer a mapping interval by dividing the regions of chromosome two into known haplotype blocks and then determining the block where the maximum SNP ratio is found. Incorporating the information on recombination hotspots to the data may provide a more accurate prediction of the mutation. In the case of Mut 43, four recombination hotspots are detected within 2Mb of the predicted mutation position (Figure 5.20). These nearby hotspots may affect the SNP ratio distribution and therefore the outcome of the analysis. However, the *Arabidopsis* recombination data that are currently available (Singer et al., 2006) have limited genetic resolution due to small sample size. Recombination data from The Multiparent Advanced Generation Inter-Cross (MAGIC) recombinant inbred lines that are expected to be publicly available in the near future (R Mott, personal communication) may help improve the accuracy of the prediction significantly. Another analysis that is worth attempting is a chastity statistical analysis that determines the position of the mutation by assessing the degree of the difference of each SNP to its reference base (Austin et al., 2011). It has been shown that this method can map a mutation with as few as 80 homozygous mutant individuals in contrast to 500 individuals in SHOREmap (Schneeberger et al., 2009). But once again, it is uncertain whether the analysis is sensitive enough to detect the subtle shift in SNP ratios when mapping with WT siblings.

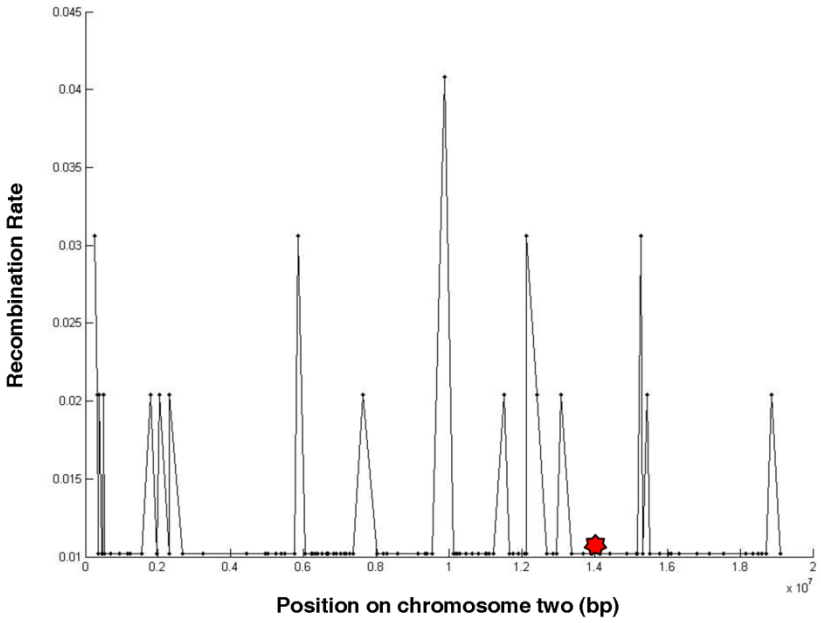

Figure 5.20. Recombination hotspots on chromosome two

Variation in recombination rate across chromosome two. Each spike represents a recombination hotspot. The predicted position of Mut 43 mutation is indicated by the red star.

Data from Singer et al., 2006; graph prepared by C Greenman (TGAC)

Once a position of maximum SNP ratio is determined, the next step is to identify the causative EMS-induced mutation. In the WT sibling sample, the causative SNP in the case of Mut 43 is expected to be found in one out of four reads. This poses a problem as the causative point mutation is only supported by a minority of reads and therefore is difficult to distinguish its signal from noise. Since it is not possible to look for homozygous SNPs in lethal mutants, a compromised alternative would be to sequence the backcrossed heterozygous mutant plants, in which homozygous SNPs are either background EMS-induced mutations or variations from the reference genome that can be discarded from the list of candidate causative mutation. Once the candidate gene loci are identified, the exact gene locus is then confirmed by complementation experiments.

5.4.5 Future Directions

The primary objective of forward genetic screening is to identify the gene that attributes to the phenotype of interest, so it is imperative to identify the genetic cause of Mut 43. Preliminary analyses of the data from deep-sequencing of WT segregants of Mut 43 mapping cross families show encouraging signs that such an approach can indeed be used to identify early-lethal mutations, but more work is required to evaluate the accuracy of the predicted causative mutation position stated in this thesis and to seek ways that can improve the method.

The intracellular secGFP accumulation phenotype was characterized with ER, Golgi and tonoplast markers. secGFP was visible in the punctate structures that do not colocalize with ER or Golgi. It is important to identify the site of secGFP accumulation to fully characterize the secretory defects in Mut 43. It would be helpful to coexpress the secGFP with markers in the late secretory pathway and the vacuolar sorting pathway (e.g. TGN, endosome or tonoplast markers).

The atypical root-tip and cotyledon cell shapes in Mut 43 raise the possibility that the mutation affects the secretory pathway in such a way that the anisotropic cell wall expansion is perturbed. Hence it may be worthwhile to investigate the elements that affect expansion in the future. As a starting point, one may want to investigate the dynamics of microtubule and/ or the polysaccharide composition of the cell wall.

Chapter 6 General Discussion

6.1 The secGFP-based forward genetic approach

The primary objective of the work presented in this thesis is to study the secretory trafficking mechanisms in plants by identifying novel and essential genes that contribute to the process. To do so, putative membrane trafficking mutants that were isolated in fluorescent protein-based forward genetic screens with a secGFP-based marker were characterized in this study. The advantage of a fluorescent imaging-based approach is that the samples do not require any fixation and can be visualized *in vivo* under physiological condition. It is particularly beneficial for studying dynamic processes like membrane trafficking such that the events can be visualized in real-time. secGFP has been established as a reliable marker to assay secretory traffic before it was adopted for forward genetic studies (Batoko et al., 2000; Zheng et al., 2004; Pinheiro et al., 2009). The underlying concept of using secGFP as a marker is that it travels along the conventional secretory pathway for soluble proteins and becomes weakly fluorescent at cell exterior. By screening for mutants that exhibit enhanced secGFP fluorescence, the screen is expected to isolate mutants that accumulate secGFP in the endomembrane system due to defects in secretion and mutants with altered properties of the cell exterior so that secGFP can now accumulate in fluorescent form. Both types of mutants have been characterized so far, with the *gsh2*, *gnl1* and Mut 43 belonging to the former as secretory mutants (Teh and Moore, 2007) and Mut 21 to the latter as a mutant with alkalized apoplast.

The rationale to screen for seedling-lethal secretory mutants is supported by both experimental and theoretical evidence. In previous secGFP-based forward genetic screen, many putative mutants with a strong secGFP-accumulating phenotype could not be recovered because of their lethal phenotypes. Those that are viable often have a weak and inconsistent secGFP-

accumulating phenotype (Zheng, 2001). It was reasoned that membrane trafficking is such an important process that any mutations in essential membrane trafficking genes that significantly perturb this process would be lethal. This is supported by the observations that complete disruption of conserved and indispensable membrane trafficking functions would provoke embryo- and gametophyte-lethality (Rojo et al., 2001; Sanderfoot et al., 2001; Surpin et al., 2003; Faso et al., 2009; Pinheiro et al., 2009). This study also showed that the strong mutant alleles of *GSH2* are seedling-lethal and only a weak allele with milder perturbation, *gsh2-6*, is viable. Furthermore, the screen was designed to isolate seedling-lethal mutants rather than embryo- or gametophyte-mutants because it is more likely to identify plant-specific genes and less likely to find mutations associated with general development and highly conserved genes from seedling-lethal mutations (Jürgens et al., 1991; Schneider et al., 1998; Berná et al., 1999; Majira et al., 2002). This reasoning is supported by the TILLING (targeted induced local lesions in genomes) analysis of the putative seedling-lethal secretory mutants in our group's collection, in which no SNP was found in 102 conserved membrane trafficking gene loci of 35 mutants (J Perez-Gomez, H Neto, I Moore, unpublished data). And indeed, *GSH2*, which has never been implicated in membrane trafficking prior to this study, was identified from four mutants from the seedling-lethal mutant screen.

This thesis has presented the characterization of *gsh2*, Mut 21 and Mut 43. In Chapter 3, four mutant alleles of *GSH2* from the collection helped establish the effects of glutathione biosynthesis on the secretory pathway and ER morphology. The four novel mutant alleles exhibit a varying degree of developmental phenotypes that correlates to the glutathione level, and all four mutants accumulate secGFP in spherical ER bodies due to γ-EC hyperaccumulation. Though loss-of-function *GSH2* alleles have been isolated in the past (Pasternak et al., 2008; Jobe et al.,

2012) and fluctuations in cytosolic redox state have been implicated in perturbation of secretory traffic (Pompa and Vitale, 2006), this is the first study to demonstrate the plant secretory pathway's sensitivity to perturbations in glutathione biosynthesis, and specifically on how an intermediate product of the glutathione biosynthesis pathway affects ER biogenesis. The *gsh2* mutants, which are the first mutants in the collection that have been fully characterized, not only demonstrate the benefits of working with multiple mutant alleles, but they also demonstrate the power of forward genetics to reveal novel function of a conserved gene.

In Chapter 4 and 5, two other temperature-sensitive mutants, Mut 21 and 43, are described. These are the only two *bona fide* temperature-sensitive mutants that were isolated from 140 000 M2 plants. Compared to the 23 complementation groups of temperature-sensitive secretory mutants that were isolated in yeast (*Saccharomyces cerevisiae*) (Novick et al., 1980), this highlights the difficulty of isolating conditional mutant alleles in higher organisms like *Arabidopsis*. Such a low occurrence of temperature-sensitive mutants is possibly attributed to the more elaborated and complex gene families in higher organisms such that many temperature-sensitive mutant phenotypes are masked by functional redundancy. Another possibility is that plants, in general, are more tolerant to changes in ambient temperature as a way to cope with the sessile lifestyle, so that a shift from 20˚C to 31˚C may not be sufficient to trigger the phenotypes of temperature-sensitive mutants. Mut 21 shows enhanced secGFP fluorescence and is therefore isolated as a putative mutant, but it is not a secretory mutant that accumulates secGFP intracellularly. Instead, it is a mutant that achieves enhanced secGFP fluorescence phenotype by accumulating fluorescent secGFP in the apoplast. A plausible explanation is that the mutation has resulted in a change in apoplastic property in cotyledon epidermal cells for secGFP to be fluorescent. Consistent with this explanation, this study has shown that Mut 21 had

an alkalized apoplast at restrictive temperature. In contrast, Mut 43 appears to be a promising secretory mutant as secGFP has been confirmed to localize in the ER as well as in small punctate structures that exclude ER and Golgi markers. In root cells, fluorescent secGFP is also localized in the vacuole at restrictive temperature. Quantitative analysis also reveals that ER export is also perturbed in the mutant. These findings suggest that the mutation affects the early secretory pathway. Preliminary mapping data show that none of the gene loci within the mapping interval of Mut 43 is associated with membrane trafficking function, suggesting that Mut 43 is a mutant allele of a novel membrane trafficking gene.

6.2 Other fluorescent protein-based imaging forward genetic screens in membrane trafficking studies

In recent years, other research groups have also taken similar fluorescent protein-based forward genetic approach to study membrane trafficking. Their research interest is reflected by their chosen fluorescent protein markers in their studies. For example, Hara-Nishimura's and Brandizzi's groups focused on the biogenesis of organelles in the early secretory pathway by using markers that normally localize in those organelles and screening for mutants that show atypical morphology or motility of organelles (Matsushima et al., 2003a; Yamada et al., 2008; Faso et al., 2009; Nakano et al., 2009; Marti et al., 2010b; Stefano et al., 2012); Raikhel's and Hara-Nishimura's groups investigate the vacuolar sorting pathways and vacuole biogenesis with vacuole-targeting markers (Tamura et al., 2005; Fuji et al., 2007; Tamura et al., 2007; Chary et al., 2008; Agee et al., 2010); Friml's group studies the PIN1-trafficking pathway with GFP-tagged PIN1 (Paciorek et al., 2005; Tanaka et al., 2009; Feraru et al., 2010; Zwiewka et al., 2011). Using the fluorescent imaging-based forward genetic approach, all these groups have identified novel and essential genes that are related to their research questions.

Comparing the membrane trafficking mutants from other imaging-based forward genetic studies with the mutants that were characterized in this study, the first notable difference is that the mutants from other groups are viable. Raikhel's group has described that half of the 211 mutants with vacuole biogenesis defects are lost due to their lethal phenotype and therefore has only focused on milder mutants for characterization (Avila et al., 2003). Brandizzi's group, who primarily screens for mutants with defects in Golgi function and biogenesis, also reports that 16% of their 188 mutants have a lethal phenotype while other viable mutants suffer noticeable growth and reproduction defects (Boulaflous et al., 2008), consistent with the notion that severe perturbation in the secretory pathway or the Golgi function impacts greatly on viability. However, it is not clear whether the other groups have also encountered a similar situation. Among the characterized mutant alleles, some belong to classical membrane trafficking genes that are partially redundant (Faso et al., 2004; Nakano et al., 2009). Another distinct feature of the reported mutants is that a number of them form atypical aggregates of endomembranes (Nakano et al., 2009; Faso et al., 2009; Marti et al., 2010; Stefano et al., 2012; Agee et al., 2010; Tamura et al., 2007; Feraru et al., 2010; Zwiewka et al., 2011). At the same time, aggregates are also observed in *gnl1* (Teh and Moore, 2007) and *gsh2*, but not in Mut 21 and 43. With regards to our secGFP-based screen, given that membrane trafficking mutants often form aggregates of different sizes, it may be a good idea to look for mutants that exhibit enhanced secGFP fluorescence and form endomembrane aggregates simultaneously in the future.

6.3 Comparison of forward genetics with other genetic approaches used for membrane trafficking research

Many groups have taken on the fluorescent protein-based forward genetic approach because forward genetic is an unbiased approach that can identify both non-redundant novel and known genes related to a particular process of function. Since it only identifies mutants with distinct phenotypes, it avoids the problem with functional redundancy. Moreover, EMS mutagenesis gives rise to a variety of hypomorphic, conditional and dominant mutations. This feature is particularly advantageous in membrane trafficking studies because membrane trafficking genes are often pleiotropic. For example, a dynamin DRP1A, which pinches off clathrin-coated vesicles from the TGN membrane (Murphy et al., 2002; Sawa et al., 2005), is implicated in fertilization, embryogenesis and leaf trichome biogenesis (Kang et al., 2003). Also, a PVC/vacuolar Qa-SNARE AtVAM3/SYP22 is also known to participate in leaf formation, flowering, shoot gravitropism and expansion, and myrosinase expression (Yano et al., 2003; Ohtomo et al., 2005; Ueda et al., 2006; Uemura et al., 2010). Having alleles with different level of gene activities of these pleiotropic genes would be helpful to probe the relationship between gene activities and mutant phenotypes. This point is exemplified by the four *GSH2* mutant alleles in this study as the difference in the developmental phenotypes between the strong and the weak alleles reveal the correlation between the level of glutathione and seedling growth, and yet all four mutant alleles show similar degree of aberrant ER morphology, thereby suggesting a small reduction in GSH2 activity is all that is required to have an effect on the ER. For these reasons, an EMS forward genetic approach is more preferable than studies with T-DNA insertion lines in membrane trafficking studies as the latter often results in knockout mutants with no gene activity.

Other than forward genetics, chemical genetics is also an approach taken to study membrane trafficking. Similar to a forward genetic screen, a chemical genetic screen requires screening of thousands of chemicals to identify compounds that can elicit a biological activity of interest. The

gene that contributes to the process is elucidated by identifying the interactor of the compound. Like forward genetics, chemical genetics evades the issue of functional redundancy. It also offers the benefits of conditional alleles in forward genetics, which are avoidance of gene lethality by adjusting the dosage, temporal control and reversibility. Considering that only two *bona fide* conditional mutants were isolated from 140 000 M2 plants in OK Teh's mutant screen (Teh, 2007), chemical genetics seems like an attractive approach. Chemical screens have been conducted to identify compounds that affect gravitropism, endocytosis and vacuolar sorting (Zouhar et al., 2004; Surpin et al., 2005; Rojas-Pierce et al., 2007; Robert et al., 2008). Despite the advantages that have been mentioned, chemical genetics have some serious shortcomings. First, the approach is limited by the ligand-protein interactions, thus it cannot identify all non-redundant components of a given process. In contrast, chemical mutagenesis can manipulate any gene that is involved in the process. Second, the specificities of the isolated compounds are variable. For example, a bioactive molecule, Gravacin, inhibits auxin transport through PGP19, but affects tonoplast marker trafficking through another PGP19-independent mechanism (Rojas-Pierce et al., 2007). Having an exogenous molecule that affects multiple pathways through different interactors is very likely to generate results that are confusing and difficult to interpret. Thirdly, the identification of interactors is a hugely laborious process. It requires another genetic screen to be conducted to isolate mutants that are resistant to the compound. Therefore, though it has been shown that chemical genetics can dissect membrane trafficking pathways and processes (Zouhar et al., 2004; Rojas-Pierce et al., 2007; Robert et al., 2008), it is not efficient for the purpose of identifying novel membrane trafficking genes.

Another popular approach in recent years is reverse genetics. Instead of working from the phenotype to the causative gene, reverse genetics starts from manipulating a gene of interest.

Arabidopsis is an ideal model species for reverse genetic studies because of the availability of the high-quality genomic sequence data and wide variety well-developed molecular techniques. This approach is widely used to study members of conserved membrane trafficking gene families and other well-known membrane trafficking genes. The biggest advantage of reverse genetics is its flexibility in genetic manipulation. One can generate random point mutations in a given gene locus by chemical mutagenesis followed by TILLING to screen out mutant alleles of the gene, or one can precisely manipulate the sequence of any genes to generate mutants with a single amino-acid residue substitution at a specific site or mutants expressing a chimeric protein consisted of domains from different proteins. Such precise gene manipulation technique has been used extensively to study Rab-GTPases (Batoko et al., 2000; Chow et al., 2008; Camacho et al., 2009; Pinheiro et al., 2009), ARF-GEFs (Geldner et al., 2003; Richter et al., 2007; Richter et al., 2012) and SNAREs (Grefen et al., 2010). Despite its power in elucidating the functions of well-known membrane trafficking genes, the efficiency of reverse genetics to discover novel membrane trafficking genes is limited by its requirement of prior gene knowledge and functional redundancy as described in Section 1.3.

Overall, a number of approaches have been employed to study the genetic basis of membrane trafficking. Each approach has its unique strengths and weaknesses in respect of a particular research question. For my purpose of identifying novel secretory trafficking genes, I need an approach that can potentially relate secretory trafficking mechanisms to novel genes or genes that have never been implicated in membrane trafficking. Based on what has been described, forward genetics, in principle, has the most potential for unravelling new components of the secretory pathway. The results in this study and a previous study (Teh, 2007) have also

demonstrated that forward genetics, combined with confocal fluorescence imaging, is a feasible way to identify membrane trafficking components.

6.4 Improvement of the secretory mutant screen

Despite its feasibility to identify membrane trafficking genes and the output that has already been generated, the use of a secretory fluorescent protein in forward genetic screen is hampered by problems associated with lethality. Prior to this work, the problem with recovering early-lethal mutants was addressed by screening individual M2 families and propagating the lethal mutations through heterozygous siblings. Another problem that is hampering the gene identification of early-lethal mutants in both the conventional map-based cloning and the new sequencing approach is the difficulty in preparing DNA samples. As has been demonstrated with Mut 43 in this study, the genome of homozygous early-lethal mutant cannot be sequenced with next-generation sequencing because sufficient good-quality DNA that is required cannot be easily extracted from small seedlings with low viability. To overcome this problem, we have looked for next-generation sequencing strategies that can map a lethal mutation by using the phenotypically WT siblings. Recently, the technology has been developed to take over the conventional process of bulked segregant analysis, fine-mapping and candidate gene identification (Hillier et al., 2008; Sarin et al., 2008; Smith et al., 2008; Srivatsan et al., 2008; Blumenstiel et al., 2009; Huang et al., 2009; Schneeberger et al., 2009; Zuryn et al., 2010; Austin et al., 2011). Instead of having to run thousands of PCRs with different samples and genetic markers, the new technology offers a more economical and effective alternative by acquiring all the information required to map a mutation from a single sequencing run on a pooled sample. Today, the strategies involving sequencing technology are well supported by established statistical analysis and high-quality reference genomic data to make it possible to perform the

entire mapping process. In this study, a new mapping method using WT siblings of heterozygous mutant families was implemented with Mut 43. This method was adopted from the SHOREmap strategy (Schneeberger et al., 2009), whose developers suggested that it is also applicable to lethal mutants. Following the recent success in mapping an early-lethal mutation by deep-sequencing and subsequently analyzing the backcrossed heterozygous mutants (Lindner et al., 2012), I have shown in this study through Mut 43 that it is feasible in predicting a plausible position of an early-lethal mutation without having to isolate DNA from the homozygous mutants for sequencing, albeit fine-tuning of the analysis is still required to improve the accuracy of the prediction. Although the method developed by Lindner et al. (2012) is feasible, it is not an efficient strategy for our purpose as it requires the discrimination between heterozygous mutant and homozygous WT plants. To do so, every individual in the sample pool has to be genotyped by propagating it to the next generation and looking for homozygous mutant offspring. On the other hand, such laborious genotyping step is not required for the strategy developed in this study. Once a systematic and robust analysis procedure is established, this mapping method through WT siblings can be applied to other seedling-lethal secretory mutants in the collection, thus immensely decreasing the time, cost and labour it takes from isolating DNA for mapping to identifying candidate gene loci.

Another major problem that was encountered in my study of membrane trafficking through confocal fluorescent imaging is the reproducibility of the secretory defect phenotype that is represented by the secGFP-accumulating phenotype. The variability of the transgene expression makes it difficult to assess and reproduce the level of enhanced secGFP fluorescence. Although ratiometric secGFP allows transgene expression to be accounted for, the accuracy of the determined ratio is compromised by weak expression where a small error in the measurement

has a significant effect on the overall ratio. The problem is exacerbated when working with seedling-lethal mutants that are losing viability soon after germination. These mutants show phenotypes associated with viability, such as increased autofluorescence, as well as secretory defects. Together, the increased autofluorescence and weak transgene expression make it difficult to quantify the true-positive secGFP signal within these mutants for the purpose of evaluating the secretory defect phenotypes. Since a key feature in gene silencing is DNA methylation (reviewed in Stam et al., 1997), one can reactivate the transgene by growing plants in growth medium containing demethylating agent or methylation inhibitor such as 5-azacytidine, trichostatin A and genistein (Kumpatla et al., 1997; Arase et al., 2012). However, by interfering with the methylation process, the expression of other genes is also likely to be affected and causes other undesirable changes in cellular processes. Another solution to bypass quantification of intracellular secGFP accumulation is to look for unique qualitative phenotype in mutants. Currently, putative secretory mutants were screened based on enhanced secGFP fluorescence but it is not necessary for the mutants to accumulate secGFP in abnormal compartments for them to be identified as a positive. Since many membrane trafficking mutants show abnormal aggregates (Section 6.2), the chance of identifying *bona fide* secretory mutants would increase if one puts greater emphasis on finding mutants that accumulate secGFP intracellularly in abnormal and characteristic endomembrane aggregates.

6.5 Conclusion

Both circumstantial evidence and empirical data have shown that specific features exist in plant membrane trafficking mechanisms. Many of these features remain to be explored and one should be cautious in transferring knowledge from other well-known systems directly to plants. In this study, forward genetics is coupled with fluorescence imaging to study the plant-specific

features of membrane trafficking. Despite its feasibility to identify novel membrane trafficking genes, it is by no means sufficient to understand everything about the mechanism. Once a novel gene is identified, other approaches may be more suitable in understanding more about the novel genes. For instance, reverse genetics can be employed to study specific protein domains; and protein biochemistry can be applied to identify interactions. The appropriate technique and approach to address a research question is highly dependent on the question itself. One should understand and evaluate what is available carefully before making a final decision. With respect to the secGFP-based forward genetic screen, the benefits include the power of genetics to manipulate any genes, the avoidance of functional redundancy and the lack of prior gene knowledge required in the screen design. One has to bear in mind that these would only be the non-redundant genes as forward genetics is designed to neglect the redundant ones. Since numerous membrane trafficking genes are members of conserved gene families (Vernoud et al., 2003; Dacks and Field, 2007), it is not surprising that many membrane trafficking genes are functionally redundant (Surpin et al., 2003; Pinheiro et al., 2009; Zhang et al., 2011). To identify novel redundant genes, one would have to seek an approach other than the one utilized in this study. One of which may be an overexpression mutant screen similar to the one that has been conducted in *Drosophila* (Rorth et al., 1998). Despite the shortcomings in the secGFP-based forward genetic approach, a look back at the mutants that have been characterized so far shows that they have helped to identify genes that were previously known to be involved in membrane trafficking (e.g. *GNL1*) as well as those genes that had previously never been associated with any roles in membrane trafficking (e.g. *GSH2*). The results highlight the unbiased nature of forward genetics that allows us to discover new participants and re-discover old ones with novel functions. It appears that the approach has lived up to the expectation and is on track to generate new knowledge on the plant membrane trafficking pathway.

References

Agee, A.E., Surpin, M., Sohn, E.J., Girke, T., Rosado, A., Kram, B.W., Carter, C., Wentzell, A.M., Kliebenstein, D.J., Jin, H.C., Park, O.K., Jin, H., Hicks, G.R., and Raikhel, N.V. (2010). MODIFIED VACUOLE PHENOTYPE1 is an *Arabidopsis* myrosinase-associated protein involved in endomembrane protein trafficking. *Plant Physiol.* **152**, 120-132.

Ahle, S., and Ungewickell, E. (1986). Purification and properties of a new clathrin assembly protein. *EMBO J.* **5**, 3143-3149.

Albertson, R., Riggs, B., and Sullivan, W. (2005). Membrane traffic: a driving force in cytokinesis. *Trends Cell Biol.* **15**, 92-101.

Albrechtova, J.T.P., Heilscher, S., Leske, L., Walczysko, P., and Wagner, E. (2003). Calcium and pH patterning at the apical meristem are specifically altered by photoperiodic flower induction in *Chenopodium* spp. *Plant Cell Environ.* **26**, 1985-1994.

Aloni, R., Aloni, E., Langhans, M., and Ullrich, C.I. (2006). Role of cytokinin and auxin in shaping root architecture: regulating vascular differentiation, lateral root initiation, root apical dominance and root gravitropism. *Ann. Bot. -London* **97**, 883-893.

Ansorge, W.J. (2009). Next-generation DNA sequencing techniques. *New Biotechnol.* **25**, 195-203.

Appenzeller-Herzog, C., and Hauri, H.P. (2006). The ER-Golgi intermediate compartment (ERGIC): in search of its identity and function. *J, Cell Sci.* **119**, 2173-2183.

Arase, S., Kasai, M., and Kanazawa, A. (2012). *In planta* assays involving epigenetically silenced genes reveal inhibition of cytosine methylation by genistein. *Plant Methods* **8**,10.

Aravind, L., and Koonin, E.V. (1999). G-patch: a new conserved domain in eukaryotic RNA-processing proteins and type D retroviral polyproteins. *Trends Biochem. Sci.* **24**, 342-344.

Arioli, T., Peng, L., Betzner, A.S., Burn, J., Wittke, W., Herth, W., Camilleri, C., Höfte, H., Plazinski, J., Birch, R., Cork, A., Glover, J., Redmond, J., and Williamson, R.E. (1998). Molecular analysis of cellulose biosynthesis in *Arabidopsis*. *Science* **279**, 717-720.

Assaad, F.F., Huet, Y., Mayer, U., and Jürgens, G. (2001). The cytokinesis gene KEULE encodes a Sec1 protein that binds the syntaxin KNOLLE. *J. Cell Biol.* **152**, 531-543.

Assaad, F.F., Qiu, J.L., Youngs, H., Ehrhardt, D., Zimmerli, L., Kalde, M., Wanner, G., Peck, S.C., Edwards, H., Ramonell, K., Somerville, C.R., and Thordal-Christensen, H. (2004). The PEN1 syntaxin defines a novel cellular compartment upon fungal attack and is required for the timely assembly of papillae. *Mol. Biol. Cell* **15**, 5118-5129.

Austin, R.S., Vidaurre, D., Stamatiou, G., Breit, R., Provart, N.J., Bonetta, D., Zhang, J., Fung, P., Gong, Y., Wang, P.W., McCourt, P., and Guttman, D.S. (2011). Next-generation mapping of *Arabidopsis* genes. *Plant J.* **67**, 715-725.

Avila, E.L., Zouhar, J., Agee, A.E., Carter, D.G., Chary, S.N., and Raikhel, N.V. (2003). Tools to study plant organelle biogenesis. Point mutation lines with disrupted vacuoles and high-speed confocal screening of green fluorescent protein-tagged organelles. *Plant Physiol.* **133**, 1673-1676.

Bainton, D.F. (1981). The discovery of lysosomes. *J. Cell Biol.* **91**, S66-S76.

Balch, W.E., Dunphy, W.G., Braell, W.A., and Rothman, J.E. (1984). Reconstitution of the transport of protein between successive compartments of the Golgi measured by the coupled incorporation of N-acetylglucosamine. Cell **39**, 405-416.

Ball, L., Accotto, G.-P., Bechtold, U., Creissen, G., Funck, D., Jimenez, A., Kular, B., Leyland, N., Mejia-Carranza, J., Reynolds, H., Karpinski, S., and Mullineaux, P.M. (2004). Evidence for a direct link between glutathione biosynthesis and stress defense gene expression in *Arabidopsis*. *Plant Cell.* **16**, 2448-2462.

Banhegyi, G., Benedetti, A., Csala, M., and Mandl, J. (2007). Stress on redox. *FEBS Lett.* **581**, 3634-3640.

Bánhegyi, G., Lusini, L., Puskás, F., Rossi, R., Fulceri, R., Braun, L., Mile, V., di Simplicio, P., Mandl, J., and Benedetti, A. (1999). Preferential transport of glutathione versus glutathione disulfide in rat liver microsomal vesicles. *J. Biol. Chem.* **274**, 12213-12216.

Bannigan, A., Wiedemeier, A.M.D., Williamson, R.E., Overall, R.L., and Baskin, T.I. (2006). Cortical microtubule arrays lose uniform alignment between cells and are oryzalin resistant in the *Arabidopsis* mutant, *radially swollen 6*. *Plant Cell Physiol.* **47**, 949-958.

Bannigan, A., Scheible, W.R., Lukowitz, W., Fagerstrom, C., Wadsworth, P., Somerville, C., and Baskin, T.I. (2007). A conserved role for kinesin-5 in plant mitosis. *J. Cell Sci.* **120**, 2819-2827.

Banowetz, G.M., Ammar, K., and Chen, D.D. (1999). Temperature effects on cytokinin accumulation and kernel mass in a dwarf wheat. *Ann. Bot. -London* **83**, 303-307.

Barlowe, C. (2002). COPII-dependent transport from the endoplasmic reticulum. *Curr. Opin. Cell Biol.* **14**, 417-422.

Barlowe, C., Orci, L., Yeung, T., Hosobuchi, M., Hamamoto, S., Salama, N., Rexach, M.F., Ravazzola, M., Amherdt, M., and Schekman, R. (1994). COPII: A membrane coat formed by Sec proteins that drive vesicle budding from the endoplasmic reticulum. *Cell* **77**, 895-907.

Batoko, H., Zheng, H.Q., Hawes, C., and Moore, I. (2000). A Rab1 GTPase is required for transport between the endoplasmic reticulum and Golgi apparatus and for normal Golgi movement in plants. *Plant Cell* **12**, 2201-2218.

Battey, N.H., James, N.C., Greenland, A.J., and Brownlee, C. (1999). Exocytosis and endocytosis. *Plant Cell* **11**, 643-659.

Baulcombe, D.C., Chapman, S., and Cruz, S.S. (1995). Jellyfish green fluorescent protein as a reporter for virus-infections. *Plant J.* **7**, 1045-1053.

Beausoleil, S.A., Jedrychowski, M., Schwartz, D., Elias, J.E., Villen, J., Li, J.X., Cohn, M.A., Cantley, L.C., and Gygi, S.P. (2004). Large-scale characterization of HeLa cell nuclear phosphoproteins. *Proc. Natl. Acad. Sci. USA* **101**, 12130-12135.

Bednarek, S.Y., and Falbel, T.G. (2002). Membrane trafficking during plant cytokinesis. *Traffic* **3**, 621-629.

Behnke, H.D., and Eschlbeck, G. (1978). Dilated cisternae in *Capparales*: An attempt towards the characterization of a specific endoplasmic reticulum. *Protoplasma* **97**, 351-363.

Benková, E., Michniewicz, M., Sauer, M., Teichmann, T., Seifertová, D., Jürgens, G., and Friml, J. (2003). Local, efflux-dependent auxin gradients as a common module for plant organ formation. *Cell* **115**, 591-602.

Berendzen, K., Searle, I., Ravenscroft, D., Koncz, C., Batschauer, A., Coupland, G., Somssich, I.E., and Ulker, B. (2005). A rapid and versatile combined DNA/RNA extraction protocol and its application to the analysis of a novel DNA marker set polymorphic between Arabidopsis thaliana ecotypes Col-0 and Landsberg *erecta*. *Plant Methods* **1**, 4.

Bergmans, H.E.N., Vandie, I.M., and Hoekstra, W.P.M. (1981). Transformation in *Escherichia coli* - stages in the process. *J. Bacteriol.* **146**, 564-570.

Berná, G., Robles, P., and Micol, J.L. (1999). A mutational analysis of leaf morphogenesis in *Arabidopsis thaliana*. *Genetics* **152**, 729-742.

Bertolotti, A., Zhang, Y., Hendershot, L.M., Harding, H.P., and Ron, D. (2000). Dynamic interaction of BiP and ER stress transducers in the unfolded protein response. *Nat. Cell. Biol.* **2**, 326-332.

Bhat, R.A., Miklis, M., Schmelzer, E., Schulze-Lefert, P., and Panstruga, R. (2005). Recruitment and interaction dynamics of plant penetration resistance components in a plasma membrane microdomain. *Proc. Natl. Acad. Sci. USA* **102**, 3135-3140.

Birnboim, H.C., and Doly, J. (1979). A rapid alkaline extraction procedure for screening recombinant plasmid DNA. *Nucleic Acids Res.* **7**, 1513-1523.

Blanco, F.A., Peltzer Meschini, E., Zanetti, M.E., and Aguilar, O.M. (2009). A small GTPase of the Rab family is required for root hair formation and preinfection stages of the common bean–*Rhizobium* symbiotic association. *Plant Cell* **21**, 2797-2810.

Block, M.R., Glick, B.S., Wilcox, C.A., Wieland, F.T., and Rothman, J.E. (1988). Purification of an N-ethylmaleimide-sensitive protein catalyzing vesicular transport. *Proc. Natl. Acad. Sci. USA* **85**, 7852-7856.

Blumenstiel, J.P., Noll, A.C., Griffiths, J.A., Perera, A.G., Walton, K.N., Gilliland, W.D., Hawley, R.S., and Staehling-Hampton, K. (2009). Identification of EMS-induced mutations in *Drosophila melanogaster* by whole-genome sequencing. *Genetics* **182**, 25-32.

Boevink, P., Martin, B., Oparka, K., Cruz, S.S., and Hawes, C. (1999). Transport of virally expressed green fluorescent protein through the secretory pathway in tobacco leaves is inhibited by cold shock and brefeldin A. *Planta* **208**, 392-400.

Boevink, P., Oparka, K., Cruz, S.S., Martin, B., Betteridge, A., and Hawes, C. (1998). Stacks on tracks: the plant Golgi apparatus traffics on an actin/ER network? *Plant J.* **15**, 441-447.

Boller, T., and Kende, H. (1979). Hydrolytic enzymes in the central vacuole of plant cells. *Plant Physiol.* **63**, 1123-1132.

Bolte, S., Talbot, C., Boutte, Y., Catrice, O., Read, N.D., and Satiat-Jeunemaitre, B. (2004). FM-dyes as experimental probes for dissecting vesicle trafficking in living plant cells. *J. Microsc.* **214**, 159-173.

Bonifacino, J.S., and Glick, B.S. (2004). The mechanisms of vesicle budding and fusion. *Cell* **116**, 153-166.

Boulaflous, A., Faso, C., and Brandizzi, F. (2008). Deciphering the Golgi apparatus: From imaging to genes. *Traffic* **9**, 1613-1617.

Bradford, J.R. (2001). *In silico* methods for prediction of signal peptides and their cleavage sites, and linear epitopes. School of Biochemistry and Molecular Biology (Leeds: University of Leeds).

Braell, W.A., Schlossman, D.M., Schmid, S.L., and Rothman, J.E. (1984). Dissociation of clathrin coats coupled to the hydrolysis of ATP: role of an uncoating ATPase. *J. Cell Biol.* **99**, 734-741.

Broadie, K., Prokop, A., Bellen, H.J., Okane, C.J., Schulze, K.L., and Sweeney, S.T. (1995). Syntaxin and synaptobrevin function downstream of vesicle docking in *Drosophila*. *Neuron* **15**, 663-673.

Brown, R.C., Lemmon, B.E., Nguyen, H., and Olsen, O.A. (1999). Development of endosperm in *Arabidopsis thaliana*. *Sex. Plant Reprod.* **12**, 32-42.

Burke, B., Griffiths, G., Reggio, H., Louvard, D., and Warren, G. (1982). A monoclonal antibody against a 135-K Golgi membrane protein. *Embo J.* **1**, 1621-1628.

Burn, J.E., Hurley, U.A., Birch, R.J., Arioli, T., Cork, A., and Williamson, R.E. (2002). The cellulose-deficient *Arabidopsis* mutant *rsw3* is defective in a gene encoding a putative glucosidase II, an enzyme processing N-glycans during ER quality control. *Plant J.* **32**, 949-960.

Cagnac, O., Bourbouloux, A., Chakrabarty, D., Zhang, M.Y., and Delrot, S. (2004). AtOPT6 transports glutathione derivatives and is induced by primisulfuron. *Plant Physiol.* **135**, 1378-1387.

Cairns, N.G., Pasternak, M., Wachter, A., Cobbett, C.S., and Meyer, A.J. (2006). Maturation of *Arabidopsis* seeds is dependent on glutathione biosynthesis within the embryo. *Plant Physiol.* **141**, 446-455.

Camacho, L., Smertenko, A.P., Pérez-Gómez, J., Hussey, P.J., and Moore, I. (2009). *Arabidopsis* Rab-E GTPases exhibit a novel interaction with a plasma-membrane phosphatidylinositol-4-phosphate 5-kinase. *J. Cell Sci.* **122**, 4383-4392.

Campbell, R.E., Tour, O., Palmer, A.E., Steinbach, P.A., Baird, G.S., Zacharias, D.A., and Tsien, R.Y. (2002). A monomeric red fluorescent protein. *Proc. Natl. Acad. Sci. USA* **99**, 7877-7882.

Cao, X., Ballew, N., and Barlowe, C. (1998). Initial docking of ER-derived vesicles requires Uso1p and Ypt1p but is independent of SNARE proteins. *Embo J.* **17**, 2156-2165.

Casimiro, I., Beeckman, T., Graham, N., Bhalerao, R., Zhang, H.M., Casero, P., Sandberg, G., and Bennett, M.J. (2003). Dissecting *Arabidopsis* lateral root development. *Trends Plant Sci* **8**, 165-171.

Chakravarthi, S., Jessop, C.E., and Bulleid, N.J. (2006). The role of glutathione in disulphide bond formation and endoplasmic reticulum-generated oxidative stress. *EMBO Rep.* **7**, 271-275.

Chalfie, M., Tu, Y., Euskirchen, G., Ward, W.W., and Prasher, D.C. (1994). Green fluorescent protein as a marker for gene expression. *Science* **263**, 802-805.

Chary, S.N., Hicks, G.R., Choi, Y.G., Carter, D., and Raikhel, N.V. (2008). Trehalose-6-phosphate synthase/phosphatase regulates cell shape and plant architecture in *Arabidopsis*. *Plant Physiol.* **146**, 97-107.

Chow, C. M., Neto, H., Foucart, C., and Moore, I. (2008). Rab-A2 and Rab-A3 GTPases define a trans-Golgi endosomal membrane domain in *Arabidopsis* that contributes substantially to the cell plate. *Plant Cell* **20**, 101-123.

Christensen, A., Svensson, K., Persson, S., Jung, J., Michalak, M., Widell, S., and Sommarin, M. (2008). Functional characterization of *Arabidopsis* calreticulin1a: a key alleviator of endoplasmic reticulum stress. *Plant Cell Physiol.* **49**, 912-924.

Clary, D.O., Griff, I.C., and Rothman, J.E. (1990). SNAPs, a family of NSF attachment proteins involved in intracellular membrane fusion in animals and yeast. *Cell* **61**, 709-721.

Clough, S.J., and Bent, A.F. (1998). Floral dip: a simplified method for *Agrobacterium*-mediated transformation of *Arabidopsis thaliana*. *Plant J.* **16**, 735-743.

Cobbett, C.S., May, M.J., Howden, R., and Rolls, B. (1998). The glutathione-deficient, cadmium-sensitive mutant, *cad2-1*, of *Arabidopsis thaliana* is deficient in γ-glutamylcysteine synthetase. *Plant J.* **16**, 73-78.

Cole, N.B., Sciaky, N., Marotta, A., Song, J., and Lippincott-Schwartz, J. (1996). Golgi dispersal during microtubule disruption: Regeneration of Golgi stacks at peripheral endoplasmic reticulum exit sites. *Mol. Biol Cell* **7**, 631-650.

Coleman, J., Blake-Kalff, M., and Davies, E. (1997). Detoxification of xenobiotics by plants: chemical modification and vacuolar compartmentation. *Trends Plant Sci.* **2**, 144-151.

Collins, N.C., Thordal-Christensen, H., Lipka, V., Bau, S., Kombrink, E., Qiu, J.L., Huckelhoven, R., Stein, M., Freialdenhoven, A., Somerville, S.C., and Schulze-Lefert, P. (2003). SNARE-protein-mediated disease resistance at the plant cell wall. *Nature* **425**, 973-977.

Conibear, E., and Stevens, T.H. (1998). Multiple sorting pathways between the late Golgi and the vacuole in yeast. *BBA-Mol. Cell Res.* **1404**, 211-230.

Costa, M.D.L., Reis, P.A.B., Valente, M.A.S., Irsigler, A.S.T., Carvalho, C.M., Loureiro, M.E., Aragao, F.J.L., Boston, R.S., Fietto, L.G., and Fontes, E.P.B. (2008). A new branch of

endoplasmic reticulum stress signaling and the osmotic signal converge on plant-specific asparagine-rich proteins to promote cell death. *J. Biol. Chem.* **283**, 20209-20219.

Cox, R., Mason-Gamer, R.J., Jackson, C.L., and Segev, N. (2004). Phylogenetic analysis of Sec7-domain–containing Arf nucleotide exchangers. *Mol. Biol. Cell* **15**, 1487-1505.

Crofts, A.J., Leborgne-Castel, N., Hillmer, S., Robinson, D.G., Phillipson, B., Carlsson, L.E., Ashford, D.A., and Denecke, J. (1999). Saturation of the endoplasmic reticulum retention machinery reveals anterograde bulk flow. *Plant Cell* **11**, 2233-2248.

Csala, M., Fulceri, R., Mandl, J., Benedetti, A., and Bánhegyi, G. (2003). Glutathione transport in the endo/sarcoplasmic reticulum. *BioFactors* **17**, 27-35.

Cutler, S.R., Ehrhardt, D.W., Griffitts, J.S., and Somerville, C.R. (2000). Random GFP::cDNA fusions enable visualization of subcellular structures in cells of *Arabidopsis* at a high frequency. *Proc. Natl. Acad. Sci. USA* **97**, 3718-3723.

Dacks, J.B., and Field, M.C. (2007). Evolution of the eukaryotic membrane-trafficking system: origin, tempo and mode. *J. Cell Sci.* **120**, 2977-2985.

Dalton, A.J., and Felix, M.D. (1954). Cytologic and cytochemical characteristics of the Golgi substance of epithelial cells of the epididymis *in situ*, in homogenates and after isolation. *Am. J. Anat.* **94**, 171-207.

DaSilva, L.L.P., Snapp, E.L., Denecke, J., Lippincott-Schwartz, J., Hawes, C., and Brandizzi, F. (2004). Endoplasmic reticulum export sites and golgi bodies behave as single mobile secretory units in plant cells. *Plant Cell* **16**, 1753-1771.

De Smet, I., Vanneste, S., Inze, D., and Beeckman, T. (2006). Lateral root initiation or the birth of a new meristem. *Plant Mol. Biol*. **60**, 871-887.

Dettmer, J., and Friml, J. (2011). Cell polarity in plants: when two do the same, it is not the same. *Curr Opin. Cell Biol.* **23**, 686-696.

Dettmer, J., Hong-Hermesdorf, A., Stierhof, Y.D., and Schumacher, K. (2006). Vacuolar H^+-ATPase activity is required for endocytic and secretory trafficking in *Arabidopsis*. *Plant Cell* **18**, 715-730.

Deutsch, D., Dafni, L., Palmon, A., Hekmati, M., Young, M.F., and Fisher, L.W. (1997). Tuftelin: enamel mineralization and amelogenesis imperfecta. *Ciba F. Symp.* **205**, 135-155.

Dhonukshe, P. (2009). Cell polarity in plants: linking PIN polarity generation mechanisms to morphogenic auxin gradients. *Commun. Integr. Biol.* **2**, 184-190.

Di Sansebastiano, G.P., Paris, N., Marc-Martin, S., and Neuhaus, J.M. (1998). Specific accumulation of GFP in a non-acidic vacuolar compartment via a C-terminal propeptide-mediated sorting pathway. *Plant J.* **15**, 449-457.

Dixon, D.P., Cummins, I., Cole, D.J., and Edwards, R. (1998). Glutathione-mediated detoxification systems in plants. *Curr Opin. Plant Biol.* **1**, 258-266.

Duman, J.G., and Forte, J.G. (2003). What is the role of SNARE proteins in membrane fusion? Am. *J. Physiolo. - Cell Ph.* **285**, C237-C249.

Ebine, K., Okatani, Y., Uemura, T., Goh, T., Shoda, K., Niihama, M., Morita, M.T., Spitzer, C., Otegui, M.S., Nakano, A., and Ueda, T. (2008). A SNARE complex unique to seed plants is required for protein storage vacuole biogenesis and seed development of *Arabidopsis thaliana*. *Plant Cell* **20**, 3006-3021.

Ebine, K., Fujimoto, M., Okatani, Y., Nishiyama, T., Goh, T., Ito, E., Dainobu, T., Nishitani, A., Uemura, T., Sato, M.H., Thordal-Christensen, H., Tsutsumi, N., Nakano, A., and Ueda, T. (2011). A membrane trafficking pathway regulated by the plant-specific RAB GTPase ARA6. *Nat Cell Biol.* **13**, 853-859.

Fahey, R.C., Newton, G.L., Dorian, R., and Kosower, E.M. (1981). Analysis of biological thiols: quantitative determination of thiols at the picomole level based upon derivatization with monobromobimanes and separation by cation-exchange chromatography. *Anal. Biochem.* **111**, 357-365.

Falbel, T.G., Koch, L.M., Nadeau, J.A., Segui-Simarro, J.M., Sack, F.D., and Bednarek, S.Y. (2003). SCD1 is required for cell cytokinesis and polarized cell expansion in *Arabidopsis thaliana*. Development **130**, 4011-4024.

Faso, C., Chen, Y.-N., Tamura, K., Held, M., Zemelis, S., Marti, L., Saravanan, R., Hummel, E., Kung, L., Miller, E., Hawes, C., and Brandizzi, F. (2009). A missense mutation in the *Arabidopsis* COPII coat protein Sec24A induces the formation of clusters of the endoplasmic reticulum and Golgi apparatus. *Plant Cell* **21**, 3655-3671.

Feraru, E., Paciorek, T., Feraru, M.I., Zwiewka, M., De Groodt, R., De Rycke, R., Kleine-Vehn, J., and Friml, J. (2010). The AP-3 β adaptin mediates the biogenesis and function of lytic vacuoles in *Arabidopsis*. *Plant Cell* **22**, 2812-2824.

Ford, M.G., Mills, I.G., Peter, B.J., Vallis, Y., Praefcke, G.J., Evans, P.R., and McMahon, H.T. (2002). Curvature of clathrin-coated pits driven by epsin. *Nature* **419**, 361-366.

Foyer, C.H., and Noctor, G. (2011). Ascorbate and glutathione: the heart of the redox hub. *Plant Physiol.* **155**, 2-18.

Fricker, M.D., May, M., Meyer, A.J., Sheard, N., and White, N.S. (2000). Measurement of glutathione levels in intact roots of *Arabidopsis*. *J. Microsc.* **198**, 162-173.

Fries, E., and Rothman, J.E. (1981). Transient activity of Golgi-like membranes as donors of vesicular stomatitis viral glycoprotein in vitro. *J. Cell Biol.* **90**, 697-704.

Fu, Y., and Yang, Z. (2001). Rop GTPase: a master switch of cell polarity development in plants. *Trends Plant Sci.* **6**, 545-547.

Fuji, K., Shimada, T., Takahashi, H., Tamura, K., Koumoto, Y., Utsumi, S., Nishizawa, K., Maruyama, N., and Hara-Nishimura, I. (2007). *Arabidopsis* vacuolar sorting mutants (green fluorescent seed) can be identified efficiently by secretion of vacuole-targeted green fluorescent protein in their seeds. *Plant Cell* **19**, 597-609.

Fujikawa, Y., and Kato, N. (2007). Split luciferase complementation assay to study protein-protein interactions in *Arabidopsis* protoplasts. *Plant J.* **52**, 185-195.

Gan, X., Stegle, O., Behr, J., Steffen, J.G., Drewe, P., Hildebrand, K.L., Lyngsoe, R., Schultheiss, S.J., Osborne, E.J., Sreedharan, V.T., Kahles, A., Bohnert, R., Jean, G., Derwent, P., Kersey, P., Belfield, E.J., Harberd, N.P., Kemen, E., Toomajian, C., Kover, P.X., Clark, R.M., Ratsch, G., and Mott, R. (2011). Multiple reference genomes and transcriptomes for *Arabidopsis thaliana*. *Nature* **477**, 419-423.

Gao, D.J., Knight, M.R., Trewavas, A.J., Sattelmacher, B., and Plieth, C. (2004). Self-reporting *Arabidopsis* expressing pH and [$Ca2^{+}$] indicators unveil ion dynamics in the cytoplasm and in the apoplast under abiotic stress. *Plant Physiol.* **134**, 898-908.

Geldner, N., Denervaud-Tendon, V., Hyman, D.L., Mayer, U., Stierhof, Y.D., and Chory, J. (2009). Rapid, combinatorial analysis of membrane compartments in intact plants with a multicolor marker set. *Plant J.* **59**, 169-178.

Geldner, N., Anders, N., Wolters, H., Keicher, J., Kornberger, W., Muller, P., Delbarre, A., Ueda, T., Nakano, A., and Jürgens, G. (2003). The *Arabidopsis* GNOM ARF-GEF mediates endosomal recycling, auxin transport, and auxin-dependent plant growth. *Cell* **112**, 219-230.

Golgi, C. (1898). Sulla struttura delle cellule nervose dei gangli spinali. *Boll. Soc. Med. Chi. Pavla* **13**, 53-63.

Gordon, C.L., and King, J. (1994). Genetic properties of temperature-sensitive folding mutants of the coat protein of phage P22. *Genetics* **136**, 427-438.

Gray, W.M., Ostin, A., Sandberg, G., Romano, C.P., and Estelle, M. (1998). High temperature promotes auxin-mediated hypocotyl elongation in *Arabidopsis*. *Proc. Natl. Acad. Sci. USA* **95**, 7197-7202.

Grebe, M. (2011). Out of the shade and into the light. *Nat. Cell Biol.* **13**, 347-349.

Greene, E.A., Codomo, C.A., Taylor, N.E., Henikoff, J.G., Till, B.J., Reynolds, S.H., Enns, L.C., Burtner, C., Johnson, J.E., Odden, A.R., Comai, L., and Henikoff, S. (2003). Spectrum of chemically induced mutations from a large-scale reverse-genetic screen in *Arabidopsis*. *Genetics* **164**, 731-740.

Grefen, C., Chen, Z.H., Honsbein, A., Donald, N., Hills, A., and Blatt, M.R. (2010). A novel motif essential for SNARE interaction with the K^+ channel KC1 and channel gating in *Arabidopsis*. *Plant Cell* **22**, 3076-3092.

Griffing, L.R. (1991). Comparisons of Golgi structure and dynamics in plant and animal-Cells. *J. Electron Micr. Tech.* **17**, 179-199.

Griffith, O.W. (1982). Mechanism of action, metabolism, and toxicity of buthionine sulfoximine and its higher homologs, potent inhibitors of glutathione synthesis. *J. Biol. Chem.* **257**, 13704-13712.

Grignon, C., and Sentenac, H. (1991). pH and ionic conditions in the apoplast. *Annu. Rev. Plant Phys.* **42,** 103-128.

Hager, A. (2003). Role of the plasma membrane H^+-ATPase in auxin-induced elongation growth: historical and new aspects. *J. Plant Res.* **116**, 483-505.

Hager, A., Menzel, H., and Krauss, A. (1971). Versuche und hypothese zur primärwirkung des auxins beim streckungswachstum. *Planta* **100**, 47-75.

Haigler, C.H., and Brown, R.M. (1986). Transport of rosettes from the Golgi apparatus to the plasma membrane in isolated mesophyll cells of *Zinnia elegans* during differentiation to tracheary elements in suspension culture. *Protoplasma* **134**, 111-120.

Hammond, A.T., and Glick, B.S. (2000). Dynamics of transitional endoplasmic reticulum sites in vertebrate cells. *Mol. Biol. Cell* **11**, 3013-3030.

Hanahan, D. (1983). Studies on transformation of *Escherichia coli* with plasmids. *J. Mol. Biol.* **166**, 557-580.

Hanton, S.L., and Brandizzi, F. (2006). Fluorescent proteins as markers in the plant secretory pathway. *Microsc. Res. Techniq.* **69**, 152-159.

Hara-Nishimura, I., Shimada, T., Hatano, K., Takeuchi, Y., and Nishimura, M. (1998). Transport of storage proteins to protein storage vacuoles is mediated by large precursor-accumulating vesicles. *Plant Cell* **10**, 825-836.

Haseloff, J., Siemering, K.R., Prasher, D.C., and Hodge, S. (1997). Removal of a cryptic intron and subcellular localization of green fluorescent protein are required to mark transgenic Arabidopsis plants brightly. *Proc. Natl. Acad. Sci. USA* **94**, 2122-2127.

Haughn, G., and Somerville, C.R. (1987). Selection for herbicide resistance at the whole-plant level. Biotechnology in Agricultural Chemistry (American Chemical Society), pp. 98-107.

Hawes, C., Saint-Jore, C., Martin, B., and Zheng, H.Q. (2001). ER confirmed as the location of mystery organelles in *Arabidopsis* plants expressing GFP! *Trends Plant Sci.* **6**, 245-246.

Hawkes, R., Grutter, M.G., and Schellman, J. (1984). Thermodynamic stability and point mutations of bacteriophage T4 lysozyme. *J. of Mol. Biol.* **175**, 195-212.

Hecht, M.H., Sturtevant, J.M., and Sauer, R.T. (1984). Effect of single amino acid replacements on the thermal stability of the NH_2-terminal domain of phage λ repressor. *Proc. Natl. Acad. Sci. USA* **81**, 5685-5689.

Heese, M., Gansel, X., Sticher, L., Wick, P., Grebe, M., Granier, F., and Jürgens, G. (2001). Functional characterization of the KNOLLE-interacting t-SNARE AtSNAP33 and its role in plant cytokinesis. *J. Cell Biol.* **155**, 239-249.

Heim, R., Cubitt, A.B., and Tsien, R.Y. (1995). Improved green fluorescence. *Nature* **373**, 663-664.

Heinlein, M., Epel, B.L., Padgett, H.S., and Beachy, R.N. (1995). Interaction of tobamovirus movement proteins with the plant cytoskeleton. *Science* **270**, 1983-1985.

Hell, R., and Bergmann, L. (1990). γ-Glutamylcysteine synthetase in higher plants: catalytic properties and subcellular localization. *Planta* **180**, 603-612.

Hellens, R.P., Edwards, E.A., Leyland, N.R., Bean, S., and Mullineaux, P.M. (2000). pGreen: a versatile and flexible binary Ti vector for *Agrobacterium*-mediated plant transformation. *Plant Mol. Biol.* **42**, 819-832.

Hicke, L., Yoshihisa, T., and Schekman, R. (1992). Sec23p and a novel 105-kDa protein function as a multimeric complex to promote vesicle budding and protein transport from the endoplasmic reticulum. *Mol. Biol. Cell* **3**, 667-676.

Hillier, L.W., Marth, G.T., Quinlan, A.R., Dooling, D., Fewell, G., Barnett, D., Fox, P., Glasscock, J.I., Hickenbotham, M., Huang, W., Magrini, V.J., Richt, R.J., Sander, S.N., Stewart, D.A., Stromberg, M., Tsung, E.F., Wylie, T., Schedl, T., Wilson, R.K., and Mardis, E.R. (2008). Whole-genome sequencing and variant discovery in *C. elegans*. *Nat. Meth.* **5**, 183-188.

Hinshaw, J.E., and Schmid, S.L. (1995). Dynamin self-assembles into rings suggesting a mechanism for coated vesicle budding. *Nature* **374**, 190-192.

Hohl, I., Robinson, D.G., Chrispeels, M.J., and Hinz, G. (1996). Transport of storage proteins to the vacuole is mediated by vesicles without a clathrin coat. *J. Cell Sci.* **109**, 2539-2550.

Hong, W. (2005). SNAREs and traffic. *BBA- Mol. Cell. Res.* **1744**, 120-144.

Hosobuchi, M., Kreis, T., and Schekman, R. (1992). *SEC21* is a gene required for ER to Golgi protein transport that encodes a subunit of a yeast coatomer. *Nature* **360**, 603-605.

Hou, X.H., Li, L.C., Peng, Z.Y., Wei, B.Y., Tang, S.J., Ding, M.Y., Liu, J.J., Zhang, F.X., Zhao, Y.D., Gu, H.Y., and Qu, L.J. (2010). A platform of high-density INDEL/CAPS markers for map-based cloning in *Arabidopsis*. *Plant J.* **63**, 880-888.

Huang, X., Feng, Q., Qian, Q., Zhao, Q., Wang, L., Wang, A., Guan, J., Fan, D., Weng, Q., Huang, T., Dong, G., Sang, T., and Han, B. (2009). High-throughput genotyping by whole-genome resequencing. *Genome Res*. **19**, 1068-1076.

Hwang, C., Sinskey, A.J., and Lodish, H.F. (1992). Oxidized redox state of glutathione in the endoplasmic reticulum. Science (New York, N.Y.) **257**, 1496-1502.

Inouye, S., and Tsuji, F.I. (1994). *Aequorea* green fluorescent protein- expression of the gene and fluorescence characteristics of the recombinant protein. *FEBS Lett.* **341**, 277-280.

Ivanov, S., Fedorova, E.E., Limpens, E., De Mita, S., Genre, A., Bonfante, P., and Bisseling, T. (2012). *Rhizobium*-legume symbiosis shares an exocytotic pathway required for arbuscule formation. *Proc. Natl. Acad. Sci. USA* **109**, 8316-8321.

Iversen, T.H. (1970). The morphology, occurrence, and distribution of dilated cisternae of the endoplasmic reticulum in tissues of plants of the *Cruciferae*. *Protoplasma* **71**, 467-477.

Iwata, Y., and Koizumi, N. (2005). An *Arabidopsis* transcription factor, AtbZIP60, regulates the endoplasmic reticulum stress response in a manner unique to plants. *Proc. Natl. Acad. Sci. USA* **102**, 5280-5285.

Jackson, C.L. (2009). Mechanisms of transport through the Golgi complex. *J. Cell Sci.* **122**, 443-452.

Jamieson, J.D., and Palade, G.E. (1967a). Intracellular transport of secretory proteins in the pancreatic exocrine cell. I. Role of the peripheral elements of the Golgi complex. *J. Cell Biol.* **34**, 577-596.

Jamieson, J.D., and Palade, G.E. (1967b). Intracellular transport of secretory proteins in the pancreatic exocrine cell. II. Transport to condensing vacuoles and zymogen granules. *J. Cell Biol.* **34,** 597-615.

Jander, G., Norris, S.R., Rounsley, S.D., Bush, D.F., Levin, I.M., and Last, R.L. (2002). *Arabidopsis* map-based cloning in the post-genome era. *Plant Physiol.* **129**, 440-450.

Jander, G., Baerson, S.R., Hudak, J.A., Gonzalez, K.A., Gruys, K.J., and Last, R.L. (2003). Ethylmethanesulfonate saturation mutagenesis in *Arabidopsis* to determine frequency of herbicide resistance. *Plant Physiol.* **131**, 139-146.

Jessop, C.E., and Bulleid, N.J. (2004). Glutathione directly reduces an oxidoreductase in the endoplasmic reticulum of mammalian cells. *J. Biol. Chem.* **279**, 55341-55347.

Ji, Q.M., Huang, C.H., Peng, J.B., Hashmi, S., Ye, T.Z., and Chen, Y. (2007). Characterization of STIP, a multi-domain nuclear protein, highly conserved in metazoans, and essential for embryogenesis in *Caenorhabditis elegans*. *Exp. Cell. Res.* **313**, 1460-1472.

Jia, W.S., and Davies, W.J. (2007). Modification of leaf apoplastic pH in relation to stomatal sensitivity to root-sourced abscisic acid signals. *Plant Physiol.* **143**, 68-77.

Jobe, T.O., Sung, D.Y., Akmakjian, G., Pham, A., Komives, E.A., Mendoza-Cozatl, D.G., and Schroeder, J.I. (2012). Feedback inhibition by thiols outranks glutathione depletion: a luciferase-based screen reveals glutathione-deficient γ-ECS and glutathione synthetase mutants impaired in cadmium-induced sulfate assimilation. *Plant J.* **70**, 783-795.

Jürgens, G. (2004). Membrane trafficking in plants. *Annu. Rev. Cell Dev. Biol.* **20**, 481-504.

Jürgens, G., Mayer, U., Ramon A, T.R., Berleth, T., and Miséra, S. (1991). Genetic analysis of pattern formation in the *Arabidopsis* embryo. *Development* **113**, 27-38.

Kaiser, C.A., and Schekman, R. (1990). Distinct sets of *SEC* genes govern transport vesicle formation and fusion early in the secretory pathway. *Cell* **61**, 723-733.

Kang, B.-H., Busse, J.S., and Bednarek, S.Y. (2003). Members of the *Arabidopsis* dynamin-like gene family, ADL1, are essential for plant cytokinesis and polarized cell growth. *Plant Cell* **15**, 899-913.

Keen, J.H., Willingham, M.C., and Pastan, I.H. (1979). Clathrin-coated vesicles: isolation, dissociation and factor-dependent reassociation of clathrin baskets. *Cell* **16**, 303-312.

Kirsch, T., Paris, N., Butler, J.M., Beevers, L., and Rogers, J.C. (1994). Purification and initial characterization of a potential plant vacuolar targeting receptor. *Proc. Natl. Acad. Sci. USA* **91**, 3403-3407.

Kleine-Vehn, J., Ding, Z.J., Jones, A.R., Tasaka, M., Morita, M.T., and Friml, J. (2010). Gravity-induced PIN transcytosis for polarization of auxin fluxes in gravity-sensing root cells. *Proc. Natl. Acad. Sci. USA* **107**, 22344-22349.

Kobayashi, H., Morisaki, N., Tago, Y., Hashimoto, Y., Iwasaki, S., Kawachi, E., Nagata, R., and Shudo, K. (1995). Identification of a major cytokinin in coconut milk. *Experientia* **51**, 1081-1084.

Koizumi, N., Martinez, I.M., Kimata, Y., Kohno, K., Sano, H., and Chrispeels, M.J. (2001). Molecular characterization of two *Arabidopsis* Ire1 homologs, endoplasmic reticulum-located transmembrane protein kinases. *Plant Physiol.* **127**, 949-962.

Koncz, C., and Schell, J. (1986). The promoter of TL-DNA gene 5 controls the tissue-specific expression of chimaeric genes carried by a novel type of *Agrobacterium* binary vector. *Mol. Gen. Genet.* **204**, 383-396.

Kornfeld, R., and Kornfeld, S. (1985). Assembly of asparagine-linked oligosaccharides. *Ann. Rev. Biochem.* **54**, 631-664.

Krebs, M., Beyhl, D., Görlich, E., Al-Rasheid, K.A.S., Marten, I., Stierhof, Y.-D., Hedrich, R., and Schumacher, K. (2010). *Arabidopsis* V-ATPase activity at the tonoplast is required for efficient nutrient storage but not for sodium accumulation. *Proc. Natl. Acad. Sci. USA* **107**, 3251-3256.

Kumpatla, S.P., Teng, W.M., Buchholz, W.G., and Hall, T.C. (1997). Epigenetic transcriptional silencing and 5-azacytidine-mediated reactivation of a complex transgene in rice. *Plant Physiol.* **115**, 361-373.

Kwaaitaal, M., Keinath, N.F., Pajonk, S., Biskup, C., and Panstruga, R. (2010). Combined bimolecular fluorescence complementation and Förster resonance energy transfer reveals ternary SNARE complex formation in living plant cells. *Plant Physiol.* **152**, 1135-1147.

Kweon, D.H., Kim, C.S., and Shin, Y.K. (2003). Regulation of neuronal SNARE assembly by the membrane. *Nat. Struct. Biol.* **10**, 440-447.

Lane, D.R., Wiedemeier, A., Peng, L., Höfte, H., Vernhettes, S., Desprez, T., Hocart, C.H., Birch, R.J., Baskin, T.I., Burn, J.E., Arioli, T., Betzner, A.S., and Williamson, R.E. (2001). Temperature-sensitive alleles of *RSW2* link the KORRIGAN endo-1,4-β-glucanase to cellulose synthesis and cytokinesis in *Arabidopsis*. *Plant Physiol.* **126**, 278-288.

Le Gall, S., Neuhof, A., and Rapoport, T. (2004). The endoplasmic reticulum membrane is permeable to small molecules. *Mol. Biol. Cell* **15**, 447-455.

Lenton, J.R., and Appleford, N.E.J. (1987). Cytokinins and early grain growth in wheat. *Monogr.-Brit. Plant Growth Reg. Group* **14,** 99-113.

Li, B.B., Gao, Z.H., Zhou, X.Y., Ren, H.B., Xie, M., Fan, Y.J., Hu, J.F., and Jia, W.S. (2008). A confocal technique applicable to studies of cellular pH-related signaling in plants. *J. Integr. Plant Biol.* **50**, 682-690.

Lindner, H., Raissig, M.T., Sailer, C., Shimosato-Asano, H., Bruggmann, R., and Grossniklaus, U. (2012). SNP-Ratio Mapping (SRM): identifying lethal alleles and mutations in complex genetic backgrounds by next-generation sequencing. *Genetics* **191**, 1381-1386

Lingwood, D., and Simons, K. (2010). Lipid rafts as a membrane-organizing principle. *Science* **327**, 46-50.

Liu, J.X., and Howell, S.H. (2010). Endoplasmic reticulum protein quality control and its relationship to environmental stress responses in plants. *Plant Cell* **22**, 2930-2942.

Liu, Y.F., Wang, F., Zhang, H.Y., He, H., Ma, L.G., and Deng, X.W. (2008). Functional characterization of the *Arabidopsis* ubiquitin-specific protease gene family reveals specific role and redundancy of individual members in development. *Plant J.* **55**, 844-856.

Lohman, J.R., and Remington, S.J. (2008). Development of a family of redox-sensitive green fluorescent protein indicators for use in relatively oxidizing subcellular environments. *Biochemistry* **47**, 8678-8688.

Long, J.A., Woody, S., Poethig, S., Meyerowitz, E.M., and Barton, K. (2002). Transformation of shoots into roots in *Arabidopsis* embryos mutant at the TOPLESS locus. *Development* **129**, 2797-2806.

Longtine, M.S., DeMarini, D.J., Valencik, M.L., Al-Awar, O.S., Fares, H., De Virgilio, C., and Pringle, J.R. (1996). The septins: roles in cytokinesis and other processes. *Curr. Opin. Cell Biol.* **8**, 106-119.

Lorenzi, R., Vernieri, P., and Ceccarelli, N. (1988). Cytokinins in endosperm of *Sechium edule* Sw. seeds. *J. Plant Physiol.* **133**, 310-315.

Lukowitz, W., Mayer, U., and Jürgens, G. (1996). Cytokinesis in the *Arabidopsis* embryo involves the syntaxin-related KNOLLE gene product. *Cell* **84**, 61-71.

Lukowitz, W., Gillmor, C.S., and Scheible, W.R. (2000). Positional cloning in *Arabidopsis*. Why it feels good to have a genome initiative working for you. *Plant Physiol.* **123**, 795-805.

Mai, H.T., Nomura, M., Takegawa, K., Asamizu, E., Sato, S., Kato, T., Tabata, S., and Tajima, S. (2006). Identification of a *Sed5*-like SNARE gene LjSYP32-1 that contributes to nodule tissue formation of *Lotus japonicus*. *Plant Cell Physiol* **47,** 829-838.

Majira, A., Domin, M., Grandjean, O., Gofron, K., and Houba-Hérin, N. (2002). Seedling lethality in *Nicotiana plumbaginifolia* conferred by *Ds* transposable element insertion into a plant-specific gene. *Plant Mol. Biol.* **50**, 551-562.

Malkus, P., Jiang, F., and Schekman, R. (2002). Concentrative sorting of secretory cargo proteins into COPII-coated vesicles. *J. Cell Biol.* **159**, 915-921.

Manchester, K.L. (1995). Value of A260/A280 ratios for measurement of purity of nucleic acids. *Biotechniques* **19**, 208-210.

Mansfield, S.G., and Briarty, L.G. (1990). Endosperm cellularization in *Arabidopsis thaliana* L. *Arabidopsis Inf. Serv.* **27**, 65-72.

Mao, Z.K., Shay, B., Hekmati, M., Fermon, E., Taylor, A., Dafni, L., Heikinheimo, K., Lustmann, J., Fisher, L.W., Young, M.F., and Deutsch, D. (2001). The human tuftelin gene: cloning and characterization. *Gene* **279**, 181-196.

Marchler-Bauer, A., Lu, S.N., Anderson, J.B., Chitsaz, F., Derbyshire, M.K., DeWeese-Scott, C., Fong, J.H., Geer, L.Y., Geer, R.C., Gonzales, N.R., Gwadz, M., Hurwitz, D.I., Jackson, J.D., Ke, Z.X., Lanczycki, C.J., Lu, F., Marchler, G.H., Mullokandov, M., Omelchenko, M.V., Robertson, C.L., Song, J.S., Thanki, N., Yamashita, R.A., Zhang, D.C., Zhang, N.G., Zheng, C.J., and Bryant, S.H. (2011). CDD: a conserved domain database for the functional annotation of proteins. *Nucleic Acids Res.* **39**, D225-D229.

Mardis, E.R. (2008). Next-generation DNA sequencing methods. *Annu. Rev. Genomics Hum. Genet.* **9**, 387-402.

Marti, L., Fornaciari, S., Renna, L., Stefano, G., and Brandizzi, F. (2010a). COPII-mediated traffic in plants. *Trends Plant Sci* **15**, 522-528.

Marti, L., Stefano, G., Tamura, K., Hawes, C., Renna, L., Held, M.A., and Brandizzi, F. (2010b). A missense mutation in the vacuolar protein GOLD36 causes organizational defects in the ER and aberrant protein trafficking in the plant secretory pathway. *Plant J.* **63**, 901-913.

Martin, R.C., Mok, M.C., Shaw, G., and Mok, D.W.S. (1989). An enzyme mediating the conversion of zeatin to dihydrozeatin in *Phaseolus* embryos. *Plant Physiol.* **90**, 1630-1635.

Marty, L., Siala, W., Schwarzländer, M., Fricker, M.D., Wirtz, M., Sweetlove, L.J., Meyer, Y., Meyer, A.J., Reichheld, J.P., and Hell, R. (2009). The NADPH-dependent thioredoxin system constitutes a functional backup for cytosolic glutathione reductase in *Arabidopsis*. *Proc. Natl. Acad. Sci. USA* **106**, 9109-9114.

Matsushima, R., Kondo, M., Nishimura, M., and Hara-Nishimura, I. (2003a). A novel ER-derived compartment, the ER body, selectively accumulates a β-glucosidase with an ER-retention signal in *Arabidopsis*. *Plant J.* **33**, 493-502.

Matsushima, R., Hayashi, Y., Kondo, M., Shimada, T., Nishimura, M., and Hara-Nishimura, I. (2002). An endoplasmic reticulum-derived structure that is induced under stress conditions in *Arabidopsis*. *Plant Physiol.* **130**, 1807-1814.

Matsushima, R., Hayashi, Y., Yamada, K., Shimada, T., Nishimura, M., and Hara-Nishimura, I. (2003b). The ER body, a novel endoplasmic reticulum-derived structure in *Arabidopsis*. *Plant Cell Physiol.* **44**, 661-666.

Matz, M.V., Fradkov, A.F., Labas, Y.A., Savitsky, A.P., Zaraisky, A.G., Markelov, M.L., and Lukyanov, S.A. (1999). Fluorescent proteins from nonbioluminescent *Anthozoa* species. *Nat. Biotechnol.* **17**, 969-973.

Maughan, S.C., Pasternak, M., Cairns, N., Kiddle, G., Brach, T., Jarvis, R., Haas, F., Nieuwland, J., Lim, B., Müller, C., Salcedo-Sora, E., Kruse, C., Orsel, M., Hell, R., Miller, A.J., Bray, P., Foyer, C.H., Murray, J.A.H., Meyer, A.J., and Cobbett, C.S. (2010). Plant homologs of the *Plasmodium falciparum* chloroquine-resistance transporter, PfCRT, are required for glutathione homeostasis and stress responses. *Proc. Natl. Acad. Sci. USA* **107**, 2331-2336.

Mayer, U., Ruiz, R.A.T., Berleth, T., Miseera, S., and Juurgens, G. (1991). Mutations affecting body organization in the *Arabidopsis* embryo. *Nature* **353**, 402-407.

McCallum, C.M., Comai, L., Greene, E.A., and Henikoff, S. (2000). Targeted screening for induced mutations. *Nat. Biotechnol.* **18**, 455-457.

Meisel, L., Xie, S.P., and Lam, E. (1996). *lem7*, a novel temperature-sensitive *Arabidopsis* mutation that reversibly inhibits vegetative development. *Dev. Biol.* **179**, 116-134.

Mellman, I., and Nelson, W.J. (2008). Coordinated protein sorting, targeting and distribution in polarized cells. *Nat. Rev. Mol. Cell Biol.* **9**, 833-845.

Meyer, A.J. (2008). The integration of glutathione homeostasis and redox signaling. *J. Plant Physiol.* **165**, 1390-1403.

Meyer, A.J., May, M.J., and Fricker, M. (2001). Quantitative *in vivo* measurement of glutathione in *Arabidopsis* cells. *Plant J.* **27**, 67-78.

Meyer, A.J., Brach, T., Marty, L., Kreye, S., Rouhier, N., Jacquot, J. P., and Hell, R. (2007). Redox-sensitive GFP in *Arabidopsis thaliana* is a quantitative biosensor for the redox potential of the cellular glutathione redox buffer. *Plant J.* **52**, 973-986.

Michelmore, R.W., Paran, I., and Kesseli, R.V. (1991). Identification of markers linked to disease-resistance genes by bulked segregant analysis - a rapid method to detect markers in specific genomic regions by using segregating populations. *Proc. Natl. Acad. Sci. USA* **88**, 9828-9832.

Michniewicz, M., Zago, M.K., Abas, L., Weijers, D., Schweighofer, A., Meskiene, I., Heisler, M.G., Ohno, C., Zhang, J., Huang, F., Schwab, R., Weigel, D., Meyerowitz, E.M., Luschnig, C., Offringa, R., and Friml, J. (2007). Antagonistic regulation of PIN phosphorylation by PP2A and PINOID directs auxin flux. *Cell* **130**, 1044-1056.

Morgan, A., Dimaline, R., and Burgoyne, R.D. (1994). The ATPase activity of N-ethylmaleimide-sensitive fusion protein (NSF) is regulated by soluble NSF attachment proteins. *J. Biol. Chem.* **269**, 29347-29350.

Morgan, T.H. (1910). Sex-limited inheritance in *Drosophila*. *Science* **32**, 120-122.

Mouratou, B., Biou, V., Joubert, A., Cohen, J., Shields, D.J., Geldner, N., Jürgens, G., Melancon, P., and Cherfils, J. (2005). The domain architecture of large guanine nucleotide exchange factors for the small GTP-binding protein Arf. *BMC Genomics* **6**.

Muller, B., and Sheen, J. (2008). Cytokinin and auxin interaction in root stem-cell specification during early embryogenesis. *Nature* **453**, 1094-1097.

Murphy, A.S., Hoogner, K.R., Peer, W.A., and Taiz, L. (2002). Identification, purification, and molecular cloning of N-1-naphthylphthalmic acid-binding plasma membrane-associated aminopeptidases from *Arabidopsis*. *Plant Physiol.* **128**, 935-950.

Nakano, R.T., Matsushima, R., Ueda, H., Tamura, K., Shimada, T., Li, L., Hayashi, Y., Kondo, M., Nishimura, M., and Hara-Nishimura, I. (2009). GNOM-LIKE1/ERMO1 and SEC24a/ERMO2 are required for maintenance of endoplasmic reticulum morphology in *Arabidopsis thaliana*. *Plant Cell* **21**, 3672-3685.

Nebenfuhr, A., Gallagher, L.A., Dunahay, T.G., Frohlick, J.A., Mazurkiewicz, A.M., Meehl, J.B., and Staehelin, L.A. (1999). Stop-and-go movements of plant Golgi stacks are mediated by the acto-myosin system. *Plant Physiol.* **121**, 1127-1141.

Nelson, B.K., Cai, X., and Nebenführ, A. (2007). A multicolored set of *in vivo* organelle markers for co-localization studies in *Arabidopsis* and other plants. *Plant J.* **51**, 1126-1136.

Neuhaus, J.M., and Rogers, J.C. (1998). Sorting of proteins to vacuoles in plant cells. *Plant Mol. Biol.* **38**, 127-144.

Nielsen, E., Cheung, A.Y., and Ueda, T. (2008). The regulatory RAB and ARF GTPases for vesicular trafficking. *Plant Physiol.* **147**, 1516-1526.

Noctor, G., Veljovic-Jovanovic, S., and Foyer, C.H. (2000). Peroxide processing in photosynthesis: antioxidant coupling and redox signalling. *Phil. Trans. R. Soc. Lond. B.* **355**, 1465-1475.

Novick, P., and Schekman, R. (1979). Secretion and cell-surface growth are blocked in a temperature-sensitive mutant of *Saccharomyces cerevisiae*. *Proc. Natl. Acad. Sci. USA* **76**, 1858-1862.

Novick, P., Field, C., and Schekman, R. (1980). Identification of 23 complementation groups required for post-translational events in the yeast secretory pathway. *Cell* **21**, 205-215.

Nziengui, H., Bouhidel, K., Pillon, D., Der, C., Marty, F., and Schoefs, B. (2007). Reticulon-like proteins in *Arabidopsis thaliana*: structural organization and ER localization. *FEBS Lett.* **581**, 3356-3362.

Oertle, T., Klinger, M., Stuermer, C.A., and Schwab, M.E. (2003). A reticular rhapsody: phylogenic evolution and nomenclature of the RTN/Nogo gene family. *FASEB J.* **17**, 1238-1247.

Ohtomo, I., Ueda, H., Shimada, T., Nishiyama, C., Komoto, Y., Hara-Nishimura, I., and Takahashi, T. (2005). Identification of an allele of VAM3/SYP22 that confers a semi-dwarf phenotype in *Arabidopsis thaliana*. *Plant Cell Physiol.* **46**, 1358-1365.

Oka, T., and Nakano, A. (1994). Inhibition of GTP hydrolysis by Sar1p causes accumulation of vesicles that are a functional intermediate of the ER-to-Golgi transport in yeast. *J. Cell Biol.* **124**, 425-434.

Onda, Y., Kumamaru, T., and Kawagoe, Y. (2009). ER membrane-localized oxidoreductase Ero1 is required for disulfide bond formation in the rice endosperm. *Proc. Natl. Acad. Sci. USA* **106**, 14156-14161.

Orci, L., Glick, B.S., and Rothman, J.E. (1986). A new type of coated vesicular carrier that appears not to contain clathrin: Its possible role in protein transport within the Golgi stack. *Cell* **46**, 171-184.

Orlando, K., and Guo, W. (2009). Membrane organization and dynamics in cell polarity. *Cold Spring Harb. Perspect. Biol.* **1**, a001321.

Ormö, M., Cubitt, A.B., Kallio, K., Gross, L.A., Tsien, R.Y., and Remington, S.J. (1996). Crystal structure of the *Aequorea victoria* green fluorescent protein. *Science* **273**, 1392-1395.

Ossowski, S., Schneeberger, K., Clark, R.M., Lanz, C., Warthmann, N., and Weigel, D. (2008). Sequencing of natural strains of *Arabidopsis thaliana* with short reads. *Genome Res.* **18,** 2024-2033.

Osterrieder, A., Carvalho, C.M., Latijnhouwers, M., Johansen, J.N., Stubbs, C., Botchway, S., and Hawes, C. (2009). Fluorescence lifetime omaging of onteractions between Golgi tethering factors and small GTPases in plants. *Traffic* **10**, 1034-1046.

Otegui, M.S., and Spitzer, C. (2008). Endosomal functions in plants. *Traffic* **9**, 1589-1598.

Otegui, M.S., Capp, R., and Staehelin, L.A. (2002). Developing seeds of *Arabidopsis* store different minerals in two types of vacuoles and in the endoplasmic reticulum. *Plant Cell* **14**, 1311-1327.

Paciorek, T., Zazimalova, E., Ruthardt, N., Petrasek, J., Stierhof, Y.-D., Kleine-Vehn, J., Morris, D.A., Emans, N., Jürgens, G., Geldner, N., and Friml, J. (2005). Auxin inhibits endocytosis and promotes its own efflux from cells. *Nature* **435**, 1251-1256.

Palade, G. (1975). Intracellular aspects of the process of protein synthesis. *Science* **189**, 867.

Palade, G.E. (1952). The fine structure of mitochondria. *Anat. Rec.* **114**, 427-451.

Parisy, V., Poinssot, B., Owsianowski, L., Buchala, A., Glazebrook, J., and Mauch, F. (2007). Identification of PAD2 as a γ-glutamylcysteine synthetase highlights the importance of glutathione in disease resistance of *Arabidopsis*. *Plant J.* **49**, 159-172.

Pasternak, M., Lim, B., Wirtz, M., Hell, R., Cobbett, C.S., and Meyer, A.J. (2008). Restricting glutathione biosynthesis to the cytosol is sufficient for normal plant development. *Plant J.* **53**, 999-1012.

Pearse, B.M. (1976). Clathrin: a unique protein associated with intracellular transfer of membrane by coated vesicles. *Proc. Natl. Acad. Sci. USA* **73**, 1255-1259.

Pinheiro, H., Samalova, M., Geldner, N., Chory, J., Martinez, A., and Moore, I. (2009). Genetic evidence that the higher plant Rab-D1 and Rab-D2 GTPases exhibit distinct but overlapping interactions in the early secretory pathway. *J. Cell Sci.* **122**, 3749-3758.

Pitann, B., Kranz, T., and Muhling, K.H. (2009). The apoplastic pH and its significance in adaptation to salinity in maize (*Zea mays* L.): comparison of fluorescence microscopy and pH-sensitive microelectrodes. *Plant Sci.* **176,** 497-504.

Pompa, A., and Vitale, A. (2006). Retention of a bean phaseolin/maize γ-zein fusion in the endoplasmic reticulum depends on disulfide bond formation. *Plant Cell* **18**, 2608-2621.

Porter, K.G., and Feig, Y.S. (1980). The use of DAPI for identifying and counting aquatic microflora. *Limnol. Oceanogr.* **25**, 943-948.

Porter, K.R., Claude, A., and Fullam, E.F. (1945). A study of tissue culture cells by electron microscopy. *J. Exp. Med.* **81**, 233-246.

Prasher, D.C., Eckenrode, V.K., Ward, W.W., Prendergast, F.G., and Cormier, M.J. (1992). Primary structure of the *Aequorea victoria* green fluorescent protein. *Gene* **111**, 229-233.

Rakusova, H., Gallego-Bartolome, J., Vanstraelen, M., Robert, H.S., Alabadi, D., Blazquez, M.A., Benkova, E., and Friml, J. (2011). Polarization of PIN3-dependent auxin transport for hypocotyl gravitropic response in *Arabidopsis thaliana*. *Plant J.* **67**, 817-826.

Rayle, D., and Cleland, R. (1970). Enhancement of wall loosening and elongation by acid solutions. *Plant Physiol.* **46,** 250-253.

Reisen, D., Leborgne-Castel, N., Ozalp, C., Chaumont, F., and Marty, F. (2003). Expression of a cauliflower tonoplast aquaporin tagged with GFP in tobacco suspension cells correlates with an increase in cell size. *Plant Mol. Biol.* **52**, 387-400.

Rennell, D., Bouvier, S.E., Hardy, L.W., and Poteete, A.R. (1991). Systematic mutation of bacteriophage T4 lysozyme. *J. Mol. Biol.* **222**, 67-87.

Richter, S., Geldner, N., Schrader, J., Wolters, H., Stierhof, Y.-D., Rios, G., Koncz, C., Robinson, D.G., and Jürgens, G. (2007). Functional diversification of closely related ARF-GEFs in protein secretion and recycling. *Nature* **448**, 488-492.

Richter, S., Muller, L.M., Stierhof, Y.D., Mayer, U., Takada, N., Kost, B., Vieten, A., Geldner, N., Koncz, C., and Jürgens, G. (2012). Polarized cell growth in *Arabidopsis* requires endosomal recycling mediated by GBF1-related ARF exchange factors. *Nat. Cell Biol.* **14**, 80-86.

Ridge, R.W., Uozumi, Y., Plazinski, J., Hurley, U.A., and Williamson, R.E. (1999). Developmental transitions and dynamics of the cortical ER of *Arabidopsis* cells seen with green fluorescent protein. *Plant Cell Physiol.* **40**, 1253-1261.

Riordan, J.F., and Vallee, B.L. (1972). Reactions with *N*-ethylmaleimide and *p*-mercuribenzoate. *Method Enzymol.* **26**, pp. 449-456.

Robatzek, S. (2007). Vesicle trafficking in plant immune responses. *Cell Microbiol.* **9,** 1-8.

Robatzek, S., Chinchilla, D., and Boller, T. (2006). Ligand-induced endocytosis of the pattern recognition receptor FLS2 in *Arabidopsis*. *Genes Dev.* **20**, 537-542.

Robert, S., Chary, S.N., Drakakaki, G., Li, S., Yang, Z., Raikhel, N.V., and Hicks, G.R. (2008). Endosidin1 defines a compartment involved in endocytosis of the brassinosteroid receptor BRI1 and the auxin transporters PIN2 and AUX1. *Proc. Natl. Acad. Sci. USA* **105,** 8464-8469.

Robinson, D.G., Jiang, L.W., and Schumacher, K. (2008). The endosomal system of plants: charting new and familiar territories. *Plant Physiol.* **147**, 1482-1492.

Robinson, J.T., Thorvaldsdottir, H., Winckler, W., Guttman, M., Lander, E.S., Getz, G., and Mesirov, J.P. (2011). Integrative genomics viewer. *Nat. Biotechnol.* **29**, 24-26.

Rojas-Pierce, M., Titapiwatanakun, B., Sohn, E.J., Fang, F., Larive, C.K., Blakeslee, J., Cheng, Y., Cuttler, S., Peer, W.A., Murphy, A.S., and Raikhel, N.V. (2007). *Arabidopsis* P-glycoprotein19 participates in the inhibition of gravitropism by gravacin. *Chem. Biol.* **14**, 1366-1376.

Rojo, E., Gillmor, C.S., Kovaleva, V., Somerville, C.R., and Raikhel, N.V. (2001). VACUOLELESS1 is an essential gene required for vacuole formation and morphogenesis in *Arabidopsis*. *Dev. Cell* **1**, 303-310.

Rorth, P., Szabo, K., Bailey, A., Laverty, T., Rehm, J., Rubin, G.M., Weigmann, K., Milan, M., Benes, V., Ansorge, W., and Cohen, S.M. (1998). Systematic gain-of-function genetics in *Drosophila*. *Development* **125**, 1049-1057.

Roth, T.F., and Porter, K.R. (1964). Yolk protein uptake in the oocyte of the mosquito *Aedes aegypti* L. *J. of Cell Biol.* **20**, 313-332.

Roudier, F., Fernandez, A.G., Fujita, M., Himmelspach, R., Borner, G.H.H., Schindelman, G., Song, S., Baskin, T.I., Dupree, P., Wasteneys, G.O., and Benfey, P.N. (2005). COBRA, an *Arabidopsis* extracellular glycosyl-phosphatidyl inositol-anchored protein, specifically controls highly anisotropic expansion through its involvement in cellulose microfibril orientation. *Plant Cell* **17**, 1749-1763.

Rutherford, S., and Moore, I. (2002). The *Arabidopsis* Rab GTPase family: another enigma variation. *Curr Opin Plant Biol.* **5**, 518-528.

Sacher, M., Stone, S., and FerroNovick, S. (1997). The synaptobrevin-related domains of Bos1p and Sec22p bind to the syntaxin-like region of Sed5p. *J. Biol. Chem.* **272**, 17134-17138.

Salminen, A., and Novick, P.J. (1987). A Ras-like protein is required for a post-Golgi event in yeast secretion. *Cell* **49**, 527-538.

Samalova, M., Fricker, M., and Moore, I. (2006). Ratiometric fluorescence-imaging assays of plant membrane traffic using polyproteins. *Traffic* **7**, 1701-1723.

Sambrook, J., and Russell, D.W. (2001). Molecular Cloning: A Laboratory Manual. (New York: Cold Spring Harbor Laboratory Press).

Sanderfoot, A. (2007). Increases in the number of SNARE genes parallels the rise of multicellularity among the green plants. *Plant Physiol.* **144**, 6-17.

Sanderfoot, A.A., and Raikhel, N.V. (1999). The specificity of vesicle trafficking: coat proteins and SNAREs. *Plant Cell* **11**, 629-641.

Sanderfoot, A.A., Kovaleva, V., Zheng, H., and Raikhel, N.V. (1999). The t-SNARE AtVAM3p resides on the prevacuolar compartment in *Arabidopsis* root cells. *Plant Physiol.* **121**, 929-938.

Sanderfoot, A.A., Pilgrim, M., Adam, L., and Raikhel, N.V. (2001). Disruption of individual members of *Arabidopsis* syntaxin gene families indicates each has essential functions. *Plant Cell* **13**, 659-666.

Sanderfoot, A.A., Ahmed, S.U., Marty-Mazars, D., Rapoport, I., Kirchhausen, T., Marty, F., and Raikhel, N.V. (1998). A putative vacuolar cargo receptor partially colocalizes with AtPEP12p on a prevacuolar compartment in *Arabidopsis* roots. *Proc. Natl. Acad. Sci. USA* **95**, 9920-9925.

Sarin, S., Prabhu, S., O'Meara, M.M., Pe'er, I., and Hobert, O. (2008). *Caenorhabditis elegans* mutant allele identification by whole-genome sequencing. *Nat. Methods* **5**, 865-867.

Sawa, S., Koizumi, K., Naramoto, S., Demura, T., Ueda, T., Nakano, A., and Fukuda, H. (2005). DRP1A is responsible for vascular continuity synergistically working with VAN3 in *Arabidopsis*. *Plant Physiol.* **138,** 819-826.

Schacter, H., and Brockhausen, I. (1992). The biosynthesis of serine (threonine)-N-acetylgalactosamine-linked carbohydrate moieties. Glycoconjugates: Composition, Structure, and Function, H.J. Allen and E.C. Kisailus, eds (New York: Marcel Dekker), pp. 263-332.

Schneeberger, K., Ossowski, S., Lanz, C., Juul, T., Petersen, A.H., Nielsen, K.L., Jorgensen, J.E., Weigel, D., and Andersen, S.U. (2009). SHOREmap: simultaneous mapping and mutation identification by deep sequencing. *Nat. Methods* **6**, 550-551.

Schneider, K., Mathur, J., Boudonck, K., Wells, B., Dolan, L., and Roberts, K. (1998). The ROOT HAIRLESS 1 gene encodes a nuclear protein required for root hair initiation in *Arabidopsis*. *Genes Dev.* **12**, 2013-2021.

Schwarzlander, M., Fricker, M.D., Muller, C., Marty, L., Brach, T., Novak, J., Sweetlove, L.J., Hell, R., and Meyer, A.J. (2008). Confocal imaging of glutathione redox potential in living plant cells. *J. Microsc.* **231**, 299-316.

Sciaky, N., Presley, J., Smith, C., Zaal, K.J.M., Cole, N., Moreira, J.E., Terasaki, M., Siggia, E., and LippincottSchwartz, J. (1997). Golgi tubule traffic and the effects of brefeldin A visualized in living cells. *J Cell. Biol.* **139**, 1137-1155.

Segev, N. (2001). Ypt/Rab GTPases: regulators of protein trafficking. *Sci. STKE* **2001,** re11.

Serafini, T., Stenbeck, G., Brecht, A., Lottspeich, F., Orci, L., Rothman, J.E., and Wieland, F.T. (1991). A coat subunit of Golgi-derived non-clathrin-coated vesicles with homology to the clathrin-coated vesicle coat protein β-adaptin. *Nature* **349**, 214-220.

Shaner, N.C., Steinbach, P.A., and Tsien, R.Y. (2005). A guide to choosing fluorescent proteins. *Nat. Methods* **2**, 905-909.

Shaner, N.C., Campbell, R.E., Steinbach, P.A., Giepmans, B.N.G., Palmer, A.E., and Tsien, R.Y. (2004). Improved monomeric red, orange and yellow fluorescent proteins derived from Discosoma sp red fluorescent protein. *Nat. Biotechnol.* **22**, 1567-1572.

Shanmugam, V., Tsednee, M., and Yeh, K.C. (2012). ZINC TOLERANCE INDUCED BY IRON 1 reveals the importance of glutathione in the cross-homeostasis between zinc and iron in *Arabidopsis thaliana*. *Plant J.* **69**, 1006-1017.

Shen, W.J., and Forde, B.G. (1989). Efficient transformation of *Agrobacterium* spp by high-voltage electroporation. *Nucleic Acids Res.* **17**, 8385-8385.

Shibata, Y., Voss, C., Rist, J.M., Hu, J., Rapoport, T.A., Prinz, W.A., and Voeltz, G.K. (2008). The reticulon and Dp1/Yop1p proteins form immobile oligomers in the tubular endoplasmic reticulum. *J. Biol. Chem*. **283**, 18892-18904.

Shih, H.P., Hales, K.G., Pringle, J.R., and Peifer, M. (2002). Identification of septin-interacting proteins and characterization of the Smt3/SUMO-conjugation system in *Drosophila*. *J. Cell Sci.* **115**, 1259-1271.

Shimada, T., Fuji, K., Tamura, K., Kondo, M., Nishimura, M., and Hara-Nishimura, I. (2003). Vacuolar sorting receptor for seed storage proteins in *Arabidopsis thaliana*. *Proc. Natl. Acad. Sci. USA* **100**, 16095-16100.

Shimomura, O., Johnson, F.H., and Saiga, Y. (1962). Extraction, purification and properties of Aequorin, a bioluminescent protein from the luminous hydromedusan, *Aequorea*. *J. Cell Comp. Physiol.* **59**, 223-239.

Shiraishi, K., Kato, S., Han, S.Y., Liu, W., Otsuka, K., Sakayori, M., Ishida, T., Takeda, M., Kanamaru, R., Ohuchi, N., and Ishioka, C. (2004). Isolation of temperature-sensitive p53 mutations from a comprehensive missense mutation library. *J. Biol. Chem.* **279**, 348-355.

Silverman, E.J., Maeda, A., Wei, J., Smith, P., Beggs, J.D., and Lin, R.J. (2004). Interaction between a G-patch protein and a spliceosomal DEXD/H-box ATPase that is critical for splicing. *Mol. Cell. Biol.* **24**, 10101-10110.

Singer, T., Fan, Y., Chang, H.S., Zhu, T., Hazen, S.P., and Briggs, S.P. (2006). A high-resolution map of *Arabidopsis* recombinant inbred lines by whole-genome exon array hybridization. *PLoS Genet.* **2**, e144.

Smith, D.R., Quinlan, A.R., Peckham, H.E., Makowsky, K., Tao, W., Woolf, B., Shen, L., Donahue, W.F., Tusneem, N., Stromberg, M.P., Stewart, D.A., Zhang, L., Ranade, S.S., Warner, J.B., Lee, C.C., Coleman, B.E., Zhang, Z., McLaughlin, S.F., Malek, J.A., Sorenson, J.M., Blanchard, A.P., Chapman, J., Hillman, D., Chen, F., Rokhsar, D.S., McKernan, K.J., Jeffries, T.W., Marth, G.T., and Richardson, P.M. (2008). Rapid whole-genome mutational profiling using next-generation sequencing technologies. *Genome Res.* **18**, 1638-1642.

Sollner, T., Whitehart, S.W., Brunner, M., Erdjumentbromage, H., Geromanos, S., Tempst, P., and Rothman, J.E. (1993). SNAP receptors implicated in vesicle targeting and fusion. *Nature* **362**, 318-324.

Sparkes, I., Tolley, N., Aller, I., Svozil, J., Osterrieder, A., Botchway, S., Mueller, C., Frigerio, L., and Hawes, C. (2010). Five *Arabidopsis* reticulon isoforms share endoplasmic reticulum location, topology, and membrane-shaping properties. *Plant Cell***,** 1333-1343.

Sparkes, I.A., Frigerio, L., Tolley, N., and Hawes, C. (2009). The plant endoplasmic reticulum: a cell-wide web. *Biochem. J.* **423**, 145-155.

Srivatsan, A., Han, Y., Peng, J., Tehranchi, A.K., Gibbs, R., Wang, J.D., and Chen, R. (2008). High-precision, whole-genome sequencing of laboratory strains facilitates genetic studies. *PLoS Genet.* **4**, e1000139.

Staal, M., De Cnodder, T., Simon, D., Vandenbussche, F., Van Der Straeten, D., Verbelen, J.P., Elzenga, T., and Vissenberg, K. (2011). Apoplastic alkalinization is instrumental for the inhibition of cell elongation in the *Arabidopsis* root by the ethylene precursor 1-aminocyclopropane-1-carboxylic acid. *Plant Physiol.* **155**, 2049-2055.

Stam, M., Mol, J.N.M., and Kooter, J.M. (1997). The silence of genes in transgenic plants. *Ann. Bot.- London* **79**, 3-12.

Stefano, G., Renna, L., Moss, T., McNew, J.A., and Brandizzi, F. (2012). In *Arabidopsis*, the spatial and dynamic organization of the endoplasmic reticulum and Golgi apparatus is influenced by the integrity of the C-terminal domain of RHD3, a non-essential GTPase. *Plant J.* **69**, 957-966.

Stephens, D.J. (2003). *De novo* formation, fusion and fission of mammalian COPII-coated endoplasmic reticulum exit sites. *EMBO Rep.* **4**, 210-217.

Stephens, D.J., Lin-Marq, N., Pagano, A., Pepperkok, R., and Paccaud, J.P. (2000). COPI-coated ER-to-Golgi transport complexes segregate from COPII in close proximity to ER exit sites. *J. Cell Sci.* **113**, 2177-2185.

Sturtevant, A.H. (1913). The linear arrangement of six sex-linked factors in *Drosophila*, as shown by their mode of association. *J. Exp. Zool.* **14**, 43-59.

Su, Y.H., Liu, Y. B., and Zhang, X.S. (2011). Auxin–cytokinin interaction regulates meristem development. *Mol. Plant* **4**, 616-625.

Suckow, J., Markiewicz, P., Kleina, L.G., Miller, J., Kisters-Woike, B., and Muller-Hill, B. (1996). Genetic studies of the Lac repressor XV: 4000 single amino acid substitutions and analysis of the resulting phenotypes on the basis of the protein structure. *J. Mol. Biol.* **261**, 509-523.

Sugiyama, M. (2003). Isolation and initial characterization of temperature-sensitive mutants of *Arabidopsis thaliana* that are impaired in root redifferentiation. *Plant Cell Physiol.* **44**, 588-596.

Surpin, M., Rojas-Pierce, M., Carter, C., Hicks, G.R., Vasquez, J., and Raikhel, N.V. (2005). The power of chemical genomics to study the link between endomembrane system components and the gravitropic response. *Proc. Natl. Acad. Sci. USA* **102**, 4902-4907.

Surpin, M., Zheng, H., Morita, M.T., Saito, C., Avila, E., Blakeslee, J.J., Bandyopadhyay, A., Kovaleva, V., Carter, D., Murphy, A., Tasaka, M., and Raikhel, N. (2003). The VTI family of SNARE proteins is necessary for plant viability and mediates different protein transport pathways. *Plant Cell* **15**, 2885-2899.

Sztul, E., and Lupashin, V. (2006). Role of tethering factors in secretory membrane traffic. *Am. J. Physiolo. Cell Physiol.* **290**, C11-C26.

Takahashi, K., Hayashi, K., and Kinoshita, T. (2012). Auxin activates the plasma membrane H^+-ATPase by phosphorylation during hypocotyl elongation in *Arabidopsis*. *Plant Physiol.* **159**, 632-641.

Takano, J., Tanaka, M., Toyoda, A., Miwa, K., Kasai, K., Fuji, K., Onouchi, H., Naito, S., and Fujiwara, T. (2010). Polar localization and degradation of *Arabidopsis* boron transporters through distinct trafficking pathways. *Proc. Natl. Acad. Sci. USA* **107**, 5220-5225.

Takei, K., Mcpherson, P.S., Schmid, S.L., and Decamilli, P. (1995). Tubular membrane invaginations coated by dynamin rings are induced by GTP-γ-S in nerve-terminals. *Nature* **374**, 186-190.

Tamura, K., Shimada, T., Kondo, M., Nishimura, M., and Hara-Nishimura, I. (2005). KATAMARI1/MURUS3 is a novel Golgi membrane protein that is required for endomembrane organization in *Arabidopsis*. *Plant Cell* **17**, 1764-1776.

Tamura, K., Takahashi, H., Kunieda, T., Fuji, K., Shimada, T., and Hara-Nishimura, I. (2007). *Arabidopsis* KAM2/GRV2 is required for proper endosome formation and functions in vacuolar sorting and determination of the embryo growth axis. *Plant Cell* **19**, 320-332.

Tamura, K., Shimada, T., Ono, E., Tanaka, Y., Nagatani, A., Higashi, S.I., Watanabe, M., Nishimura, M., and Hara-Nishimura, I. (2003). Why green fluorescent fusion proteins have not been observed in the vacuoles of higher plants. *Plant J.* **35**, 545-555.

Tanaka, H., Kitakura, S., De Rycke, R., De Groodt, R., and Friml, J. (2009). Fluorescence imaging-based screen identifies ARF GEF component of early endosomal trafficking. *Curr Biol.* **19**, 391-397.

Tanksley, S.D., Young, N.D., Paterson, A.H., and Bonierbale, M.W. (1989). RFLP mapping in plant breeding: new tools for an old science. *Nat. Biotechnol.* **7**, 257-264.

Tannukit, S., Wen, X., Wang, H.J., and Paine, M.L. (2008). TFIP11, CCNL1 and EWSR1 protein-protein interactions, and their nuclear localization. *Int. J. Mol. Sci.* **9**, 1504-1514.

Teh, O.K. (2007). Characterisation of membrane trafficking mutants in *Arabidopsis thaliana.* Department of Plant Sciences (Oxford: University of Oxford).

Teh, O.K., and Moore, I. (2007). An ARF-GEF acting at the Golgi and in selective endocytosis in polarized plant cells. *Nature* **448**, 493-496.

The Arabidopsis Genome Initiative (2000). Analysis of the genome sequence of the flowering plant *Arabidopsis thaliana*. *Nature* **408**, 796-815.

Thomas, J.H., Birnby, D.A., and Vowels, J.J. (1993). Evidence for parallel processing of sensory information controlling dauer formation in *Caenorhabditis elegans*. *Genetics* **134**, 1105-1117.

Tolley, N., Sparkes, I.A., Hunter, P.R., Craddock, C.P., Nuttall, J., Roberts, L.M., Hawes, C., Pedrazzini, E., and Frigerio, L. (2008). Overexpression of a plant reticulon remodels the lumen of the cortical endoplasmic reticulum but does not perturb protein transport. *Traffic* **9**, 94-102.

Toyooka, K., Okamoto, T., and Minamikawa, T. (2000). Mass transport of proform of a KDEL-tailed cysteine proteinase (SH-EP) to protein storage vacuoles by endoplasmic reticulum–derived vesicle is involved in protein mobilization in germinating seeds. J. Cell Biol. **148**, 453-464.

Toyooka, K., Goto, Y., Asatsuma, S., Koizumi, M., Mitsui, T., and Matsuoka, K. (2009). A mobile secretory vesicle cluster involved in mass transport from the Golgi to the plant cell exterior. *Plant Cell* **21**, 1212-1229.

Ueda, H., Nishiyama, C., Shimada, T., Koumoto, Y., Hayashi, Y., Kondo, M., Takahashi, T., Ohtomo, I., Nishimura, M., and Hara-Nishimura, I. (2006). AtVAM3 is required for normal specification of idioblasts, myrosin cells. *Plant Cell Physiol.* **47**, 164-175.

Ueda, T., Yamaguchi, M., Uchimiya, H., and Nakano, A. (2001). Ara6, a plant-unique novel type Rab GTPase, functions in the endocytic pathway of *Arabidopsis thaliana*. *EMBO J.* **20**, 4730-4741.

Uemura, T., Morita, M.T., Ebine, K., Okatani, Y., Yano, D., Saito, C., Ueda, T., and Nakano, A. (2010). Vacuolar/pre-vacuolar compartment Qa-SNAREs VAM3/SYP22 and PEP12/SYP21 have interchangeable functions in *Arabidopsis*. *Plant J.* **64**, 864-873.

Vale, R.D. (2003). The molecular motor toolbox for intracellular transport. *Cell* **112**, 467-480.

Vernoud, V., Horton, A.C., Yang, Z.B., and Nielsen, E. (2003). Analysis of the small GTPase gene superfamily of *Arabidopsis*. *Plant Physiol.* **131**, 1191-1208.

Vernoux, T., Wilson, R.C., Seeley, K.A., Reichheld, J.P., Muroy, S., Brown, S., Maughan, S.C., Cobbett, C.S., Van Montagu, M., Inze, D., May, M.J., and Sung, Z.R. (2000). The *ROOT MERISTEMLESS1/CADMIUM SENSITIVE2* gene defines a glutathione-dependent pathway involved in initiation and maintenance of cell division during postembryonic root development. *Plant Cell* **12**, 97-109.

Vida, T.A., and Emr, S.D. (1995). A new vital stain for visualizing vacuolar membrane dynamics and endocytosis in yeast. *J. Cell Biol.* **128**, 779-792.

Voeltz, G.K., Prinz, W.A., Shibata, Y., Rist, J.M., and Rapoport, T.A. (2006). A class of membrane proteins shaping the tubular endoplasmic reticulum. *Cell* **124**, 573-586.

Völker, A., Stierhof, Y.D., and Jürgens, G. (2001). Cell cycle-independent expression of the *Arabidopsis* cytokinesis-specific syntaxin KNOLLE results in mistargeting to the plasma membrane and is not sufficient for cytokinesis. *J. Cell Sci.* **114**, 3001-3012.

Vos, P., Hogers, R., Bleeker, M., Reijans, M., Vandelee, T., Hornes, M., Frijters, A., Pot, J., Peleman, J., Kuiper, M., and Zabeau, M. (1995). AFLP- a new technique for DNA-fingerprinting. *Nucleic Acids Res.* **23**, 4407-4414.

Wachter, A., Wolf, S., Steininger, H., Bogs, J., and Rausch, T. (2005). Differential targeting of GSH1 and GSH2 is achieved by multiple transcription initiation: implications for the compartmentation of glutathione biosynthesis in the *Brassicaceae*. *Plant J.* **41**, 15-30.

Wada, Y., Nakamura, N., Ohsumi, Y., and Hirata, A. (1997). Vam3p, a new member of syntaxin related protein, is required for vacuolar assembly in the yeast *Saccharomyces cerevisiae*. *J.Cell Sci.* **110**, 1299-1306.

Waizenegger, I., Lukowitz, W., Assaad, F., Schwarz, H., Jürgens, G., and Mayer, U. (2000). The *Arabidopsis* KNOLLE and KEULE genes interact to promote vesicle fusion during cytokinesis. *Curr. Biol.* **10**, 1371-1374.

Wang, J., Howles, P.A., Cork, A.H., Birch, R.J., and Williamson, R.E. (2006a). Chimeric proteins suggest that the catalytic and/or C-terminal domains give CesA1 and CesA3 access to their specific sites in the cellulose synthase of primary walls. *Plant Physiol.* **142**, 685-695.

Wang, X.H., Teng, Y., Wang, Q.L., Li, X.J., Sheng, X.Y., Zheng, M.Z., Samaj, J., Baluska, F., and Lin, J.X. (2006b). Imaging of dynamic secretory vesicles in living pollen tubes of *Picea meyeri* using evanescent wave microscopy. *Plant Physiol.* **141**, 1591-1603.

Ward, W.W. (1981). Properties of the coelenterate green-fluorescent proteins. Bioluminescence and Chemiluminescence: Basic Chemistry and Analytical Applications, M. DeLuca, McElroy, W.D., ed (New York: Academic Press, Inc.), pp. 235-242.

Wen, X., Tannukit, S., and Paine, M.L. (2008). TFIP11 interacts with mDEAH9, an RNA helicase involved in spliceosome disassembly. *Int. J. Mol. Sci.* **9**, 2105-2113.

Wen, X., Lei, Y.P., Zhou, Y.L., Okamoto, C.T., Snead, M.L., and Paine, M.L. (2005). Structural organization and cellular localization of tuftelin-interacting protein 11 (TFIP11). *Cell Mol. Life Sci.* **62**, 1038-1046.

West, M., Zurek, N., Hoenger, A., and Voeltz, G.K. (2011). A 3D analysis of yeast ER structure reveals how ER domains are organized by membrane curvature. *J. Cell Biol.* **193**, 333-346.

Whittington, A.T., Vugrek, O., Wei, K.J., Hasenbein, N.G., Sugimoto, K., Rashbrooke, M.C., and Wasteneys, G.O. (2001). MOR1 is essential for organizing cortical microtubules in plants. *Nature* **411**, 610-613.

Whyte, J.R.C., and Munro, S. (2002). Vesicle tethering complexes in membrane traffic. *J. Cell Sci.* **115**, 2627-2637.

Wightman, R., and Turner, S. (2010). Trafficking of the plant cellulose synthase complex. *Plant Physiol.* **153**, 427-432.

Williams, J.G.K., Reiter, R.S., Young, R.M., and Scolnik, P.A. (1993). Genetic-mapping of mutations using phenotypic pools and mapped RAPD markers. Nucleic Acids Res. **21**, 2697-2702.

Wiśniewska, J., Xu, J., Seifertová, D., Brewer, P.B., Růžička, K., Blilou, I., Rouquié, D., Benková, E., Scheres, B., and Friml, J. (2006). Polar PIN localization directs auxin flow in plants. *Science* **312**, 883-883.

Xiang, Y., and Wang, Y. (2010). GRASP55 and GRASP65 play complementary and essential roles in Golgi cisternal stacking. *J. Cell Biol.* **188**, 237-251.

Xu, H., Boulianne, G.L., and Trimble, W.S. (2002). *Drosophila* syntaxin 16 is a Q-SNARE implicated in Golgi dynamics. *J. Cell Sci.* **115**, 4447-4455.

Yamada, K., Hara-Nishimura, I., and Nishimura, M. (2011). Unique defense strategy by the endoplasmic reticulum body in plants. *Plant Cell Physiol.* **52**, 2039-2049.

Yamada, K., Nagano, A.J., Nishina, M., Hara-Nishimura, I., and Nishimura, M. (2008). NAI2 is an endoplasmic reticulum body component that enables ER body formation in *Arabidopsis thaliana*. *Plant Cell* **20**, 2529-2540.

Yang, F., Moss, L.G., and Phillips, G.N., Jr. (1996). The molecular structure of green fluorescent protein. *Nat. Biotechnol.* **14**, 1246-1251.

Yang, X., Boateng, K.A., Yuan, L., Wu, S., Baskin, T.I., and Makaroff, C.A. (2011). The *radially swollen 4* separase mutation of *Arabidopsis thaliana* blocks chromosome disjunction and disrupts the radial microtubule system in meiocytes. *PLoS One* **6**, e19459.

Yano, D., Sato, M., Saito, C., Sato, M.H., Morita, M.T., and Tasaka, M. (2003). A SNARE complex containing SGR3/AtVAM3 and ZIG/VTI11 in gravity-sensing cells is important for *Arabidopsis* shoot gravitropism. *Proc. Natl. Acad. Sci. USA* **100**, 8589-8594.

Yasutani, I., Ozawa, S., Nishida, T., Sugiyama, M., and Komamine, A. (1994). Isolation of temperature-sensitive mutants of *Arabidopsis thaliana* that are defective in the redifferentiation of shoots. *Plant Physiol.* **105**, 815-822.

Yu, I.M., and Hughson, F.M. (2010). Tethering factors as organizers of intracellular vesicular traffic. *Annu. Rev. Cell Dev. Biol.* **26,** 137-156.

Zechmann, B., Mauch, F., Sticher, L., and Müller, M. (2008). Subcellular immunocytochemical analysis detects the highest concentrations of glutathione in mitochondria and not in plastids. *J. Exp. Bot.* **59**, 4017-4027.

Zeitlin, S.G., and Sullivan, K.F. (2001). Animal cytokinesis: breaking up is hard to do. *Curr. Biol.* **11,** R514-R516.

Zerial, M., and McBride, H. (2001). Rab proteins as membrane organizers. *Nat. Rev. Mol. Cell Biol.* **2**, 107-117.

Zhang, L., Zhang, H., Liu, P., Hao, H., Jin, J.B., and Lin, J. (2011). *Arabidopsis* R-SNARE proteins VAMP721 and VAMP722 are required for cell plate formation. *PLoS One* **6**, e26129.

Zhang, Y., He, J.M., Lee, D., and McCormick, S. (2010). Interdependence of endomembrane trafficking and actin dynamics during polarized growth of *Arabidopsis* pollen tubes. *Plant Physiol.* **152**, 2200-2210.

Zheng, H. (2001). Green fluorescent protein as a marker for genetic analysis of the plant secretory pathway. School of Life Sciences (Oxford: Oxford Brookes University).

Zheng, H., Kunst, L., Hawes, C., and Moore, I. (2004). A GFP-based assay reveals a role for RHD3 in transport between the endoplasmic reticulum and Golgi apparatus. *Plant J.* **37**, 398-414.

Zheng, H., Camacho, L., Wee, E., Batoko, H., Legen, J., Leaver, C.J., Malho, R., Hussey, P.J., and Moore, I. (2005). A Rab-E GTPase mutant acts downstream of the Rab-D subclass in biosynthetic membrane traffic to the plasma membrane in tobacco leaf epidermis. *Plant Cell* **17**, 2020-2036.

Zheng, H.Y., Bednarek, S.Y., Sanderfoot, A.A., Alonso, J., Ecker, J.R., and Raikhel, N.V. (2002). NPSN11 is a cell plate-associated SNARE protein that interacts with the syntaxin KNOLLE. *Plant Physiol* **129**, 530-539.

Zhou, C., Yin, Y.B., Dam, P., and Xu, Y. (2010). Identification of novel proteins involved in plant cell-wall synthesis based on protein-protein interaction data. *J. Proteome Res.* **9**, 5025-5037.

Zouhar, J., Hicks, G.R., and Raikhel, N.V. (2004). Sorting inhibitors (Sortins): Chemical compounds to study vacuolar sorting in *Arabidopsis*. *Proc. Natl. Acad. Sci. USA* **101**, 9497-9501.

Zuryn, S., Le Gras, S., Jamet, K., and Jarriault, S. (2010). A strategy for direct mapping and identification of mutations by whole-genome sequencing. *Genetics* **186**, 427-430.

Zwiewka, M., Feraru, E., Moller, B., Hwang, I., Feraru, M.I., Kleine-Vehn, J., Weijers, D., and Friml, J. (2011). The AP-3 adaptor complex is required for vacuolar function in *Arabidopsis*. *Cell Res.* **21**, 1711-1722.

Appendix A List of Oligonucleotides

Table A1. List of oligonucleotides used in this study

	Primer name	Sequence (5' to 3')	Restriction enzyme required to digest the PCR product (if applicable)
gsh2 **genotyping markers**	G4_U	GCTTACCATTTAACTGGCTCCA	*XmnI*
	G4_L	GATATTGGGGGACTCAATTGGGTGAAAAC	
	N37_U	TGTACGATCAACATTTGCTGAG	*XhoI*
	N37_L	GCCTGCTTGACAATTTCTGAG	
	S6_U	GTGGCTGCTCTTCTCTCTCTTACTC	*XmnI*
	S6_L	CTGATTTCTGATAACTTTTGTCACCAAGAACGAG	
	S10_U2	CTTGCCCACCACTAAAGTTCC	*XmnI*
	S10_L	CATTGAAAAGAGGAGTAACATTACAAGAATGCTT	
rml1 **genotyping marker**	rml1_U	GAGTCAGGCAGTAAGATTTGACATAGTGTA	*XmnI*
	rml1_L	GAAACTTCCTGATCATATCAGCTTCTGAGAAAAAA	
GFP transgene genotyping marker	GFP_U	GTC CCA ATT CTT GTT GAA TTA GAT GGT	
	GFP_L	CAG ATT GTG TGG ACA GGT AAT GGT T	
Genetic markers used for mapping Mut 21	F21M12_fwd	GGCTTTCTCGAAATCTGTCC	
	F21M12_rev	TTACTTTTTGCCTCTTGTCATTG	
	F3F19_fwd	CGACGCATCAACAATGTACT	
	F3F19_rev	GCTTGGAATCGGCTTCTCTT	
	T24D18_fwd	TAGCACGGGTCTTTACAAC	
	T24D18_rev	AGCTGATAGATCCACTTCG	
	F19K19_fwd	AAAGAATCACCAGCCAGAT	
	F19K19_rev	ATTTAACAGTCGCAAGTCG	
	F17F16_fwd	TTCACTTTGCGGCAGTTG	*MfeI*
	F17F16_rev	TTGTTGTTGTGCATGGTAGA	
	PERL42164_fwd	GTAAGGGCTCAAAAACAGGTC	*AvaII*
	PERL42164_rev	CAAGATCCTATACAACGGATTCA	
	PERL42230_fwd set 2	CAAATATGTTTTCAGGGTTTCTAGATAAC	*BsaBI*
	PERL42230_rev set 2	TTAAGTACCAAATCAGTGGGAAA	
	F20D23_fwd	TTATGCCAACTCATGTGGAAAG	
	F20D23_rev	TGTCAAAGCGTCTGGTTCTG	
	F11A6_fwd	TGCGTTTAGATTTGATTTTC	*BfaI*
	F11A6_rev	TCAGGTTTAAGTGGGACG	
	F15H18_fwd	AGTCGTCGTCGGTCTACTA	*HaeIII*
	F15H18_rev	TTTGTCCCAAGTATTTATGT	
	F6A14_fwd	GGGAAGTGGATGGTTATGT	*ScaI*
	F6A14_rev	GGAAATATGGCCAGAAAAT	
	T26F17_fwd	TGAATCACATGAACCGTAGA	
	T26F17_rev	CGTGCATGTACCAGGAAT	

	T17H3_fwd	GTTTTTTACCCGCGTTTG	
	T17H3_rev	AAGCATAGAAACCTTTAAGA	
	F7P12_fwd	TCGAGGATATGTTTCGTGTTTG	
	F7P12_rev	ACAGTTTTGATGCATTGTGTGAG	
	ciw12_fwd	AGGTTTTATTGCTTTTCACA	
	ciw12_rev	CTTTCAAAAGCACATCACA	
	NF514a_fwd	GTTGAGTCTTGGCATCACAGTTC	
	NF514a_rev	CTGCCTGAAATTGTCGAAAC	
	F18P14_fwd	ATTCCCGCAATTTATTTTGTTC	
	F18P14_rev	GTTTGATGGCAGATTTGTTTTC	
	nga1126_fwd	GCACAGTCCAAGTCACAACC	
	nga1126_rev	CGCTACGCTTTTCGGTAAAG	
	nga168_fwd	GAGGACATGTATAGGAGCCTCG	
	nga168_rev	TCGTCTACTGCACTGCCG	
	nga172_fwd	AGCTGCTTCCTTATAGCGTCC	
	nga172_rev	CCATCCGAATGCCATTGTTC	
	N7N14_fwd	CAATACACTTTATCCAGATGCTG	
	N7N14_rev	GGGATTTGTTGATTGAAAAAGGAC	
	T6H20_fwd	CGGCTGAAACTTGGAAGGGAC	
	T6H20_rev	AGGAAGAACGTGTGATTGTG	
	K27K19_fwd	TGCTTTTGAAGAGATGGTTATTAGG	
	K27K19_rev	CCCCATTTCACTTATCATTGG	
	ciw5_fwd	GGTTAAAAATTAGGGTTACGA	
	ciw5_rev	AGATTTACGTGGAAGCAAT	
	F14G16_fwd	ACAAACCGATCAGCATTCAAG	
	F14G16_rev	GCCTTTGTCACGGATTCAAC	
	F6E21_fwd	TTCTTTGTTCAAGTTCCATGTCTC	
	F6E21_rev	CGGTGATTGTCTCAAGTGTTTG	
	nga151a_fwd	ATCTCATACTGACCCATATGTTCC	
	nga151a_rev	ATTGTACAGTCTAAAAGCGAGAG	
	PHYC_fwd	CTCAGAGAATTCCCAGAAAAATCT	
	PHYC_rev	AAACTCGAGAGTTTTGTCTAGATC	
	ciw9_fwd	CAGACGTATCAAATGACAAATG	
	ciw9_rev	GACTACTGCTCAAACTATTCGG	
	MPL12_fwd	TAGCCATAAACTTGGAAGA	
	MPL12_rev	CCTCATTCGCTACCTAGA	
	K9P8_fwd	TTATGGGTTTCTCAGAGTTTCTCAC	
	K9P8_rev	TTGTATGCGTTTGCTTTTTCC	
	MNC17_fwd	GTACCGGATCTGTGTTGTGAAG	
	MNC17_rev	GTGCTCAAGGAAATGGGATAG	
	K9I9_fwd	TTTCTAATCAACTGCTAAAG	
	K9I9_rev	TACAGATAATGGCAGTATCA	
Mut 21/ *rrd4* genotyping marker	rrd4_fwd	CGCTGGACTCACTTGCTATTCG	*ApaI*
	rrd4_rev	CACTGCATCACTAAGAGGGGCC	
	At1g17070_2_fwd	AGGAAGAGAAACAAAAAAGACAC	*AvaII*
	At1g17070_2_rev	TTGGCTATAAGGCGTTGAGA	

Appendix B Publication from this work

A perturbation in glutathione biosynthesis disrupts endoplasmic reticulum morphology and secretory membrane traffic in *Arabidopsis thaliana*

Kenneth K. C. Au, José Pérez-Gómez, Hélia Neto, Christopher Müller, Andreas J. Meyer, Mark D. Fricker and Ian Moore